THE UNIVERSITY OF CHICAGO

# ISOLATION, CHARACTERIZATION, AND REACTIVITY OF CO-OXO COMPLEXES SUPPORTED BY TRIS(IMIDAZOL-2-YLIDENE)PHENYLBORATE LIGANDS

A DISSERTATION SUBMITTED TO

THE FACULTY OF THE DIVISION OF THE PHYSICAL SCIENCES

IN CANDIDACY FOR THE DEGREE OF

DOCTOR OF PHILOSOPHY

DEPARTMENT OF CHEMISTRY

BY

MCKENNA KATHLEEN GOETZ

CHICAGO, ILLINOIS

DECEMBER 2021

# Table of Contents

# List of Figures

Chapter 1



Chapter 2



Chapter 3



Chapter 4

Chapter 5



Appendix 1

Appendix 4

# List of Schemes

Chapter 1



Chapter 2



Chapter 3



Chapter 4



Chapter 5



Appendix 1

Appendix 2



Appendix 4

# List of Tables

Chapter 2



Chapter 3



Chapter 4



Appendix 1

Appendix 2

Appendix 4

# List of Equations

Chapter 2



Chapter 3

Chapter 5



Appendix 1



Appendix 2

# List of Abbreviations

| | |
|---|---|
| $\{^{1}H\}$ | Proton decoupled |
| ° | degree |
| °C | degree Celcius |
| $^{11}B$ | Boron-11 |
| $^{13}C$ | Carbon-13 |
| $^{19}F$ | Fluorine-19 |
| $^{1}H$ | Hydrogen-1 |
| $^{2}H$ | Hydrogen-2 or deuterium |
| $^{7}Li$ | Lithium-7 |
| $^{31}P$ | Phosphorus-31 |
| A | absorbance |
| Å | Angstrom |
| Ad | adamantyl |
| $^{Ad}Im$ | 1-adamantyl-imidazol-2-ylidene |
| $^{Ad}ImH$ | 1-adamantyl-imidazolium |
| Avg | average |
| B.M. | Bohr magnetons |

| | |
|---|---|
| $BAr^F_4$ | tetrakis(3,5-bis(trifluoromethyl)phenyl)borate |
| BD(F)E | bond dissociation (free) energy |
| br | broad |
| Bu | butyl |
| Bz | benzoyl |
| *C* | Standard reduction potential of $H^+/H^\bullet$ in a given solvent |
| $C_{3v}$ | pseudo-tetrahedral |
| $C_{4v}$ | pseudo-octahedral |
| CHD | 1,3-cyclohexadiene |
| cm | centimeter |
| $cm^{-1}$ | wavenumber |
| COSMO, CPMC | Solvation models for DFT |
| COSY | correlation spectroscopy |
| CPET | concerted proton-electron transfer |
| crypt | Kryptofix 2,2,1 (4,7,13,16,21-pentaoxa-1,10-diazabicyclo[8.8.5]tricosane) |
| CV | cyclic voltammetry or cyclic voltammogram |
| δ | chemical shift |
| d | deuterium or doublet |

| | |
|---|---|
| DCM | dichloromethane |
| def2-SVP, etc. | DFT basis sets |
| DFB | 1,2-difluorobenzene |
| DFT | density functional theory |
| DHA | 9,10-dihydroanthracene |
| DI | delocalization index |
| DMSO | dimethylsulfoxide |
| $d_x$ | Compound with x deuterium atoms |
| ε | Absorption extinction coefficient |
| e | electron |
| $E^0$ | Standard reduction potential |
| $E_{1/2}$ | Reduction potential of a compound under any conditions |
| EI | electron ionization |
| $E_p$ | Peak potential of a CV feature |
| EPR | electron paramagnetic resonance |
| equiv. | equivalents |
| ET | electron tranfer |
| Et | ethyl |

| | |
|---|---|
| Fc | ferrocene |
| Fl | fluorene |
| G | Gibbs free energy or Gauss |
| g | gram |
| *g* | electron g-factor |
| GC | gas chromatography |
| η | Asynchronicity |
| H | enthalpy |
| HMDS | hexamethyldisilazide |
| HSQC | heteronuclear single quantum coherence |
| Hz | Hertz |
| IBO | intrinsic bond orbital |
| Im | imidazol-2-ylidene |
| $^{i}$Pr | isopropyl |
| IR | infrared |
| K | Kelvin |
| *k* | rate constant |
| $K_a$ | acid equilibrium constant |

| | |
|---|---|
| kcal | kilocalorie |
| $K_{eq}$ | general equilibrium constant |
| KIE | kinetic isotope effect |
| $K_{ip}$ | ion-paired equilibrium constant |
| λ | wavelength |
| μ | reduced mass |
| M | molarity |
| m | medium |
| *m* | meta |
| μA | microamp |
| Me | methyl |
| $\mu_{eff}$ | magnetic moment |
| mg | milligram |
| MHz | megahertz |
| mL | milliliter |
| μL | microliter |
| mM | millimolar |
| μM | micromolar |

| | |
|---|---|
| mm | millimeter |
| mmol | millimole |
| mol | mole |
| MS | mass spectrometry |
| MTBD | 7-methyl-1,5,7-triazabicyclo[4.4.0]dec-5-ene |
| mV | millivolt |
| ν | frequency |
| nm | nanometer |
| NMR | nuclear magnetic resonance |
| NOESY | nuclear Overhauser effect spectroscopy |
| *o* | ortho |
| O3LYP, etc. | DFT functional |
| Oh | octahedral |
| OTf | $CF_3SO_3$ |
| *p* | para |
| PCET | proton-coupled electron transfer |
| PCI | positive chemical ionization |
| Ph | phenyl |

| | |
|---|---|
| p$K_a$ | –log($K_a$) |
| PT | proton transfer |
| R | generic organic group or R-factor |
| r | radius |
| RT | room temperature |
| S | entropy |
| s | second, strong, or singlet |
| *S* | spin |
| sh | shoulder |
| Std. Dev. | standard deviation |
| t | time or triplet |
| T | temperature |
| $^t$Bu | *tert*-butyl |
| $^t$BuIm | 1-*tert*-butyl-imidazol-2-ylidene |
| $^t$BuImH | 1-*tert*-butyl-imidazolium |
| TD-DFT | time dependent density functional theory |
| THF | tetrahydrofuran |
| TMS | trimethylsilyl |

| | |
|---|---|
| UV | ultraviolet |
| V | volt |
| vis | visible |
| w | weak |
| wR | weighted R-factor |
| XAS | X-ray absorption spectroscopy |
| XRD | X-ray diffraction |
| Z | collision frequency |

# Acknowledgments

First and foremost, I would like to thank my advisor, Prof. John Anderson, for all of his support and guidance over the years. I am particularly grateful for his never-ending faith in me and my abilities, his infectious enthusiasm for my projects and chemistry in general, and his willingness to let me pursue additional opportunities throughout my graduate career. Next, I would like to thank my committee members, Prof. Greg Engel and Prof. Mark Levin, for their role in my defense. I would also like to thank the Anderson lab as a whole for their willingness to help out when needed, for helpful discussions about science, and for some fun times outside the lab.

In particular, I need to thank the oxo subgroup for everything over the years. From lunch breaks, to coffee breaks, to sharing the glovebox and talking about science, I couldn't have gotten to where I am without the subgroup. I must give special thanks to Prof. Ethan Hill, who taught me so much about how to do chemistry and was always a useful sounding board. I don't think I'd have had as much success without his mentorship. Next, I want to thank Norman Zhao for being such a great lab buddy, especially during covid when we shared a shift and glovebox. I would also like to thank Maggie Kelty for being a wonderful lab mate and friend. Her help and support were invaluable for making it through the marathon that is grad school and I am so grateful that our life paths crossed.

I would like to thank Dr. Alex Filatov, Dr. Andrew McNeece, Dr. Kate Jesse, and also Sophie Anferov for all their help with crystal structures over the years. My compounds were notoriously awful, and I appreciate all the help with data collection and analysis. I must also thank Dr. Britni Ratliff for being a wonderful additional mentor during my graduate career. I've learned so much about many different aspects of teaching from her and am endlessly grateful for the opportunities I had to work with her in various capacities.

The work described here was primarily funded by the University of Chicago and the National Science Foundation. I have personally received additional financial support over the years from the Eckhardt Fellowship, various Department of Chemistry awards including the Seymour Goodman Fellowship, the Helen Sellei-Beretvas Fellowship, and the Benjamin Ball Freud Teaching Fellowship, and the William Rainey Harper Dissertation Fellowship. This work was greatly supported by these fellowships and I want to thank those responsible for the availability of these funds.

Finally, I would like to thank all of those who have supported me outside of my academic career. First, my parents, who have always believed in me, supported me when I've needed it, and encouraged me to be the best that I can be. I couldn't ask for better parents. Next, my siblings, who have also always been in my corner, even if it's just to annoy me. I would like to thank my friends, those here at the University of Chicago and those from before, especially Anna Kellner and Courtney Smith who were some of the best bridesmaids a girl could ask for. I would also like to thank my parents- and sister-in-law, for welcoming me into their family and offering support as I finish up graduate school. And finally, I must thank my wonderful husband, Nick Smith, for all of his unwavering support over the past 5 years. Thank you for reminding me there is more to life than chemistry, for the laughter, for planning a wedding in the middle of graduating, for everything. I couldn't ask for a better partner in life.

# Abstract

C–H activation and O–O bond formation are extremely important reactions for efficient complex organic synthesis and water oxidation, respectively. The catalysts that mediate these fundamental processes are proposed to utilize transition metal-oxo intermediates, which has inspired decades of research into the isolation and characterization of such species. In particular, late transition metal-oxo complexes such as those with Co have been implicated in these reactions. However, due to their high d-electron counts, these complexes are difficult to isolate and characterize. Thus, there is a dearth of examples of isolable Co-oxo complexes, resulting in a lack of general understanding of their properties and reactivity. Specifically, prior to the work described here, no characterizable examples of terminal $Co^{III}$-oxo complexes were reported. Strategies such as the use of strongly donating ligands and low-coordinate geometries enable the isolation of these intermediates. Subsequent characterization of their bonding and thermodynamic properties, as well as examination of their reactivity towards C–H activation and O–O bond formation, provides fundamental insight into the nature of these species which have often been invoked, but rarely observed, in the key reactions described above.

Chapter 2 describes the use of strongly donating tris(imidazol-2-ylidene)phenylborate ligands that enforce a low-coordinate, pseudo-tetrahedral geometry to enable the isolation and characterization of three $Co^{III}$-oxo complexes. These complexes have 6 d-electrons, yet maintain a strong Co–O multiple bond. All have been crystallographically characterized and display H–atom abstraction and O–atom transfer reactivity. Their stability enables thorough characterization of the thermodynamic properties of the two terminal $Co^{III}$-oxo complexes, which reveal ligand substituent-dependent oxidation potentials and p$K_a$ values. Interestingly, the Co–O multiple bond

itself is unaffected by the identity of the ligand substituents and DFT analysis reveals the presence of two strong π bonding interactions and one weak σ bonding interaction.

Given the importance of metal-oxo intermediates in C–H activation reactions, the C–H activation reactivity of the $^{t}$Bu-substituted $Co^{III}$-oxo complex was explored and is described in Chapter 3. Broadly, transition metal-oxo complexes react most quickly with the homolytically weakest C–H bond in a molecule, resulting in selectivity solely based on bond strengths. However, thorough kinetic studies reveal that this $Co^{III}$-oxo complex reacts most quickly with the most acidic C–H bond, opening up possibilities of alternative selectivity in metal-oxo mediated C–H activation. Additionally, it is shown that these C–H activation reactions are concerted but proceed through an imbalanced transition state, so-called "asynchronous" CPET, which had only been explored computationally previously.

The relevance of asynchronicity has seen a resurgence in the field of transition metal-oxo chemistry, resulting in questions about the limits of this mechanism. Chapter 4 describes the C–H and O–H activation reactivity of the Ad-substituted $Co^{III}$-oxo complex which is more basic and less oxidizing than the $^{t}$Bu-substituted complex. As expected, this results in C–H activation that proceeds with greater asychronicity, as evidenced by Hammett analysis. Additionally, a clear switch from an asynchronous CPET mechanism to a stepwise PTET mechanism is observed for O–H activation reactions. This highlights the limits of asynchronous CPET and provides additional support for the concerted reactivity invoked in the C–H activations described in Chapter 3.

Most isolable transition metal-oxo complexes engage in endergonic C–H activation reactions at very slow rates. This is true for the $Co^{III}$-oxo complexes described here, prompting attempts at oxidation to $Co^{IV}$ to generate a more active oxidant. These experiments are summarized in Chapter

5, and reveal ligand substituent-dependent reactivity. For the $^{t}$Bu-substituted $Co^{III}$-oxo, preliminary evidence indicates likely oxo-oxo coupling after oxidation to form a $Co^{III}_2$-peroxo complex. For the Ad-substituted $Co^{III}$-oxo, oxidation results in the formation of a transient $Co^{IV}$-oxo complex, as assayed by EPR spectroscopy. This intermediate reacts endergonically with a ligand C–H at rates comparable to P450 enzymes, before engaging in exergonic rebound to form hydroxylated product. This reactivity pattern mirrors that proposed to be operative in enzymatic and catalytic systems, providing support for these mechanisms.

This thesis also contains multiple appendices which have supporting data for each chapter.

# Preface

All chapters have an independent compound numbering system. Characterization spectra are provided in the corresponding appendix for each chapter.

# Chapter 1: Introduction to Transition Metal-Oxo Complexes

## 1.1 Importance of Transition Metal-Oxo Complexes

Transition metal-oxo complexes are a ubiquitous class of compounds that mediate a wide variety of reactions that are important in biology, industry, and organic synthesis. These reactions include C–H activation, O–atom transfer, and O–O bond formation (Scheme 1.1). In biology, C–H activation reactions carried out by enzymes such as cytochrome P450s or α-ketoglutarate dependent hydroxylases are mediated by high-valent iron-oxo species.[1] These Fe-oxo intermediates abstract an H–atom from a substrate, producing a carbon radical that can be fed into further reactions, such as hydroxylation (Scheme 1.1). In cytochrome P450 enzymes in particular, which are responsible for the degradation of pharmaceuticals in the body, these reactions proceed at extremely fast rates.[1a] The success of these enzymatic systems has motivated development of synthetic catalysts for complex organic synthesis[2] and prompted intense study of the mechanism of these reactions in model complexes.[3]

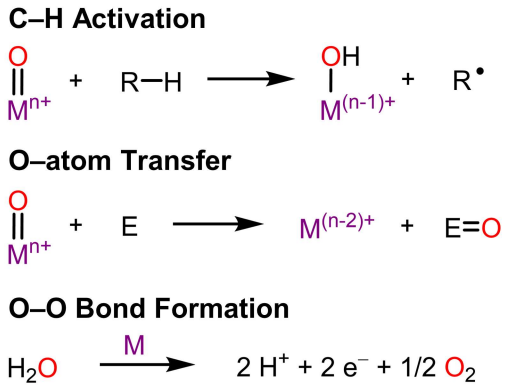


**Scheme 1.1.** Reactions mediated by key transition metal-oxo intermediates.

The transfer of a net H–atom from a C–H bond to a metal-oxo unit to form an O–H bond, the initial step in any transition metal-oxo mediated C–H activation reaction, involves the movement of both a proton and electron. The mechanisms by which this transfer can occur fall under the umbrella of proton-coupled electron transfer (PCET) reactions.[3] These reactions can be concerted proton-electron transfer (CPET), stepwise proton transfer-electron transfer (PTET), or stepwise electron transfer-proton transfer (ETPT) and have important implications for the rate and selectivity of a given reaction.[3b] Understanding the intricacies by which this PCET reaction occurs is therefore vital for the development of catalysts with exquisite control over selectivity and rates of reaction. Thus, the study of model transition metal-oxo complexes that mediate C–H activation reaction is invaluable for providing insight into enzymatic and synthetic systems.

Transition metal-oxo complexes are also implicated as key intermediates in the O–O bond forming step of water oxidation (Scheme 1.1). The oxidation of water to produce protons, electrons, and oxygen is central in the life processes of plants.[4] The protons and electrons are used to produce fuel for the plant while the oxygen is released as a benign byproduct. Mirroring this process is an attractive strategy in the development of clean energy sources,[5] motivating the development of synthetic water oxidation catalysts.[6] In all of these cases, a terminal transition metal-oxo intermediate is proposed to be the key intermediate prior to O–O bond formation and $O_2$ release. In biology, this is a Mn-oxo intermediate,[4a] and a variety of metals have been utilized synthetically, with Co-based catalysts being particularly promising.[6a] Given the centrality of metal-oxo intermediates in the O–O bond forming step, there has been significant interest in understanding the mechanism of this O–O bond formation.[7] There are two main mechanisms for O–O bond formation: nucleophilic attack of a (metal)-hydroxide on a terminal metal-oxo

intermediate or bimetallic coupling of two metal-oxo complexes to form a bridging peroxo complex. Study of model complexes has therefore been focused on linking metal-oxo properties with O–O bond formation mechanistic preference.[8]

## 1.2 Terminal Transition Metal-Oxo Complexes with High d-electron Counts

The centrality of transition metal-oxo complexes in many important processes described above motivates the study of isolable examples of these intermediates. In-depth understanding of the bonding, structure, and reactivity of these complexes provides valuable insight into Nature's design principles and also provides guidelines for the development of efficient synthetic catalysts. While Nature primarily utilizes Mn and Fe as the metal centers for metal-oxo mediated reactivity, the utility of other metals, such as Co, has been demonstrated in synthetic systems.[6a] However, study of late transition metal-oxo complexes is significantly hindered by their high d-electron counts (Figure 1.1). This can be understood by considering the d-orbital diagram for a transition metal-oxo complex in a pseudo-octahedral ($C_{4v}$) geometry, a common geometry observed for these species. This d-orbital diagram was initially derived for the vanadyl ion, and reveals that upon replacing an axial ligand with a π donor oxo ligand, the $d_{yz}$ and $d_{xz}$ orbitals, which are formally non-bonding in an octahedral ($O_h$) geometry, take on π antibonding character with respect to the metal-oxygen bond (Figure 1.1).[9]

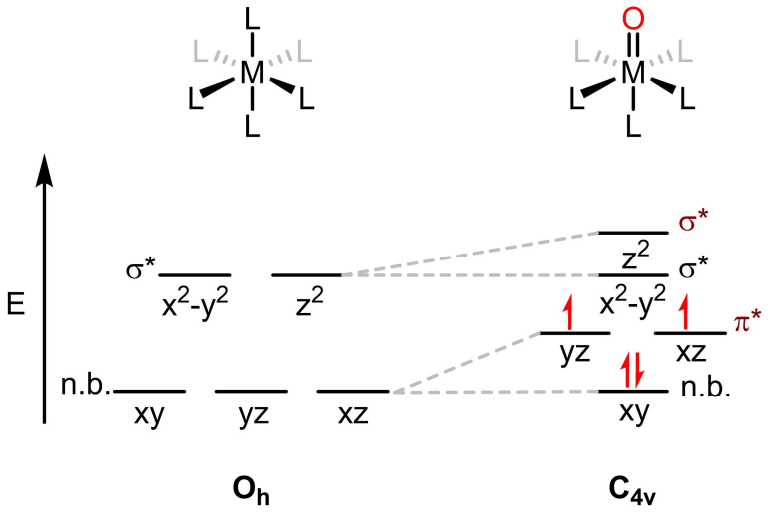


**Figure 1.1.** The d-orbital splitting diagrams for an octahedral complex (left) and pseudo-octahedral complex (right) with an axial π donor O ligand and 4 d-electrons. Red symmetry labels indicate the symmetry with respect to the M–O bond.

The d-orbital splitting diagram shown for a $C_{4v}$ complex in Figure 1.1 has an important implication: when there are more than 4 d-electrons in the complex, the M–O π* orbitals will be populated to the extent that both π bonds are almost or fully broken. This reduction of multiple bonding between the metal and oxygen will result in an unstable complex that cannot be isolated or studied. This fact can be summarized in the concept of the "oxo wall", which states that no stable, terminal metal-oxo complex can be isolated past group 8. Indeed, the vast majority of isolable examples of transition metal-oxo complexes adhere to this principle.[3c,10]

Nonetheless, a handful of examples of transition metal-oxo complexes with > 4 d-electrons have been isolated and characterized (Figure 1.2).[11,12] However, few of these have been truly isolated and crystallographically characterized (Figure 1.2 A-D),[12] limiting the understanding of their structure and the study of their reactivity. In particular, Co-oxo complexes, which are known to be important intermediates in water oxidation catalysis,[13] had yet to be crystallized as of the beginning

of this body of work in 2017. This emphasizes the need to study well-defined examples of such complexes in order to understand their properties and reactivity. Co-oxo complexes will have 5 ($Co^{IV}$) or 6 ($Co^{III}$) d-electrons and determining what implications these higher d-counts have for the reactivity of these complexes remains an open question.

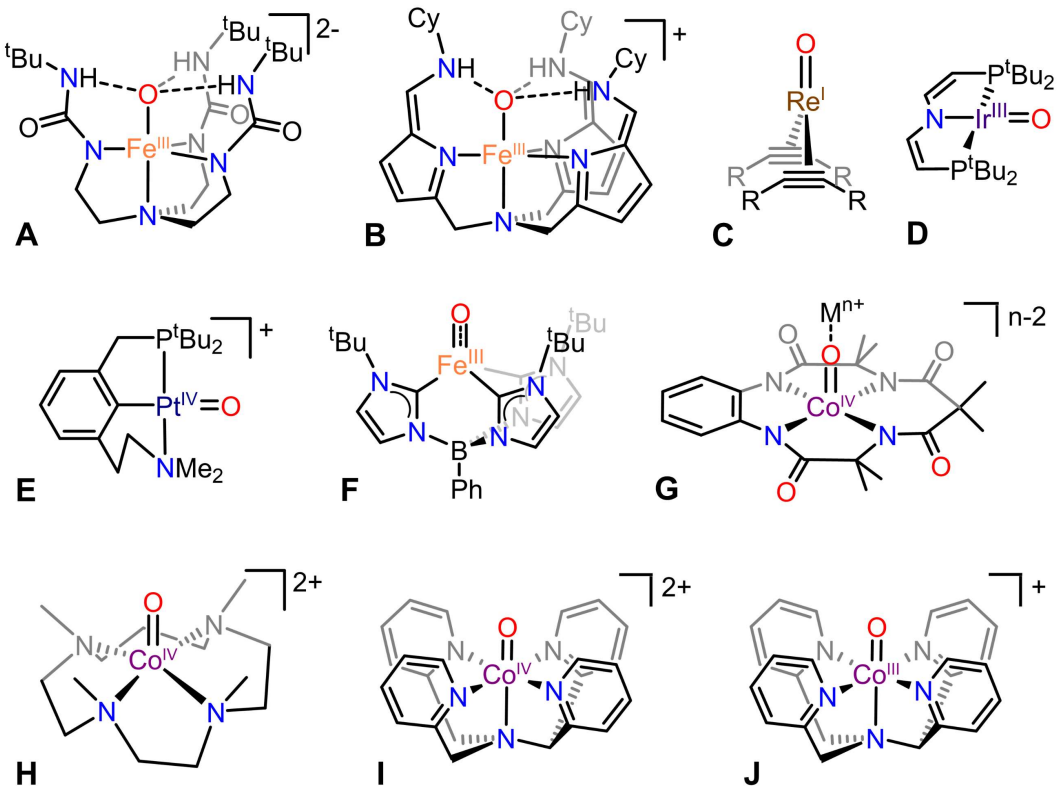


**Figure 1.2.** Transition metal-oxo complexes with > 4 d-electrons. (A) Reference 12a. (B) Reference 12b. (C) Reference 12c. (D) Reference 12d (E) Reference 11e. (F) Reference 11a. (G) Reference 11b. (H) Reference 11c. (I) Reference 11d. (J) Reference 11d.

## 1.3 Strategies for the Isolation and Study of Late Transition Metal-Oxo Complexes

Given the interest in late transition metal-oxo complexes with high d-electron counts, appropriate strategies must be employed to stabilize these elusive and interesting intermediates. One strategy that has had success previously includes the use of secondary sphere interactions, such as hydrogen bonding, to protect the reactive metal-oxygen unit (Figure 1.2 A, B).[12a,b] Another strategy involves protecting the oxo ligand by binding a redox-inactive metal ion (Figure 1.2G).[11b] A third strategy is the use of alternate geometries that afford different d-orbital splittings and consequently avoid population of metal-oxygen antibonding orbitals (Figure 1.2 C, D, E, F).[11a,11e,12c,12d]

Pseudo-tetrahedral geometries (Figure 1.3) are particularly attractive in this regard. In this geometry, the two lowest lying orbitals are non-bonding with respect to the metal-oxygen bond. The two highest lying orbitals are the M–O $\pi^*$ orbitals with the $d_{z^2}$ orbital lying between those two sets. The $d_{z^2}$ orbital is of the correct symmetry to have $\sigma^*$ character with respect to the metal-oxygen bond, but it is also of the correct symmetry to hybridize with the metal s-orbital. This hybridization lowers $d_{z^2}$ in energy and gives it some degree of non-bonding character, making population of this orbital less destabilizing.[14] Thus, in a pseudo-tetrahedral geometry, it is possible to accommodate up to 6 d-electrons before populating M–O $\pi^*$ orbitals (Figure 1.3), maintaining at least a double bond between the metal and oxygen, which would likely result in a stable metal-oxo complex.

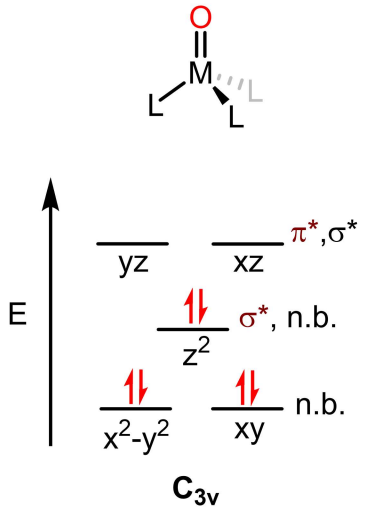


**Figure 1.3.** The d-orbital splitting diagram for a pseudo-tetrahedral complex with an axial π donor O ligand and 6 d-electrons. Red symmetry labels indicate the symmetry with respect to the M–O bond.

Indeed, this strategy has been used successfully previously. Isolation of a terminal $Ir^{V}$-oxo complex in a pseudo-tetrahedral geometry reveals a metal-oxygen triple bond, despite the presence of 4 d-electrons.[15] In a pseudo-octahedral geometry, 4 d-electrons would allow for a maximum bond order of 2 (Figure 1.1). Additionally, many examples of $d^6$ $Co^{III}$-imide complexes, which are isoelectronic to oxo complexes, have been isolated and characterized.[16] These observations make use of pseudo-tetrahedral geometries a particularly attractive target for the isolation and characterization of Co-oxo complexes with 5 or 6 d-electrons. There are many choices of pseudo-tetrahedral enforcing ligands, with tris(pyrazolyl)borates being the canonical example. However, these are weakly donating ligands that aren't capable of supporting the highly oxidized metal centers of metal-oxo complexes.[17] Tris(imidazol-2-ylidene)phenylborate ligands are an analogous scaffold that features much stronger N-heterocyclic carbene donors. These ligands have been

shown to support highly oxidized metal centers previously (Figure 1.4),[18] motivating their use in the pursuit of high-valent Co-oxo complexes.

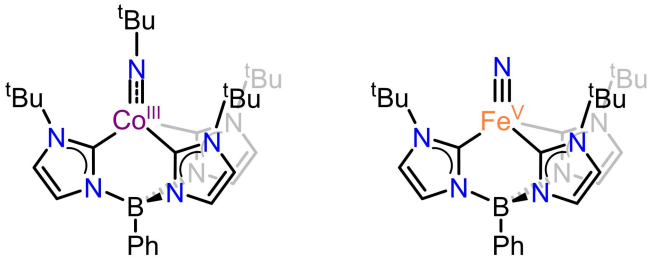


**Figure 1.4.** High-valent compounds supported by tris(imidazol-2-ylidene)phenylborate ligands. Left: Reference 16d. Right: Reference 18.

In this thesis, use of tris(imidazol-2-ylidene)phenylborate ligands enables the isolation and thorough characterization of three $Co^{III}$-oxo complexes. These remain the sole examples of crystallographically characterized terminal Co-oxo complexes. These isolable complexes provide a platform from which to explore detailed C–H and O–H activation reactivity, which is shown to follow unusual kinetic trends, consistent with the unusual nature of these $d^6$ metal-oxo complexes. Additionally, oxidation of these complexes gives varied results depending on the identity of ligand substituents. Preliminary evidence indicates O–O bond formation with *tert*-butyl substituents, while adamantyl substituents enable the formation of a $Co^{IV}$-oxo intermediate which engages in rapid uphill C–H activation reactivity. Overall, the isolation, characterization, and study of the reactivity of these unusual $Co^{III}$-oxo complexes provides fundamental insight into the properties and reactivity of late transition metal-oxo complexes, which has been lacking thus far.

## 1.4 References


[1] (a) Rittle, J.; Green, M. T. "Cytochrome P450 Compound I: Capture, Characterisation, and C-H Bond Activation Kinetics." *Science.* **2010**, *330*, 933–937. (b) Hausinger, R. P. "Critical Reviews in Biochemistry and Molecular Biology Fe(II)/α-Ketoglutarate-Dependent Hydroxylases and Related Enzymes Fe(II)/α-Ketoglutarate-Dependent Hydroxylases and Related Enzymes." *Crit. Rev. Biochem. Mol. Biol.* **2004**, *39* (1), 21–68. (c) Gray, H. B.; Winkler, J. R. "Living with Oxygen." *Acc. Chem. Res.* **2018**, *51* (8), 1850–1857. (d) Montellano, P. R. O. de. "Hydrocarbon Hydroxylation by Cytochrome P450 Enzymes." *Chem. Rev.* **2009**, *110* (2), 932–948. (e) Huang, X.; Groves, J. T. "Beyond Ferryl-Mediated Hydroxylation: 40 Years of the Rebound Mechanism and C–H Activation." *J. Biol. Inorg. Chem.* **2017**, *22* (2–3), 185–207.

[2] (a) Chen, M. S.; White, M. C. "A Predictably Selective Aliphatic C H Oxidation Reaction for Complex Molecule Synthesis." *Science.* **2007**, *318* (5851), 783–787. (b) White, M. C.; Zhao, J. "Aliphatic C–H Oxidations for Late-Stage Functionalization." *J. Am. Chem. Soc.* **2018**, *140* (43), 13988–14009. (c) Milan, M.; Salamone, M.; Costas, M.; Bietti, M. "The Quest for Selectivity in Hydrogen Atom Transfer Based Aliphatic C–H Bond Oxygenation." *Acc. Chem. Res.* **2018**, *51* (9), 1984–1995. (d) Kal, S.; Xu, S.; Que, L. "Bio-inspired Nonheme Iron Oxidation Catalysis: Involvement of Oxoiron(V) Oxidants in Cleaving Strong C−H Bonds." *Angew. Chem., Int. Ed.* **2020**, *59* (19), 7332–7349. (e) Chen, J.; Jiang, Z.; Fukuzumi, S.; Nam, W.; Wang, B. "Artificial Nonheme Iron and Manganese Oxygenases for Enantioselective Olefin Epoxidation and Alkane Hydroxylation Reactions." *Coord. Chem. Rev.* **2020**, *421*, 213443.

[3] (a) Huynh, M. H. V.; Meyer, T. J. "Proton-Coupled Electron Transfer." *Chem. Rev.* **2007**, *107* (11), 5004–5064. (b) Warren, J. J.; Tronic, T. A.; Mayer, J. M. "Thermochemistry of Proton-Coupled Electron Transfer Reagents and Its Implications." *Chem. Rev.* **2010**, *110* (12), 6961–7001. (c) Gunay, A.; Theopold, K. H. "C-H Bond Activations by Metal Oxo Compounds." *Chem. Rev.* **2010**, *110* (2), 1060–1081.

[4] (a) Cox, N.; Pantazis, D. A.; Neese, F.; Lubitz, W. "Biological Water Oxidation." *Acc. Chem. Res.* **2013**, *46* (7), 1588–1596. (b) Kern, J.; Chatterjee, R.; Young, I. D.; Fuller, F. D.; Lassalle, L.; Ibrahim, M.; Gul, S.; Fransson, T.; Brewster, A. S.; Alonso-Mori, R.; Hussein, R.; Zhang, M.; Douthit, L.; de Lichtenberg, C.; Cheah, M. H.; Shevela, D.; Wersig, J.; Seuffert, I.; Sokaras, D.; Pastor, E.; Weninger, C.; Kroll, T.; Sierra, R. G.; Aller, P.; Butryn, A.; Orville, A. M.; Liang, M.; Batyuk, A.; Koglin, J. E.; Carbajo, S.; Boutet, S.; Moriarty, N. W.; Holton, J. M.; Dobbek, H.; Adams, P. D.; Bergmann, U.; Sauter, N. K.; Zouni, A.; Messinger, J.; Yano, J.; Yachandra, V. K. "Structures of the Intermediates of Kok's Photosynthetic Water Oxidation Clock." *Nature* **2018**, *563* (7731), 421–425. (c) Suga, M.; Akita, F.; Yamashita, K.; Nakajima, Y.; Ueno, G.; Li, H.; Yamane, T.; Hirata, K.; Umena, Y.; Yonekura, S.; Yu, L.-J.; Murakami, H.; Nomura, T.; Kimura, T.; Kubo, M.; Baba, S.; Kumasaka, T.; Tono, K.; Yabashi, M.; Isobe, H.; Yamaguchi, K.; Yamamoto, M.; Ago, H.; Shen, J.-R. "An Oxyl/Oxo Mechanism for Oxygen-Oxygen Coupling in PSII Revealed by an x-Ray Free-Electron Laser." *Science.* **2019**, *366* (6463), 334–338.

[5] Nocera, D. G. "The Artificial Leaf." *Acc. Chem. Res.* **2012**, *45* (5), 767–776.

[6] (a) Kanan, M. W.; Nocera, D. G. "In Situ Formation of an Oxygen-Evolving Catalyst in Neutral Water Containing Phosphate and Co2+." *Science.* **2008**, *321* (5892), 1072–1075. (b) McMillion, N. D.; Wilson, A. W.; Goetz, M. K.; Chang, M.-C.; Lin, C.-C.; Feng, W.-J.; McCrory, C. C. L.; Anderson, J. S. "Imidazole for Pyridine Substitution Leads to Enhanced Activity Under Milder Conditions in Cobalt Water Oxidation Electrocatalysis." *Inorg. Chem.* **2019**, *58* (2), 1391–1397. (c) Pokhrel, R.; Goetz, M. K.; Shaner, S. E.; Wu, X.; Stahl, S. S. "The 'Best Catalyst' for Water Oxidation Depends on the Oxidation Method Employed: A Case Study of Manganese Oxides." *J. Am. Chem. Soc.* **2015**, *137* (26), 8384–8387. (d) Blakemore, J. D.; Crabtree, R. H.; Brudvig, G. W. "Molecular Catalysts for Water Oxidation." *Chem. Rev.* **2015**, *115* (23), 12974–13005. (e) Hunter, B. M.; Gray, H. B.; Müller, A. M. "Earth-Abundant Heterogeneous Water Oxidation Catalysts." *Chem. Rev.* **2016**, *116* (22), 14120–14136.

[7] (a) Liu, H.; Frei, H. "Observation of O–O Bond Forming Step of Molecular Co 4 O 4 Cubane Catalyst for Water Oxidation by Rapid-Scan FT-IR Spectroscopy." *ACS Catal.* **2020**, *10* (3), 2138–2147. (b) Surendranath, Y.; Kanan, M. W.; Nocera, D. G. "Mechanistic Studies of the Oxygen Evolution Reaction by a Cobalt-Phosphate Catalyst at Neutral PH." *J. Am. Chem. Soc.* **2010**, *132* (46), 16501–16509.

[8] Betley, T. A.; Surendranath, Y.; Childress, M. V; Alliger, G. E.; Fu, R.; Cummins, C. C.; Nocera, D. G. "A Ligand Field Chemistry of Oxygen Generation by the Oxygen-Evolving Complex and Synthetic Active Sites." *Philos. Trans. R. Soc. B Biol. Sci.* **2008**, *363* (1494), 1293–1303.

[9] Ballhausen, C. J.; Gray, H. B. "The Electronic Structure of the Vanadyl Ion." *Inorg. Chem.* **1962**, *1* (1), 111–122.

[10] (a) McDonald, A. R.; Que, L. "High-Valent Nonheme Iron-Oxo Complexes: Synthesis, Structure, and Spectroscopy." *Coord. Chem. Rev.* **2013**, *257* (2), 414–428. (b) Gupta, R.; Taguchi, T.; Lassalle-Kaiser, B.; Bominaar, E. L.; Yano, J.; Hendrich, M. P.; Borovik, A. S. "High-Spin Mn-Oxo Complexes and Their Relevance to the Oxygen-Evolving Complex within Photosystem II." *Proc. Natl. Acad. Sci. U. S. A.* **2015**, *112* (17), 5319–5324.

[11] (a) Smith, J. M.; Mayberry, D. E.; Margarit, C. G.; Sutter, J.; Wang, H.; Meyer, K.; Bontchev, R. P. "N-O Bond Homolysis of an Iron(II) TEMPO Complex Yields an Iron(III) Oxo Intermediate." *J. Am. Chem. Soc.* **2012**, *134* (15), 6516–6519. (b) Hong, S.; Pfaff, F. F.; Kwon, E.; Wang, Y.; Seo, M.-S.; Bill, E.; Ray, K.; Nam, W. "Spectroscopic Capture and Reactivity of a Low-Spin Cobalt(IV)-Oxo Complex Stabilized by Binding Redox-Inactive Metal Ions." *Angew. Chem., Int. Ed.* **2014**, *53* (39), 10403–10407. (c) Wang, B.; Lee, Y.-M.; Tcho, W.-Y.; Tussupbayev, S.; Kim, S.-T.; Kim, Y.; Seo, M. S.; Cho, K.-B.; Dede, Y.; Keegan, B. C.; Ogura, T.; Kim, S. H.; Ohta, T.; Baik, M.-H.; Ray, K.; Shearer, J.; Nam, W. "Synthesis and Reactivity of a Mononuclear Non-Haem Cobalt(IV)-Oxo Complex." *Nat. Commun.* **2017**, *8*, 14839. (d) Andris, E.; Navrátil, R.; Jašík, J.; Srnec, M.; Rodríguez, M.; Costas, M.; Roithová, J. "M−O Bonding Beyond the Oxo Wall: Spectroscopy and Reactivity of Cobalt(III)-Oxyl and Cobalt(III)-Oxo Complexes." *Angew. Chem., Int. Ed.* **2019**, *58* (28), 9619–9624. (e) Poverenov,

E.; Efremenko, I.; Frenkel, A. I.; Ben-David, Y.; Shimon, L. J. W.; Leitus, G.; Konstantinovski, L.; Martin, J. M. L.; Milstein, D. "Evidence for a Terminal Pt(IV)-Oxo Complex Exhibiting Diverse Reactivity." *Nature* **2008**, *455* (7216), 1093–1096.

[12] (a) MacBeth, C. E.; Golombek, A. P.; Young, V. G.; Yang, C.; Kuczera, K.; Hendrich, M. P.; Borovik, A. S. "$O_2$ Activation by Nonheme Iron Complexes: A Monomeric Fe(III)-Oxo Complex Derived from $O_2$." *Science.* **2000**, *289* (5481), 938–941. (b) Matson, E. M.; Park, Y. J.; Fout, A. R. "Facile Nitrite Reduction in a Non-Heme Iron System: Formation of an Iron(III)-Oxo." *J. Am. Chem. Soc.* **2014**, *136* (50), 17398–17401. (c) Spaltenstein, E.; Conry, R. R.; Critchlow, S. C.; Mayer, J. M. "Synthesis, Characterization, and Reactivity of a Formally Rhenium(I) Terminal Oxo Complex, NaRe(O)(RC=CR)$_2$." *J. Am. Chem. Soc.* **1989**, *111*, 8741–8742. (d) Delony, D.; Kinauer, M.; Diefenbach, M.; Demeshko, S.; Würtele, C.; Holthausen, M. C.; Schneider, S. "A Terminal Iridium Oxo Complex with a Triplet Ground State." *Angew. Chem., Int. Ed.* **2019**, *58* (32), 10971–10974.

[13] (a) McAlpin, J. G.; Surendranath, Y.; Dincă, M.; Stich, T. A.; Stoian, S. A.; Casey, W. H.; Nocera, D. G.; Britt, R. D. "EPR Evidence for Co(IV) Species Produced during Water Oxidation at Neutral PH." *J. Am. Chem. Soc.* **2010**, *132* (20), 6882–6883. (b) Ullman, A. M.; Brodsky, C. N.; Li, N.; Zheng, S. L.; Nocera, D. G. "Probing Edge Site Reactivity of Oxidic Cobalt Water Oxidation Catalysts." *J. Am. Chem. Soc.* **2016**, *138* (12), 4229–4236.

[14] Betley, T. A.; Wu, Q.; Van Voorhis, T.; Nocera, D. G. "Electronic Design Criteria for O-O Bond Formation via Metal-Oxo Complexes." *Inorg. Chem.* **2008**, *47* (6), 1849–1861.

[15] Hay-Motherwell, R. S.; Wilkinson, G.; Hussain-Bates, B.; Hursthouse, M. B. "Synthesis and X-Ray Crystal Structure of Oxotrimesityliridium(V)." *Polyhedron* **1993**, *12* (16), 2009–2012.

[16] (a) Liu, Y.; Du, J.; Deng, L. "Synthesis, Structure, and Reactivity of Low-Spin Cobalt(II) Imido Complexes [$(Me_3P)_3$Co(NAr)]." *Inorg. Chem.* **2017**, *56*, 8278–8286. (b) Saouma, C. T.; Peters, J. C. "M≡E and M=E Complexes of Iron and Cobalt That Emphasize Three-Fold Symmetry (E=O, N, NR)." *Coord. Chem. Rev.* **2011**, *255* (7–8), 920–937. (c) Jenkins, D. M.; Betley, T. A.; Peters, J. C. "Oxidative Group Transfer to Co(I) Affords a Terminal Co(III) Imido Complex." *J. Am. Chem. Soc.* **2002**, *124* (38), 11238–11239. (d) Cowley, R. E.; Bontchev, R. P.; Sorrell, J.; Sarracino, O.; Feng, Y.; Wang, H.; Smith, J. M. "Formation of a Cobalt(III) Imido from a Cobalt(II) Amido Complex. Evidence for Proton-Coupled Electron Transfer." *J. Am. Chem. Soc.* **2007**, *129* (9), 2424–2425. (e) Shay, D. T.; Yap, G. P. A.; Zakharov, L. N.; Rheingold, A. L.; Theopold, K. H. "Intramolecular C-H Activation by an Open-Shell Cobalt(III) Imido Complex." *Angew. Chem., Int. Ed.* **2005**, *44* (10), 1508–1510. (f) Hu, X.; Meyer, K. "Terminal Cobalt(III) Imido Complexes Supported by Tris(Carbene) Ligands: Imido Insertion into the Cobalt-Carbene Bond." *J. Am. Chem. Soc.* **2004**, *126* (50), 16322–16323.

[17] (a) Reinaud, O. M.; Theopold, K. H. "Hydrogen Tunneling in the Activation of Dioxygen by a Tris(Pyrazolyl)Borate Cobalt Complex." *J. Am. Chem. Soc.* **1994**, *116* (15), 6979–6980. (b) Hill, E. A.; Kelty, M. L.; Filatov, A. S.; Anderson, J. S. "Isolable Iodosylarene and Iodoxyarene

Adducts of Co and Their O-Atom Transfer and C–H Activation Reactivity." *Chem. Sci.* **2018**, *9* (19), 4493–4499.

[18] Scepaniak, J. J.; Vogel, C. S.; Khusniyarov, M. M.; Heinemann, F. W.; Meyer, K.; Smith, J. M. "Synthesis, Structure, and Reactivity of an Iron(V) Nitride." *Science.* **2011**, *331* (6020), 1049–1052.

# Chapter 2: Isolation of Terminal Co(III)-Oxo Complexes

This chapter has been adapted from the following three sources with permission: (1) Goetz, M. K.; Hill, E. A.; Filatov, A. S.; Anderson, J. S. *J. Am. Chem. Soc.* **2018**, *140*, 13176-13180.  (2) Goetz, M. K.; Anderson, J. S. *J. Am. Chem. Soc.* **2019**, *141*, 4051-4062.  (3) Goetz, M. K.; Schneider, J. E.; Filatov, A. S.; Jesse, K. A.; Anderson, J. S. *J. Am. Chem. Soc.* Submitted for publication. 

## 2.1 Introduction

Transition metal-oxo complexes have been proposed as intermediates in a variety of important catalytic reactions. For example, these species have been invoked in biological oxidations such as the degradation of pharmaceuticals by cytochrome P450 enzymes and the formation of oxygen from water during photosynthesis.[1] Metal-oxo intermediates are also cited in synthetic systems such as cobalt oxide catalyzed water oxidation and catalytic epoxidations.[2] The ubiquity of transition metal-oxo complexes in these reactions has motivated synthetic studies to probe their reactivity and plausibility as intermediates. While many examples of terminal oxo complexes have been studied,[3] classic bonding theory and experiment suggests that examples with d-electron counts > 4 have weakened metal-oxygen bonds making them highly reactive.[4] Indeed, only a handful of such species had been reported at the time this work was done, with many displaying weak metal-oxygen bonding and instability that has limited their characterization.[5,6]

Complexes with six d-electrons are exceptionally difficult to isolate and have been mischaracterized in some cases.[6a] A $Re^{I}$ complex utilizing π-accepting acetylene ligands, a $Pt^{IV}$

complex with limited structural information, and an $Ir^{III}$ complex in a square planar geometry remain the sole examples.[6b,c,d] A strategy which should allow for the isolation of multiply bonded, high d-electron count complexes is the use of lower coordinate geometries.[7] For example, pseudo-tetrahedral geometries can stabilize M–L multiple bonds with late transition metals as evidenced by several examples of M–N multiply bonded species.[8] Nevertheless, outside of Wilkinson's $d^4$ Ir oxo complex reported 25 years ago,[9] efforts to generate related late transition metal-oxo species in pseudo-tetrahedral ligand environments have proven unsuccessful, as exemplified with tris(pyrazolyl)borate ligands.[3b] We rationalized that the stronger carbene donors of the tris(imidazol-2-ylidene)borate ligand $PhB(^tBuIm)_3^-$ ($PhB(^tBuIm)_3^-$ = tris(1-*tert*-butyl-imidazol-2-ylidene)phenylborate) employed by Smith and coworkers might enable isolation of a $d^6$ terminal oxo complex.[5b,10] Additionally, alteration of the substituents on the imidazol-2-ylidene ligand arms should be a facile way to investigate how ligand donor strength and steric profile affect the reactivity of terminal $d^6$ transition metal-oxo complexes.

Here we report that use of strongly donating tris(imidazol-2-ylidene)borate scaffolds enables the isolation of three highly unusual $Co^{III}$-oxo complexes which have been thoroughly characterized by a suite of physical techniques including single crystal X-ray diffraction. These complexes display O–atom and H–atom transfer reactivity and demonstrate that terminal metal-oxo complexes with six d-electrons can display strong metal-oxygen bonding and sufficient stability to enable their characterization. The unambiguous assignment of these complexes supports the viability of related species that are frequently invoked, but rarely observed, in the types of catalytic reactions mentioned above.

## 2.2 Results and Discussion

### 2.2.1 Synthesis and Characterization of PhB($^t$BuIm)$_3$Co$^{III}$O

We found that treatment of the previously reported PhB($^t$BuIm)$_3$Co$^{II}$Cl with NaOH in THF generates a new species, PhB($^t$BuIm)$_3$Co$^{II}$OH (**1**, Scheme 2.1).[11] Complex **1** has been characterized by a suite of spectroscopic techniques including X-ray diffraction (XRD) that confirm the assignment of a terminal, pseudo-tetrahedral, $S$ = 3/2 Co$^{II}$ hydroxide complex with a Co–O bond length of 1.876(2) Å (Figure 2.1, Figure A1.1-Figure A1.3, Figure A1.33, Figure A1.36, Figure A1.42). This bond length is comparable to other pseudo-tetrahedral Co$^{II}$-hydroxide complexes.[12] Cyclic voltammetry of **1** in MeCN shows a quasi-reversible couple at –230 mV vs. Fc/Fc$^+$ (Fc = ferrocene) which is assigned to the Co$^{II}$/Co$^{III}$ redox couple and suggests a Co$^{III}$–OH species may be chemically accessible (Figure A1.54). Monitoring the addition of one equivalent of FcBF$_4$ to **1** in THF at –78 °C by UV-vis spectroscopy shows an isosbestic conversion from violet **1** to a green species assigned as the one-electron oxidized product, [PhB($^t$BuIm)$_3$Co$^{III}$OH][BF$_4$] (**2**, Figure A1.43). This oxidation is also reversible as addition of cobaltocene to in situ generated **2** cleanly regenerates **1** (Figure A1.44).

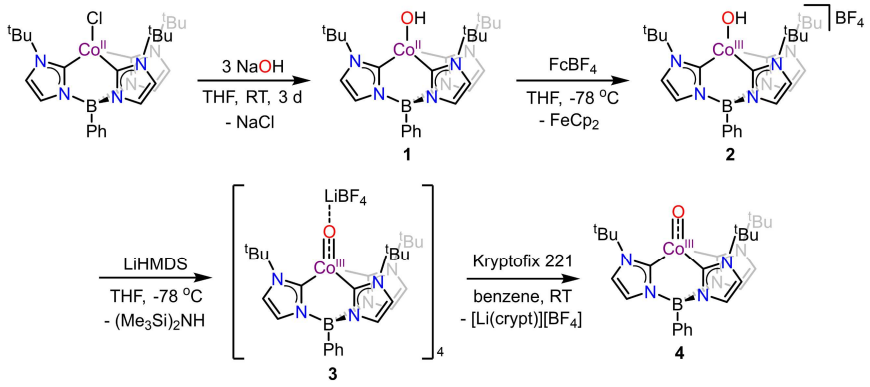


**Scheme 2.1.** Synthesis of complexes **1**-**4**.

While **2** is thermally unstable, it is long-lived enough at temperatures < –35 °C to allow for isolation and characterization. Accordingly, single crystals of **2** were obtained at low temperature and the structure reveals a monomeric $Co^{III}$–OH complex in a highly distorted, near see-saw geometry. This distorted geometry may be due to a hydrogen bonding interaction with a THF molecule present in the unit cell, but may also have electronic origins.[13] The Co–O bond length in **2** has contracted by ~0.1 Å from that in **1** to 1.776(7) Å (Figure 2.1, Table A1.5), which is comparable to another four-coordinate $Co^{III}$–OH complex.[14] Complex **2** is diamagnetic and its NMR features demonstrate that this complex is $C_3$ symmetric in solution (Figure A1.4-Figure A1.7).

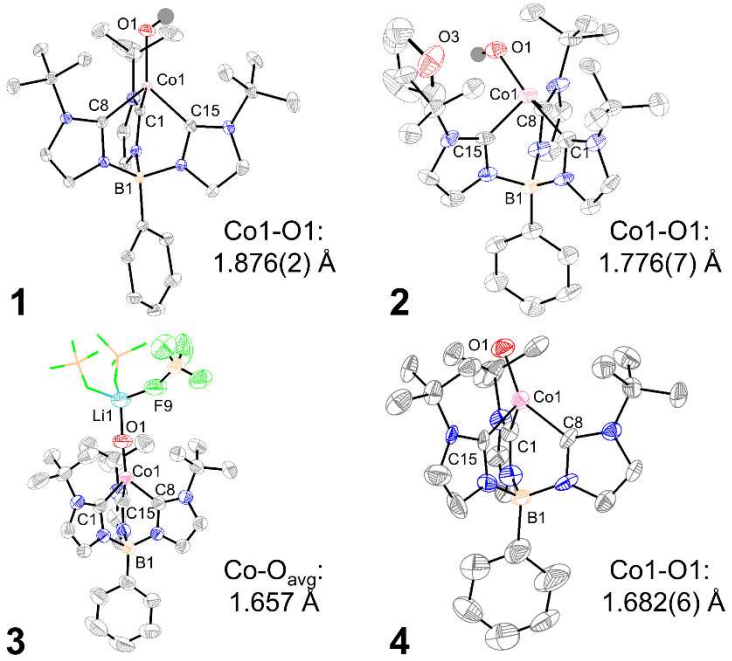


**Figure 2.1.** Crystal structures of complexes **1**-**4**. Thermal ellipsoids are shown at 50% probability. All H–atoms besides those bound to O are omitted for clarity. Counterions and solvent molecules except for the THF in **2** are also omitted. Only one unit of tetrameric **3** is shown with two of the $BF_4^-$ counter-anions interacting with the $Li^+$ shown in wireframe. The complete structure is shown in Figure A1.58.

Using **2** as a synthon, we found that treatment with strong bases such as LiHMDS (HMDS = hexamethyldisilazide) results in generation of a new magenta species (**3**, Figure A1.45). The reversibility of this reaction by addition of $[HNEt_3][BF_4]$ suggested the new species may be a Co-oxo complex (Figure A1.46). Analysis of single crystals grown at −35 °C by XRD reveals a tetrameric species with four $PhB(^tBuIm)_3Co^{III}O$ units each capped by a $Li^+$ ion and bridged by $BF_4^-$ anions to give a monomeric formula of $PhB(^tBuIm)_3Co^{III}O{\bullet}LiBF_4$ (Figure 2.1, Figure A1.58). In this structure, the average Co–O bond length has shortened by an additional ~0.1 Å to 1.657 Å, consistent with deprotonation and an increase in formal bond order. In contrast to **2**, the B–Co–O angle is nearly linear at 170.1°. Additionally, isotopically labeled **3** was synthesized from **1-$^{18}$O** and comparison of the IR spectra of **3-$^{16}$O** and **3-$^{18}$O** shows one isotope dependent feature at 839 $cm^{-1}$ which shifts to 802 $cm^{-1}$ upon $^{18}O$ incorporation, as expected for a simple harmonic oscillator (Figure 2.2A, Figure A1.37A). Finally, **3** is diamagnetic and displays solvent-dependent speciation by NMR spectroscopy in deuterated benzene, THF, and MeCN (Figure A1.8-Figure A1.12). This suggested to us that the $LiBF_4$ units in **3** could be separated to isolate a bona fide terminal oxo complex.

Addition of Kryptofix 2,2,1 (4,7,13,16,21-pentaoxa-1,10-diazabicyclo[8.8.5]tricosane, crypt) to a benzene solution of **3** results in formation of a purple solution of $PhB(^tBuIm)_3Co^{III}O$ (**4**) and precipitation of $[Li(crypt)][BF_4]$. The successful removal of $Li^+$ was confirmed by the loss of signal by $^7Li$ NMR spectroscopy. We also note that addition of KHMDS to in situ generated **2** results in formation of **4** directly (see Appendix 1). Furthermore, XRD analysis of single crystals of **4** verifies a monomeric complex and shows a Co–O bond length of 1.682(6) Å (Figure 2.1). There is also a change in the B–Co–O angle upon $Li^+$ sequestration from an average of 170.1° in **3** to 160.2(3)°

in **4** giving a slight but noticeably bent structure in the solid state (Table A1.5). However, similar to complexes **2** and **3**, **4** is diamagnetic and its NMR spectra are consistent with a $C_3$ symmetric species in solution (Figure A1.13-Figure A1.15). Finally, IR spectroscopic studies of **4-$^{16}$O** and **4-$^{18}$O** show a feature at 815 cm$^{-1}$ in the natural abundance complex that shifts to 782 cm$^{-1}$ in the $^{18}$O-isotopologue as expected from a simple harmonic oscillator approximation (Figure 2.2B, Figure A1.37B). This vibrational frequency is lower than that in **3**, consistent with the slightly longer (~0.02 Å) Co–O bond length in **4**.[15]

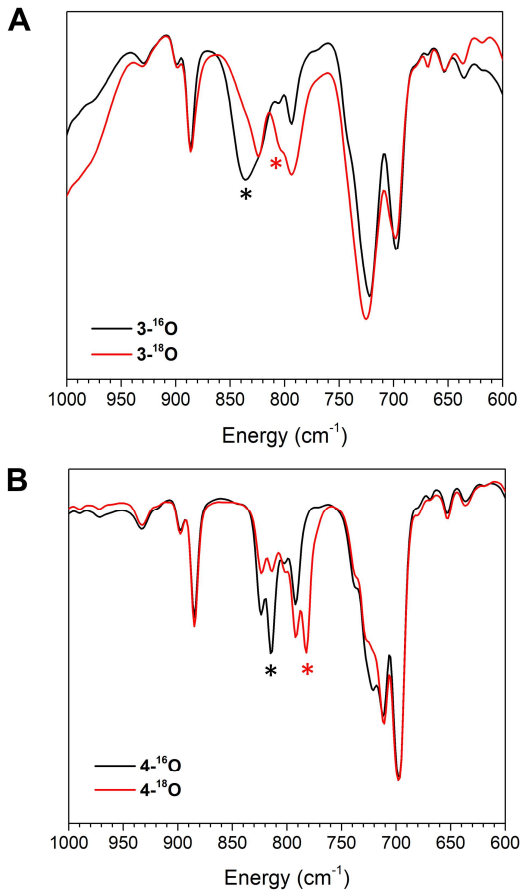


**Figure 2.2.** Overlay of IR spectra of $^{18}$O-labeled and natural abundance (A) **3** and (B) **4**. Asterisks indicate the feature assigned to the Co–O stretching frequency and its corresponding shift in the $^{18}$O-labeled compound. Difference spectra are shown in Figure A1.37.

The isolation of these species enabled us to investigate their reactivity with H–atom donors and O–atom acceptors. While **3** and **4** are thermally unstable with solution half-lives of ~6.5-8 hours at room temperature (Table A1.4), this background reaction is sufficiently slow to allow study of their reactivity with substrates (Figure 2.3, Figure A1.47, and Figure A1.48). Both **3** and **4** react with the H–atom source DHA (DHA = 9,10-dihydroanthracene) and the O–atom acceptor $PMe_3$ at similar rates (Table A1.4).

Analysis of UV-vis spectra of the reactions with DHA support the formation of anthracene and **1**, consistent with net H–atom transfer. Similarly, the products of the reactions with $PMe_3$ are $OPMe_3$ from $^{31}P$ NMR spectroscopy and what is assigned as $PhB(^{t}BuIm)_3Co^{II}Cl$ based on previously reported spectral data (Figure A1.16 and Figure A1.17).[11] We speculate that a putative $Co^{I}$ complex resulting from O–atom transfer could react with adventitious chlorine atom sources such as trace dichloromethane (DCM) to give $PhB(^{t}BuIm)_3Co^{II}Cl$ as the major Co-containing product. Attempts to rigorously exclude DCM from the reaction solution led to formation of trimethylphosphine oxide and **1** as the major Co-containing product (Figure A1.18), leading us to conclude that the mechanism of this reaction is likely not a simple O–atom transfer. Nevertheless, net O–atom transfer from Co to P was confirmed by GC-MS analysis of the reaction mixture using $^{18}O$-labeled **3** and **4** (Figure A1.57).

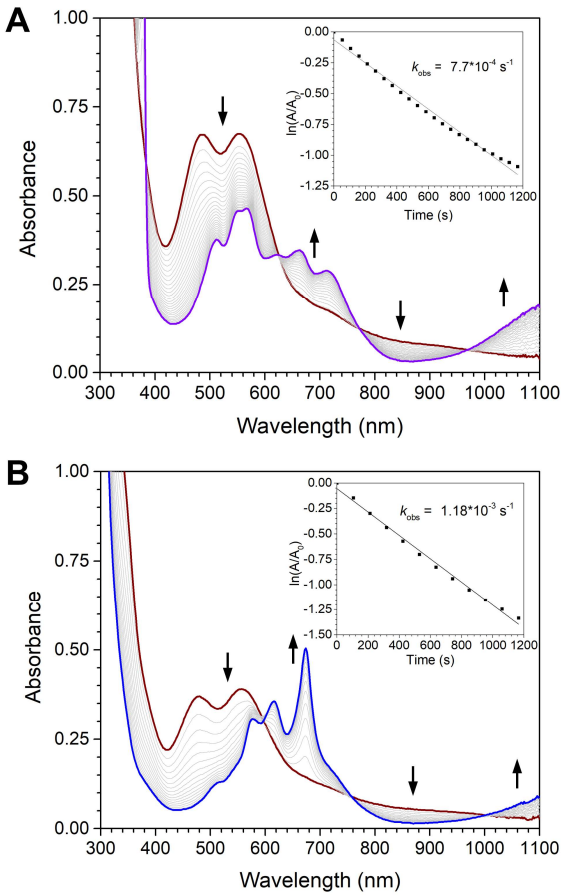


**Figure 2.3.** UV-vis spectra of (A) the reaction between **3** (dark red trace) and excess DHA, resulting in formation of **1** (purple trace) and (B) the reaction between **4** (dark red trace) and excess $PMe_3$ resulting in formation of $PhB(^tBuIm)_3Co^{II}Cl$ (blue trace). Gray traces indicate one- and two-minute time intervals, respectively. Insets: first order kinetic plots of the reaction monitored at 470 nm.

Having established **4** as a competent H–atom abstractor, we sought to estimate the bond dissociation free energy (BDFE) of the O–H bond in **1** using the relationship between p$K_a$, $E^0$, and BDFE outlined in Equation 2.1 and Scheme A1.1.[16] The $Co^{II}/Co^{III}$ (**1**/**2**) redox potential was measured by cyclic voltammetry as –0.23 V vs $Fc/Fc^+$ (see above). We determined the p$K_a$ of **2** by titration of **4** with an acid, $[HMTBD][BF_4]$ (MTBD = 7-methyl-1,5,7-triazabicyclo[4.4.0]dec-5-ene, $pK_{aMeCN}$ = 25.49[17]), in MeCN-$d_3$. The titration was monitored by $^1H$ NMR spectroscopy at

–35 °C where all species in solution (**4**, $HMTBD^+$, **2**, and MTBD) were in rapid equilibrium. As a result, the concentration of each species in solution was evaluated by examination of the observed chemical shift ($\delta_{obs}$) of the methyl protons of $HMTBD^+$/MTBD in the $^1H$ NMR spectra (See Chapter 2.4, Figure A1.19). From this data, an equilibrium constant for the reaction between **3** and [HMTBD][$BF_4$] was determined to be 1.2(1) (Table A1.1). Using the known p$K_a$ value of [HMTBD][$BF_4$] we calculated a p$K_a$ value of 25.58(5) for **2** in MeCN. Together with the **1**/**2** redox potential and a *C* value (*C* = standard reduction potential of $H^+/H^\bullet$ in a particular solvent) of 54.9 kcal/mol in MeCN,[16] we get an experimentally determined $BDFE_{O–H}$ of 84.6 kcal/mol (Equation 2.1, Scheme A1.1). This is consistent not only with the value of 85 kcal/mol predicted by DFT calculations (Table A1.8) but also the instantaneous reaction between **4** and 2,4,6-tri(*tert*-butyl)phenol (BDE ≈ 82 kcal/mol) to produce the corresponding phenoxyl radical and **1** (Figure A1.49).

Equation 2.1 $$BDFE = 1.37pK_a + 23.06E^0 + C$$

### 2.2.2 Synthesis and Characterization of $PhB(^{Ad}Im)_3Co^{III}O$

Another $Co^{III}$-oxo complex, $PhB(^{Ad}Im)_3Co^{III}O$ (**8**, $PhB(^{Ad}Im)_3^-$ = tris(1-adamantyl-imidazol-2-ylidene)phenyl borate), and the relevant precursors were synthesized analogously to the methods described in Chapter 2.2.1 (Scheme 2.2). Deprotonation of the proligand, $[PhB(^{Ad}ImH)_3][OTf]_2$, with 3.05 equivalents of lithium diisopropylamide followed by addition of 1 equivalent of $CoCl_2$ results in the formation of $PhB(^{Ad}Im)_3Co^{II}Cl$ (**5**) which can be isolated as a bright blue solid in 78% yield. Thorough characterization including NMR and EPR spectroscopies confirm the assignment and purity of this *S* = 3/2, pseudo-tetrahedral chloride complex (See Appendix 1). Single crystal X-ray diffraction (SXRD) reveals that the Co–Cl and Co–C bond lengths in the first

coordination sphere (Figure 2.4, Table A1.7) are slightly shorter than those observed in the analogous complex with *tert*-butyl ($^t$Bu) substituents on the ligand.[11] This observation is consistent with the stronger donation from the adamantyl (Ad) substituents.

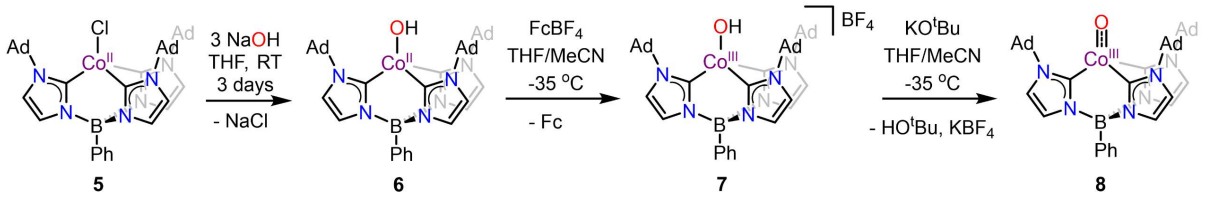


**Scheme 2.2.** Synthesis of complexes **5**-**8**.

Treatment of complex **5** with 3 equivalents of NaOH in THF over 3 days at room temperature produces the Co$^{II}$-hydroxide complex, PhB($^{Ad}$Im)$_3$Co$^{II}$OH as a bright violet powder in 57% yield (**6**, Scheme 2.2). NMR and EPR spectroscopic characterization confirm the assignment of this $S$ = 3/2 complex (See Appendix 1). Cyclic voltammetry of **6** collected in THF shows a quasi-reversible couple at –440 mV vs. Fc/Fc$^+$. This couple is substantially more negative than that observed for the $^t$Bu substituted system (–230 mV vs. Fc/Fc$^+$) suggesting that this compound is more easily oxidized as expected from the stronger donation of the Ad-substituents. Consistently, the SXRD structure of **2** (Figure 2.4, Table A1.7) also displays shorter Co–O and Co–C bonds.

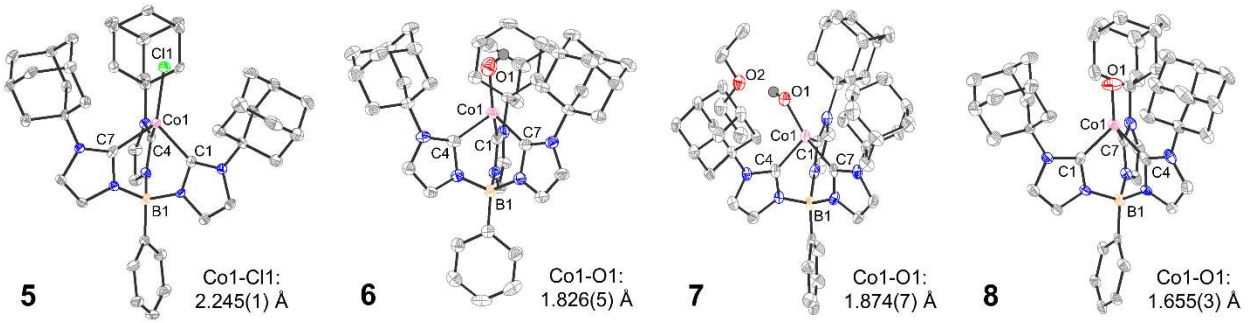


**Figure 2.4.** Crystal structures of complexes **5**-**8**. Thermal ellipsoids are shown at 50% probability. All H–atoms besides those bound to O are omitted for clarity. Counterions and solvent molecules except for the $Et_2O$ hydrogen-bonding to the O–H in **7** are also omitted.

Oxidation of **6** with 1 equivalent of $FcBF_4$ in THF at –35 °C provides the diamagnetic $Co^{III}$-hydroxide complex, $[PhB(^{Ad}Im)_3Co^{III}OH][BF_4]$ (**7**, Scheme 2.2), as a bright green species. Similarly to the $^{t}$Bu-substituted system, **7** is thermally unstable. Nonetheless, it is long-lived enough at –35 °C for characterization by low temperature NMR and UV-vis spectroscopies which reveal a diagnostic O–*H* resonance (Figure A1.26) and a strong absorbance at 718 nm (Figure A1.52), respectively. Single crystals of **7** can also be obtained by layering in situ generated solutions of **7** in THF under cold pentane and allowing them to diffuse at –35 °C. The SXRD structure of **7** (Figure 2.4) displays a distortion away from pseudo- tetrahedral symmetry, similar to that observed in the $^{t}$Bu-substituted complex.[13] Nonetheless, the complex is $C_3$ symmetric in solution, as evidenced by the observation of only two Im-*H* resonances in the $^{1}$H NMR spectrum (Figure A1.26).

Deprotonation of complex **7** should result in the formation of the desired $Co^{III}$-oxo complex. However, use of the previously used base hexamethyldisilazide ($HMDS^{-}$) resulted in impure mixtures of **6** and a new species, $PhB(^{Ad}Im)_3Co^{III}O$ (**8**). We hypothesized this was due to slow deprotonation from the steric hindrance between $HMDS^{-}$ and the Ad groups, which allowed for

competitive reduction of **7** by $HMDS^-$, consistent with the lower oxidation potential of **6** in this system. Indeed, switching to a sterically less encumbered and less reducing base in the form of potassium *tert*-butoxide ($KO^tBu$) enabled the isolation of the pure terminal oxo complex **8** as dark purple crystals in variable yields (22%-55%, Scheme 2.2). Complex **8** is diamagnetic and has been thoroughly characterized by a variety of techniques including IR spectroscopy and SXRD (See Appendix 1). Comparison of the IR spectra of as synthesized **8** and its $^{18}O$-isotopologue reveal a Co–O vibration at 807 $cm^{-1}$ which shifts to 775 $cm^{-1}$ upon labeling, as expected from a simple harmonic oscillator approximation (Figure A1.41). This stretching frequency is consistent with a strong Co–O multiple bond. Additionally, a short Co–O bond length of 1.655(3) Å is observed in the SXRD structure (Figure 2.4), also consistent with a strong multiple bond.[18]

Similar to complex **1**, we sought to characterize the $BDFE_{O–H}$ of complex **6** using the relationship between p$K_a$, $E^0$, and BDFE outlined in Equation 2.1 and Scheme A1.2.[16] The $Co^{II}/Co^{III}$ (**6**/**7**) redox potential was measured by cyclic voltammetry as –0.44 V vs $Fc/Fc^+$ (see above). We determined the p$K_a$ of **7** by titration of **8** with the same acid used previously, [HMTBD][$BF_4$] (p$K_{aMeCN}$ = 25.49[17]), in MeCN-$d_3$. The titration was monitored by $^1H$ NMR spectroscopy at –35 °C where all species in solution (**8**, $HMTBD^+$, **7**, and MTBD) were in rapid equilibrium. As a result, the ratios of the concentration of each species in solution was evaluated by examination of the observed chemical shift ($\delta_{obs}$) of the resonances in the $^1H$ NMR spectra (See Experimental, Figure A1.31 and Figure A1.32). From this data, and using the methods describe in the Experimental section below, we calculated a p$K_a$ value of 22.6 for **7** in THF. Together with the **6**/**7** redox potential and a *C* value of 66 kcal/mol in THF,[19] we get an experimentally determined $BDFE_{O–H}$ of 86.8 kcal/mol (Equation 2.1, Scheme A1.2).

### 2.2.3 Comparison of the Co–O Bonding in PhB($^{t}$BuIm)$_3$Co$^{III}$O and PhB($^{Ad}$Im)$_3$Co$^{III}$O

Given their unusual nature, the bonding in **3**, **4**, and **8** merits further discussion. When compared to M–E species with formal triple bonds, **3**, **4**, and **8** display relatively longer M–E bonds (1.655(3)-1.682(6) Å vs. 1.50-1.59 Å) and correspondingly lower M–E stretching frequencies (800-850 cm$^{-1}$ vs. 950-1000 cm$^{-1}$).[8b,20] However, comparison to an example of a terminal Co$^{IV}$-oxo complex with a formal Co–O double bond shows that **3**, **4**, and **8** have higher Co–O bond orders based on their bond lengths (1.657-1.682(6) Å vs. 1.72 Å) and vibrational frequencies (800-850 cm$^{-1}$ vs. 770 cm$^{-1}$).[5e] Alternatively, comparison with isoelectronic, pseudo-tetrahedral Fe$^{II}$- and Co$^{III}$-imide complexes shows very similar M–O/N bond lengths.[8b] However, direct comparison of the M–E vibrational frequencies is convoluted by mixing of other ligand vibrational modes in the case of the imide complexes.[21]

To further examine the Co–O interaction in **4** we turned to density functional theory calculations (Figure 2.5). Analysis of the frontier orbitals reveals two Co–O π* interactions with $d_{xz}$ and $d_{yz}$ parentage as the two highest lying orbitals. These orbitals support the presence of two π-bonds as would be expected for a formal triple bond. The highest occupied orbital in this set is primarily of $d_{z2}$ parentage and shows a mixed σ*/non-bonding Co–O interaction. The lowest two orbitals are primarily of $d_{xy}$ and $d_{x2-y2}$ parentage and have non-bonding character with respect to the Co–O bond. On the surface, this orbital picture is consistent with three bonding interactions between Co and O, or a triple bond. However, the σ interaction is weakened significantly by its antibonding character, which has been thoroughly examined computationally.[18] This study suggests the σ interaction is only a partial bond, and therefore a triple bond is an inaccurate descriptor for the interaction between Co and O. Nonetheless, the Co–O bond appears to be stronger than a formal

double bond by some metrics, and is likely best described as lying between and double and a triple bond.[18] This orbital picture is analogous to that in related imide complexes suggesting that the bonding in these isoelectronic species is very similar. However, the complex reported here demonstrates an off-axis tilt of the oxo ligand which is not observed in the imide complexes, although computations suggest a relatively low barrier to linearization of ~2 kcal/mol (Table A1.8). The preference for this bending in the oxo complex is not entirely clear but may likely be attributed to orbital mixing enabled by the weaker ligand field arising from an oxo versus an imide ligand.[22]

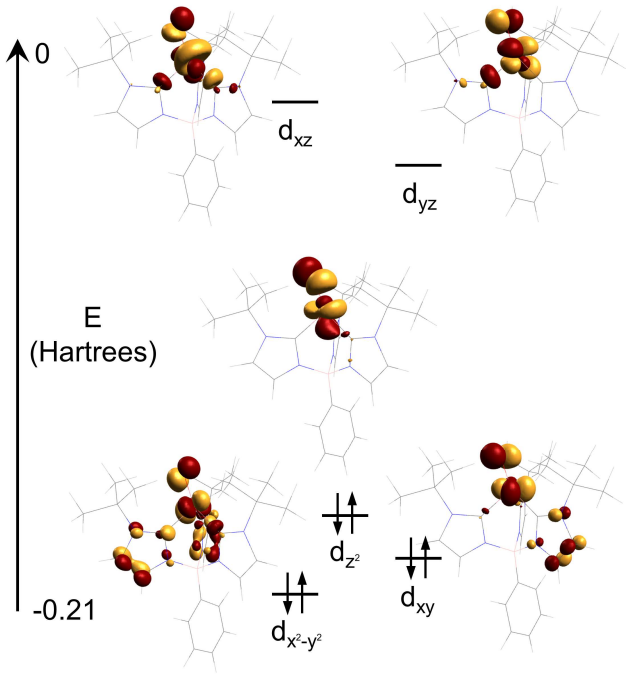


**Figure 2.5.** Frontier primarily Co-based molecular orbitals of **4**. The z-axis is oriented parallel to the energy axis shown. Note that x and y are arbitrary.

We can also directly compare the bonding interactions in **4** and **8** to elucidate any substituent effects on the nature of these complexes. Initial comparison of the Co–C bond lengths in these two

complexes shows that on average, the Co–C bond lengths are ~0.02 Å shorter in **4** (Table 2.1). This is consistent with the increased donation of the Ad-substituted ligand. Additionally, the Co–O bond length is observed to be ~0.03 Å shorter in **8** than **4** (Table 2.1). This could suggest a stronger Co–O bond in **8**. However, IR spectroscopic data and DFT analysis of the Co–O bonding in these two complexes suggests this is not the case. The Co–O stretching frequency in **8** is 807 $cm^{-1}$, compared to 815 $cm^{-1}$ in **4** (Table 2.1). This difference in stretching frequency corresponds to a bond length difference of only ~0.005 Å according to a Badger's Law analysis,[15] which is approximately the error on the SXRD bond lengths. The similarity in Co–O stretching frequencies is more consistent with a comparable Co–O bond between the two complexes. DFT analysis further supports this similarity. The DFT predicted Co–O bond lengths and stretching frequencies are identical (Table 2.1) and the computed delocalization index[18] (DI, a measure of the covalent bond order) is the same for both bonds (Table 2.1). Together, the DFT analysis and IR spectroscopic data support an almost identical bonding interaction between Co and O in complex **4** and **8** despite the slightly different Co–O stretching frequencies. The observed shorter bond length in the crystal structure of **8** may reasonably be attributed to crystal packing effects instead of a stronger Co–O bond.

**Table 2.1.** Comparison of the bonding in **4** and **8**.

| Compound | $Co–C_{avg}$ (Å) | Co–O (Å) | | $\nu_{Co–O}$ ($cm^{-1}$) | | DI[b] |
|---|---|---|---|---|---|---|
| | | exp | calc[a] | exp | calc[a] | |
| **4** | 1.929 | 1.682(6) | 1.651 | 815 | 829 | 2.293 |
| **8** | 1.912 | 1.655(3) | 1.651 | 807 | 827 | 2.293 |

[a]From DFT calculated structures (See Appendix 1). [b]Delocalization index (See Chapter 2.4).

Finally, we can compare the redox potentials, p$K_a$, and $BDFE_{O–H}$ values between these two systems.[16] Examining the values reported in Table 2.2, we can see that the Ad-substituted system is ~200 mV less oxidizing than the $^t$Bu-substituted system, but is ~3 p$K_a$ units more basic once the experimentally measured values are extrapolated to DMSO for more direct comparison. This results in a ~2 kcal/mol stronger O–H bond in **6** than in **1**. Therefore, we might expect **8** to be a slightly more potent H–atom abstractor for X–H bond activation reactions. Additionally, the p$K_a$ and $E_{1/2}$ contributions to the $BDFE_{O–H}$ are more imbalanced in the Ad-substituted system than in the $^t$Bu-substituted system, i.e. the Ad-substituted system is less oxidizing yet more basic. We might therefore expect to observe differences in the C–H activation reactivity of **4** and **8**.

**Table 2.2.** Comparison of thermodynamic parameters of **4** and **8**.

| Compound | p$K_a$[a] | | $E_{1/2}$[c] | $BDFE_{O–H}$[d] |
|---|---|---|---|---|
| | exp | DMSO[b] | (V vs $Fc/Fc^+$) | (kcal/mol) |
| **4** | 25.58(5)[e] | 15 | –0.23[e] | 84.6[e] |
| **8** | 22.6[f] | 18 | –0.44[f] | 86.8[f] |

[a]p$K_a$ value for the deprotonation of the $Co^{III}$-hydroxide complex to form the $Co^{III}$-oxo complex. [b]p$K_a$ values extrapolated to DMSO given that p$K_a$ values correlate linearly between many solvents. [c]$Co^{II}$-hydroxide/$Co^{III}$-hydroxide redox potential. [d]For the O–H bond in the corresponding $Co^{II}$-hydroxide complex. [e]Measured in MeCN. [f]Measured in THF.

## 2.3 Conclusions

Taken together the results presented here unequivocally validate the assignment of terminal $d^6$ transition metal-oxo complexes. The computational and experimental analyses are consistent with the presence of a strong Co–O interaction with multiple bond character despite a high d-electron count. While the precise nature of this bonding has been an interesting point of discussion and investigation,[18] it is nevertheless clear that these studies provide concrete examples of this unusual

class of compounds. The isolation of these complexes facilitates further detailed analysis of the properties and reactivity of this and related late transition metal oxo species.

## 2.4 Experimental

**General Considerations.** All manipulations were performed under a dry nitrogen atmosphere using either standard Schlenk techniques or in an mBraun Unilab Pro glove box unless otherwise stated. All chemicals were obtained from commercial sources and used as received unless otherwise stated. Solvents were dried on a solvent purification system from Pure Process Technologies before storing over 4 Å molecular sieves under $N_2$. Tetrahydrofuran (THF), THF-$d_8$, and diethyl ether ($Et_2O$) were stirred over NaK alloy and passed through a column of activated alumina prior to storing over 4 Å sieves under $N_2$. 9,10-dihydroanthracene (DHA), ferrocenium tetrafluoroborate ($FcBF_4$), and tetrabutylammonium hexafluorophosphate ($TBAPF_6$) were recrystallized prior to use. The proligands, $[PhB(^tBuIm)_3][OTf]_2$ and $[PhB(^{Ad}Im)_3][OTf]_2$, were prepared according to literature procedures.[11,23] $PhB(^tBuIm)_3Co^{II}Cl$ was also synthesized following the reported procedure[11] and crystallized by either liquid diffusion of pentanes into a diethyl ether solution of the chloride complex or liquid diffusion of hexamethyldisiloxane into a toluene solution of the chloride complex.

UV-vis spectra were recorded on a Thermo Scientific Evolution 300 spectrometer with the VISIONpro software suite. For low temperature UV-vis spectroscopic measurements for complexes **1**-**4**, a Hellma Analytics Excalibur Immersion Probe with a 10 mm path length (Article No. 661-202-10-S-46) was used. These low temperature UV-vis spectra were smoothed using the 10 points adjacent averaging function in Origin (OriginLab, Northampton, MA). For low temperature UV-vis spectroscopic measurements for complexes **5**-**8**, a Unisoku CoolSpek cryostat

was used. A standard 1 cm quartz cuvette was used for room temperature measurements. IR spectra were recorded on a Bruker Tensor II spectrometer with the OPUS software suite as mulls in Nujol oil pressed between KBr plates. EPR spectra were recorded on a Bruker Elexsys E500 spectrometer with an Oxford ESR 900 X-band cryostat and a Bruker Cold-Edge Stinger. NMR spectra for $^{1}H$, $^{13}C\{^{1}H\}$, $^{31}P\{^{1}H\}$, $^{11}B\{^{1}H\}$, $^{19}F$, and $^{7}Li$ were recorded or either Bruker DRX-400 or AVANCE-500 spectrometers. $^{1}H$ and $^{13}C\{^{1}H\}$ spectra were referenced to residual proteo-solvent peaks. $^{11}B\{^{1}H\}$ spectra were baseline corrected to remove the signal from the borosilicate tube. Combustion analysis was performed by Midwest Microlab. GC-MS data were collected using an Agilent 7890B GC equipped with an Agilent HP-5MS column coupled to an Agilent 5977A EI-MS. Isotope patterns were compared to the NIST library to confirm assignments. Electrochemical measurements were carried out using a BAS Epsilon potentiostat and analyzed using BAS Epsilon software version 1.40.67NT. Magnetic moments were determined using the Evans method.[24]

**Synthesis of Complex 1.** $PhB(^{t}BuIm)_3Co^{II}Cl$ (500 mg, 0.91 mmol) was dissolved in 8 mL THF. NaOH (109 mg, 2.72 mmol) was ground to a fine powder and added to the THF solution. The deep blue solution was stirred for three days at room temperature, during which the color changed to dark violet. The solution was then filtered through Celite to remove NaCl and excess NaOH after which the THF was removed *in vacuo*. The violet solid was dissolved in a minimal amount of diethyl ether, filtered through glass wool, and layered under pentane at −35 °C. After 48 hours, the supernatant was decanted and the violet crystals dried under vacuum to yield pure **1** (247 mg, 51% yield). Single crystals suitable for X-ray diffraction were grown from liquid diffusion of petroleum ether into a concentrated diethyl ether solution of the complex at −35 °C over two days. $^{1}H$ NMR

($CD_3CN$, 400 MHz): δ 95.13 (3H, Im-H), 45.35 (3H, Im-H), 8.14 (2H, *o/m*-H), 7.74 (2H, *o/m*-H), 7.65 (1H, *p*-H), 7.02 (27H, $^t$Bu). $^1$H NMR (THF-$d_8$, 500 MHz): δ 95.38 (3H, Im-H), 45.40 (3H, Im-H), 8.23 (2H, *o/m*-H), 7.70 (2H, *o/m*-H), 7.57 (1H, *p*-H), 7.29 (27H, $^t$Bu). $^1$H NMR ($C_6D_6$, 400 MHz): δ 94.59 (3H, Im-H), 45.53 (3H, Im-H), 8.48 (2H, *o/m*-H), 7.69 (2H, *o/m*-H), 7.56 (1H, *p*-H), 7.16 (27H, $^t$Bu). $^1$H NMR ($CD_2Cl_2$, 400 MHz): δ 94.34 (3H, Im-H), 44.84 (3H, Im-H), 8.09 (2H, *o/m*-H), 7.69 (2H, *o/m*-H), 7.58 (1H, *p*-H), 7.06 (27H, $^t$Bu). $^{13}$C NMR ($CD_3CN$, 100 MHz): δ 247.1, 140.9, 131.5, 128.9, 84.5. $^{11}$B NMR ($CD_3CN$, 128 MHz): δ 133.8. $\mu_{eff}$ ($CD_3CN$): 4.13 B.M. IR (Nujol, cm$^{-1}$): 3142 (w, $\nu_{O-H}$), 2978 (s), 2935 (m), 2878 (m), 2787 (w), 1969 (w), 1901 (w), 1836 (w), 1659 (w), 1617 (m), 1534 (m), 1480 (m), 1467 (m), 1433 (m), 1398 (s), 1372 (s), 1335 (m), 1275 (s), 1235 (m), 1200 (s), 1190 (s), 1149 (s), 1109 (s), 1082 (w), 1032 (w), 1020 (w), 933 (w), 880 (m), 825 (m), 805 (m), 787 (m), 732 (s). UV-vis, nm in THF (ε, M$^{-1}$cm$^{-1}$): 510 (284), 548 (356), 567 (357), 620 (255), 645 (sh, 234), 722 (335), 1100 (217). Anal. Calc. for $C_{27}H_{39}N_6OBCo$: C 60.80, H 7.37, N 15.76, Found: C 60.44, H 7.12, N 15.52.

**Synthesis of Complex 2.** PhB($^t$BuIm)$_3$Co$^{II}$OH (11 mg, 0.021 mmol) was dissolved in 1 mL THF and cooled to −78 °C. A 0.20 M stock solution of $FcBF_4$ was prepared by dissolution of 14 mg of $FcBF_4$ in 250 μL of MeCN. Addition of 100 μL of the deep blue $FcBF_4$ stock solution to the violet solution of **1** resulted in an immediate color change to green. This solution was then layered under cold pentane and stored in a −35 °C freezer overnight to yield green single crystals suitable for X-ray diffraction. NMR spectra were collected on an in situ generated solution of **2** in THF-$d_8$. UV-vis spectra were collected on an in situ generated solution of **2** in THF at −78 °C. $^1$H NMR ($CD_3CN$, 500 MHz, −35 °C): δ 7.77 (2H, d, *o*-H), 7.52 (3H, m, *m/p*-H), 7.38 (3H, d, Im-H), 7.17 (3H, d, Im-H), 1.64 (27H, s, $^t$Bu). $^1$H NMR (THF-$d_8$, 500 MHz, −78 °C): δ 7.85 (2H, d, *o*-H), 7.52

(3H, m, *m/p*-H), 7.34 (3H, d, Im-H), 6.94 (3H, d, Im-H), 1.82 (27H, s, $^{t}$Bu). $^{13}$C NMR (THF-$d_8$, 126 MHz, −78 °C): δ 135.4, 129.0, 122.6, 121.9, 68.1, 60.0, 32.6, 25.9. $^{19}$F NMR ($CD_3CN$, 471 MHz, −35 °C): δ −151.1. $^{11}$B NMR ($CD_3CN$, 128 MHz): δ −0.07 (Ph*B*($^{t}$BuIm)$_3^-$), −0.5 (*B*$F_4^-$). UV-vis, nm in THF (ε, $M^{-1}cm^{-1}$): 450 (1239), 606 (346), 718 (599). Due to thermal instability, elemental analysis and IR spectra were unable to be collected for this complex.

**Synthesis of Complex 3.** To an in situ generated solution of **2** at −78 °C (0.19 mmol, 3 mL) was added a solution of LiHMDS (31 mg, 0.19 mmol) in THF (1 mL) pre-cooled to −78 °C. The initially green solution instantly changed color to give a magenta solution. The solution was then warmed to room temperature and the solvent removed *in vacuo* to yield a magenta solid. Dissolution in a minimal amount of toluene followed by filtration through glass wool to remove black solids and layering under pentane at −35 °C gave pure **3** as a crystalline solid after two days (82 mg, 71% yield). The solid was stored in the freezer to avoid decomposition. Single crystals suitable for X-ray diffraction were grown from liquid diffusion of pentanes into a toluene solution of **3** at −35 °C over the course of a week. $^{1}$H NMR ($CD_3CN$, 500 MHz): δ 7.74 (2H, d, *o*-H), 7.50 (3H, m, *m/p*-H), 7.31 (3H, d, Im-H), 7.03 (3H, d, Im-H), 1.89 (27H, s, $^{t}$Bu). $^{1}$H NMR ($C_6D_6$, 400 MHz): δ 7.89 (2H, d, *o*-H), 7.39 (3H, m, *m/p*-H), 6.96 (3H, d, Im-H), 6.69 (3H, d, Im-H), 1.96 (27H, s, $^{t}$Bu). $^{13}$C NMR ($C_6D_6$, 126 MHz): δ 152.7, 134.7, 123.0, 121.1, 59.1, 31.4. $^{19}$F NMR ($CD_3CN$, 471 MHz): δ −151.6. $^{19}$F NMR (THF, 471 MHz): δ −156.8. $^{11}$B NMR ($C_6D_6$, 128 MHz): δ −0.1. $^{7}$Li NMR ($C_6D_6$, 156 MHz): δ 2.4 (br). $^{7}$Li NMR (THF, 156 MHz): δ 2.9 (very br). IR (Nujol, $cm^{-1}$): 2728 (w), 1460 (s), 1416 (m), 1375 (s), 1332 (s), 1291 (w), 1277 (w), 1213 (m), 1198 (m), 1155 (m), 1130 (w), 1062 (br, m), 1024 (m), 929 (w), 899 (w), 887 (m), 839 (m, $\nu_{Co-O}$), 794 (w), 722 (m), 698 (m). UV-vis, nm in THF (ε, $M^{-1}cm^{-1}$): 346 (sh, 1110), 486 (456), 555 (470),

718 (sh, 134). Due to thermal instability, satisfactory combustion analysis was not able to be obtained for this complex.

**Synthesis of Complex 4.** Magenta solid **3** (100 mg, 0.16 mmol) was dissolved in 6 mL benzene after which Kryptofix 2,2,1 (48 μL, 0.16 mmol) was added, resulting in an immediate color change from magenta to dull purple and formation of a fine precipitate. The solution was filtered through Celite and the benzene removed by lyophilization. The purple powder was dissolved in a minimum amount of diethyl ether and layered under pentane at −35 °C to yield pure **4** as a purple crystalline solid after a few hours (69 mg, 81% yield). Single crystals suitable for X-ray diffraction were grown from liquid diffusion of pentanes into a concentrated THF solution of **4** at −35 °C over the course of a week. $^{1}$H NMR ($C_6D_6$, 400 MHz): δ 7.97 (2H, d, *o*-H), 7.40 (3H, m, *m/p*-H), 7.02 (3H, d, Im-H), 6.75 (3H, d, Im-H), 1.88 (27H, s, $^{t}$Bu). $^{13}$C NMR ($C_6D_6$, 126 MHz): δ 134.8, 122.6, 120.1, 68.3, 58.2, 31.6. $^{11}$B NMR ($C_6D_6$, 128 MHz): δ −1.2. IR (Nujol, cm$^{-1}$): 2722 (w), 1460 (s), 1411 (m), 1392 (w), 1377 (s), 1369 (m), 1332 (s), 1288 (w), 1275 (m), 1232 (w), 1213 (m), 1198 (m), 1153 (m), 1125 (w), 1042 (m), 1023 (m), 932 (w), 898 (w), 885 (m), 825 (w), 815 (m, $\nu_{Co-O}$), 802 (w), 792 (m), 737 (w), 721 (w), 713 (w), 698 (m), 653 (w). UV-vis, nm in THF (ε, M$^{-1}$cm$^{-1}$): 342 (sh, 1150), 484 (427), 564 (457), 718 (sh, 116). Due to thermal instability, satisfactory combustion analysis was not able to be obtained for this complex.

**Alternative synthesis of Complex 4.** To an in situ generated solution of **2** in THF at −35 °C (0.19 mmol, 3 mL) was added a solution of KHMDS (37 mg, 0.19 mmol) in THF (1 mL) pre-cooled to −35 °C. The initially green solution instantly changed color to give a dull purple solution. The solution was then warmed to room temperature and the solvent removed *in vacuo* to yield a purple solid. Dissolution in a minimal amount of diethyl ether followed by filtration through glass

wool to remove black solids and layering under pentane at –35 °C gave pure **4** as a crystalline solid overnight (50 mg, 50% yield).

**Synthesis of Complex 5.** To a suspension of 5.0 g (5.0 mmol) of $PhB(^{Ad}ImH)_3OTf_2$ in 100 mL THF at –78 °C was added 3.05 equivalents of LDA (15.4 mmol, prepared in situ from a 1:1 mixture of n-BuLi and $HN(^{i}Pr)_2$ in 25 mL THF at –78 °C). This heterogeneous mixture was allowed to stir at –78 °C for 1-1.5 h until the mixture became homogeneous and yellowy-pink in color. Solid $CoCl_2$ (650 mg, 5.0 mmol) was added and the reaction allowed to warm to room temperature with stirring overnight. The solution was pumped down and dried at ~75 °C to ensure complete removal of THF. The blue residue was dissolved in DCM and filtered through Celite to remove LiCl and LiOTf salts. This solution was pumped down and washed with THF. A bright blue solid was collected by filtration and dried to give **5** in 78% yield (3.1 g, 3.9 mmol). Single crystals suitable for X-ray diffraction were grown from a toluene solution of **5** layered under pentane at –35 °C and had a toluene molecule in the unit cell. $^{1}$H NMR ($C_6D_6$, 400 MHz): δ 92.71 (3H, Im-*H*), 33.69 (3H, Im-*H*), 12.92 (18H, Ad-*H*), 5.55 (1H, Ph-*H*), 5.42 (9H, Ad-*H*), 5.13 (2H, Ph-*H*), 4.25 (9H, Ad-*H*), 1.80 (2H, Ph-*H*), 0.72 (9H, Ad-*H*). $^{13}$C NMR ($C_6D_6$, 100 MHz): δ 199.3, 130.6, 128.3, 125.9, 123.8, 112.5, 57.5, 32.5. $^{11}$B NMR ($C_6D_6$, 128 MHz): δ 68.8. $\mu_{eff}$ ($C_6D_6$): 4.32 B.M. IR (KBr, $cm^{-1}$): 3145 (w), 3070 (w), 3033 (w), 2908 (s), 2853 (s), 1549 (w), 1477 (w), 1453 (m), 1387 (m), 1375 (w), 1359 (m), 1329 (m), 1309 (m), 1273 (s), 1240 (w), 1159 (s), 1119 (m), 1103 (m), 1076 (w), 1016 (s), 938 (w), 895 (w), 879 (m), 834 (m), 816 (m), 804 (m), 786 (s), 771 (w), 736 (sh), 725 (sh), 712 (s), 681 (s). UV-vis, nm in THF (ε, $M^{-1}cm^{-1}$): 584 (514), 616 (774), 674 (1007). Anal. Calc. for $C_{52}H_{64}BClCoN_6$ (**5**•toluene): C 71.11, H 7.34, N 9.57, Found: C 71.16, H 7.30, N 9.57.

**Synthesis of Complex 6.** To a solution of **5** in 15 mL THF (450 mg, 0.57 mmol) was added 3 equivalents of solid NaOH (69 mg, 1.7 mmol) that was ground up to a fine powder. This reaction was allowed to stir at room temperature for 3 days, during which the solution color changed from blue to purple. The solution was filtered to remove excess NaOH and NaCl and then pumped down. The purple residue was redissolved in THF and layered under pentane at –35 °C to afford pure **6** as a bright violet solid in 72% yield (320 mg, 0.41 mmol). Single crystals suitable for X-ray diffraction were grown from a toluene solution of **6** layered under pentane at –35 °C. $^{1}$H NMR ($C_6D_6$, 400 MHz): δ 91.32 (3H, Im-*H*), 44.94 (3H, Im-*H*), 8.27 (2H, Ph-*H*), 7.60 (2H, Ph-*H*), 7.52 (1H, Ph-*H*), 5.16 (18H, Ad-*H*), 4.35 (9H, Ad-*H*), 4.00 (9H, Ad-*H*), 1.24 (9H, Ad-*H*). $^{13}$C NMR ($C_6D_6$, 100 MHz): δ 222.1, 139.8, 129.6, 128.3, 126.9, 105.7, 55.3, 39.5. $^{11}$B NMR ($C_6D_6$, 128 MHz): δ 127.3. $\mu_{eff}$ ($C_6D_6$): 4.22 B.M. IR (KBr, $cm^{-1}$): 3142 (w, $\nu_{O-H}$), 3042 (w), 2906 (s), 2850 (s), 1616 (br), 1534 (br), 1477 (w), 1453 (m), 1433 (w), 1386 (m), 1359 (m), 1329 (m), 1309 (m), 1273 (s), 1239 (w), 1165 (s), 1155 (s), 1121 (s), 1103 (s), 1076 (w), 1014 (s), 879 (m), 835 (m), 816 (w), 802 (m), 785 (m), 731 (s), 709 (s), 676 (m). UV-vis, nm in THF (ε, $M^{-1}cm^{-1}$): 514 (251), 550 (317), 568 (322), 624 (sh, 238), 646 (247), 716 (179), 1100 (169). Anal. Calc. for $C_{45}H_{57}BCoN_6O$: C 70.40, H 7.48, N 10.95, Found: C 70.23, H 7.53, N 10.66.

**Synthesis of Complex 7.** A solution of **6** in 2.0 mL of THF (25 mg, 33 μmol) was cooled to –35 °C before $FcBF_4$ (8.9 mg, 33 μmol) dissolved in minimal MeCN was added. A color change from violet to bright green was observed and this solution was layered under $Et_2O$ at –35 °C to afford single crystals of **7**. NMR spectra were recorded on an in situ generated solution of **7** in THF-$d_8$ and UV-vis spectra were recorded on an in situ generated solution of **7** in THF. $^{1}$H NMR (THF-$d_8$, 500 MHz, –35 °C): δ 10.61 (1H, O–*H*), 7.82 (2H, Ph-*H*), 7.66 (3H, Im-*H*), 7.56 (3H, Ph-

*H*), 7.29 (3H, Im-*H*), 2.35 (18H, Ad-*H*), 2.25 (9H, Ad-*H*), 1.78 (18H, Ad-*H*). $^{19}$F NMR (THF-$d_8$, 471 MHz, –35 °C): δ 162.1. UV-vis, nm in THF at –80 °C (ε, $M^{-1}cm^{-1}$): 458 (1267), 636 (sh, 503), 718 (898). Due to thermal instability, $^{11}$B NMR, $^{13}$C NMR, and IR spectroscopic data and elemental analysis were not able to be collected for this complex.

**Synthesis of Complex 8.** A solution of **6** in 12 mL THF (60 mg, 78 μmol) was cooled to –35 °C. A solution of $FcBF_4$ (22 mg, 78 μmol) in 0.5 mL MeCN was added to result in a color change from violet to green. Next, a solution of KO$^t$Bu (8.8 mg, 78 μmol) in 1.0 mL THF was added, which resulted in a color change to red-purple. The reaction was allowed to stir for ~5 minutes at –35 °C before pumping down at room temperature. The dark purple and blue residue was triterated with pentane and dried extensively to remove HO$^t$Bu and leave a lighter purple only residue. This was washed with MeCN to remove Fc and other Co-containing impurities. The solid was dried extensively to remove traces of MeCN before being dissolved in toluene and layered under pentane at –35 °C. Dark purple crystals of pure **8** were collected in variable yields (13-33 mg, 17-43 μmol, 22-55% yield). Single crystals suitable for X-ray diffraction were grown from a toluene solution of **8** layered under pentane at –35 °C. $^1$H NMR ($C_6D_6$, 400 MHz): δ 7.95 (2H, Ph-*H*), 7.39 (2H, Ph-*H*), 7.35 (1H, Ph-*H*), 7.06 (3H, Im-*H*), 6.84 (3H, Im-*H*), 2.77 (18H, Ad-*H*), 2.10 (9H, Ad-*H*), 1.87 (9H, Ad-*H*), 1.57 (9H, Ad-*H*). $^{13}$C NMR ($C_6D_6$, 100 MHz): δ 134.5, 122.4, 118.8, 58.2, 43.0, 36.1, 30.5. $^{11}$B NMR ($C_6D_6$, 128 MHz): δ –1.8. IR (Nujol, $cm^{-1}$): 1459 (s), 1410 (m), 1376 (s), 1360 (sh), 1340 (m), 1326 (s), 1307 (m), 1275 (m), 1235 (m), 1186 (s), 1168 (s), 1129 (w), 1105 (m), 1073 (w), 1023 (s), 885 (m), 832 (m), 807 (m, $\nu_{Co–O}$), 792 (w), 714 (m), 694 (s). UV-vis, nm in THF (ε, $M^{-1}cm^{-1}$): 488 (529), 554 (506), 712 (sh, 178), 940 (tr, 76). Anal. Calc. for $C_{45}H_{56}BCoN_6O$: C 70.49, H 7.36, N 10.96, Found: C 70.35, H 7.33, N 10.89.

**Synthesis of $Na^{18}OH$.** Sodium metal (0.574 g, 25 mmol) was placed in a Schlenk tube equipped with a #2 size ground glass plug and a 14/20 ground glass joint to which 7 mL of THF was added. $^{18}O$-labeled water (0.5 g, 25 mmol) was added slowly under a positive pressure of $N_2$, resulting in vigorous gas evolution and formation of a fine white solid. The reaction was stirred at room temperature under nitrogen for 11 days, after which the THF was removed *in vacuo* and the unreacted Na metal separated from the white solid. The white solid was dried to yield $Na^{18}OH$ as a powder (0.85 g, 81% yield).

**Synthesis of $^{18}O$-labeled compounds.** $^{18}O$-labeled **1** and **6** were prepared as described above, using $Na^{18}OH$ in the place of natural abundance NaOH. Purity of the crystalline violet solid was confirmed by $^1H$ NMR spectroscopy. $^{18}O$-labeled **3**, **4**, and **8** were prepared as described above, using the $^{18}O$-labeled precursor complexes where necessary. Purity of the crystalline solids was confirmed by $^1H$ NMR spectroscopy.

**Synthesis of [HMTBD][$BF_4$].** To a solution of MTBD in $Et_2O$ was added an equimolar amount of $HBF_4 \bullet Et_2O$. The resulting precipitate was collected and dried under vacuum to yield pure [HMTBD][$BF_4$] (500 mg, 64% yield). $^1H$ NMR ($CD_3CN$, 400 MHz): δ 5.95 (1H, s, N–H), 3.28 (8H, m, $CH_2$), 2.88 (3H, s, Me), 1.95 (4H, m, $CH_2$). $^{13}C$ NMR ($CD_3CN$, 100 MHz): δ 151.2, 48.8, 48.3, 47.8, 39.6, 37.5, 21.5, 21.3.

**General Procedure for UV-vis Spectroscopy of Complex Syntheses.** In a typical experiment, 4.0 mL of a 1.25 mM solution of $PhB(^tBuIm)_3Co^{II}OH$ in THF was transferred to a custom made, air-tight apparatus equipped with a 14/20 ground glass joint, #2 size ground glass plug, and #25 size threated Teflon plug for the dip probe to go through which was sealed with a Teflon coated o-ring. The entire apparatus was sealed inside the glovebox and removed before cooling to −78 °C

under a positive pressure of $N_2$ through the ground glass plug. Stock solutions of $FcBF_4$ (50 mM in 2:1 THF/MeCN), LiHMDS (200 mM in THF), $CoCp_2$ (100 mM in MeCN), and $HNEt_3BF_4$ (75 mM in THF) were prepared in the glovebox and transferred to the reaction flask in gas tight microsyringes through a rubber septum placed in the 14/20 ground glass joint. For each reaction, one equivalent of solution was added in partial equivalent additions after which no further spectral changes were observed (see Appendix 1).

**Titration of PhB($^t$BuIm)$_3$Co$^{III}$O with [HMTBD][BF$_4$].** The titration of **4** with [HMTBD][$BF_4$] was monitored by $^1$H NMR spectroscopy. As the product of the reaction, **2**, is unstable above −35 °C, the samples were prepared and stored cold and the spectra were collected at −35 °C. Spectra were collected on three separate samples for each amount of acid added. To prepare a typical sample, 0.25 mL of a 20 mM solution of **4** in $CD_3CN$ was transferred to a J. Young NMR tube. Next, 0.10 mL of a 50 mM solution of hexamethyldisiloxane ($TMS_2O$) in $CD_3CN$ was added as an internal standard followed by addition of varying volumes of a 50 mM solution of [HMTBD][$BF_4$] in $CD_3CN$ to reach 0.25, 0.50, 0.75, 1.0, or 1.5 equivalents of added acid relative to **4**. Finally, the samples were diluted with $CD_3CN$ to reach a total volume of 0.50 mL and initial concentrations of 10 mM **4**, 10 mM $TMS_2O$, and 2.5-15 mM [HMTBD][$BF_4$]. It was discovered upon collecting the spectra that all species in solution (**2**, **4**, [HMTBD][$BF_4$], and MTBD) were in rapid equilibrium. The concentration of each species in solution at equilibrium was determined using Equation 2.2–Equation 2.6 and the observed chemical shift for the methyl protons of MTBD/[HMTBD][$BF_4$]. From this data the equilibrium constant for the reaction shown in Equation 2.7, $K_{eq}$, was calculated and the values obtained from each initial concentration tested averaged. Finally, the relationship shown in Equation 2.8 was used to calculate the $K_a$ of **2**.

Equation 2.2 $\delta_{obs} = \mathrm{X}_{MTBD}\delta_{MTBD} + X_{HMTBD}\delta_{HMTBD}$

Equation 2.3 $[HTMBD]_{eq} = \frac{[HMTBD]_i(\delta_{obs} - \delta_{MTBD})}{\delta_{HMTBD} - \delta_{MTBD}}$

Equation 2.4 $[MTBD]_{eq} = [HMTBD]_i - [HMTBD]_{eq}$

Equation 2.5 $[\mathbf{2}]_{eq} = [MTBD]_{eq}$

Equation 2.6 $[\mathbf{3}]_{eq} = [\mathbf{3}]_i - [\mathbf{2}]_{eq}$

Equation 2.7 $\mathbf{3} + [HMTBD][BF_4] \xrightarrow{K_{eq}} \mathbf{2} + MTBD$

Equation 2.8 $K_{eq} = \frac{K_{a,HMTBD}}{K_{a,\mathbf{2}}}$

**Procedure for Determining the p$K_a$ of 7.** The p$K_a$ of **7** was determined by titrating **8** with [HMTBD][$BF_4$]. The titration of **8** with [HMTBD][$BF_4$] was monitored by $^1$H NMR spectroscopy. As the product of the reaction, **7**, is unstable above –35 °C, the samples were prepared and stored cold and the spectra were collected at –35 °C. Spectra were collected on three separate samples for each amount of acid added. To prepare a typical sample, 0.25 mL of a 10 mM solution of **8** in THF-$d_8$ was transferred to an NMR tube. Next, 0.10 mL of a 25 mM solution of $TMS_2O$ in THF-$d_8$ was added as an internal standard followed by addition of varying volumes of a 25 mM solution of [HMTBD][$BF_4$] in THF-$d_8$ to reach 0.75, 1.0, or 1.5 equivalents of added acid relative to **8**. Finally, the samples were diluted with THF-$d_8$ to reach a total volume of 0.50 mL and initial concentrations of 5 mM **8**, 5 mM $TMS_2O$, and 3.75-7.5 mM [HMTBD][$BF_4$]. It was discovered upon collecting the spectra that all species in solution (**7**, **8**, [HMTBD][$BF_4$], and MTBD) were in rapid equilibrium resulting in the appearance of coalesced peaks in the $^1$H NMR spectra. The ratios of the concentrations of **7**:**8** and [HMTBD][$BF_4$]:MTBD were determined according to Equation

2.9-Equation 2.11. The peaks used for analysis were an Im-*H* peak and two Ad-*H* peaks for **7**/**8** and the methyl protons of MTBD/[HMTBD][$BF_4$] (Table A1.2). From this data the equilibrium constant for the reaction shown in Equation 2.12, $K_{eq}$, was calculated and the values obtained from each **7**/**8** peak averaged. In THF, these species exist as ion pairs in solution so the calculated equilibrium constant is for those ion pairs, not the true p$K_a$ values. Using Equation 2.13 and Equation 2.14,[25] we can calculate $\Delta pK_a$ relative to the p$K_a$ of $[HMTBD]^+$ (18.0 in THF[25]) using the methods described in Reference 26 to estimate $K_d$ values (Table A1.3). Finally, the relationship shown in Equation 2.15 was used to calculate the p$K_a$ of **7**.

Equation 2.9 $$\delta_{obs} = \delta_A \chi_A + \delta_B \chi_B$$

Equation 2.10 $$\frac{[\mathbf{7}]}{[\mathbf{8}]} = \frac{\delta_{obs} - \delta_{\mathbf{4}}}{\delta_{\mathbf{3}} - \delta_{obs}}$$

Equation 2.11 $$\frac{[\mathrm{MTBD}]}{[\mathrm{HMTBD^+}]} = \frac{\delta_{\mathrm{HMTBD^+}} - \delta_{\boldsymbol{obs}}}{\delta_{\boldsymbol{obs}} - \delta_{\mathrm{MTBD}}}$$

Equation 2.12 $$K_{\mathrm{eq}} = \frac{[\mathbf{7}][\mathrm{MTBD}]}{[\mathbf{8}][\mathrm{HMTBD^+}]} = \frac{\delta_{obs} - \delta_{\mathbf{8}}}{\delta_{\mathbf{7}} - \delta_{obs}} \cdot \frac{\delta_{\mathrm{HMTBD^+}} - \delta_{\boldsymbol{obs}}}{\delta_{\boldsymbol{obs}} - \delta_{\mathrm{MTBD}}}$$

Equation 2.13 $$\Delta \mathrm{p}K_{\mathrm{ip}} = \log\left(K_{\mathrm{eq}}\right)$$

Equation 2.14 $$\Delta \mathrm{p}K_{\mathrm{a}} = \Delta \mathrm{p}K_{\mathrm{ip}} - \log\left(\frac{K_{\mathrm{d,HMTBD^+}}}{K_{\mathrm{d,7}}}\right)$$

Equation 2.15 $$\Delta \mathrm{p}K_{\mathrm{a}} = \mathrm{p}K_{\mathrm{a,7}} - \mathrm{p}K_{\mathrm{a,HMTBD^+}}$$

**Procedure for Electrochemical Data Collection.** A 3 mM solution of cobalt complex (**1**) was prepared in MeCN containing 0.1 M $TBAPF_6$ as the electrolyte. Cyclic voltammetry was collected at a scan rate of 50 mV/s (**1**) or 100 mV/s (**5** and **6**) and referenced to the $Fc/Fc^+$ couple. A glassy

carbon working electrode with a diameter of 3 mm was used, polished with alumina before use. The counter electrode was a platinum wire and the reference electrode was a silver wire.

**General Procedure for Monitoring Reactivity with Substrates by UV-vis Spectroscopy.** Data for rate determination were collected in triplicate unless otherwise noted. In a typical experiment, 2.0 mL of a 1.25 mM solution of cobalt complex (**3** or **4**) in THF was placed in a cuvette with a #2 ground glass plug to apply positive $N_2$ pressure. The initial scan was collected followed by injection of 50 μL of a 0.50 M solution of substrate in THF (10 equivalents). The reactions were monitored by UV-vis spectroscopy until completion (≤ 40 min). Self-decay rates were obtained by monitoring a 1.25 mM solution of cobalt complex (**3** or **4**) in THF by UV-vis spectroscopy in a cuvette sealed with a Teflon plug. In both cases, the data were analyzed by plotting the natural log of the absorbance at 470 nm at time *t* divided by the initial absorbance vs time in seconds to give the observed rate $k_{obs}$ as the slope of the linear fit of the data. The reaction of **3** and **4** with 2,4,6-tri(*tert*-butyl)phenol was instantaneous upon mixing and therefore no rate data were obtained.

**Procedure for Monitoring Reactivity with $PMe_3$ by $^{31}P$ NMR.** A 10 mM solution of **3** was prepared in 0.5 mL of THF and placed into an NMR tube. $PMe_3$ (10 equivalents, 5 μL) was added and the solution allowed to react for 30 minutes after which one equivalent of an internal standard of $OPPh_3$ was added (10 μL of a 0.5 M solution). $^{31}P$ NMR spectra were collected on three separate trials.

**Procedure for Monitoring Reactivity with $PMe_3$ in the absence of DCM by NMR spectroscopy.** In a J. Young NMR tube, a 10 mM solution of **3** was prepared in 0.5 mL of THF-$d_8$ that had been stirred over NaK alloy and vacuum transferred to a clean flask before use. $PMe_3$

(10 equivalents, 5 μL) was added and the solution allowed to react for 30 minutes after which a $^{1}H$ NMR spectrum was collected. Subsequently, one equivalent of an internal standard of $OPPh_3$ was added (10 μL of a 0.5 M solution in proteo-THF) and a $^{31}P$ NMR spectrum was collected.

**Procedure for GC-MS Determination of $^{18}O$ Incorporation During Reaction with $PMe_3$.** A 10 mM solution of **4** in THF was prepared (1.0 mL) and $PMe_3$ (11 μL) was added. The solution was allowed to stand at room temperature for approximately 30 minutes, over the course of which it changed from a dark purple to a bright blue. The solution was then diluted by approximately a factor of 10, filtered through a 0.2 micron syringe filter, and subjected to GC-MS analysis.

**Crystallographic Details.** The diffraction data for **2-4** and **7** were measured at 100 K on a Bruker D8 fixed-chi with PILATUS1M (CdTe) pixel array detector (synchrotron radiation, $\lambda$ = 0.41328 Å (30 KeV)) at the Chem-MatCARS 15-ID-B beamline at the Advanced Photon Source (Argonne National Laboratory). The diffraction data for **1**, **5**, **6**, and **8** were measured at 100 K on a Bruker D8 VENTURE diffractometer equipped with a microfocus Mo-target X-ray tube ($\lambda$ = 0.71073 Å) and PHOTON 100 CMOS detector. Data reduction and integration were performed with the Bruker APEX3 software package (Bruker AXS, version 2017.3-0, 2018). Data were scaled and corrected for absorption effects using the multi-scan procedure as implemented in SADABS (Bruker AXS, version 2014/5).[27] The structures were solved by SHELXT (Version 2014/5)[28] and refined by a full-matrix least-squares procedure using OLEX2 (XL refinement program version 2018/1)[29]. Structure solutions were performed with the use of standard restraints and constraints as implemented in ShelXL. Additional crystallographic and refinement data can be found in Table A1.6 in Appendix 1.

**Computational Methods for the Data in Table A1.8 and Figure 2.5.** Geometry optimizations were performed using the ORCA program suite.[30] The B3LYP hybrid functional was used for all calculations. The basis sets for each atom were as follows: TZVPP for Co, N, and O; 6-31G for C and H. The COSMO solvation model for THF solvation was included in all calculations. A full frequency calculation was performed on each structure to ensure that there were no imaginary frequencies and ensure true minima in the energies. The initial geometries were generated with a simple molecular mechanics geometry optimization in the Hyperchem program suite.[31] The computed energies were corrected for thermal energy contributions. Bond dissociation energies were obtained by comparison of the energies of each optimized structure along with the computed energy for a free hydrogen atom. The geometry plots were created from the optimized xyz cartesian coordinates in Diamond 3.2.[32] The free energies of the respective species are shown in Table S3. The Kohn-Sham molecular orbitals were plotted in Avogadro[33] with ISO values for the surface set at 0.06.

**Computational Methods for the Data in Table 2.1.** DFT calculations were performed in ORCA 5.0.0 using the O3LYP functional with default grid settings.[34] The CPCM continuum polarization model with gaussian charges and the dielectric constant of THF was included.[35] The basis sets of Aldrich and coworkers was employed: cobalt was given def2-TZVPP; all ligands bound to cobalt were given def2-TZVP; all other atoms were given def2-SV(P).[36] Frequency calculations were performed numerically. All minima were confirmed to have zero imaginary frequencies, excepting for a few modes with magnitudes less than 40 $cm^{-1}$ which all corresponded to rotating adamantyl groups. The delocalization index, which measures the number of electron

pairs shared in a bond and can serve as an estimate of the bond order,[37] was calculated in Becke fuzzy atomic space using the Multiwfn program.[38]

## 2.5 References


[1] (a) Rittle, J.; Green, M. T. "Cytochrome P450 Compound I: Capture, Characterisation, and C-H Bond Activation Kinetics." *Science.* **2010**, *330*, 933–937. (b) Cox, N.; Pantazis, D. A.; Neese, F.; Lubitz, W. "Biological Water Oxidation." *Acc. Chem. Res.* **2013**, *46* (7), 1588–1596.

[2] (a) Surendranath, Y.; Kanan, M. W.; Nocera, D. G. "Mechanistic Studies of the Oxygen Evolution Reaction by a Cobalt-Phosphate Catalyst at Neutral PH." *J. Am. Chem. Soc.* **2010**, *132* (46), 16501–16509. (b) Lane, B. S.; Burgess, K. "Metal-Catalyzed Epoxidations of Alkenes with Hydrogen Peroxide." *Chem. Rev.* **2003**, *103* (7), 2457–2473.

[3] (a) McDonald, A. R.; Que, L. "High-Valent Nonheme Iron-Oxo Complexes: Synthesis, Structure, and Spectroscopy." *Coord. Chem. Rev.* **2013**, *257* (2), 414–428. (b) Gunay, A.; Theopold, K. H. "C−H Bond Activations by Metal Oxo Compounds." *Chem. Rev.* **2010**, *110* (2), 1060–1081. (c) Gupta, R.; Taguchi, T.; Lassalle-Kaiser, B.; Bominaar, E. L.; Yano, J.; Hendrich, M. P.; Borovik, A. S. "High-Spin Mn-Oxo Complexes and Their Relevance to the Oxygen-Evolving Complex within Photosystem II." *Proc. Natl. Acad. Sci. U. S. A.* **2015**, *112* (17), 5319–5324. (d) Neu, H. M.; Baglia, R. A.; Goldberg, D. P. "A Balancing Act: Stability versus Reactivity of Mn(O) Complexes." *Acc. Chem. Res.* **2015**, *48* (10), 2754–2764.

[4] (a) Ballhausen, C. J.; Gray, H. B. "The Electronic Structure of the Vanadyl Ion." *Inorg. Chem.* **1962**, *1* (1), 111–122. (b) Betley, T. A.; Wu, Q.; Van Voorhis, T.; Nocera, D. G. "Electronic Design Criteria for O-O Bond Formation via Metal-Oxo Complexes." *Inorg. Chem.* **2008**, *47* (6), 1849–1861.

[5] (a) MacBeth, C. E.; Golombek, A. P.; Young, V. G.; Yang, C.; Kuczera, K.; Hendrich, M. P.; Borovik, A. S. "$O_2$ Activation by Nonheme Iron Complexes: A Monomeric Fe(III)-Oxo Complex Derived from $O_2$." *Science.* **2000**, *289* (5481), 938–941. (b) Smith, J. M.; Mayberry, D. E.; Margarit, C. G.; Sutter, J.; Wang, H.; Meyer, K.; Bontchev, R. P. "N-O Bond Homolysis of an Iron(II) TEMPO Complex Yields an Iron(III) Oxo Intermediate." *J. Am. Chem. Soc.* **2012**, *134* (15), 6516–6519. (c) Hong, S.; Pfaff, F. F.; Kwon, E.; Wang, Y.; Seo, M.-S.; Bill, E.; Ray, K.; Nam, W. "Spectroscopic Capture and Reactivity of a Low-Spin Cobalt(IV)-Oxo Complex Stabilized by Binding Redox-Inactive Metal Ions." *Angew. Chem., Int. Ed.* **2014**, *53* (39), 10403–10407. (d) Matson, E. M.; Park, Y. J.; Fout, A. R. "Facile Nitrite Reduction in a Non-Heme Iron System: Formation of an Iron(III)-Oxo." *J. Am. Chem. Soc.* **2014**, *136* (50), 17398–17401. (e) Wang, B.; Lee, Y. M.; Tcho, W. Y.; Tussupbayev, S.; Kim, S. T.; Kim, Y.; Seo, M. S.; Cho, K. Bin; Dede, Y.; Keegan, B. C.; Ogura, T.; Kim, S. H.; Ohta, T.; Baik, M. H.; Ray, K.; Shearer, J.; Nam, W. "Synthesis and Reactivity of a Mononuclear Non-Haem Cobalt(IV)-Oxo Complex." *Nat. Commun.* **2017**, *8*.

[6] (a) O'Halloran, K. P.; Zhao, C.; Ando, N. S.; Schultz, A. J.; Koetzle, T. F.; Piccoli, P. M. B.; Hedman, B.; Hodgson, K. O.; Bobyr, E.; Kirk, M. L.; Knottenbelt, S.; Depperman, E. C.; Stein, B.; Anderson, T. M.; Cao, R.; Geletii, Y. V; Hardcastle, K. I.; Musaev, D. G.; Neiwert, W. A.; Fang, X.; Morokuma, K.; Wu, S.; Kögerler, P.; Hill, C. L. "Revisiting the Polyoxometalate-Based Late-Transition-Metal-Oxo Complexes: The 'Oxo Wall' Stands." *Inorg. Chem.* **2012**, *51* (13), 7025–7031. (b) Spaltenstein, E.; Conry, R. R.; Critchlow, S. C.; Mayer, J. M. "Synthesis, Characterization, and Reactivity of a Formally Rhenium(I) Terminal Oxo Complex, $NaRe(O)(RC{=}CR)_2$." *J. Am. Chem. Soc.* **1989**, *111*, 8741–8742. (c) Poverenov, E.; Efremenko, I.; Frenkel, A. I.; Ben-David, Y.; Shimon, L. J. W.; Leitus, G.; Konstantinovski, L.; Martin, J. M. L.; Milstein, D. "Evidence for a Terminal Pt(IV)-Oxo Complex Exhibiting Diverse Reactivity." *Nature* **2008**, *455* (7216), 1093–1096. (d) Delony, D.; Kinauer, M.; Diefenbach, M.; Demeshko, S.; Würtele, C.; Holthausen, M. C.; Schneider, S. "A Terminal Iridium Oxo Complex with a Triplet Ground State." *Angew. Chem., Int. Ed.* **2019**, *58* (32), 10971–10974.

[7] (a) Mindiola, D. J.; Hillhouse, G. L. "Terminal Amido and Imido Complexes of Three-Coordinate Nickel." *J. Am. Chem. Soc.* **2001**, *123* (19), 4623–4624. (b) Dai, X.; Kapoor, P.; Warren, T. H. "$[Me_2NN]Co(\eta^6$-Toluene): O=O, N=N, and O=N Bond Cleavage Provides β-Diketiminato Cobalt μ-Oxo and Imido Complexes." *J. Am. Chem. Soc.* **2004**, *126* (15), 4798–4799. (c) Kogut, E.; Wiencko, H. L.; Zhang, L.; Cordeau, D. E.; Warren, T. H. "A Terminal Ni(III)-Imide with Diverse Reactivity Pathways." *J. Am. Chem. Soc.* **2005**, *127* (32), 11248–11249. (d) Cowley, R. E.; Holland, P. L. "Ligand Effects on Hydrogen Atom Transfer from Hydrocarbons to Three-Coordinate Iron Imides." *Inorg. Chem.* **2012**, *51* (15), 8352–8361. (e) King, E. R.; Sazama, G. T.; Betley, T. A. "Co(III) Imidos Exhibiting Spin Crossover and C-H Bond Activation." *J. Am. Chem. Soc.* **2012**, *134* (43), 17858–17861. (f) Zhang, L.; Liu, Y.; Deng, L. "Three-Coordinate Cobalt(IV) and Cobalt(V) Imido Complexes with N-Heterocyclic Carbene Ligation: Synthesis, Structure, and Their Distinct Reactivity in C-H Bond Amination." *J. Am. Chem. Soc.* **2014**, *136* (44), 15525–15528. (g) Wilding, M. J. T.; Iovan, D. A.; Betley, T. A. "High-Spin Iron Imido Complexes Competent for C–H Bond Amination." *J. Am. Chem. Soc.* **2017**, *139* (34), 12043–12049.

[8] (a) Liu, Y.; Du, J.; Deng, L. "Synthesis, Structure, and Reactivity of Low-Spin Cobalt(II) Imido Complexes $[(Me_3P)_3Co(NAr)]$." *Inorg. Chem.* **2017**, *56*, 8278–8286. (b) Saouma, C. T.; Peters, J. C. "M≡E and M=E Complexes of Iron and Cobalt That Emphasize Three-Fold Symmetry (E=O, N, NR)." *Coordination Chemistry Reviews*. 2011, pp 920–937. (c) Jenkins, D. M.; Betley, T. A.; Peters, J. C. "Oxidative Group Transfer to Co(I) Affords a Terminal Co(III) Imido Complex." *J. Am. Chem. Soc.* **2002**, *124* (38), 11238–11239. (d) Cowley, R. E.; Bontchev, R. P.; Sorrell, J.; Sarracino, O.; Feng, Y.; Wang, H.; Smith, J. M. "Formation of a Cobalt(III) Imido from a Cobalt(II) Amido Complex. Evidence for Proton-Coupled Electron Transfer." *J. Am. Chem. Soc.* **2007**, *129* (9), 2424–2425. (e) Shay, D. T.; Yap, G. P. A.; Zakharov, L. N.; Rheingold, A. L.; Theopold, K. H. "Intramolecular C-H Activation by an Open-Shell Cobalt(III) Imido Complex." *Angew. Chem., Int. Ed.* **2005**, *44* (10), 1508–1510. (f) Wu, B.; Hernández Sánchez, R.; Bezpalko, M. W.; Foxman, B. M.; Thomas, C. M. "Formation of Heterobimetallic Zirconium/Cobalt Diimido Complexes via a Four-Electron Transformation." *Inorg. Chem.* **2014**, *53* (19), 10021–10023. (g) Hu, X.; Meyer, K. "Terminal Cobalt(III) Imido Complexes Supported

by Tris(Carbene) Ligands: Imido Insertion into the Cobalt-Carbene Bond." *J. Am. Chem. Soc.* **2004**, *126* (50), 16322–16323.

[9] Hay-Motherwell, R. S.; Wilkinson, G.; Hussain-Bates, B.; Hursthouse, M. B. "Synthesis and X-Ray Crystal Structure of Oxotrimesityliridium(V)." *Polyhedron* **1993**, *12* (16), 2009–2012.

[10] Scepaniak, J. J.; Vogel, C. S.; Khusniyarov, M. M.; Heinemann, F. W.; Meyer, K.; Smith, J. M. "Synthesis, Structure, and Reactivity of an Iron(V) Nitride." *Science.* **2011**, *331* (6020), 1049–1052.

[11] Cowley, R. E.; Bontchev, R. P.; Duesler, E. N.; Smith, J. M. "Removing the Sting from the Tail: Reversible Protonation of Scorpionate Ligands in Cobalt(II) Tris(Carbene)Borate Complexes." *Inorg. Chem.* **2006**, *45* (24), 9771–9779.

[12] (a) Bergquist, C.; Fillebeen, T.; Morlok, M. M.; Parkin, G. "Protonation and Reactivity towards Carbon Dioxide of the Mononuclear Tetrahedral Zinc and Cobalt Hydroxide Complexes, [$Tp^{But,Me}$]ZnOH and [$Tp^{But,Me}$]CoOH: Comparison of the Reactivity of the Metal Hydroxide Function in Synthetic Analog." *J. Am. Chem. Soc.* **2003**, *125* (20), 6189–6199. (b) Singh, U. P.; Babbar, P.; Tyagi, P.; Weyhermüller, T. "A Mononuclear Cobalt(II) Hydroxo Complex: Synthesis, Molecular Structure, and Reactivity Studies." *Transit. Met. Chem.* **2008**, *33* (8), 931–940.

[13] Cirera, J.; Ruiz, E.; Alvarez, S. "Stereochemistry and Spin State in Four-Coordinate Transition Metal Compounds." *Inorg. Chem.* **2008**, *47* (7), 2871–2889.

[14] Hana, F.; Lough, A. J.; Lavoie, G. G. "Coordinatively- and Electronically-Unsaturated Square Planar Cobalt(III) Complexes of a Pyridine Dianionic Pincer Ligand." *Dalt. Trans.* **2017**, *46*, 16228–16235.

[15] (a) Green, M. T. "Application of Badger's Rule to Heme and Non-Heme Iron-Oxygen Bonds: An Examination of Ferryl Protonation States." *J. Am. Chem. Soc.* **2006**, *128* (6), 1902–1906. (b) Spaeth, A. D.; Gagnon, N. L.; Dhar, D.; Yee, G. M.; Tolman, W. B. "Determination of the Cu(III)-OH Bond Distance by Resonance Raman Spectroscopy Using a Normalized Version of Badger's Rule." *J. Am. Chem. Soc.* **2017**, *139* (12), 4477–4485.

[16] Warren, J. J.; Tronic, T. A.; Mayer, J. M. "Thermochemistry of Proton-Coupled Electron Transfer Reagents and Its Implications." *Chem. Rev.* **2010**, *110* (12), 6961–7001.

[17] Kaljurand, I.; Kütt, A.; Sooväli, L.; Rodima, T.; Mäemets, V.; Leito, I.; Koppel, I. A. "Extension of the Self-Consistent Spectrophotometric Basicity Scale in Acetonitrile to a Full Span of 28 p$K_a$ Units: Unification of Different Basicity Scales." *J. Org. Chem.* **2005**, *70* (3), 1019–1028.

[18] Gardner, J. G.; Schneider, J. E.; Anderson, J. S. "Two, Three, or Not to Be? Elucidating Multiple Bonding in d 6 Pseudotetrahedral Oxo and Imide Complexes." *Inorg. Chem.* **2021**, acs.inorgchem.1c01022.

[19] Dhar, D.; Tolman, W. B. "Hydrogen Atom Abstraction from Hydrocarbons by a Copper(III)-Hydroxide Complex." *J. Am. Chem. Soc.* **2015**, *137* (3), 1322–1329.

[20] (a) Evans, J. C. "The Vibrational Spectra and Structure of the Vanadyl Ion in Aqueous Solution." *Inorg. Chem.* **1963**, *2* (2), 372–375. (b) Zaragoza, J. P. T.; Siegler, M. A.; Goldberg, D. P. "A Reactive Manganese(IV)-Hydroxide Complex: A Missing Intermediate in Hydrogen Atom Transfer by High-Valent Metal-Oxo Porphyrinoid Compounds." *J. Am. Chem. Soc.* **2018**, *140* (12), 4380–4390.

[21] Mehn, M. P.; Brown, S. D.; Jenkins, D. M.; Peters, J. C.; Que, L. "Vibrational Spectroscopy and Analysis of Pseudo-Tetrahedral Complexes with Metal Imido Bonds." *Inorg. Chem.* **2006**, *45* (18), 7417–7427.

[22] McGarvey, B. R.; Telser, J. "Simple Ligand-Field Theory of $d^4$ and $d^6$ Transition Metal Complexes with a $C_3$ Symmetry Axis." *Inorg. Chem.* **2012**, *51* (11), 6000–6010.

[23] Hill, E. A.; Zhao, N.; Filatov, A. S.; Anderson, J. S. "Nickel(II)-Methyl Complexes Adopting Unusual Seesaw Geometries." *Chem. Commun.* **2020**, *56* (57), 7861–7864.

[24] Jenkins, D. M.; Peters, J. C. "Spin-State Tuning at Pseudotetrahedral $d^7$Ions: Examining the Structural and Magnetic Phenomena of Four-Coordinate $[BP_3]Co^{II}$-X Systems." *J. Am. Chem. Soc.* **2005**, *127* (19), 7148–7165.

[25] Kolomeitsev, A. A.; Koppel, I. A.; Rodima, T.; Barten, J.; Lork, E.; Röschenthaler, G.-V.; Kaljurand, I.; Kütt, A.; Koppel, I.; Mäemets, V.; Leito, I. "Guanidinophosphazenes: Design, Synthesis, and Basicity in THF and in the Gas Phase." *J. Am. Chem. Soc.* **2005**, *127* (50), 17656–17666.

[26] Abdur-Rashid, K.; Fong, T. P.; Greaves, B.; Gusev, D. G.; Hinman, J. G.; Landau, S. E.; Lough, A. J.; Morris, R. H. "An Acidity Scale for Phosphorus-Containing Compounds Including Metal Hydrides and Dihydrogen Complexes in THF: Toward the Unification of Acidity Scales." *J. Am. Chem. Soc.* **2000**, *122* (38), 9155–9171.

[27] Krause, L.; Herbst-Irmer, R.; Sheldrick, G. M.; Stalke, D. "Comparison of Silver and Molybdenum Microfocus X-Ray Sources for Single-Crystal Structure Determination." *J. Appl. Crystallogr.* **2015**, *48* (1), 3–10.

[28] Sheldrick, G. M. "SHELXT - Integrated Space-Group and Crystal-Structure Determination." *Acta Crystallogr. Sect. A Found. Crystallogr.* **2015**, *71* (1), 3–8.

[29] (a) Dolomanov, O. V; Bourhis, L. J.; Gildea, R. J.; Howard, J. A. K.; Puschmann, H. "OLEX2: A Complete Structure Solution, Refinement and Analysis Program." *J. Appl. Crystallogr.* **2009**, *42* (2), 339–341. (b) Sheldrick, G. M. "Crystal Structure Refinement with SHELXL." *Acta Crystallogr. Sect. C Struct. Chem.* **2015**, *71*, 3–8.

[30] Neese, F. "The Orca Program System." *Wiley Interdiscip. Rev. Mol. Sci.* **2012**, *2*, 73–78.

[31] "HyperChem(TM) Professional 7.51." Hypercube, Inc.: 1115 NW 4th Street, Gainesville, Florida 32601, USA.

[32] Putz, D. H.; Brandenburg, D. K. "Diamond - Crystal and Molecular Structure Visualization, Crystal Impact." GbR, Kreuzherrenstr. 102, 53227 Bonn, Germany.

[33] Hanwell, M. D.; Curtis, D. E.; Lonie, D. C.; Vandermeerschd, T.; Zurek, E.; Hutchison, G. R. "Avogadro: An Advanced Semantic Chemical Editor, Visualization, and Analysis Platform." *J. Cheminform.* **2012**, *4* (8).

[34] (a) Neese, F.; Wennmohs, F.; Becker, U.; Riplinger, C. "The ORCA Quantum Chemistry Program Package." *J. Chem. Phys.* **2020**, *152* (22), 224108. (b) Handy, N. C.; Cohen, A. J. "Left-Right Correlation Energy." *Mol. Phys.* **2001**, *99* (5), 403–412. (c) Cohen, A. J.; Handy, N. C. "Dynamic Correlation." *Mol. Phys.* **2001**, *99* (7), 607–615. (d) Lee, C.; Yang, W.; Parr, R. G. "Development of the Colle-Salvetti Correlation-Energy Formula into a Functional of the Electron Density." *Phys. Rev. B* **1988**, *37* (2), 785–789.

[35] York, D. M.; Karplus, M. "A Smooth Solvation Potential Based on the Conductor-Like Screening Model." *J. Phys. Chem. A* **1999**, *103* (50), 11060–11079.

[36] (a) Weigend, F.; Ahlrichs, R. "Balanced Basis Sets of Split Valence, Triple Zeta Valence and Quadruple Zeta Valence Quality for H to Rn: Design and Assessment of Accuracy." *Phys. Chem. Chem. Phys.* **2005**, *7* (18), 3297. (b) Weigend, F. "Accurate Coulomb-Fitting Basis Sets for H to Rn." *Phys. Chem. Chem. Phys.* **2006**, *8* (9), 1057.

[37] (a) Poater, J.; Solà, M.; Duran, M.; Fradera, X. "The Calculation of Electron Localization and Delocalization Indices at the Hartree-Fock, Density Functional and Post-Hartree-Fock Levels of Theory." *Theor. Chem. Accounts Theory, Comput. Model. (Theoretica Chim. Acta)* **2002**, *107* (6), 362–371. (b) Matito, E.; Poater, J.; Solà, M.; Duran, M.; Salvador, P. "Comparison of the AIM Delocalization Index and the Mayer and Fuzzy Atom Bond Orders." *J. Phys. Chem. A* **2005**, *109* (43), 9904–9910. (c) Outeiral, C.; Vincent, M. A.; Martín Pendás, Á.; Popelier, P. L. A. "Revitalizing the Concept of Bond Order through Delocalization Measures in Real Space." *Chem. Sci.* **2018**, *9* (25), 5517–5529.

[38] (a) Becke, A. D. "A Multicenter Numerical Integration Scheme for Polyatomic Molecules." *J. Chem. Phys.* **1988**, *88* (4), 2547–2553. (b) Lu, T.; Chen, F. "Multiwfn: A Multifunctional Wavefunction Analyzer." *J. Comput. Chem.* **2012**, *33* (5), 580–592.

# Chapter 3: Experimental Evidence for p$K_a$-Driven Asynchronicity in C–H Activation by a Terminal Co(III)-Oxo Complex

This chapter has been adapted from the following with permission: Goetz, M. K.; Anderson, J. S. *J. Am. Chem. Soc.* **2019**, *141*, 4051-4062. 

## 3.1 Introduction

Transition metal-oxo complexes are a remarkable class of intermediates that mediate important C–H activation reactivity in many fields including biology and organic synthesis. As an archetypal example, cytochrome P450 enzymes employ high valent iron-oxo species to facilitate the oxidative degradation of pharmaceuticals.[1] Inspired by the success of nature, a variety of synthetic transition metal-oxo complexes have been made and their C–H activation reactivity studied thoroughly.[2] Transition metal catalyzed C–H activation has also been increasingly investigated as a synthetic strategy, with particular emphasis on controlling selectivity.[3] C–H activation by a transition metal-oxo complex involves the net transfer of a hydrogen atom and discussion of the intricacies of this transfer has also been a topic of intense interest.[4] Understanding this process in detail is crucial for providing a framework for the factors that govern reactivity and selectivity in both natural and synthetic systems.

A broad body of research dedicated to understanding C–H activation by transition metal-oxo complexes has established that the reactivity is generally dictated by the thermodynamics of the bond dissociation (free) energies (BD(F)Es) of the C–H bond being broken and the O–H bond

being formed. This paradigm, which follows the Bell-Evans-Polanyi principle,[5] suggests that in the simplest case, electronic selectivity should be exclusive for the homolytically weakest C–H bond in the substrate.[2a,4a,6] However, net hydrogen atom transfer from an organic substrate to a transition metal-oxo complex can occur via multiple possible mechanisms (Scheme 3.1).[4a,7] This process involves the transfer of both a proton and an electron which can be transferred simultaneously in a coupled fashion (concerted proton-electron transfer, CPET) or stepwise (proton transfer-electron transfer, PTET, or electron transfer-proton transfer, ETPT). It is generally accepted that coupling movement of the proton and electron is energetically favorable; thus, the details of how a proton and electron may couple in these transfers has important implications in C–H activation reactivity.[4e,8]

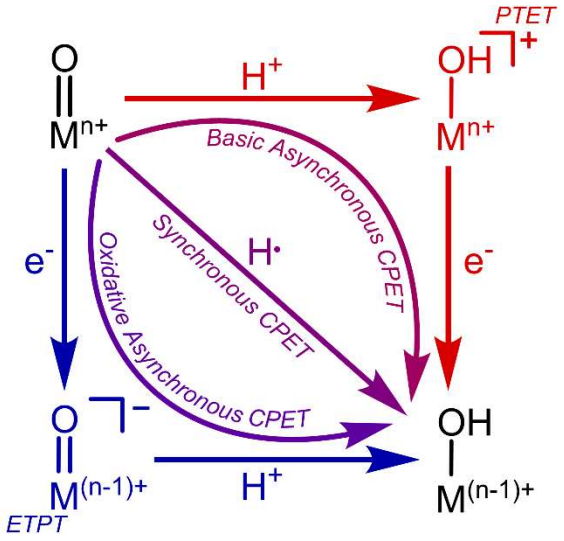


Scheme 3.1. Mechanisms of net H–atom transfer.

In addition to the limiting extremes mentioned above, it has been proposed that concerted proton and electron transfer can occur along a spectrum of "asynchronicity" in which the transition state for the net hydrogen atom transfer can contain either more proton transfer or electron transfer

character (Scheme 3.1).[7a,7c] Computational quantification of this distinction has been newly developed and suggests that more synchronous processes actually have higher activation barriers.[7b] This computational proposal has intriguing implications for the selectivity of transition metal oxo mediated C–H activation, but there is a dearth of experimental support for this theory as the vast majority of well-studied oxo complexes display rates which depend on BD(F)Es as discussed above.

There are some limited examples that demonstrate alternative basicity controlled mechanisms of C–H activation.[7a,9] For instance, Borovik and coworkers report that their $[(H_3buea)Mn^{III}O]^{2-}$ complex activates the weak C–H bond of 9,10-dihydroanthracene by utilizing a PTET mechanism due the high basicity of the $Mn^{III}$-oxo complex ($pK_{aDMSO}$ = 28.3).[9c] The effects of oxo or hydroxo ligand basicity have been invoked in other systems as well. For instance, compensation for low oxidation potentials with increased basicity to maintain a high $BDFE_{O–H}$ (Equation 3.1) has been seen in both synthetic and natural systems such as cytochrome P450 enzymes.[6b,10] Nonetheless "basic asynchronous CPET" has not been studied in a systematic fashion but may be vitally important to these systems.[7a,7b]

We have previously reported an unusual late transition metal-oxo complex $PhB(^tBuIm)_3Co^{III}O$ (**3**, Scheme 3.2) and preliminary studies of its C–H activation reactivity.[11] In the current chapter, we have compared key thermodynamic parameters and the reactivity of **3** with 9,10-dihydroanthracene (DHA) to related examples reported in the literature. This comparison reveals that **3** is one of the more basic metal-oxo complexes reported in the literature. In addition to these experiments, we have thoroughly investigated the reactivity of **3** with a variety of H–atom donors and found that contrary to the generally established pattern, the reactivity of **3** is dependent on the

p$K_a$ of the substrate instead of its BDE$_{C–H}$. Experimental and computational examination of the transition state provides insight into the mechanism of H–atom transfer in the current system and supports the agency of a basic asynchronous CPET mechanism in the C–H activation reactivity of **3** (Scheme 3.1). This work represents a clear example of experimental evidence for asynchronicity in C–H activation and opens the door for employing this concept in designing new oxidative reactivity with alternative electronic selectivity.

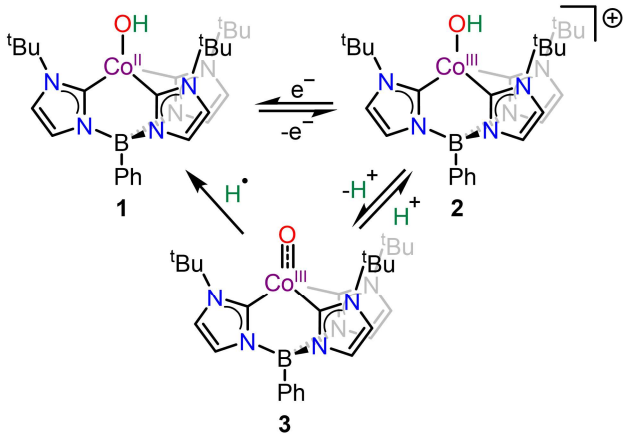


**Scheme 3.2.** Co complexes discussed in this chapter.

## 3.2 Results and Discussion

### 3.2.1 Thermodynamics

In beginning to examine the C–H activation reactivity in this system, we first sought to compare the BDFE for the O–H bond in **1** to other examples in the literature. This was done using the relationship between p$K_a$, $E^0$, and BDFE outlined in Equation 3.1 and Scheme A2.1. Previously, cyclic voltammetry data were collected that showed that the $Co^{II}/Co^{III}$ oxidation potential is –0.23 V versus $Fc/Fc^+$ in acetonitrile (MeCN, Fc = ferrocene, Figure A2.1).[11] Additionally, the p$K_a$ of **2** was measured as 25.58(5) in MeCN after $^1$H NMR spectroscopic analysis of a titration of **3** with

[HMTBD][$BF_4$] (p$K_{aMeCN}$ = 25.49[12]) in MeCN-$d_3$ (See Chapter 2.2.1). Using the *C* value of 54.9 kcal/mol in MeCN,[4a] we calculated a $BDFE_{O–H}$ of 84.6 kcal/mol (Equation 3.1, Scheme A2.1). This value gives a useful benchmark for the types of C–H bonds that might be expected to be activated by **3**.

Equation 3.1 $$BDFE = 1.37pK_a + 23.06E^0 + C$$

The $BDFE_{O–H}$ of **1** is comparable to a sample of other well-studied transition metal oxo/hydroxo complexes (Table 3.1), and it therefore might be expected that **3** would activate C–H bonds analogously to these other species. However, it appears that the balance between p$K_a$ and oxidation potential for the cobalt complex discussed here is weighted in favor of the basicity of the oxo ligand instead of the oxidizing potential of the complex. Additionally, when compared to computed p$K_a$ and $E^0$ values for a series of non-heme $Fe^{IV}$-oxo complexes, complex **3** is much more basic and much less oxidizing.[7b] This imbalance could affect the mechanism of C–H activation and has been proposed to be a determining factor in asynchronicity.[7b]

**Table 3.1.** Thermodynamic data for selected transition metal oxo/hydroxo complexes and their reactivity parameters with DHA.

| Complex | $\Delta H^{\ddagger}$ (kcal/mol)[a] | $\Delta S^{\ddagger}$ (e.u.)[a] | $k_2$ ($M^{-1}s^{-1}$)[a] | KIE ($k_H/k_D$) | p$K_a$ (DMSO)[b] | $E^0$ (V vs $Fc/Fc^+$)[c] | $BDFE_{O-H}$ (kcal/mol) | Ref. |
|---|---|---|---|---|---|---|---|---|
| $PhB(^tBuIm)_3Co^{III}O$[d] | 13(2) | –20(6) | 0.0584(8) | 9.2(6) | ~15 | –0.23 | 84.6 | this work |
| $[(H_3buea)Fe^{IV}O]^-$[e] | n.r. | n.r. | n.r. | n.r. | 11 | 0.036 | 87 | 1 |
| $[(H_3buea)Mn^{IV}O]^-$[e] | 5(1) | –49(4) | 0.026(2) | 6.8 | 15 | –0.11 | 89 | 9c |
| $[(H_3buea)Mn^{III}O]^{2-}$[e] | 14(2) | –14(6) | 0.48(4) | 2.6 | 28.3 | –1.51 | 77 | 9c |
| $[Fe^{IV}O(TMC)(MeCN)]^{2+}$[f] | n.r. | n.r. | 0.14 | 10 | n.r. | n.r. | 84(1) | 6d |
| $(Cz)Mn^VO$[g] | n.r. | n.r. | $1.8(5)\cdot10^{-5}$ | n.r. | ~11 | –0.33 | ~80 | 6b |
| $LCu^{III}OH$[h] | 5.4(2) | –30(2) | 186 | 29 | ~18 | –0.076 | 90(3) | 6e |
| $[Ru^{IV}O(bpy)_2py]^{2+}$ | n.r. | n.r. | 125 | 35(5) | <–2 | >2.2 | 84.8 | 1 |
| $Fe^{IV}O(TPFPP)$[i] | n.r. | n.r. | 13(2) | 20 | n.r. | n.r. | n.r. | 1 |

[a]Values for reaction with DHA at room temperature. [b]p$K_a$ value for $M^{n+}$-O/$M^{n+}$-OH adjusted using the correlation between p$K_a$ values in DMSO, MeCN, THF, and $H_2O$ as necessary. [c]$E^0$ for $M^{n+}$-OH/$M^{(n-1)+}$-OH adjusted versus $Fc/Fc^+$ as necessary. [d]$PhB(^tBuIm)_3^-$ = tris(1-*tert*-butylimidazol-2-ylidene)phenylborate. [e]$H_3buea^{3-}$ = tris[($N_3$-*tert*-butylureayl)-N-ethylene]aminato. [f]TMC = 1,4,8,11-tetramethyl-1,4,8,11-tetraazacyclotetradecane. [g]$Cz^{3-}$ = octakis(para-tert-butylphenyl)corrolazinato. [h]$L^{2-}$ = N,N’ -bis(2,6-diisopropylphenyl)-2,6-pyridinedicarboxamide. [i]$TPFPP^{2-}$ = meso-tetrakis(pentafluorophenyl)porphinato. Entries depicting n.r. indicate values not reported to the best of our knowledge.

### 3.2.2 Reactivity of PhB($^t$BuIm)$_3$Co$^{III}$O with 9,10-Dihydroanthracene

As was previously reported, **3** reacts cleanly with DHA to produce **1** and anthracene (Figure 3.1) under pseudo-first order conditions. Due to the common use of DHA as a model substrate for the C–H activation reactivity of transition metal-oxo/hydroxo species (Table 3.1), we chose to investigate the reactivity of **3** and DHA further. Collecting rate data at variable concentrations of DHA showed a dependence of the rate of reaction on the concentration of DHA, giving a second order rate constant, $k_2$ = 5.84(8)•10$^{-2}$ M$^{-1}$s$^{-1}$ (Figure A2.5, Figure A2.6). This demonstrates that the reaction follows a second order rate law overall, being first order in [Co] and first order in [DHA]. This $k_2$ value falls in the middle of the range of other transition metal-oxo/hydroxo complexes.

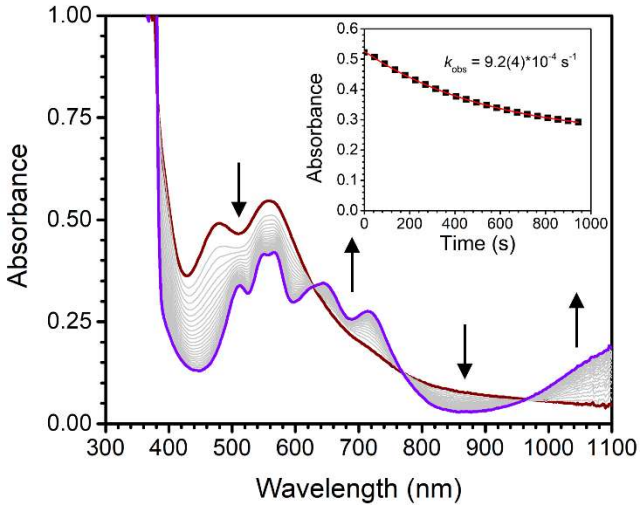


**Figure 3.1.** UV-vis spectra of the reaction between **3** (dark red trace) and 10 equivalents of DHA to produce **1** and anthracene (purple trace). Gray traces indicate 1-minute time points. Inset: pseudo-first order kinetic analysis of the reaction monitored at 470 nm.

Additionally, we measured a kinetic isotope effect (KIE) when **3** was reacted with DHA-$d_4$ of 9.2±0.6 (Figure A2.7). A KIE of this magnitude is common for C–H activation reactions carried

out by transition metal oxo/hydroxo species (Table 3.1) and is slightly beyond the "classical limit" of ~7, implying some degree of contribution from tunneling effects.[13] This is not surprising, given that this reaction involves the overall transfer of both a proton and an electron, but our measured value is far from the extremely high (~30) KIE values determined for some metal oxo/hydroxo complexes.[6e] Generally, larger KIE values are consistent with concerted mechanistic processes where the transfer of the electron is intimately coupled to the transfer of the proton, potentially through tunneling. However, KIEs can vary widely depending on the exact nature of the transition state.[4e,14] This fact makes conclusive interpretation of KIEs difficult.

Finally, we sought to determine the activation parameters, $\Delta H^{\ddagger}$ and $\Delta S^{\ddagger}$, for the reaction between **3** and DHA. This information has been reported for some transition metal oxo/hydroxo complexes that react with DHA, allowing for comparison of our system to those previously reported. Collection of rate data at various temperatures and fitting using the Eyring equation (Figure A2.8, Figure A2.9) gave the values $\Delta H^{\ddagger}$ = 13(2) kcal/mol and $\Delta S^{\ddagger}$ = –20(6) e.u. The negative entropy of activation is consistent with a bimolecular transition state in which two species must come together for the reaction to proceed. Such a transition state would be consistent with any of the mechanistic reaction pathways laid out in Scheme 3.1 and cannot be used to distinguish between them. The activation parameters determined for **3** are typical in the series of transition metal oxo/hydroxo complexes shown in Table 3.1, with activation enthalpies between 5 to 15 kcal/mol and activation entropies between −15 to −50 e.u.

### 3.2.3 Hydrogen Atom Transfer Reactivity with Various Substrates

As was mentioned above, the general trend in reactivity for transition metal oxo complexes with various H–atom donors is that substrates with stronger C–H bonds react more slowly.[4a,6b] In an

effort to investigate whether or not the reactivity of complex **3** follows this same trend, we examined the reactivity of **3** with a series of H–atom donors with different $BDE_{C–H}$ values (Figure A2.10-Figure A2.20) and the results of these studies are presented in Table 3.2 as observed rate constants ($k_{obs}$). All of these reactions demonstrate isosbestic conversion from **3** to **1** by UV-vis spectroscopy (Figure 3.1). Additionally, the reactions of **3** with DHA and fluorene were examined by GC-MS and the expected products of the reaction (anthracene and 9,9'-bifluorenyl, respectively) were observed with 75-100% conversion (Figure A2.26, Table A2.1), supporting the clean transformations seen by UV-vis spectroscopy.

**Table 3.2.** Kinetic data for the reaction of **3** with various C–H substrates.

| Substrate | $k_{obs}$ ($10^{-4}s^{-1}$)[a] | $k_2$ ($10^{-2}M^{-1}s^{-1}$) | KIE ($k_H/k_D$) | p$K_a$ (DMSO)[b] | $BDE_{C–H}$ (kcal/mol)[c] |
|---|---|---|---|---|---|
| 9,10-dihydroanthracene[d] | 9.2(4) | 5.84(8) | 9.2(6) | 30.1 | 76.3 |
| xanthene | 14.1(8) | n.d. | n.d. | 30.0 | 75 |
| 1,1,3,3-tetraphenylpropene | 1.0(3) | n.d. | n.d. | 25.8 | 77 |
| diphenylmethane | 1.5(4) | 1.2(4) | n.d. | 32.3 | 84.5 |
| 1,3-cyclohexadiene[d] | 0.60(7) | 0.27(2) | n.d. | 35 | 74.3 |
| 9-X-9*H*-fluorene | | | | | |
| X = H | 95(3) | 61(4) | 3.1(1) | 22.6 | 82 |
| $^t$Bu | 11(3) | n.d. | n.d. | 24.4 | 79.9 |
| Ph | 3700(500) | n.d. | n.d. | 17.9 | 74 |

[a]Determined using 10 equivalents of substrate per equivalent of Co complex either directly or from the $k_2$ value. [b]Data taken from the Bordwell p$K_a$ table.[15] [c]Data taken from the CRC's Handbook of Bond Dissociation Energies.[16] [d]Rates corrected for stoichiometry. Entries depicting n.d. indicate values that were not determined.

Surprisingly, when the kinetic data are plotted as the log($k_{obs}$) versus $BDE_{C–H}$ of substrate (Figure 3.2A) no discernible correlation between the $BDE_{C–H}$ of the substrate and the rate of reactivity is observed. This is contrary to what might be expected based on literature precedent. As a particularly illustrative series, the reactivity of **3** with 1,3-cyclohexadiene (CHD), DHA, and fluorene shows an inverse relationship with $BDE_{C–H}$. To explain this discrepancy, we considered additional parameters that could correlate with reactivity. Two likely thermodynamic parameters are the p$K_a$ or $E^0$ of the C–H substrate. Such parameters might be expected to dictate the reactivity if the mechanism were stepwise or asynchronous (Scheme 3.1). Plotting the log of the $k_{obs}$ values versus the gas phase ionization energies (Figure A2.21) shows little correlation between these two quantities, as might be expected due to the low oxidation potential of our system. Alternatively, examination of a plot of the log of the $k_{obs}$ values versus the p$K_a$ of each substrate (Figure 3.2B) reveals a linear correlation where substrates with higher p$K_a$ values react with slower rates. It is prudent to note that while there is a definitive correlation between the rate of C–H activation and the p$K_a$ of the substrate being studied, there are a few substrates that deviate from the line. Most notable in this regard are 9-(*tert*-butyl)-9*H*-fluorene and 1,1,3,3-tetraphenylpropene. Both of these substrates contain tertiary C–H bonds, likely introducing steric clashing with the three *tert*-butyl groups that surround the Co–O bond in **3**. We argue that this steric effect likely leads to aberrantly slow observed rates for these substrates.

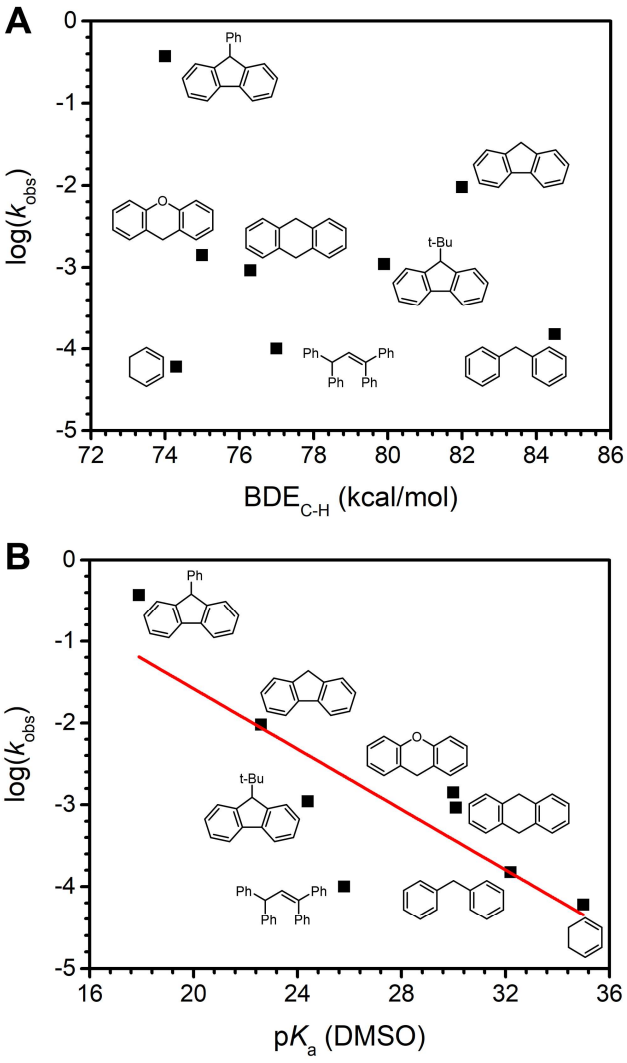


**Figure 3.2.** Plots of log($k_{obs}$) vs (A) BDE$_{C–H}$ of substrate and (B) p$K_a$ of substrate. Each $k_{obs}$ value is that for the reaction of **3** with 10 equivalents of substrate either determined directly or from the $k_2$ value (see Chapter 3.4 and Appendix 2). Linear fit in (B): log($k_{obs}$) = –0.18p$K_a$ + 2.1, $R^2$ = 0.65.

This correlation with p$K_a$ of the substrate suggests a basicity-controlled mechanism of H–atom transfer and could be consistent with a stepwise transfer of the proton and electron (PTET mechanism) or a concerted mechanism in which the transition state contains a significant amount of proton transfer character (i.e. basic asynchronous CPET). Stepwise C–H activation has been

observed previously in the literature,[9c,9d] with one well-studied example being the reactivity of a $Mn^{V}$-imide complex with substituted phenol substrates reported by Abu-Omar and coworkers. In this study, it was found that for acidic enough substituted phenols, the data were consistent with a stepwise PTET mechanism, while for the more basic substituted phenols, the data were consistent with a CPET process.[9d] On the other hand, asynchronous mechanisms of hydrogen atom transfer have also been proposed in some systems.[7a,7b] We therefore set out to distinguish between these two mechanisms.

### 3.2.4 Mechanism of C–H Activation by $PhB(^{t}BuIm)_3Co^{III}O$

In order to better understand the mechanism of C–H activation employed by **3**, we turned to various experimental techniques for studying the characteristics of the transition state of this reaction. Hammett analysis is a powerful technique in this regard that informs on the type of charge build-up on the atom of interest in the transition state. In this instance, we are probing the character of the charge build-up on the carbon of the C–H bond being broken. We therefore carried out Hammett analysis for *p*-substituted 9-phenyl-9*H*-fluorenes. It has been shown previously that for a synchronous CPET process, a negative Hammett correlation is expected.[6b] However, for mechanisms such as PTET or basic asynchronous CPET a positive Hammett correlation would be expected due to the build-up of negative charge.

The results of the Hammett analysis (Figure A2.22-Figure A2.24) are summarized in the first half of Table 3.3 and graphically represented in Figure 3.3. There is a positive Hammett correlation with $\rho = 0.87(3)$. This positive slope supports our hypothesis that the reactivity of **3** with H–atom donors is proton-controlled, consistent with either a stepwise PTET or basic asynchronous CPET mechanism. While this trend is clear in this series, we also wanted to carry out this analysis for

another class of substrates with C–H bonds at the upper end of the p$K_a$ range studied due to the fact that the substituted phenylfluorenes are relatively acidic (p$K_a$ ~19 in DMSO). Thus, we chose to look at 3-substituted xanthenes (p$K_a$ ~30 in DMSO). However, due to synthetic challenges in obtaining three or more 3-substituted xanthene substrates, kinetic analysis was carried out only with 3-methylxanthene (Figure A2.25) and xanthene and we were unable to obtain a meaningful Hammett slope. Nonetheless, if this class of substrates is reacting via the same mechanism as the *p*-substituted 9-phenyl-9*H*-fluorene derivatives, it would be expected that 3-methylxanthene would react at a slower rate than xanthene. Indeed, this is what was observed, with the rate of reaction for 3-methylxanthene being ~3x slower than that for xanthene (Table 3.3). Thus, we can say with confidence that these two classes of substrates appear to be reacting via the same basicity-controlled mechanism despite the large (~12 log units) difference in p$K_a$ between the two. This supports the assertion that the same mechanism is operative for all substrates studied in this work.

**Table 3.3.** Rates for substrates used in Hammett analyses.

| Substrate | | $k_{obs}$ ($10^{-2}$ $s^{-1}$)[a] | $\sigma_p^-$[b] |
|---|---|---|---|
| 9-(4-X-phenyl)-9*H*-fluorene | | | |
| X = | OMe | 22(3) | –0.26 |
| | Me | 28(4) | –0.17 |
| | H | 37(5) | 0.00 |
| | $CF_3$ | 140(40) | 0.65 |
| 3-X-xanthene | | | |
| X = | Me | 0.11(2) | –0.17 |
| | H | 0.141(8) | 0.00 |

[a]Values obtained using 10 equivalents of substrate. [b]Hammett parameters obtained from Hansch, Leo, and Taft.[17]

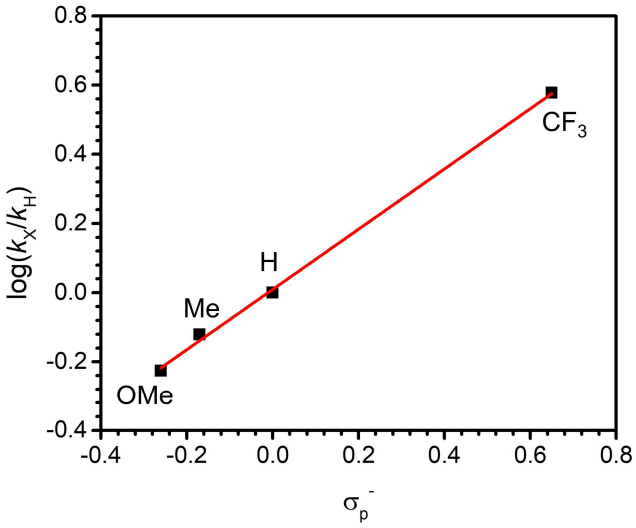


**Figure 3.3.** Hammett substituent plot for the reaction of **3** with 9-(4-X-phenyl)-9*H*-fluorenes. The red line shows the linear fit of the data: $\rho = 0.87(3)$, $R^2 = 0.996$.

In addition to the KIE data discussed earlier for DHA, we also determined the KIE for fluorene (Figure A2.20, Table 3.2). As has been previously established,[13] large KIE values beyond the classical limit of ~7 are indicative of contributions from tunneling effects, a common observation with transition metal oxo complexes that activate C–H bonds via synchronous CPET. We observed such a KIE with DHA (KIE = 9.2(6)) which indicated to us that there may be some contribution from tunneling. However, in the case of the more acidic fluorene, we observed a KIE of 3.1(1) which is well within the classical limit. As noted above, it is difficult to interpret KIE values without a detailed picture of the transition state.[4d,14] Nevertheless, we can propose a speculative interpretation of these comparative values. The observed KIEs could suggest that a stepwise PTET mechanism is operative for fluorene and there is a p$K_a$-dependent mechanism switch as seen in the $Mn^V$-imide system.[9d] Alternatively, this difference in KIE values may be explained by one asynchronous CPET mechanism where a larger degree of asynchronicity results in a smaller KIE (i.e. the proton is less coupled to the electron).[7b] The reaction between **3** and fluorene would be

expected to be more asynchronous than that between **3** and DHA due to the smaller p$K_a$ difference between **3** and fluorene.

All of the experimental data presented above support that proton transfer plays an integral role in the C–H activation reactivity of **3**, but these experiments cannot discern between a stepwise or concerted mechanism. As discussed above, we envision two likely mechanistic scenarios (Scheme 3.3). Firstly, one plausible possibility is a PTET mechanism where a pre-equilibrium PT to generate **2** and substrate anion is followed by ET to result in net H–atom transfer. Secondly, an alternative pathway where a basic asynchronous CPET is operative may also be feasible. Experimentally distinguishing between these two mechanisms is difficult, but we reasoned that if **2** were a genuine intermediate in the reactivity of **3**, we should be able to show that this species is kinetically competent to carry out the reaction and that we might be able to intercept it in some way to verify its agency.

It is reasonable to assume that the stepwise mechanism shown in Scheme 3.3 would occur under steady-state conditions. This imposes a $k_{et}$ (homogeneous electron transfer rate constant) value for the electron transfer between **2** and the substrate carbanion that can be determined from the measured $k_2$ value for a given reaction and the p$K_a$ difference between the substrate and **2** (See derivation in Appendix 2). Taking fluorene as an example substrate, a $k_{et}$ value of ~$10^6$ $M^{-1}s^{-1}$ at room temperature is required to be in agreement with the experimentally determined kinetics.

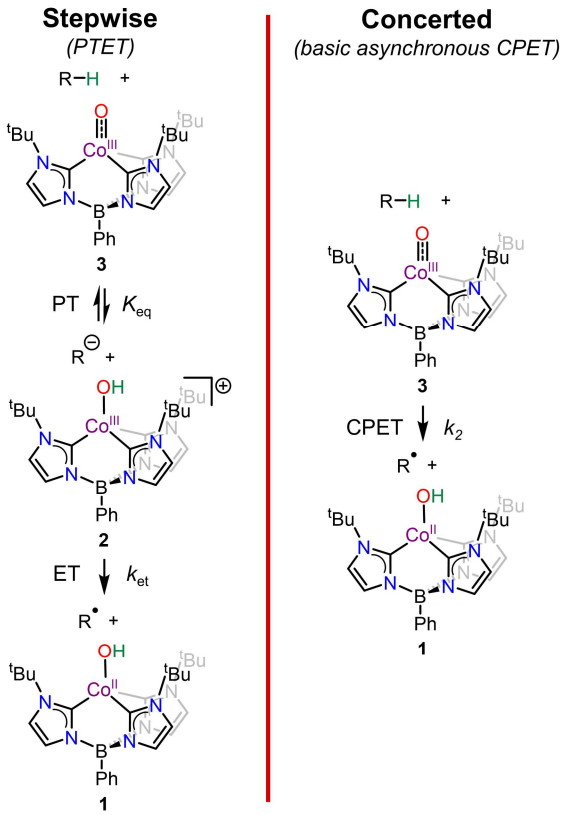


**Scheme 3.3.** Possible mechanisms of C–H activation by complex **3**.

We can estimate the upper bound of $k_{et}$ by measuring the intrinsic ability of **1**/**2** to give up/accept an electron using cyclic voltammetry (CV) and analyzing the change in $\Delta E_p$ with varying scan rate.[18] This measurement gives a $k_s$ value (the heterogeneous electron transfer rate constant) which can be correlated to $k_{et}$ given the assumption that $\Delta G^{\ddagger}$ changes negligibly from heterogeneous to homogeneous conditions, as has been previously shown.[19] We conducted this measurement (Figure A2.2-Figure A2.4, see Chapter 3.4 for mathematical details) and found that the upper bound $k_{et}$ for **1**/**2** is on the order of $10^3$ $M^{-1}s^{-1}$ at room temperature. However, this does not take into account the likely rate enhancement from what would be an exergonic electron transfer between **2** and the fluorenide anion. Thus, while it is likely that **2** cannot accept an electron fast

enough to match the measured kinetics for the reaction of **3** and fluorene (Table 3.2), this cannot be determined explicitly without direct measurement of $k_{et}$ for the reaction between **2** and fluorenide anion. Nonetheless, this provides indirect evidence against a stepwise PTET mechanism of C–H activation (Scheme 3.3).

We also attempted to intercept **2** to see if it were a bona-fide intermediate in the C–H activation reactivity of **3**. Given the steady-state approximation discussed earlier, it might be expected that in the presence of an appropriate deuterated acid, such as [DMTBD][$BF_4$], scrambling of deuterium into the organic product and the excess substrate would occur due to the presence of **2** and the substrate carbanion in solution. This hypothesis hinges on the equilibrium exchange being appropriately fast while the electron transfer rate from **2** to the carbanion is suitably slow. We can estimate a lower bound for the rate of equilibrium proton exchange from the p$K_a$ determination experiment described above, where the peaks in the $^1$H NMR spectrum were fully coalesced at −35 °C. This implies a minimum rate of exchange on the order of $10^2$ $s^{-1}$ at this temperature.[20] From the room temperature experimentally estimated $k_{et}$ presented above, we can expect that $k_{et}$ at −35 °C should be on the order of $10^1$ $M^{-1}s^{-1}$ (See Chapter 3.4). Thus, we can reasonably expect to observe deuterium incorporation if a pre-equilibrium is involved in the mechanism of C–H activation.

We carried out the scrambling experiment by reacting **3** with fluorene in the presence of excess [DMTBD][$BF_4$] and MTBD at −35 °C and evaluating the organic products by GC-MS to test for deuterium incorporation. Comparison of the mass spectra of both fluorene and 9,9'-bifluorenyl in the reaction mixtures with and without added deuterated acid reveals no deuterium incorporation in any of the fluorene-derived species (Figure A2.27). This observation strongly implies that there

is no buildup of **2** or substrate carbanion in the reaction mixture and thus supports a concerted net H–atom transfer mechanism, in this case basic asynchronous CPET.

### 3.2.5 Computational Analysis

While these experimental results are consistent with a concerted asynchronous process, we also wanted to obtain computational support for this pathway. We have performed two sets of DFT studies to probe these C–H activation reactions in detail. Firstly, we followed the procedure laid out by Srnec and coworkers for calculating the asynchronicity parameters, η, for the reactions of **3** with CHD, DHA, and fluorene (Table A2.2).[7b] The value η is a parameter that quantitatively informs on the relative thermodynamic contributions of p$K_a$ and redox potential to the driving force for a net H–atom transfer reaction. A negative η value implies that the p$K_a$ is the dominant driving force whereas a positive η value implies that the redox potential is dominant. Additionally, a larger magnitude of η demonstrates a greater imbalance of the contributions of p$K_a$ and redox potential to the driving force which results in a propensity for asynchronicity in the H–atom transfer reaction. In the current system, all three of the computed η values are negative, implying that the reactions proceed via asynchronous mechanisms with proton transfer character in the transition state. Additionally, η becomes more negative as the p$K_a$ of the substrate decreases, indicating that the reaction is more asynchronous for more acidic substrates. Finally, it is worth noting that the $k_2$ values reported in Table 3.2 trend logarithmically with η (Figure A2.28), with faster rates of reactivity seen for more asynchronous processes. These results are consistent with the theory of asynchronicity as laid out by Srnec, supporting the idea that lower barriers resulting from higher degrees of asynchronicity lead to faster rates of reactivity, which is observed experimentally in our system.

Secondly, we analyzed the reaction coordinate for C–H activation. As a starting point, we note that while both starting materials are singlets, we have been unable to locate a maximum along a singlet spin manifold. Instead, a maximum is observed along a triplet spin surface (Figure 3.4). The overall reaction to form **1** and the organic radical mandates a net spin change from $S = 0$ to $S = 1$ (or potentially $S = 2$ if the radical couples ferromagnetically) so the relevance of multiple spin manifolds is not surprising. The relative importance of different spin manifolds has been extensively invoked in transition metal oxo C–H activation reactivity as well as in the reactivity of related Fe carbene systems.[21] While we have largely focused this discussion on probing the relative importance of an asynchronous C–H activation mechanism, we acknowledge that the involvement of multiple spin states is a convolution that we have not yet thoroughly addressed.

To obtain further detail on the flow of protons and electrons along the reaction coordinate and in the transition state, we employed an intrinsic bond orbital (IBO) analysis as reported by Knizia and coworkers and recently applied to C–H activation by Fe-oxo complexes (Figure 3.4, Figure A2.29).[22] This computational technique enables analysis of the movement and localization of orbitals along a reaction coordinate. This allows us to visualize and quantify how the orbitals associated with electron transfer (Figure 3.4, blue orbital) and proton transfer (Figure 3.4, red orbital) change as the O–H bond forms. This analysis clearly indicates that both protons and electrons move along the reaction coordinate in a coupled manner. To further test the concept of asynchronicity, we plotted the normalized orbital movement as a function of the O–H distance along the reaction coordinate (Figure 3.4). This analysis supports that the proton and electron move in a concerted manner, but also shows that the degree of proton movement is greater than the degree of electron movement at intermediate steps along the reaction coordinate. This observation

is consistent with the concept of asynchronicity and supports our overall picture of the reaction and experimental results.

## 3.3 Conclusions

We have presented a thorough study of the C–H activation reactivity carried out by a $Co^{III}$-oxo complex and have determined that this reactivity occurs via basic asynchronous CPET. DFT calculations and experimental evidence indicate that the reaction does not employ a stepwise mechanism and the dependence of the rate on the p$K_a$ of the substrate indicates that proton movement is paramount. This is in direct contrast to the vast majority of previous systems where the reactivity is controlled by the substrate $BDE_{C–H}$. While such proton-controlled reactivity has been observed previously, these systems have invoked stepwise PTET mechanisms to explain their observations. To the best of our knowledge, this is the first example demonstrating experimental evidence for asynchronicity in C–H activation. This asynchronous pathway offers a compelling alternative to mechanisms that have been traditionally invoked. For instance, a basic asynchronous mechanism would imply selectivity for the most acidic C–H bond in a substrate as opposed to the homolytically weakest bond. Furthermore, asynchronous mechanisms may be relevant in a number of processes, as potentially indicated by the important role of basicity noted in cytochrome P450 enzymes.[10a] This observation could open the door to new selectivity in reactions carried out by transition metal-oxo complexes and adds to our growing understanding of C–H bond activation.

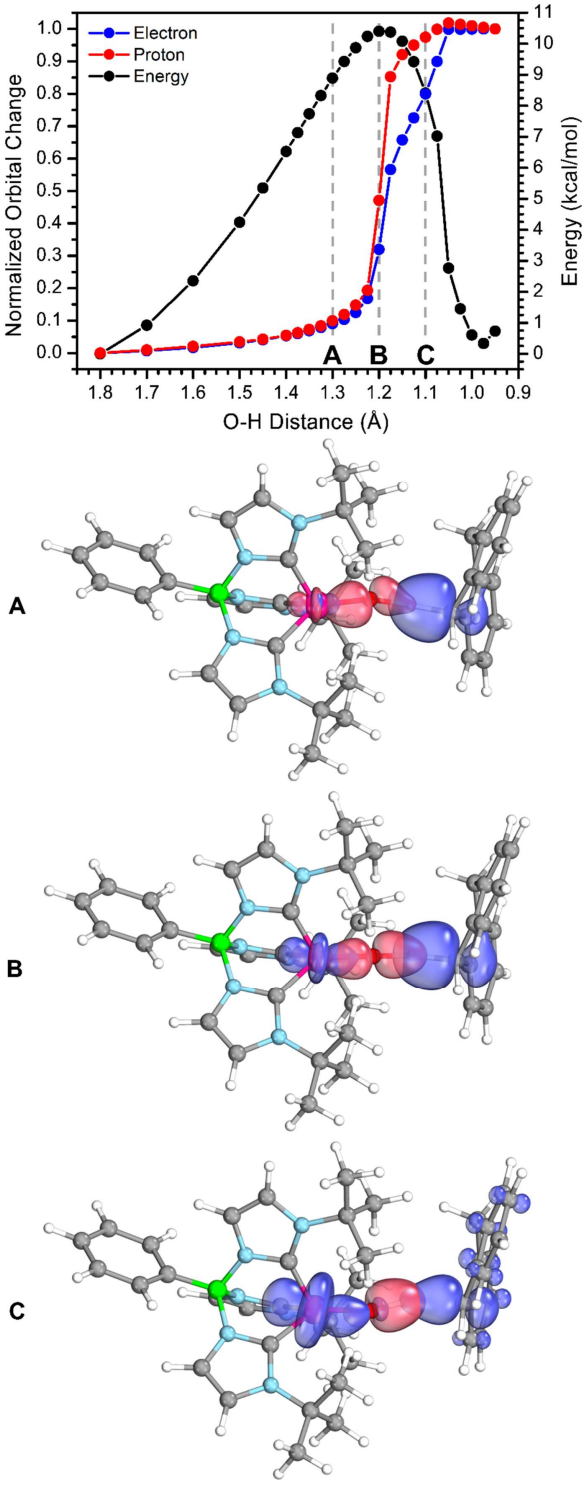


**Figure 3.4.** IBO analysis showing the normalized orbital movements involved in the proton transfer (red) and the electron transfer (blue). A, B, and C indicate the stationary points at O–H

distances of 1.3, 1.2, and 1.1 Å respectively with the blue orbital involved in the electron transfer and the red orbital involved in proton transfer.

## 3.4 Experimental

**General Considerations.** All manipulations were performed under a dry nitrogen atmosphere using either standard Schlenk techniques or in an mBraun Unilab Pro glovebox unless otherwise stated. All chemicals were obtained from commercial sources and used as received unless otherwise stated. Solvents were dried on a solvent purification system from Pure Process Technologies before storing over 4 Å molecular sieves under $N_2$. Tetrahydrofuran (THF) was stirred over NaK alloy and passed through a column of activated alumina prior to storing over 4 Å sieves under $N_2$. 9,10-dihydroanthracene, and xanthene were recrystallized from hexanes and fluorene and diphenylmethane were recrystallized from methanol prior to use. 1,3-cyclohexadiene was distilled and stored over 4 Å molecular sieves prior to use. DHA-$d_4$ was prepared according to a literature procedure and recrystallized prior to use.[23] All other substrates were synthesized using slightly modified literature procedures (see below). $PhB(^tBuIm)_3Co^{III}O$ was synthesized according to the previously reported procedure using potassium hexamethyldisilazide as the base.[11] UV-vis spectra were recorded on a Thermo Scientific Evolution 300 spectrometer with the VISIONpro software suite. The UV-vis spectra for the reaction of **3** with 9-(4-(trifluoromethyl)phenyl)-9*H*-fluorene were recorded using an Agilent HP 8453 spectrometer with the UV-vis ChemStation software suite. A Hellma Analytics Excalibur Immersion Probe with a 10 mm path length (Article No. 661-202-10-S-46) was used for variable temperature UV-vis spectroscopic measurements and a standard 1 cm quartz cuvette with an air tight screw cap with a puncturable Teflon seal was used for room temperature measurements. Variable temperature UV-

vis spectra were smoothed using the 10 points adjacent averaging function in Origin (OriginLab, Northhampton, MA). $^{1}H$ and $^{13}C$ NMR spectra were recorded on a Bruker DRX-400 spectrometer and referenced to residual proteo-solvent peaks. GC-MS data were collected using an Agilent 7890B GC equipped with an Agilent HP-5MS column coupled to an Agilent 5977A EI/PCI-MS. Isotope patterns were compared to the NIST library to confirm assignments. Electrochemical measurements were carried out using a BAS Epsilon potentiostat and using BAS Epsilon software version 1.40.67NT.

**Synthesis of 9-phenyl-9*H*-fluorene**. To a solution of lithium diisopropylamide (0.30 mmol made in situ from a 1:1 mixture of 2.5 M n-BuLi and diisopropylamine) in THF (3 mL) in the glovebox was added a solution of fluorene (166 mg, 0.10 mmol) in THF (3 mL). The bright orange solution was stirred for 30 minutes at room temperature after which fluorobenzene (141 μL, 0.15 mmol) was added. The resulting dark solution was stirred for 3 hours at room temperature before removal from the glovebox and addition of methanol (1 mL). Ethyl acetate was added to the pale yellow solution which was then washed twice with brine. The organic layer was dried over $MgSO_4$, filtered, and pumped down to a pale yellow solid. Recrystallization from ethanol (EtOH) gave pure 9-phenyl-9*H*-fluorene (90 mg, 37% yield) as a white solid which matched the reported $^{1}H$ NMR spectrum.[24] $^{1}H$ NMR ($CDCl_3$, 400 MHz): δ 7.80 (2H, d), 7.41-7.23 (9H, m), 7.10 (2H, d), 5.05 (1H, s).

**Synthesis of 9-(4-X-phenyl)-9*H*-fluorene (X = OMe, Me, or $CF_3$).** To a solution of 9-fluorenone (0.50 g, 2.8 mmol) in toluene (30 mL) under air was added $TsNHNH_2$ (0.775 g, 4.2 mmol) and the mixture heated at 80 °C for 2 hours. To the bright yellow homogeneous solution was added $K_2CO_3$ (0.575 g, 4.2 mmol) and 4-X-phenylboronic acid (4.2 mmol). The heterogenous

mixture was heated at reflux at 110 °C for 5 hours before cooling to room temperature. Dichloromethane (DCM) and saturated aqueous $NaHCO_3$ were added and the layers separated. The aqueous layer was washed twice with DCM followed by washing the combined organic layers once each with saturated aqueous $NaHCO_3$ and brine. The organic layer was dried with $MgSO_4$, filtered, and pumped down to a yellow solid. Recrystallization from EtOH afforded the desired compounds in pure forms which matched the reported $^1$H NMR spectra.[25] Yields were 47%, 32%, and 30% for X = OMe, Me, and $CF_3$, respectively. $^1$H NMR ($CDCl_3$, 400 MHz, X = OMe): δ 7.78 (2H, d), 7.37 (2H, t), 7.30-7.23 (4H, m), 7.00 (2H, d), 6.82 (2H, d), 5.01 (1H, s), 3.78 (3H, s). $^1$H NMR ($CDCl_3$, 400 MHz, X = Me): δ 7.78 (2H, d), 7.37 (2H, t), 7.32-7.23 (4H, m), 7.07 (2H, d), 6.99 (2H, d), 5.02 (1H, s), 2.31 (3H, s). $^1$H NMR ($CDCl_3$, 400 MHz, X = $CF_3$): δ 7.81 (2H, d), 7.53 (2H, t), 7.41 (2H, m), 7.27 (4H, m), 7.21 (2H, d), 5.10 (1H, s).

**Synthesis of 9-(*tert*-butyl)-9*H*-fluorene.** To a suspension of 9-fluorenone (1.05 g, 5.8 mmol) in 20 mL of hexanes was added a solution of $^t$BuLi dropwise (1.5 M in pentanes, 6.0 mL). The dark solution was allowed to stir at room temperature overnight after which $H_2O$ (25 mL) was added and the layers separated. The aqueous layer was extracted twice with hexanes and the combined organic layers washed once with $H_2O$. The organic layer was dried over $MgSO_4$, filtered, and the solvent evaporated. The residue was dissolved in DCM (20 mL) after which $Et_3SiH$ (2 mL) and $BF_3$•$Et_2O$ (1.6 mL) were added. The resulting homogeneous solution was stirred at room temperature for two days after which $H_2O$ (20 mL) was added. The aqueous layer was extracted twice with DCM and the combined organic layers dried over $MgSO_4$, filtered, and pumped down to an orange residue. The residue was dissolved in hexanes and run through a silica plug to remove orange impurities. The hexanes were removed and the resulting residue recrystallized from

methanol to give the desired product (220 mg, 17% yield) in pure form which matches the reported $^1$H NMR spectrum.[26] $^1$H NMR ($CDCl_3$, 400 MHz): δ 7.68 (2H, dt), 7.54 (2H, ddd), 7.33 (2H, tdd), 7.22 (2H, td), 3.63 (1H, s), 1.00 (9H, s).

**Synthesis of 1,1,3,3-tetraphenylpropene.** 1,1-diphenylethylene (353 μL, 2.0 mmol) and benzhydrol (184 mg, 1.0 mmol) were dissolved in DCM (30 mL). p-toluenesulfonic acid (190 mg, 1.1 mmol) and $FeCl_3$•$6H_2O$ (27 mg, 0.01 mmol) were added and the solution heated at reflux for 4 hours. The resulting green solution was cooled to room temperature and the solvent evaporated. The residue was extracted with $Et_2O$ and filtered through silica. Recrystallization from EtOH gave the desired product (289 mg, 83% yield) which matched the reported $^1$H NMR spectrum.[27] $^1$H NMR ($CDCl_3$, 400 MHz): δ 7.37-7.15 (20H, m), 6.53 (1H, d), 4.83 (1H, d).

**Synthesis of 3-methylxanthene.** This synthesis was carried out in two steps. First, the corresponding 3-methylxanthone was made following a modified literature procedure.[28] 2-nitrobenzaldehyde (2.00 g, 13.2 mmol), *m*-cresol (1.86 g, 19.8 mmol), $CuCl_2$ (89 mg, 0.66 mmol), $PPh_3$ (260 mg, 0.99 mmol), and $K_3PO_4$•$H_2O$ (6.70 g, 29.0 mmol) were mixed in ~100 mL of dry toluene. The heterogeneous mixture was refluxed at 110 °C under an active flow of $N_2$, during which it darkened. After cooling to room temperature, ~250 mL of DCM was added and the combined organic layers washed twice with $H_2O$ and once with brine. The organic layers were dried over $MgSO_4$, filtered, and pumped down to a dark residue. This residue was dissolved in pure DCM, washed twice with 1 M NaOH, dried over $MgSO_4$, filtered through silica to remove dark colored impurities, and pumped down to a brown solid. This solid was recrystallized from EtOH to give pure 3-methylxanthone (376 mg, 14% yield) which was carried on into the next step. $^1$H NMR ($CDCl_3$, 400 MHz): δ 8.35 (1H, dd), 8.22 (1H, d), 7.72 (1H, td), 7.48 (1H, dd), 7.38 (1H,

td), 7.30 (1H, s), 7.22 (1H, d), 2.52 (3H, s). A previously reported reduction procedure was used to produce 3-methylxanthene.[29] 3-methylxanthone (300 mg, 1.4 mmol) was dissolved in dry THF. $BH_3SMe_2$ (1.78 mL of a 2.0 M solution in THF) was added under $N_2$ and the reaction stirred at room temperature overnight. The THF was removed under vacuum and the residue dissolved in DCM. The organic layer was washed twice with 2 M NaOH and filtered. The filtrate was acidified with concentrated HCl and filtered again. The filtrate was then washed with $H_2O$, dried over $MgSO_4$, filtered, and pumped down to an off-white powder that was pure 3-methylxanthene (185 mg, 66% yield). The $^1$H NMR spectrum matched that reported in the literature. $^1$H NMR ($CDCl_3$, 400 MHz): δ 7.16 (2H, m), 7.03 (3H, m), 6.87 (2H, m), 4.01 (2H, s), 2.32 (3H, s).

**Synthesis of fluorene-*d*$_2$.** Fluorene (250 mg, 1.5 mmol) was dissolved in DMSO-$d_6$ (~0.8 M) and three equivalents of solid NaH were added. The suspension was stirred for 3-6 hours before addition of excess $D_2O$. The mixture was extracted with hexanes and the aqueous layer washed again with hexanes. The combined organic layers were washed with $H_2O$, dried over $MgSO_4$, filtered, and pumped down. The residue was recrystallized from methanol (90 mg, 36% yield). $^1$H NMR spectroscopy showed 95% deuterium incorporation.[30]

**Synthesis of [DMTBD][BF$_4$].** This was made analogously to [HMTBD][$BF_4$] described in Chapter 2.4, but $DBF_4$ was used instead of $HBF_4$•$Et_2O$. The $DBF_4$ was prepared *in situ* by mixing together $HBF_4$•$Et_2O$ and $D_2O$ in a 1:3 ratio by volume.[31] The product was recrystallized by layering a THF solution under $Et_2O$ at −35 °C and showed 90% deuterium incorporation at the acidic position by $^1$H NMR (200 mg, 51% yield).

**Procedure for kinetic studies.** Data for rate determination were collected in triplicate at ambient temperature unless otherwise noted. In a typical experiment, 2.0 mL of a 1.25 mM solution of **3** in THF was transferred to an air tight screw top cuvette. After an initial scan (or single absorbance data point at 470 nm) was collected, a solution of substrate in THF was injected through the septum in the screw top. The reaction was monitored for an appropriate amount of time to either reach completion or ~3 half-lives. To determine the observed rate $k_{obs}$ values, the data were analyzed by plotting the absorbance at 470 nm at time $t$ versus time in seconds and fitting the data to an exponential function, $A_t = A_{inf} + (A_0 - A_{inf})e^{-kt}$, where $A_{inf}$ is the absorbance at infinite time, $A_0$ is the initial absorbance, and k is the observed rate constant, $k_{obs}$. For diphenylmethane, this plot was generated using the absorbance at 556 nm due to a convoluting absorbance at 470 nm upon injection of substrate. To determine the second order rate constants $k_2$ for various substrates, the $k_{obs}$ values were collected at various concentrations of substrate and plotted vs the substrate concentration to give $k_2$ as the slope of the linear fit of the data. These $k_2$ values were used to estimate $k_{obs}$ at 10 equivalents of substrate for diphenylmethane and 1,3-CHD due to the kinetically competitive self-decay rate of **3** at low substrate concentration. KIE values were obtained by evaluating $k_H/k_D$ for DHA and fluorene using the $k_{obs}$ values obtained with 10 equivalents of substrate. Hammett analysis was carried out by comparing the relative rates ($k_{obs}$ obtained using 10 equivalents of substrate) of reaction of the substituted substrates to the unsubstituted 9-phenyl-9*H*-fluorene or xanthene.

**Determination of activation parameters for the reaction between 3 and DHA.** Data for rate determination were collected in triplicate at each temperature used for the Eyring analysis. In a typical experiment, 4.0 mL of a 1.25 mM solution of **3** in THF was transferred to a custom made,

air-tight apparatus equipped with a 14/20 ground glass joint, #2 size ground glass plug, and #25 size threaded Teflon plug for the immersion probe to go through which was sealed with a Teflon coated O-ring. The entire apparatus was sealed inside the glovebox and removed before cooling to the appropriate temperature (10 °C, 0 °C, −10 °C, −20 °C, and −30 °C) under a positive pressure of $N_2$ through the ground glass plug. After collecting an initial scan, 50 equivalents of DHA were added as a 1.25 M solution in THF (200 μL) injected through a rubber septum in the ground glass joint. The reaction was monitored until ~3 half-lives had been completed. To determine the observed rate $k_{obs}$ values, the data were analyzed by plotting $\ln((A_t-A_{inf})/(A_0-A_{inf}))$ (where $A_{inf}$ was estimated from reactions carried out in a cuvette at room temperature) vs time in seconds to give $k_{obs}$ as the slope of the linear fit of the data. Using the relationship $k_{obs} = [DHA]^*k_2$, the $k_2$ values were determined at each temperature and a plot of $\ln(k_2/T)$ vs 1/T was generated (where T is the temperature in Kelvin). The activation parameters $\Delta H^‡$ and $\Delta S^‡$ were determined from the linear fit via the Eyring equation (Figure A2.9, Table 3.1).

**Determination of the upper bound $k_{et}$ for 2 from CV measurements.** A 3 mM solution of **1** in MeCN was prepared with 0.1 M $TBAPF_6$ as the electrolyte. A glassy carbon working electrode with a 3 mm diameter was used along with a Pt wire counter electrode and a Ag wire reference electrode that was externally referenced to the $Fc/Fc^+$ couple. CVs were collected from −964 mV to +235 mV versus $Fc/Fc^+$ at varying scan rates (10 mV/s, 25 mV/s, 50 mV/s, 75 mV/s, 100 mV/s, 150 mV/s, 200 mV/s, 250 mV/s, 300 mV/s, 400 mV/s, and 800 mV/s). The peak anodic and cathodic current densities, $j_p$, were plotted versus the square roots of the scan rates ($\nu^{1/2}$). The linear fits of these data were used with Equation 3.2 (for quasi-reversible electron transfer) to determine the diffusion coefficients, $D_R$ and $D_O$, respectively, for the reduced (**1**) and oxidized (**2**) species. α

was assumed to be 0.5, n = 1 for the single electron transferred, and c is the concentration. The spread in the anodic and cathodic peak potentials ($\Delta E_p$) for each scan rate was converted to the dimensionless parameter $\Psi$ according to Reference 18. $\Psi$ was plotted versus $\nu^{-1/2}$ and the slope of the linear fit of this data was used with Equation 3.3 to determine $k_s$. Equation 3.4 shows the relationship between $\Delta G^{\ddagger}$ and $k$, where $Z$ is the collision frequency for the heterogeneous ($Z_E$, Equation 3.5, M = the mass of the complex, 533 g/mol) or homogeneous ($Z_H$, Equation 3.6, $\mu$ = the reduced mass of the reactant pair, 126 g/mol, r = the distance between the reactant pair, $7*10^{-8}$ cm) process. Assuming that the difference between $\Delta G^{\ddagger}$ for these processes is negligible (see Reference 19), $k_{et}$ can be estimated from $k_s$ using Equation 3.7. Estimating $k_{et}$ at different temperatures is done using Equation 3.8 which is derived from Equation 3.4 and Equation 3.6 and assumes $\Delta H^{\ddagger} \sim 10$ kcal/mol.

Equation 3.2 $$j_p = (3 * 10^5) n (n\alpha)^{1/2} D^{1/2} c \nu^{1/2}$$

Equation 3.3 $$\Psi = \left(\frac{D_O}{D_R}\right)^{\alpha} k_s \left(\frac{\pi D_O n F \nu}{RT}\right)^{-1/2}$$

Equation 3.4 $$\Delta G^{\ddagger} = -RT \ln\left(\frac{k}{Z}\right)$$

Equation 3.5 $$Z_E = \left(\frac{RT}{2\pi M}\right)^{1/2}$$

Equation 3.6 $$Z_H = (6.022 * 10^{20}) \left(\frac{8\pi RT}{\mu}\right)^{1/2} r^2$$

Equation 3.7 $$\frac{k_s}{Z_E} = \frac{k_{et}}{Z_H}$$

Equation 3.8 $$\frac{k_{T_2}}{k_{T_1}} = \left(\frac{T_2}{T_1}\right)^{\frac{1}{2}} e^{\frac{-\Delta H^{\ddagger}}{R}\left(\frac{1}{T_2} - \frac{1}{T_1}\right)}$$

**Reaction of 3 and fluorene in the presence of [DMTBD][$BF_4$] and MTBD at –35 °C.** Reactions were carried out in the glovebox on a 1.0 mL scale at –35 °C with the same initial concentrations used for kinetic measurements (see above). Before addition of substrate, 2.0 equivalents of [DMTBD][$BF_4$] and 3.2 equivalents of MTBD were added to the solution of **3**. The reactions were left in the freezer for ~24 hours after which they were diluted by a factor of ~10, filtered through silica gel, and analyzed by GC-MS to screen for any deuterium incorporation into aromatic hydrocarbon products.

**Evaluation of representative reaction conversion percentages by GC-MS.** Reactions were carried out in the glovebox on a 1.0 mL scale with the same initial concentrations used for kinetic measurements (see above). After the reaction was complete, mesitylene was added as an internal standard (0.5 equivalents relative to the initial amount of **3** present). The reaction solutions were then diluted by a factor of 10, passed through silica to remove Co, and analyzed by GC-MS. For analysis of the reaction with DHA, EI-MS was used. For analysis of the reaction with fluorene, PCI-MS was used. Integration of the peaks in the chromatograms and comparison to a calibration curve of pure mesitylene allowed for the determination of the concentration of the products in solution from which the percent conversion was calculated.

**Computational methods.** Geometry optimizations and numerical frequency calculations were performed using the ORCA program suite.[32] The O3LYP hybrid functional was used for these calculations. The basis sets for each atom were as follows: def2-TZVPP for Co, N, O, the carbene carbons of the ligand, and the carbon undergoing C–H activation in each substrate; def2-SVP for all other atoms. The COSMO solvation model for THF solvation was included in all geometry calculations. A full frequency calculation was performed on each structure to ensure that there

were no imaginary frequencies and ensure true minima in the energies. The initial geometries were generated with a simple molecular mechanics geometry optimization in the Hyperchem program suite.[33] The computed energy for each species was corrected for thermal energy contributions. Calculation of p$K_a$ values, $E^0$ values, and η values were performed analogously to methods reported in Reference 7b. The intrinsic bond orbital (IBO) analysis[22] was carried out by scanning the reaction coordinate as a function of O–H distance from 1.8 Å to 0.95 Å. This scan was carried out in the ORCA program suite. Each point's energy was minimized during this scan. For these calculations, the BP86 functional was used with the TZVPP basis set on Co, N, and O and 6-31G on the remaining atoms. The results from this scan were examined in the IboView software (http://www.iboview.org/index.html). The orbitals involved in the reaction were identified by analysis of the orbitals along the reaction coordinate (Figure A2.29). Orbital movement was normalized versus the starting and endpoints of the overall orbital movement.

## 3.5 References


[1] Rittle, J.; Green, M. T. "Cytochrome P450 Compound I: Capture, Characterisation, and C-H Bond Activation Kinetics." *Science.* **2010**, *330*, 933–937.

[2] (a) Que, L. "The Road to Non-Heme Oxoferryls and Beyond." *Acc. Chem. Res.* **2007**, *40* (7), 493–500. (b) Nam, W.; Lee, Y.-M.; Fukuzumi, S. "Hydrogen Atom Transfer Reactions of Mononuclear Nonheme Metal–Oxygen Intermediates." *Acc. Chem. Res.* **2018**, *51* (9), 2014–2022. (c) Gunay, A.; Theopold, K. H. "C-H Bond Activations by Metal Oxo Compounds." *Chem. Rev.* **2010**, *110* (2), 1060–1081. (d) Wang, B.; Lee, Y.-M.; Tcho, W.-Y.; Tussupbayev, S.; Kim, S.-T.; Kim, Y.; Seo, M. S.; Cho, K.-B.; Dede, Y.; Keegan, B. C.; Ogura, T.; Kim, S. H.; Ohta, T.; Baik, M.-H.; Ray, K.; Shearer, J.; Nam, W. "Synthesis and Reactivity of a Mononuclear Non-Haem Cobalt(IV)-Oxo Complex." *Nat. Commun.* **2017**, *8*, 14839.

[3] (a) White, M. C.; Zhao, J. "Aliphatic C–H Oxidations for Late-Stage Functionalization." *J. Am. Chem. Soc.* **2018**, *140* (43), 13988–14009. (b) Sun, C.-L.; Li, B.-J.; Shi, Z.-J. "Direct C−H Transformation via Iron Catalysis." *Chem. Rev.* **2011**, *111* (3), 1293–1314. (c) Milan, M.;

Salamone, M.; Costas, M.; Bietti, M. "The Quest for Selectivity in Hydrogen Atom Transfer Based Aliphatic C–H Bond Oxygenation." *Acc. Chem. Res.* **2018**, *51* (9), 1984–1995.

[4] (a) Warren, J. J.; Tronic, T. A.; Mayer, J. M. "Thermochemistry of Proton-Coupled Electron Transfer Reagents and Its Implications." *Chem. Rev.* **2010**, *110* (12), 6961–7001. (b) Weinberg, D. R.; Gagliardi, C. J.; Hull, J. F.; Murphy, C. F.; Kent, C. A.; Westlake, B. C.; Paul, A.; Ess, D. H.; McCafferty, D. G.; Meyer, T. J. "Proton-Coupled Electron Transfer." *Chem. Rev.* **2012**, *112* (7), 4016–4093. (c) Huynh, M. H. V.; Meyer, T. J. "Proton-Coupled Electron Transfer." *Chem. Rev.* **2007**, *107* (11), 5004–5064. (d) Cukier, R. I.; Nocera, D. G. "Proton-Coupled Electron Transfer." *Annu. Rev. Phys. Chem.* **1998**, *49* (1), 337–369. (e) Mayer, J. M. "Understanding Hydrogen Atom Transfer: From Bond Strengths to Marcus Theory." *Acc. Chem. Res.* **2011**, *44* (1), 36–46.

[5] (a) Bell, R. P. "The Theory of Reactions Involving Proton Transfers." *Proc. R. Soc. A Math. Phys. Eng. Sci.* **1936**, *154* (882), 414–429. (b) Evans, M. G.; Polanyi, M. "Inertia and Driving Force of Chemical Reactions." *Trans. Faraday Soc.* **1938**, *34*, 11–24.

[6] (a) Zaragoza, J. P. T.; Siegler, M. A.; Goldberg, D. P. "A Reactive Manganese(IV)-Hydroxide Complex: A Missing Intermediate in Hydrogen Atom Transfer by High-Valent Metal-Oxo Porphyrinoid Compounds." *J. Am. Chem. Soc.* **2018**, *140* (12), 4380–4390. (b) Lansky, D. E.; Goldberg, D. P. "Hydrogen Atom Abstraction by a High-Valent Manganese(V)−Oxo Corrolazine." *Inorg. Chem.* **2006**, *45*, 5119–5125. (c) McDonald, A. R.; Que, L. "High-Valent Nonheme Iron-Oxo Complexes: Synthesis, Structure, and Spectroscopy." *Coord. Chem. Rev.* **2013**, *257* (2), 414–428. (d) Sastri, C. V; Lee, J.; Oh, K.; Lee, Y. J.; Lee, J.; Jackson, T. A.; Ray, K.; Hirao, H.; Shin, W.; Halfen, J. A.; Kim, J.; Que, L.; Shaik, S.; Nam, W. "Axial Ligand Tuning of a Nonheme Iron(IV) Oxo Unit for Hydrogen Atom Abstraction." *Proc. Natl. Acad. Sci.* **2007**, *104* (49), 19181–19186. (e) Dhar, D.; Tolman, W. B. "Hydrogen Atom Abstraction from Hydrocarbons by a Copper(III)-Hydroxide Complex." *J. Am. Chem. Soc.* **2015**, *137* (3), 1322–1329.

[7] (a) Usharani, D.; Lacy, D. C.; Borovik, A. S.; Shaik, S. "Dichotomous Hydrogen Atom Transfer vs Proton-Coupled Electron Transfer During Activation of X–H Bonds (X = C, N, O) by Nonheme Iron–Oxo Complexes of Variable Basicity." *J. Am. Chem. Soc.* **2013**, *135* (45), 17090–17104. (b) Bím, D.; Maldonado-Domínguez, M.; Rulíšek, L.; Srnec, M. "Beyond the Classical Thermodynamic Contributions to Hydrogen Atom Abstraction Reactivity." *Proc. Natl. Acad. Sci.* **2018**, *115* (44), E10287–E10294. (c) Hodgkiss, J. M.; Rosenthal, J.; Nocera, D. G. The Relation between Hydrogen Atom Transfer and Proton-Coupled Electron Transfer in Model Systems. In *Hydrogen-Transfer Reactions*; Hynes, J. T., Klinman, J. P., Limbach, H.-H., Schowen, R. L., Eds.; WILEY-VCH Verlag GmbH: Weinheim, 2007; pp 503–562.

[8] Hammes-Schiffer, S. "Theory of Proton-Coupled Electron Transfer in Energy Conversion Processes." *Acc. Chem. Res.* **2009**, *42* (12), 1881–1889.

[9] (a) Fulton, J. R.; Sklenak, S.; Bouwkamp, M. W.; Bergman, R. G. "A Comprehensive Investigation of the Chemistry and Basicity of a Parent Amidoruthenium Complex." *J. Am.*

*Chem. Soc.* **2002**, *124* (17), 4722–4737. (b) Roth, J. P.; Mayer, J. M. "Hydrogen Transfer Reactivity of a Ferric Bi-Imidazoline Complex That Models the Activity of Lipoxygenase Enzymes." *Inorg. Chem.* **1999**, *38* (12), 2760–2761. (c) Parsell, T. H.; Yang, M. Y.; Borovik, A. S. "C-H Bond Cleavage with Reductants: Re-Investigating the Reactivity of Monomeric $Mn^{III/IV}$-Oxo Complexes and the Role of Oxo Ligand Basicity." *J. Am. Chem. Soc.* **2009**, *131* (8), 2762–2763. (d) Zdilla, M. J.; Dexheimer, J. L.; Abu-Omar, M. M. "Hydrogen Atom Transfer Reactions of Imido Manganese(V) Corrole: One Reaction with Two Mechanistic Pathways." *J. Am. Chem. Soc.* **2007**, *129* (37), 11505–11511.

[10] (a) Yosca, T. H.; Rittle, J.; Krest, C. M.; Onderko, E. L.; Silakov, A.; Calixto, J. C.; Behan, R. K.; Green, M. T. "Iron(IV)Hydroxide PK(a) and the Role of Thiolate Ligation in C-H Bond Activation by Cytochrome P450." *Science.* **2013**, *342* (6160), 825–829. (b) Green, M. T.; Dawson, J. H.; Gray, H. B. "Oxoiron(IV) in Chloroperoxidase Compound II Is Basic: Implications for P450 Chemistry." *Science.* **2004**, *304* (5677), 1653–1656. (c) Donoghue, P. J.; Tehranchi, J.; Cramer, C. J.; Sarangi, R.; Solomon, E. I.; Tolman, W. B. "Rapid C–H Bond Activation by a Monocopper(III)–Hydroxide Complex." *J. Am. Chem. Soc.* **2011**, *133* (44), 17602–17605. (d) Dhar, D.; Yee, G. M.; Markle, T. F.; Mayer, J. M.; Tolman, W. B. "Reactivity of the Copper(III)-Hydroxide Unit with Phenols." *Chem. Sci.* **2017**, *8* (2), 1075–1085.

[11] Goetz, M. K.; Hill, E. A.; Filatov, A. S.; Anderson, J. S. "Isolation of a Terminal Co(III)-Oxo Complex." *J. Am. Chem. Soc.* **2018**, *140* (41), 13176–13180.

[12] Kolomeitsev, A. A.; Koppel, I. A.; Rodima, T.; Barten, J.; Lork, E.; Röschenthaler, G.-V.; Kaljurand, I.; Kütt, A.; Koppel, I.; Mäemets, V.; Leito, I. "Guanidinophosphazenes: Design, Synthesis, and Basicity in THF and in the Gas Phase." *J. Am. Chem. Soc.* **2005**, *127* (50), 17656–17666.

[13] Caldin, E. F. "Tunneling in Proton-Transfer Reactions in Solution." *Chem. Rev.* **1969**, *69* (1), 135–156.

[14] (a) Cong, Z.; Kinemuchi, H.; Kurahashi, T.; Fujii, H. "Factors Affecting Hydrogen-Tunneling Contribution in Hydroxylation Reactions Promoted by Oxoiron(IV) Porphyrin π-Cation Radical Complexes." *Inorg. Chem.* **2014**, *53* (19), 10632–10641. (b) Mandal, D.; Mallick, D.; Shaik, S. "Kinetic Isotope Effect Determination Probes the Spin of the Transition State, Its Stereochemistry, and Its Ligand Sphere in Hydrogen Abstraction Reactions of Oxoiron(IV) Complexes." *Acc. Chem. Res.* **2018**, *51* (1), 107–117. (c) Edwards, S. J.; Soudackov, A. V; Hammes-Schiffer, S. "Analysis of Kinetic Isotope Effects for Proton-Coupled Electron Transfer Reactions." *J. Phys. Chem. A* **2009**, *113* (10), 2117–2126.

[15] Bordwell, F. G. "Equilibrium Acidities in Dimethyl Sulfoxide Solution." *Acc. Chem. Res* **1988**, *21* (7), 456–463.

[16] Luo, Y.-R. "Handbook of Bond Dissociation Energies in Organic Compounds;" CRC Press: Boca Raton, 2003.

[17] Hansch, C.; Leo, A.; Taft, R. W. "A Survey of Hammett Substituent Constants and Resonance and Field Parameters." *Chem. Rev.* **1991**, *91* (2), 165–195.

[18] Nicholson, R. S. "Theory and Application of Cyclic Voltammetry for Measurement of Electrode Reaction Kinetics." *Anal. Chem.* **1965**, *37* (11), 1351–1355.

[19] Klingler, R. J.; Kochi, J. K. "Electron-Transfer Kinetics from Cyclic Voltammetry. Quantitative Description of Electrochemical Reversibility." *J. Phys. Chem.* **1981**, *85* (12), 1731–1741.

[20] Bryant, R. G. "The NMR Time Scale." *J. Chem. Educ.* **1983**, *60* (11), 933–935.

[21] (a) Klinker, E. J.; Shaik, S.; Hirao, H.; Que, L. "A Two-State Reactivity Model Explains Unusual Kinetic Isotope Effect Patterns in C-H Bond Cleavage by Nonheme Oxoiron(IV) Complexes." *Angew. Chem., Int. Ed.* **2009**, *48* (7), 1291–1295. (b) Mandal, D.; Mallick, D.; Shaik, S. "Kinetic Isotope Effect Determination Probes the Spin of the Transition State, Its Stereochemistry, and Its Ligand Sphere in Hydrogen Abstraction Reactions of Oxoiron(IV) Complexes." *Acc. Chem. Res.* **2018**, *51* (1), 107–117. (c) Hickey, A. K.; Lutz, S. A.; Chen, C.-H.; Smith, J. M. "Two-State Reactivity in C–H Activation by a Four-Coordinate Iron(0) Complex." *Chem. Commun.* **2017**, *53* (7), 1245–1248.

[22] (a) Knizia, G. "Intrinsic Atomic Orbitals: An Unbiased Bridge between Quantum Theory and Chemical Concepts." *J. Chem. Theory Comput.* **2013**, *9* (11), 4834–4843. (b) Knizia, G.; Klein, J. E. M. N. "Electron Flow in Reaction Mechanisms-Revealed from First Principles." *Angew. Chem., Int. Ed.* **2015**, *54* (18), 5518–5522. (c) Klein, J. E. M. N.; Knizia, G. "CPCET versus HAT: A Direct Theoretical Method for Distinguishing X-H Bond-Activation Mechanisms." *Angew. Chem., Int. Ed.* **2018**, *57* (37), 11913–11917.

[23] Goldsmith, C. R.; Jonas, R. T.; Stack, T. D. P. "C-H Bond Activation by a Ferric Methoxide Complex: Modeling the Rate-Determining Step in the Mechanism of Lipoxygenase." *J. Am. Chem. Soc.* **2002**, *124* (1), 83–96.

[24] Ji, X.; Huang, T.; Wu, W.; Liang, F.; Cao, S. "LDA-Mediated Synthesis of Triarylmethanes by Arylation of Diarylmethanes with Fluoroarenes at Room Temperature." *Org. Lett.* **2015**, *17* (20), 5096–5099.

[25] Shen, X.; Gu, N.; Liu, P.; Ma, X.; Xie, J.; Liu, Y.; He, L.; Dai, B. "A Simple and Efficient Synthesis of 9-Arylfluorenes via Metal-Free Reductive Coupling of Arylboronic Acids and N-Tosylhydrazones in Situ." *RSC Adv.* **2015**, *5* (78), 63726–63731.

[26] Li, H.; Aquino, A. J. A.; Cordes, D. B.; Hung-Low, F.; Hase, W. L.; Krempner, C. "A Zwitterionic Carbanion Frustrated by Boranes - Dihydrogen Cleavage with Weak Lewis Acids via an 'Inverse' Frustrated Lewis Pair Approach." *J. Am. Chem. Soc.* **2013**, *135* (43), 16066–16069.

[27] Liu, Z. Q.; Zhang, Y.; Zhao, L.; Li, Z.; Wang, J.; Li, H.; Wu, L. M. "Iron-Catalyzed Stereospecific Olefin Synthesis by Direct Coupling of Alcohols and Alkenes with Alcohols." *Org. Lett.* **2011**, *13* (9), 2208–2211.

[28] Hu, J.; Adogla, E. A.; Ju, Y.; Fan, D.; Wang, Q. "Copper-Catalyzed Ortho-Acylation of Phenols with Aryl Aldehydes and Its Application in One-Step Preparation of Xanthones." *Chem. Commun.* **2012**, *48* (91), 11256.

[29] Stopka, T.; Marzo, L.; Zurro, M.; Janich, S.; Würthwein, E.-U.; Daniliuc, C. G.; Alemán, J.; Mancheño, O. G. "Oxidative C-H Bond Functionalization and Ring Expansion with $TMSCHN_2$: A Copper(I)-Catalyzed Approach to Dibenzoxepines and Dibenzoazepines." *Angew. Chem., Int. Ed.* **2015**, *54* (17), 5049–5053.

[30] Franz, J. A.; Alnajjar, M. S.; Barrows, R. D.; Kaisaki, D. L.; Camaioni, D. M.; Suleman, N. K. "Reactions of the 2-Allylbenzyl Radical: Relative and Absolute Rate Constants for Abstraction of Hydrogen Atom from Thiophenol, Dicyclohexylphosphine, Phenols, and Arylalkyl Donors." *J. Org. Chem.* **1986**, *51* (9), 1446–1456.

[31] Jia, G.; Morris, R. H. "Wide Range of p$K_a$ Values of Coordinated Dihydrogen. Synthesis and Properties of Some $\eta^2$-Dihydrogen and Dihydride Complexes of Ruthenium." *J. Am. Chem. Soc.* **1991**, *113* (3), 875–883.

[32] Neese, F. "The Orca Program System." *Wiley Interdiscip. Rev. Mol. Sci.* **2012**, *2*, 73–78.

[33] "HyperChem(TM) Professional 7.51." Hypercube, Inc.: 1115 NW 4th Street, Gainesville, Florida 32601, USA.

# Chapter 4: Pushing the Boundaries of Asynchronicity in the PCET Reactivity of a Terminal Co(III)-Oxo Complex

## 4.1 Introduction

Proton-coupled electron transfer (PCET) reactions are a ubiquitous class of reactions that are central to many processes both in biology and synthesis.[1] In particular, X–H bond activation often proceeds through a PCET mechanism, and understanding the intricacies by which the net H–atom is transferred from the X–H bond to the corresponding proton and electron acceptors is invaluable for controlling selectivity and designing effective catalysts.[2] Transition metal-oxo species are often invoked as key intermediates in these X–H bond activations and have a range of PCET mechanisms to choose from when activating these bonds (Scheme 4.1).[3] Different mechanisms have important implications for the rate and selectivity of a given reaction.

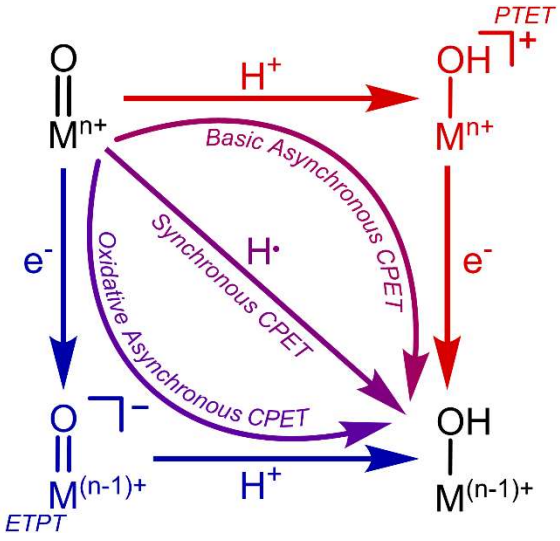


**Scheme 4.1.** Mechanisms of net H–atom transfer to a metal-oxo complex (reproduced from Chapter 3).

Within the realm of specifically concerted proton-electron transfer (CPET) mechanisms, there is a spectrum of "synchronicity" of the CPET that must be considered given that the transfer of a net H–atom involves the transfer of both proton and electron components (Scheme 4.1). Historically, transition metal oxo species have been observed to favor a completely synchronous CPET mechanism, whereby rates of reaction are solely dependent on the driving force for the H–atom transfer reaction, as outlined by the Bell-Evans-Polanyi principle.[4] In these cases, the proton and electron transfers have equal contributions to the transition state of the reaction. However, there has recently been discussion of and experimental evidence for asynchronous CPET mechanisms, which can be conceptualized as reactions proceeding through an imbalanced transition state.[5] In these instances, reaction rates can depend on parameters other than the driving force for net H–atom transfer, such as the driving forces for proton transfer or electron transfer.[5e]

This discussion of asynchronicity and imbalanced transition states has recently been brought into question.[6] The idea of transition state asymmetry is inherently rooted in semiclassical transition state theory,[5a] which does not account for quantum mechanical phenomena such as tunneling. However, PCET reactions are known to have a large degree of tunneling present.[7] The question of whether or not these two conflicting viewpoints can be resolved is relatively unexplored, but a recent study of temperature dependent kinetic isotope effects allowed for the development of a model that reproduces the idea of an "imbalanced transition state" from a quantum mechanical framework.[8] Thus, asynchronicity is entirely consistent with our quantum mechanical understanding of how H–atoms move in chemical reactions and is appropriate to include in discussion of PCET reactions carried out by transition metal-oxo complexes.

While these studies support the viability of concerted but asynchronous CPET reactions, there remain questions about possible overlap or boundaries between asynchronous and stepwise mechanisms. How asynchronous can a concerted reaction be? One could imagine that at some point, asynchronicity in a concerted reaction will be so great that mechanistic crossover occurs and a stepwise ETPT or PTET mechanism will become operative. Our terminal $Co^{III}$-oxo complexes provide an ideal platform from which to interrogate these questions (Scheme 4.2), as they are known to activate X–H bonds via a basic asynchronous CPET mechanism.[5e,9,10]

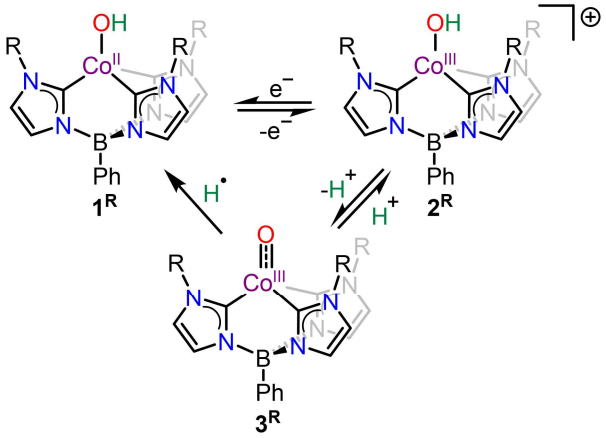


**Scheme 4.2.** Metal complexes discussed in this chapter. R = $^{t}$Bu, Ad.

In this chapter, it is shown that reactivity with C–H bonds proceeds more asynchronously for PhB($^{Ad}$Im)$_3$Co$^{III}$O (**3$^{Ad}$**) than for PhB($^{t}$BuIm)$_3$Co$^{III}$O (**3$^{tBu}$**). This is consistent with the greater imbalance in the contributions of basicity and oxidation potential to the $BDFE_{O–H}$ in PhB($^{Ad}$Im)$_3$Co$^{II}$OH (**1$^{Ad}$**) than in PhB($^{t}$BuIm)$_3$Co$^{II}$OH (**1$^{tBu}$**).[10] Additionally, despite a higher $BDFE_{O–H}$ for **1$^{Ad}$**, **3$^{Ad}$** activates C–H bonds more slowly than **3$^{tBu}$**, likely due to steric hindrance. This highlights the importance of factors other than thermodynamics when considering these systems.

Furthermore, reactivity with a set of 4-X-2,6-di(*tert*-butyl)phenols, which are sterically identical, demonstrates mechanistic crossover from a CPET mechanism to a stepwise PTET mechanism. This provides an example that highlights the limit of asynchronicity in CPET reactions in this system. Additionally, this explicit observation of a mechanistic switch to a stepwise PTET mechanism provides additional support for distinct *concerted* asynchronous C–H activation, as presented in the previous chapter.

## 4.2 Results and Discussion

### 4.2.1 Reactivity of PhB($^{Ad}$Im)$_3$Co$^{III}$O with C–H Bonds

To examine the limits of asynchronicity, we began by studying the C–H activation reactivity of **3$^{Ad}$**. Reaction of **3$^{Ad}$** with 10 equivalents of 9-phenyl-9*H*-fluorene was followed by UV-vis spectroscopy at room temperature (Figure 4.1). Kinetic analysis of the absorbance data at 714 nm allowed for the determination of the observed rate constant, $k_{obs}$, for this reaction (Table 4.1). Surprisingly, this $k_{obs}$ value is three orders of magnitude smaller than that measured for **3$^{tBu}$** ($k_{obs}$ = 3.7(5)•10$^{-1}$ s$^{-1}$).[5] At first glance, one would expect the rate constants for the C–H activation reactivity of **3$^{Ad}$** to be greater than those measured for **3$^{tBu}$** due to the larger BDFE$_{O–H}$ in **1$^{Ad}$** and greater imbalance in the thermodynamic contributions to this BDFE$_{O–H}$.[10] The larger BDFE$_{O–H}$ would predict a greater rate constant following the Bell-Evans-Polanyi principle,[4] and the greater imbalance in thermodynamic contributions would predict a more asynchronous reaction that would also be expected to be faster.[5a,e] We hypothesized that the larger steric profile of the adamantyl (Ad) substituents could be affecting the observed rates for the reactivity of **3$^{Ad}$**.

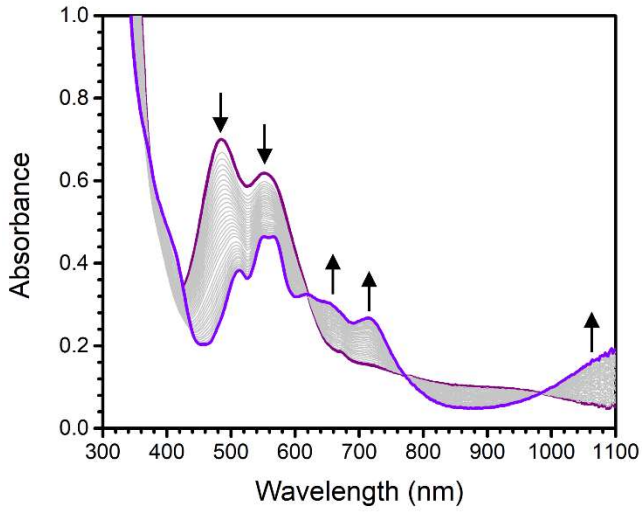


**Figure 4.1.** Representative UV-vis spectrum showing the clean reaction between $\mathbf{3^{Ad}}$ (dark purple) and 10 equivalents of 9-phenyl-9*H*-fluorene in THF at room temperature to produce $\mathbf{1^{Ad}}$ (violet). Gray traces indicate 3 minute timepoints.

To test this hypothesis, we examined the reactivity of $\mathbf{3^{Ad}}$ with indene. Based on both BDE and p$K_a$ arguments (consistent with the asynchronous reactivity previously shown for $\mathbf{3^{tBu}}$), indene should react more slowly with $\mathbf{3^{Ad}}$ than 9-phenyl-9*H*-fluorene (Table 4.1). However, indene is a much smaller substrate than 9-phenyl-9*H*-fluorene and therefore could reasonably be expected to react more quickly if the degree of steric hindrance is important in this system. Indeed, analysis of the reaction of $\mathbf{3^{Ad}}$ with indene show an observed rate constant that is ~2x larger than that observed for 9-phenyl-9*H*-fluorene. This confirms that for this bulky Ad-substituted ligand, steric considerations dominate for this substrate pair. Care must be taken in comparing rate constants for this system, since trends with thermodynamic parameters may be masked be steric effects.

**Table 4.1.** Kinetic data for the C–H activation reactions of $\mathbf{3^{Ad}}$.

| Substrate | $k_{obs}$ ($10^{-4}$ $s^{-1}$) | BDE (kcal/mol)[b] | p$K_a$ (DMSO)[c] | $\sigma_p^{-}$[d] |
|---|---|---|---|---|
| indene | 4.4[a] | 83 | 20.1 | n/a |
| 9-phenyl-9*H*-fluorene | 2.6(8) | 74 | 17.9 | 0 |
| 9-(4-(trifluoromethyl)phenyl)-9*H*-fluorene | 39(4) | n/a | n/a | 0.65 |

[a]Data from only one trial. [b]From the Handbook of Bond Dissociation Energies.[11] [c]From the Bordwell p$K_a$ tables.[12] [d]From Hansch, Leo, and Taft.[13] See also Figure A3.1-Figure A3.3.

To avoid convolutions from steric effects, we decided to examine the asynchronicity trends in C–H activation mediated by this Ad-substituted system by examining the rate constants obtained for a set of sterically identical substrates: 9-(4-X-phenyl)-9*H*-fluorenes. This set of substrates allows for carrying out a Hammett analysis, which was done previously for $\mathbf{3^{tBu}}$.[5e] A Hammett analysis will inform on the polarity (or imbalance) of the transition state, which is directly related to the degree of asynchronicity in the C–H activation reaction. A more asynchronous reaction (or equivalently, a more polar transition state) will be more sensitive to the X substituent on the 9-(4-X-phenyl)-9*H*-fluorene substrate. Therefore, for a more asynchronous CPET mechanism of C–H activation, we'd expect a steeper Hammett slope.

Reliable data has only been able to be obtained for two substrates so far. Nonetheless, we can compare the initial trend to the previous Hammett analysis for $\mathbf{3^{tBu}}$ to examine how the asynchronicity in C–H activation by $\mathbf{3^{Ad}}$ compares (Figure 4.2). From this data, it is apparent that the reactivity of $\mathbf{3^{Ad}}$ is more sensitive to the X substituent than $\mathbf{3^{tBu}}$. This is consistent with a greater degree of asynchronicity in the C–H activation reactivity of $\mathbf{3^{Ad}}$, as is expected from the greater imbalance in the thermodynamic contributions to the $BDFE_{O–H}$ of $\mathbf{1^{Ad}}$. This comparison

demonstrates that by simple ligand modification, the degree of asynchronicity in a CPET mechanism of C–H activation can be tuned and pushed to greater limits, while maintaining the benefits of a concerted reaction that avoids high energy intermediates. It is reasonable to expect that this larger degree of asynchronicity could lead to more effective selectivity in synthetic systems.

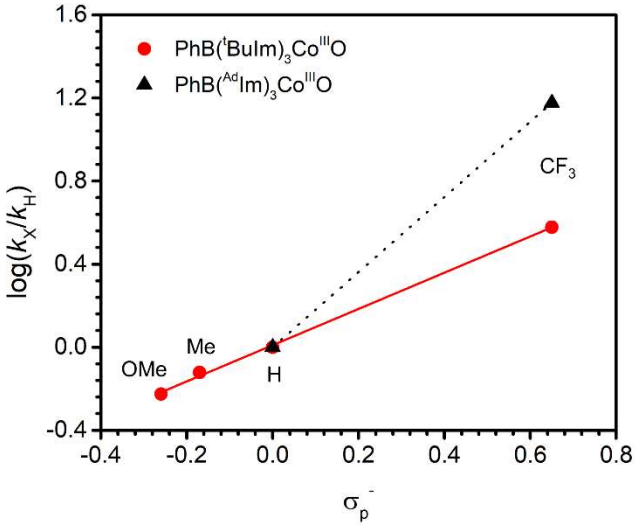


**Figure 4.2.** Hammett substituent plot for the reactions of $\mathbf{3^{R}}$ with 9-(4-X-phenyl)-9*H*-fluorenes (the data for $\mathbf{3^{tBu}}$ are reproduced from Chapter 3.2.4). The red line shows the linear fit of the data for $\mathbf{3^{tBu}}$: $\rho = 0.87(3)$, $R^2 = 0.996$. The black dotted line shows the greater dependence on X substituent for $\mathbf{3^{Ad}}$.

### 4.2.2 Reactivity of PhB($^{Ad}$Im)$_3$Co$^{III}$O with 4-X-2,6-Di(*tert*-butyl)-phenol Substrates

To further explore the limits of asynchronous CPET reactions, we turned to the study of O–H bond activation in phenols. These O–H bonds are much more acidic than C–H bonds, which is likely to have important consequences for the *basic* asynchronous CPET mechanism employed by these terminal Co$^{III}$-oxo complexes. We initially examined the $k_{obs}$ values obtained for the reaction of $\mathbf{3^{Ad}}$ with 7 different 4-X-2,6-di(*tert*-butyl)phenols. This set of substrates ensures a consistent

steric profile across the series. The data for these reactions is presented in Table 4.2 (see also Figure A3.4-Figure A3.10).

**Table 4.2.** Kinetic data for the reaction of $\mathbf{3^{Ad}}$ with 4-X-2,6-di(*tert*-butyl)phenol substrates.

| X | $k_{obs}$ ($10^{-2}$ $s^{-1}$) | BDE (kcal/mol)[a] | p$K_a$ (DMSO)[a] | $E_{ox}$ ($PhO^-$) (V vs. $Fc/Fc^+$)[a] |
|---|---|---|---|---|
| OMe | 1.8(2) | 79.7 | 18.2 | –0.806 |
| Me | 1.2(3) | 80.1 | 17.73 | –0.755 |
| $^t$Bu | 0.6(1) | 82.6 | 17.8 | –0.665 |
| H | 1.0(2) | 82.7 | 17.3 | –0.619 |
| Br | 1.5(2)[b] | n.r. | 15.1[c] | n.r. |
| COOMe | 1.6(9)[b] | 84.3 | 11.9 | –0.229 |
| $NO_2$ | 2(1)[b] | 86.2 | 7.3 | 0.127 |

[a]Data from Bordwell.[14] [b]Rate constant for proton transfer to form $\mathbf{2^{Ad}}$ and the corresponding phenoxide. [c]Estimated from the reported value in methanol (Figure A3.13).[15] n.r. = not reported.

Plotting the log($k_{obs}$) versus the BDEs of the phenols (Figure 4.3) or their p$K_a$ values (Figure 4.4) reveals an interesting trend across this series of substrates. In both plots, there is an obvious discontinuity in the trend of the data (marked by the gray dashed line). This discontinuity occurs between X = H and X = Br. Such a discontinuity suggests a mechanism switch between the two sets of substrates (X = OMe, Me, $^t$Bu, H and X = Br, COOMe, $NO_2$), similar to mechanistic crossovers that have been proposed previously.[5d,16] Closer examination of the reactions of $\mathbf{3^{Ad}}$ with the substrates with X = Br, COOMe, and $NO_2$ explicitly reveals this to be the case. In these cases, $\mathbf{2^{Ad}}$ is initially produced at –100 °C as would be expected for the first step of a PTET mechanism of net H–atom transfer (see Figure A3.11 for a representative example). Therefore, the rate constants reported in Table 4.2 for these substrates are in fact the rate constants for proton transfer, not H–atom transfer. Indeed, these rate constants display a linear trend with the p$K_a$ of the phenols, as expected for a proton transfer reaction (Figure 4.4).

Warming these reactions to at least 0 °C is necessary before the electron transfer step will proceed at an appreciable rate (see Figure A3.12 for a representative example). This confirms that these substrates still participate in net H–atom transfer via a stepwise PTET mechanism. An important consequence of this clearly observed stepwise reactivity and the discontinuities in Figure 4.3 and Figure 4.4 is that it strongly suggests that all the other reactivity that has been observed with these systems is in fact concerted since there is no observation of the $\mathbf{2^R}$ intermediates in those cases (see above, reference 5e). While this was indirectly shown previously, the data presented here provides more explicit evidence for concerted basic asynchronous reactivity.

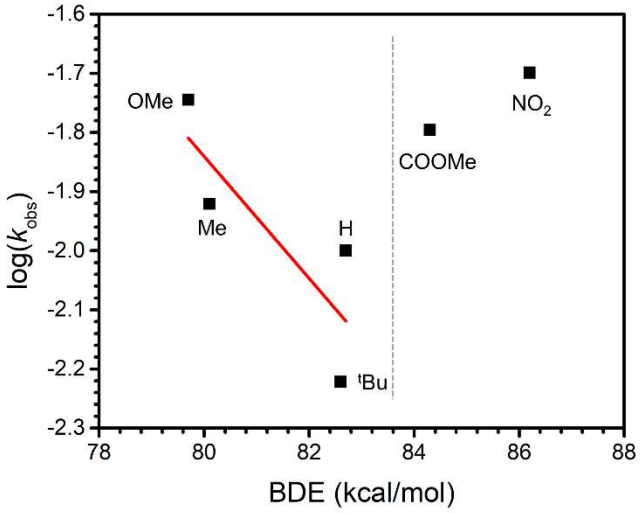


**Figure 4.3.** Plot of log($k_{obs}$) versus BDE for the reaction of $\mathbf{3^{Ad}}$ with various 4-X-2,6-di(*tert*-butyl)phenols. The gray dotted line indicates a discontinuity in the data trend. The red line shows the linear fit for X = OMe, Me, $^t$Bu, H (log($k_{obs}$) = –0.10(5)*BDE + 6(4), $R^2$ = 0.54).

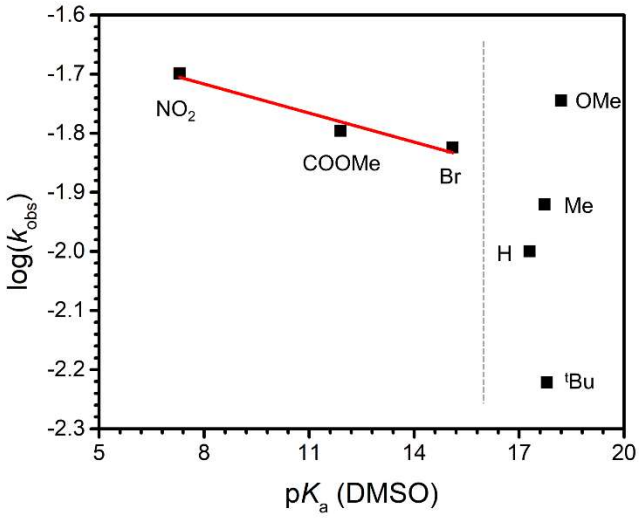


**Figure 4.4.** Plot of log($k_{obs}$) versus p$K_a$ for the reaction of $\mathbf{3^{Ad}}$ with various 4-X-2,6-di(*tert*-butyl)phenols. The gray dotted line indicates a discontinuity in the data trend. The red line shows the linear fit for X = Br, COOMe, $NO_2$ ($R^2$ = 0.92).

Interestingly, the rate constants for the reaction of $\mathbf{3^{Ad}}$ with substrates with X = OMe, Me, $^t$Bu, H display a marked dependence on the BDEs of these substrates, and essentially no dependence on the p$K_a$ values. This is in direct contrast to what is expected for a basic asynchronous CPET mechanism of net H–atom transfer to $\mathbf{3^{Ad}}$. However, there are two key observations that explain this apparent discrepancy. First, the difference in p$K_a$ across these 4 substrates is only 0.9 p$K_a$ units as compared to the ~17 p$K_a$ unit difference across the series of C–H substrates studied with $\mathbf{3^{tBu}}$ where the trend with p$K_a$ was noticed. For such a narrow range of p$K_a$ values, we may not expect to observe such a subtle effect (slope for $\mathbf{3^{tBu}}$ was –0.18). Second, it has recently been demonstrated that reactivity trends for transition metal-oxo complexes can be explained by a weighted sum of the contributions from the driving forces for PCET, PT, and ET.[5f,17] Thus, it should be the case that when the driving force for PT is almost constant, the driving force for PCET may become dominant in explaining the reactivity trend. This therefore explains the linear correlation with BDE

seen in Figure 4.3. Additionally, for a synchronous CPET mechanism, a slope of –0.5 is expected in a plot of log($k_{obs}$) versus BDE.[5b] However, in this case the dependence is shallow (slope = –0.10), consistent with an asynchronous mechanism of CPET that has large contributions from off-diagonal thermodynamic elements (Scheme 4.1).

## 4.3 Conclusions

In this chapter we have demonstrated that we can traverse the boundary between concerted asynchronous reactions and stepwise reactions in the PCET reactivity of a terminal Co-oxo complex. Simple ligand modification has been shown to be an effective method for altering the degree of asynchronicity in the activation of C–H bonds which has important implications for selectivity in synthetic applications. However, such ligand modifications may lead to unwanted effects, such as the slowing of reaction rates due to steric hindrance. Careful consideration of all factors must accompany any ligand design. Additionally, we observed explicit mechanistic crossover in the CPET reactivity of $\mathbf{3^{Ad}}$ with a set of sterically identical phenols. This gives additional support for concerted reactivity in the case of substrates that aren't observed to form $\mathbf{2^{Ad}}$, as concluded previously. Explicit determination of electron transfer rate constants, which is likely possible with this set of reactions in a separate study, can provide further support for this conclusion. Finally, it was observed that the rate constants for the concerted reactions of $\mathbf{3^{Ad}}$ with phenols correlate logarithmically with the BDEs. This is still consistent with a basic asynchronous CPET mechanism due to the shallow dependence and narrow range of p$K_a$ values surveyed. This underscores that asynchronicity is a subtle effect and demonstrates a regime where the different thermodynamic parameters can have varying importance.

## 4.4 Experimental

**General Considerations**. All manipulations were performed under a dry nitrogen atmosphere using either standard Schlenk techniques or in an mBraun Unilab Pro glovebox unless otherwise stated. All chemicals were obtained from commercial sources and used as received unless otherwise stated. Solvents were dried on a solvent purification system from Pure Process Technologies before storing over 4 Å molecular sieves under $N_2$. Tetrahydrofuran (THF) was stirred over NaK alloy and passed through a column of activated alumina prior to storing over 4 Å sieves under $N_2$. $PhB(^{Ad}Im)_3Co^{III}O$ was prepared as described in Chapter 2.4. All substituted phenols were obtained commercially and used as received. Indene was obtained commercially and used as received. 9-phenyl-9*H*-fluorene and 9-(4-(trifluoromethyl)phenyl)-9*H*-fluorene were prepared according to previously reported procedures.[5e] UV-vis spectra were recorded on a Thermo Scientific Evolution 300 spectrometer with the VISIONpro software suite. A standard 1 cm quartz cuvette with an air-tight screw cap with a puncturable Teflon seal was used for all measurements. A Unisoku CoolSpek cryostat was used for low temperature measurements.

**Procedure for kinetic studies with C–H substrates.** Data for rate determination were collected in triplicate at 23 °C unless otherwise noted. In a typical experiment, 2.0 mL of a 1.25 mM solution of $\mathbf{3^{Ad}}$ in THF was transferred to an air tight screw top cuvette. After an initial scan was collected, a solution of substrate in THF was injected through the septum in the screw top. The reaction was monitored for an appropriate amount of time to reach completion, collected spectra from 300-1100 nm every 45 seconds. To determine the observed rate $k_{obs}$ values, the data were analyzed by plotting the absorbance at 714 nm at time $t$ versus time in seconds and fitting the data to an

exponential function, $A_t = A_{inf} + (A_0 - A_{inf})e^{-kt}$, where $A_{inf}$ is the absorbance at infinite time, $A_0$ is the initial absorbance, and $k$ is the observed rate constant, $k_{obs}$.

**Procedure for kinetic studies with O–H substrates.** Data for rate determination were collected in triplicate at –100 °C unless otherwise noted. In a typical experiment, 2.0 mL of a 1.25 mM solution of **3$^{Ad}$** in THF was transferred to an air tight screw top cuvette. After allowing the cuvette to equilibrate to –100 °C, single wavelength data collection at 714 nm was started, with a data collection interval of 1 second. Within a few seconds, a solution of substrate in THF was injected through the septum in the screw top. The reaction was monitored for an appropriate amount of time to reach completion. To determine the observed rate $k_{obs}$ values, the data were analyzed by plotting the absorbance at 714 nm at time $t$ versus time in seconds and fitting the data to an exponential function, $A_t = A_{inf} + (A_0 - A_{inf})e^{-kt}$, where $A_{inf}$ is the absorbance at infinite time, $A_0$ is the initial absorbance, and $k$ is the observed rate constant, $k_{obs}$.

**Procedure for UV-vis spectroscopy of the reaction between 3$^{Ad}$ and methyl 4-hydroxy-3,5-di(*tert*-butyl)benzoate.** For this experiment, 2.0 mL of a 1.25 mM solution of **3$^{Ad}$** in THF was transferred to an air tight screw top cuvette. The cuvette was cooled to –80 °C in the cryostat and allowed to equilibrate before injecting 10 equivalents of methyl 4-hydroxy-3,5-di(*tert*-butyl)benzoate via syringe. The reaction was monitored every 45 seconds until the spectrum stopped changing. The final spectrum matched that of **2$^{Ad}$** (Figure A3.11). At this point, the cryostat was rapidly warmed to 0 °C and the reaction monitored for ~1 hour until the formation of **1$^{Ad}$** was complete (Figure A3.12). This reactivity is representative of what was observed for the reactions of **3$^{Ad}$** with 4-bromo-2,6-di(*tert*-butyl)phenol and 4-nitro-2,6-di(*tert*-butyl)phenol.

## 4.5 References


[1] (a) Weinberg, D. R.; Gagliardi, C. J.; Hull, J. F.; Murphy, C. F.; Kent, C. A.; Westlake, B. C.; Paul, A.; Ess, D. H.; McCafferty, D. G.; Meyer, T. J. "Proton-Coupled Electron Transfer." *Chem. Rev.* **2012**, *112* (7), 4016–4093. (b) Migliore, A.; Polizzi, N. F.; Therien, M. J.; Beratan, D. N. "Biochemistry and Theory of Proton-Coupled Electron Transfer." *Chem. Rev.* **2014**, *114* (7), 3381–3465.

[2] (a) White, M. C.; Zhao, J. "Aliphatic C–H Oxidations for Late-Stage Functionalization." *J. Am. Chem. Soc.* **2018**, *140* (43), 13988–14009. (b) Milan, M.; Salamone, M.; Costas, M.; Bietti, M. "The Quest for Selectivity in Hydrogen Atom Transfer Based Aliphatic C–H Bond Oxygenation." *Acc. Chem. Res.* **2018**, *51* (9), 1984–1995. (c) Mittra, K.; Green, M. T. "Reduction Potentials of P450 Compounds I and II: Insight into the Thermodynamics of C–H Bond Activation." *J. Am. Chem. Soc.* **2019**, *141* (13), 5504–5510. (d) Mayer, J. M. "Understanding Hydrogen Atom Transfer: From Bond Strengths to Marcus Theory." *Acc. Chem. Res.* **2011**, *44* (1), 36–46. (e) Warren, J. J.; Tronic, T. A.; Mayer, J. M. "Thermochemistry of Proton-Coupled Electron Transfer Reagents and Its Implications." *Chem. Rev.* **2010**, *110* (12), 6961–7001.

[3] (a) Rittle, J.; Green, M. T. "Cytochrome P450 Compound I: Capture, Characterisation, and C-H Bond Activation Kinetics." *Science.* **2010**, *330*, 933–937. (b) Que, L. "The Road to Non-Heme Oxoferryls and Beyond." *Acc. Chem. Res.* **2007**, *40* (7), 493–500. (c) Gunay, A.; Theopold, K. H. "C-H Bond Activations by Metal Oxo Compounds." *Chem. Rev.* **2010**, *110* (2), 1060–1081. (d) Chen, M. S.; White, M. C. "A Predictably Selective Aliphatic C H Oxidation Reaction for Complex Molecule Synthesis." *Science.* **2007**, *318* (5851), 783–787.

[4] (a) Bell, R. P. "The Theory of Reactions Involving Proton Transfers." *Proc. R. Soc. A Math. Phys. Eng. Sci.* **1936**, *154* (882), 414–429. (b) Evans, M. G.; Polanyi, M. "Inertia and Driving Force of Chemical Reactions." *Trans. Faraday Soc.* **1938**, *34*, 11–24.

[5] (a) Bím, D.; Maldonado-Domínguez, M.; Rulíšek, L.; Srnec, M. "Beyond the Classical Thermodynamic Contributions to Hydrogen Atom Abstraction Reactivity." *Proc. Natl. Acad. Sci.* **2018**, *115* (44), E10287–E10294. (b) Darcy, J. W.; Kolmar, S. S.; Mayer, J. M. "Transition State Asymmetry in C-H Bond Cleavage by Proton-Coupled Electron Transfer." *J. Am. Chem. Soc.* **2019**, *141* (27), 10777–10787. (c) Usharani, D.; Lacy, D. C.; Borovik, A. S.; Shaik, S. "Dichotomous Hydrogen Atom Transfer vs Proton-Coupled Electron Transfer During Activation of X–H Bonds (X = C, N, O) by Nonheme Iron–Oxo Complexes of Variable Basicity." *J. Am. Chem. Soc.* **2013**, *135* (45), 17090–17104. (d) Bailey, W. D.; Dhar, D.; Cramblitt, A. C.; Tolman, W. B. "Mechanistic Dichotomy in Proton-Coupled Electron-Transfer Reactions of Phenols with a Copper Superoxide Complex." *J. Am. Chem. Soc.* **2019**, *141* (13), 5470–5480. (e) Goetz, M. K.; Anderson, J. S. "Experimental Evidence for p$K_a$-Driven Asynchronicity in C–H Activation by a Terminal Co(III)–Oxo Complex." *J. Am. Chem. Soc.* **2019**, *141* (9), 4051–4062. (f) Barman, S. K.; Jones, J. R.; Sun, C.; Hill, E. A.; Ziller, J. W.;

Borovik, A. S. "Regulating the Basicity of Metal-Oxido Complexes with a Single Hydrogen Bond and Its Effect on C-H Bond Cleavage." *J. Am. Chem. Soc.* **2019**, *141* (28), 11142–11150.

[6] (a) Costentin, C.; Savéant, J.-M. "Hydrogen and Proton Exchange at Carbon. Imbalanced Transition State and Mechanism Crossover." *Chem. Sci.* **2020**, *11* (4), 1006–1010. (b) Liu, T.; Tyburski, R.; Wang, S.; Fernández-Terán, R.; Ott, S.; Hammarström, L. "Elucidating Proton-Coupled Electron Transfer Mechanisms of Metal Hydrides with Free Energy- and Pressure-Dependent Kinetics." *J. Am. Chem. Soc.* **2019**, *141* (43), 17245–17259. (c) Tyburski, R.; Liu, T.; Glover, S. D.; Hammarström, L. "Proton-Coupled Electron Transfer Guidelines, Fair and Square." *J. Am. Chem. Soc.* **2021**, *143* (2), 560–576.

[7] Layfield, J. P.; Hammes-Schiffer, S. "Hydrogen Tunneling in Enzymes and Biomimetic Models." *Chem. Rev.* **2013**, *114* (7), 3466–3494.

[8] Schneider, J. S.; Goetz, M. K.; Anderson, J. S. "Reconciling Imbalanced Transition State Effects with Nonadiabatic CPET Reactions." *ChemRxiv*. **2021**. This content is a preprint and has not been peer-reviewed.

[9] Goetz, M. K.; Hill, E. A.; Filatov, A. S.; Anderson, J. S. "Isolation of a Terminal Co(III)-Oxo Complex." *J. Am. Chem. Soc.* **2018**, *140* (41), 13176–13180.

[10] See Chapter 2.4 for the synthesis and Chapter 2.2 for the characterization of the Ad-substituted compound.

[11] Luo, Y.-R. "Handbook of Bond Dissociation Energies in Organic Compounds;" CRC Press: Boca Raton, 2003.

[12] Bordwell, F. G. "Equilibrium Acidities in Dimethyl Sulfoxide Solution." *Acc. Chem. Res* **1988**, *21* (7), 456–463.

[13] Hansch, C.; Leo, A.; Taft, R. W. "A Survey of Hammett Substituent Constants and Resonance and Field Parameters." *Chem. Rev.* **1991**, *91* (2), 165–195.

[14] Bordwell, F. G.; Zhang, X.-M. "Acidities and Homolytic Bond Dissociation Enthalpies of 4-Substituted-2,6-Di-Tert-Butylphenols." *J. Phys. Org. Chem.* **1995**, *8* (8), 529–535.

[15] Rochester, C. H.; Rossall, B. "Steric Hindrance and Acidity. Part 3.—Enthalpies and Entropies of Ionization of Phenols in Methanol." *Trans. Faraday Soc.* **1969**, *65* (0), 1004–1013.

[16] (a) Dhar, D.; Yee, G. M.; Markle, T. F.; Mayer, J. M.; Tolman, W. B. "Reactivity of the Copper(III)-Hydroxide Unit with Phenols." *Chem. Sci.* **2017**, *8* (2), 1075–1085. (b) Zdilla, M. J.; Dexheimer, J. L.; Abu-Omar, M. M. "Hydrogen Atom Transfer Reactions of Imido Manganese(V) Corrole: One Reaction with Two Mechanistic Pathways." *J. Am. Chem. Soc.* **2007**, *129* (37), 11505–11511.

[17] Schneider, J. E.; Goetz, M. K.; Anderson, J. S. "Statistical Analysis of C–H Activation by Oxo Complexes Supports Diverse Thermodynamic Control over Reactivity." *Chem. Sci.* **2021**, *12* (11), 4173–4183.

# Chapter 5: Enzyme-Like Hydroxylation of Aliphatic C–H Bonds From an Isolable Co-Oxo Complex

This chapter has been adapted from the following with permission: Goetz, M. K.; Schneider, J. E.; Filatov, A. S.; Jesse, K. A.; Anderson, J. S. *J. Am. Chem. Soc.* Submitted for publication. 

## 5.1 Introduction

Direct C–H activation and hydroxylation of unactivated aliphatic bonds is a challenging but powerful transformation for the efficient synthesis of complex organic molecules and pharmaceuticals, many of which have oxygenated functionalities.[1] Nature has evolved enzymatic systems that rapidly and selectively hydroxylate aliphatic C–H bonds.[2] An archetypal example is CYP119, a cytochrome P450 enzyme that hydroxylates the C–H bonds in fatty acids (BDE ~ 101 kcal/mol) with second order rate constants as large as $10^4$-$10^7$ $M^{-1}s^{-1}$ at 4 °C.[3] The remarkable reactivity of this system has motivated intense efforts to understand what factors underpin its activity. A recent analysis of the thermodynamics of this system shows that the initial C–H activation step is uphill, but extremely fast rates are enabled by a highly favorable rebound to the in situ generated carbon radical.[3c,4]

In addition to biological systems, there has been concerted effort in discovering catalysts that mediate C–H hydroxylation reactivity in a synthetic context.[5] Many of these systems invoke transition metal-oxo intermediates,[5e,5f,6] and selectivity is noted to be greater in systems that have an extremely fast rebound step that avoids long-lived radical intermediates that can engage in side

reactions.[5f,6b,6c] In parallel, there has been significant interest in the detailed study of C–H activation by isolable, well-characterized transition metal-oxo complexes in order to better understand what factors govern the reactivity of enzymatic and synthetic catalysts. However, in most of these cases the activation of strong bonds, such as aliphatic C–H bonds, is rarely observed or slow, in direct contrast to the rates of C–H oxidation by P450s. This muted reactivity with strong C–H bonds by well-defined systems is often attributed to free energy considerations. These relatively stable transition metal-oxo intermediates frequently have $BDFE_{O–H} < BDE_{C–H}$ which, as illustrated by the Bell-Evans-Polanyi relationship and extensive literature precedent, results in inhibited reactivity.[7] The dichotomy of stabilization at the expense of reactivity results in a scarcity of metal-oxo complexes that activate strong C–H bonds where the thermodynamics are known with fidelity,[8] and in these limited examples the rates of reaction are slow when $BDE_{C–H} > BDFE_{O–H}$.[8f,g,h] In particular, late transition metal-oxo complexes, which are frequently invoked as potent oxidants, have not displayed this reactivity from well-characterized examples.[9] The activation of strong *tert*-butyl C–H bonds in Co complexes has been observed, but hydroxyl radicals are invoked in these reactions and it's unclear whether this reactivity stems from bona fide metal-oxo intermediates.[8a,b,d] Gas phase C–H activation of cyclohexane (BDE = 99.5 kcal/mol) by a transient $Co^{IV}$-oxo complex has been reported, but the relevant reaction free energies are unknown.[8c] Thus, while it has been proposed that endergonic C–H activation followed by exergonic rebound is central to selective catalysis by both molecular and enzymatic systems, examples of well-characterized transition metal-oxo systems where these steps can be studied are rare.

Chapter 3 describes the C–H activation reactivity of an isolable $Co^{III}$-oxo complex which displays unusual kinetic trends. As expected, the comparatively low $BDFE_{O–H}$ of this system

resulted in no reactivity with strong C–H bonds.[9c] Additionally, no evidence for oxygenated products arising from rebound was observed. We rationalized that a $Co^{IV}$ oxidation state would provide a more potent oxidant for strong C–H bonds. Furthermore, rebound to produce oxygenated products might be facilitated by the more favorable generation of a $Co^{II}$ complex as opposed to a $Co^{I}$ product. However, oxidation of the previously reported $PhB(^{t}BuIm)_3Co^{III}O$ results in intractable mixtures of products. Additionally, the cleanest product isolated from these reactions is most consistent with a dimeric product, detailed below in Chapter 5.2.1. Therefore, we decided to pursue a $Co^{IV}$ oxidation state with a $PhB(^{Ad}Im)_3Co^{III}O$ (see Chapter 2.2.2), which features a bulkier and more donating ligand with adamantyl (Ad) groups to support an oxidized metal center, protect the reactive Co–O unit, and inhibit bimetallic side reactions.[10]

Here, we show that 1 $e^-$ oxidation of $PhB(^{Ad}Im)_3Co^{III}O$ results in a more active oxidant which activates aliphatic C–H bonds with subsequent rebound. C–H activation proceeds through a transient and highly reactive $Co^{IV}$-oxo intermediate. This unusual high valent late transition metal-oxo species can nonetheless be observed spectroscopically. Detailed characterization of the thermodynamics of this system shows an endergonic initial C–H activation step. Nonetheless, this reaction is exceptionally fast, with a first order rate constant $>10^2$ $M^{-1}s^{-1}$, comparable to those measured for P450 enzymes. Computational analysis supports that these fast rates are driven by extremely favorable rebound, which parallels and supports mechanistic proposals for enzymatic hydroxylations. These results provide detailed experimental validation on how unfavorable C–H activation can be facilitated by favorable radical rebound.

## 5.2 Results and Discussion

### 5.2.1 Oxidation of PhB($^t$BuIm)$_3$Co$^{III}$O

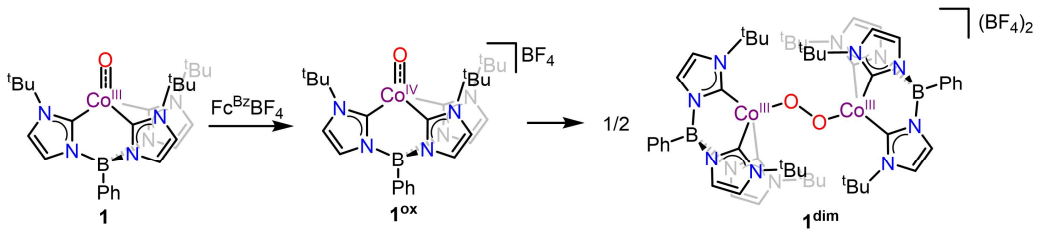


**Scheme 5.1.** Synthesis of compounds discussed in this section.

To initially explore the oxidation of PhB($^t$BuIm)$_3$Co$^{III}$O (**1**, Scheme 5.1), a cyclic voltammogram was collected in MeCN (Figure 5.1). This shows interesting electrochemical behavior that changes over time. On the first scan, there is an initial sharp irreversible feature with a peak potential at +0.055 V vs. Fc/Fc$^+$ (Fc = ferrocene) followed very closely by a second quasi-reversible feature with $E_{1/2}$ = +0.124 V vs. Fc/Fc$^+$. On the second scan, the initial sharp feature is almost entirely gone while the second quasi-reversible feature remains (Figure 5.1). This suggests that upon 1 e$^-$ oxidation, a rapid chemical reaction occurs to produce a new stable species (**1$^{dim}$**, Scheme 5.1) which can be oxidized further and reversibly reduced. Further examination of this quasi-reversible feature reveals that the peak-to-peak separation of the oxidation and reduction peaks is only 98 mV. Interestingly, under the same conditions, the peak-to-peak separation of the features for a sample of Fc is ~200 mV. The Fc/Fc$^+$ redox event is most definitely a reversible 1 e$^-$ redox event, which establishes an expected peak-to-peak separation for analogous 1 e$^-$ redox processes. However, multi-electron redox processes would be expected to have smaller peak-to-peak separations, as observed in Figure 5.1. This led us to hypothesize that 1 e$^-$ oxidation of **1**, which could reasonably produce a Co$^{IV}$-oxo intermediate (**1$^{ox}$**, Scheme 5.1), results in the formation of a

$Co^{III}/Co^{III}$-peroxo dimer complex (**1**$^{dim}$, Scheme 5.1) via O–O bond formation, similar to a $Ni^{III}/Ni^{III}$-peroxo complex isolated in our lab.[11]

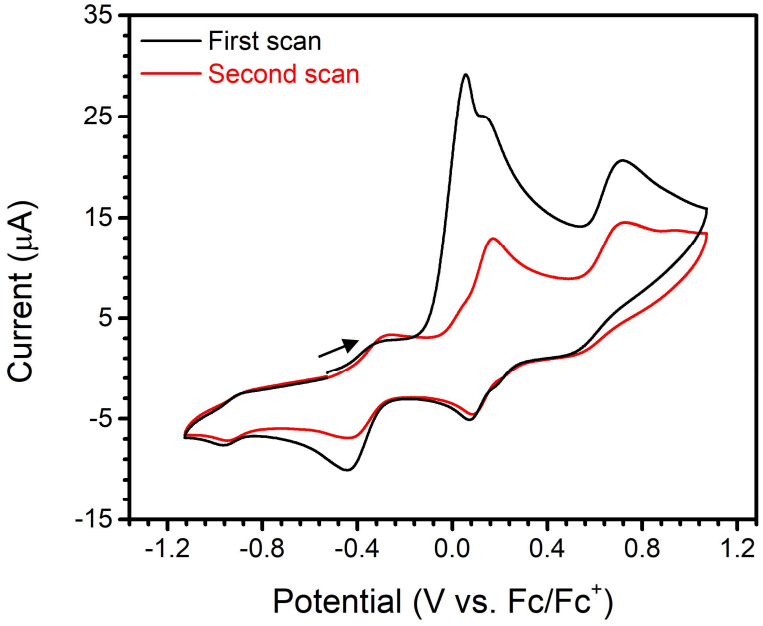


**Figure 5.1.** CV of **1** in MeCN (3 mM, 0.1 M $TBAPF_6$) collected at 100 mV/s.

To further examine this hypothesis, **1**$^{dim}$ was synthesized in bulk. Addition of benzoylferrocenium tetrafluoroborate ($Fc^{Bz}BF_4$) to solutions of **1** in THF at room temperature results in the initial formation of an orange-brown solution. Removal of solvent followed by rigorous washing of the orange-brown residue with $Et_2O$ and toluene affords a dark purple-red residue. $^1H$ NMR spectroscopic characterization of this material reveals that it is silent by NMR spectroscopy. This characterization also revealed the presence of impurities that varied in amount every attempt at synthesis (see Figure A4.1 for the cleanest $^1H$ NMR spectrum collected). Interestingly, attempts at determining the magnetic moment via Evans method demonstrate that this material is paramagnetic. However, due to the presence of impurities an accurate value for the magnetic moment could not be determined. This material is also silent by EPR spectroscopy,

indicating that it is $S = 0$ or has integer spin. Given the observation of a magnetic moment by Evans method, it is likely that this material is $S = 1$. This is consistent with the $Co^{III}_2$ formulation of $\mathbf{1^{dim}}$, which has an even number of electrons. Cyclic voltammetry of this isolated material demonstrates that the bulk of the material is redox active, and shows a reversible redox feature (Figure A4.27) consistent with the 2 $e^-$ redox event expected for $\mathbf{1^{dim}}$ and observed in the voltammogram of **1**.

Vibrational data were collected in an effort to identify the O–O bond that should be present in $\mathbf{1^{dim}}$. Collection of IR spectra of as synthesized $\mathbf{1^{dim}}$ and its $^{18}O$ and $^{16}O/^{18}O$ isotopologues revealed one isotope dependent stretch at 889 $cm^{-1}$ that shifts to 875 $cm^{-1}$ and 855 $cm^{-1}$ in the partially and fully labeled compounds, respectively (Figure A4.25). These shifts are consistent with those expected for an O–O bond that behaves as a simple harmonic oscillator. Finally, X-ray absorption spectroscopic (XAS) data were collected on this material and on **1** for comparison. This data reveals that both of the compounds have the same oxidation state at Co, as assessed by their identical Co K-edge positions (Figure 5.2B). Additionally, the pre-edge feature for the putative $\mathbf{1^{dim}}$ material decreases in intensity relative to the pre-edge feature observed in **1** (Figure 5.2A), consistent with a loss of multiple bonding upon going from **1** to $\mathbf{1^{dim}}$, as expected (Scheme 5.1).

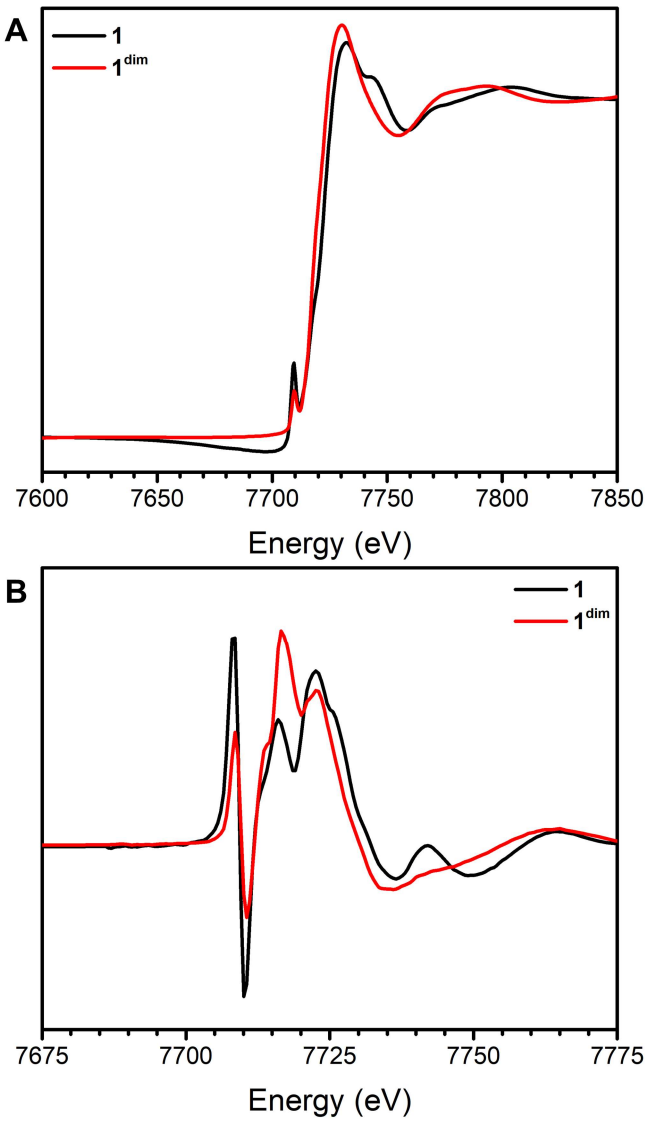


**Figure 5.2.** XAS data for **1** and **1**$^{\mathbf{dim}}$. (A) Full spectrum showing the pre-edge features. (B) First derivative showing overlapping K-edge positions.

Taken together, the silent NMR and EPR spectra, the CV data, the vibrational data, and the XAS data are all consistent with the formulation of **1**$^{\mathbf{dim}}$ shown in Scheme, formed via O–O bond formation between two **1**$^{\mathbf{ox}}$ intermediates generated by oxidation of **1**. This would be an example of direct observation of O–O bond formation between two terminal oxo complexes, as proposed for radical coupling mechanisms.[12] However, this structure could not be confirmed due to the

spectroscopic silence of this species. Additionally, all attempts at crystallization for structural characterization failed. Various solvent conditions, ion-exchanges to attempt to crystallize a different salt, and temperatures of crystallization all produced the same amorphous solids and also didn't increase the purity of the material. Thus, while all available data supports the assignment of the major product formed during the oxidation of **1** as the above-mentioned dimer, the impurity of the isolated material prevents a definitive assignment. Given these challenges, we turned to the investigation of PhB($^{Ad}$Im)$_3$Co$^{III}$O with the hypothesis that the bulkier ligand would inhibit this bimetallic reactivity and allow for clean generation of a Co$^{IV}$-oxo complex instead.

### 5.2.2 Oxidation of PhB($^{Ad}$Im)$_3$Co$^{III}$O

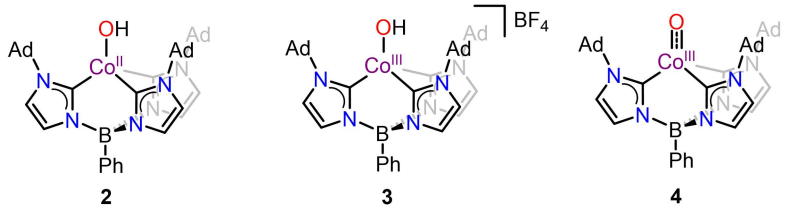


**Scheme 5.2.** Complexes discussed in this section.

To initially explore the oxidation of PhB($^{Ad}$Im)$_3$Co$^{III}$O (**4**, Scheme 5.2), a cyclic voltammogram (CV) was collected in THF (Figure A4.28). This shows an irreversible oxidation feature near 0 V vs Fc/Fc$^+$. Closer examination of this feature reveals an initial shoulder with a peak potential $E_{p,sh}$ = –0.12 V vs Fc/Fc$^+$ that appears before the main feature with $E_p$ = +0.085 V vs Fc/Fc$^+$. We hypothesized that these features could correspond to an initial oxidation to a putative Co$^{IV}$-oxo intermediate (**4$^{ox}$**) followed by a rapid chemical step to produce a second intermediate that could be further oxidized at a similar potential.

The initial oxidation seen by CV should reasonably produce a $Co^{IV}$-oxo intermediate that could engage in C–H activation reactivity to produce **3** as the metal-containing product. Therefore, we sought to characterize the $BDFE_{O–H}$ in **3** (Scheme 5.2, Equation 5.1, Scheme A4.1). Using $E_{p,sh}$ as the upper bound for the true value of the **4**/**4**$^{ox}$ redox potential and the p$K_a$ of **3** (22.6 in THF, see Chapter 2.2.2), we can calculate an upper bound for the $BDFE_{O–H}$ in **3** of 94 kcal/mol. This is ~7 kcal/mol stronger of an O–H bond than that in **2** (Scheme 5.2, 84.6 kcal/mol, see Chapter 2.2.1). As predicted, oxidation to produce a putative $Co^{IV}$-oxo intermediate results in a species that has a greater driving force for H–atom abstraction. This high $BDFE_{O–H}$, and the commensurately high reactivity of this putative $Co^{IV}$ intermediate, could explain the irreversibility observed in the CV collected at room temperature. Nonetheless, related species with comparable $BDFE_{O–H}$ values have been observed and characterized previously at low temperatures,[13] so we pursued the low-temperature oxidation of **4** to investigate possible intermediates as well as C–H oxidation reactivity.

Equation 5.1 $$\mathrm{BDFE_{O-H}} = 1.37\mathrm{p}K_\mathrm{a} + 23.06\mathrm{E}_{1/2} + C$$

We initially monitored these reactions by UV-vis spectroscopy in THF at –80 °C. Addition of 1 equivalent of $FcBF_4$ to a solution of **4** results in a very rapid (complete within <3 minutes) and relatively clean transformation to a new spectrum with absorbances at 434 nm, 478 nm, 534 nm, and 708 nm (Figure A4.15). This resulting spectrum does not change appreciably until warming above 0 °C. The absorbance at 708 nm is similar to the diagnostic 718 nm band observed in the UV-vis spectrum of **3** (Figure A4.13). This suggests that instead of observing **4**$^{ox}$ as a discrete intermediate, **3** is produced by rapid C–H activation by **4**$^{ox}$.

We turned to low temperature NMR spectroscopy to provide further insight into the products of this reaction. A solution of $FcBF_4$ in $CD_3CN$ was mixed with a solution of **4** in THF-$d_8$ at –35 °C and allowed to react for ~15 minutes before a $^1$H NMR spectrum was collected at –30 °C. No paramagnetic species are observed, precluding non-integer spin $\mathbf{4^{ox}}$ as a likely component in this reaction mixture. On the other hand, some amount of **3** was produced in this reaction as indicated by a set of $^1$H NMR features (blue highlighted peaks in Figure 5.3A) that match those observed for independently prepared **3** (Figure A4.13). Interestingly, the observation of the diagnostic O–*H* resonance of **3** at 10.60 ppm indicates that solvent C–H activation is not the source of that H–atom, since this experiment was carried out in deuterated solvent. The $^1$H NMR spectrum also shows there is another species in solution (red highlighted peaks in Figure 5.3A, **5**) that is highly asymmetric, resulting in each imidazol-2-ylidene arm being inequivalent to each other and giving rise to 6 separate Im-*H* resonances. The observation of these asymmetric signals is consistent with C–H activation of the Ad group on one arm of the ligand (Scheme 5.3A), putatively by $\mathbf{4^{ox}}$.

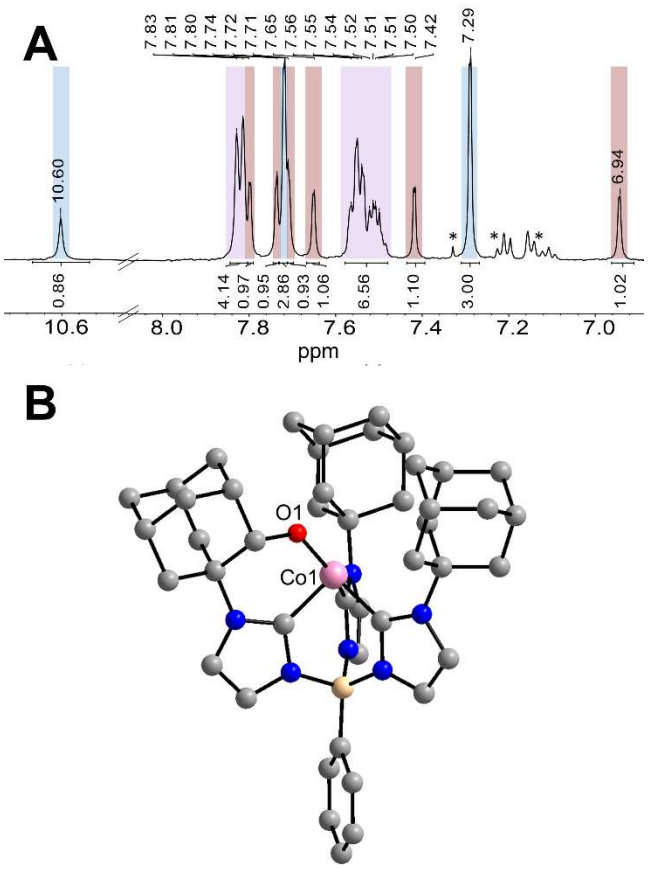


**Figure 5.3.** (A) $^{1}$H NMR spectrum at –35 °C in THF-$d_8$ of the reaction of **4** with $FcBF_4$. Only the aromatic region is shown for clarity. The full spectrum is shown in Figure A4.10. The resonances associated only with **3** are highlighted in blue and those associated only with **5** are in red. Overlapping resonances from **3** and **5** are in purple. Asterisks indicate toluene and benzene impurities in the THF-$d_8$. (B) Crystal structure of **5** shown as a ball and stick model. All H–atoms and the counterion are omitted for clarity.

While **3** decays at room temperature (see Chapter 2.2.2), the new diamagnetic species **5** is thermally stable which allowed for detailed 1D and 2D NMR spectroscopic characterization (See Appendix 4). Based on these results, complex **5** can be assigned as the chiral $Co^{III}$-alkoxide product, $[PhB(^{Ad}Im)_2(^{OAd}Im)Co^{III}][BF_4]$ (Scheme 5.3B). The formulation of **5** is just one H–atom away from the expected $Co^{II}$ product (**4$^{reb}$**, Scheme 5.3A) that might be expected as a result of C–H activation of an Ad group by **4$^{ox}$** followed by rebound to form a C–O bond. We propose that this

net H–atom is lost to form **5** via in situ oxidation of $\mathbf{4}^{reb}$ by $Fc^{+}$ with subsequent proton transfer to **4** (Scheme 5.3B). This explains the observation of **3** as a product in this reaction mixture which should be formed in a 1:1 molar ratio with **5**. Indeed, integration of the $^{1}H$ NMR spectrum reveals ratios consistent with this mechanistic proposal (Figure 5.3A). The resonance at 6.94 ppm corresponds to 1 Im-*H* in asymmetric **5** while the resonance at 7.29 ppm corresponds to 3 Im-*H* in symmetric **3**. As expected for a 1:1 molar ratio of **5**:**3**, these resonances integrate in a 1:3 ratio.

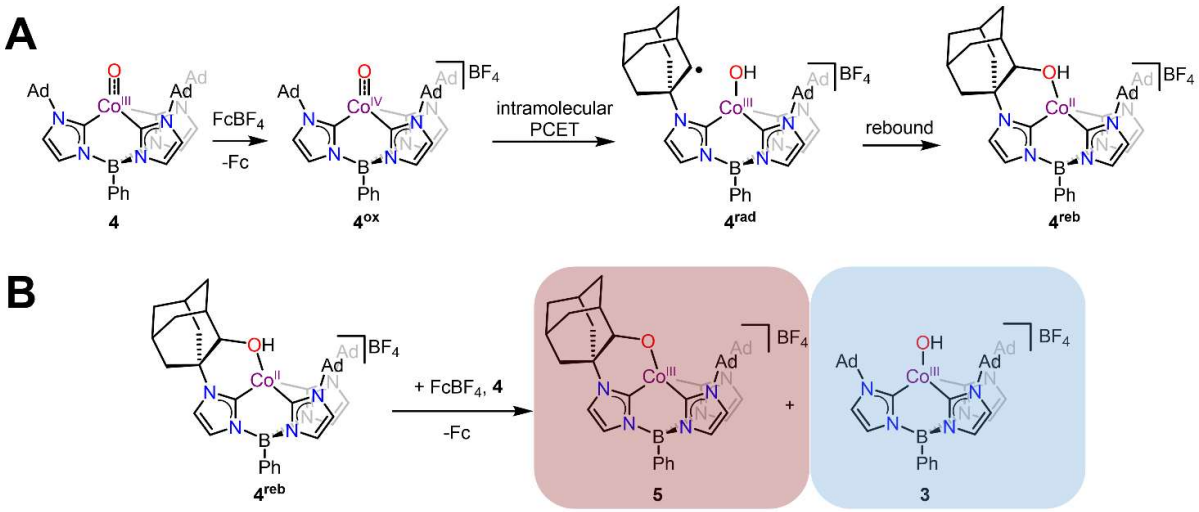


**Scheme 5.3.** Proposed reaction mechanisms following the oxidation of **4**.

The overall reaction shown in Scheme 5.3 should result in a maximum 50% yield of **5** relative to the Fc formed during the reaction. Indeed, this yield is observed in $^{1}H$ NMR spectra collected of solutions warmed to room temperature after oxidation. Additional support for the proposed formation of **5** from $\mathbf{4}^{reb}$ shown in Scheme 5.3B comes from experiments carried out with the addition of 2 equivalents of $FcBF_4$ to **4** in the presence of 1 equivalent of KO$^{t}$Bu. When this reaction is monitored by UV-vis spectroscopy at –80 °C, the growth of a strong absorbance near 700 nm, diagnostic for the presence of **3** in solution, is dramatically attenuated (Figure A4.18).

Additionally, monitoring this reaction by $^1$H NMR spectroscopy at –35 °C shows very little **3** as assayed by the diagnostic O–*H* resonance (Figure A4.12). Analysis of these solutions by $^1$H NMR spectroscopy after the reaction has been warmed to room temperature shows that the yield of **5** relative to Fc is increased to ~90% (Figure A4.11).

Complex **5** was therefore synthesized in bulk using 2 equivalents of $FcBF_4$ and 1 equivalent of $KO^tBu$ and isolated in 64% yield. This compound has been thoroughly characterized, including by elemental analysis (See Chapter 5.4 and Appendix 4). The assignment of **5** was also confirmed by X-ray diffraction data collected on single crystals of the ion-exchanged $BAr^F{}_4^-$ salt ($BAr^F{}_4^-$ = tetrakis(3,5-bis(trifluoromethyl)phenyl)borate, see Chapter 5.4) grown from an $Et_2O$ solution layered under pentane (Figure 5.3B). Due to complicated disorder of the O–atom over multiple positions, the data quality is only suitable to confirm the connectivity of the atoms in **5**. Nonetheless, the Co–O–C unit is clearly observed and the presence of a single $BAr^F{}_4$ anion supports a $Co^{III}$ complex with an alkoxide ligand. Taken together, these observations support the formation of the terminal product **5** from rapid intramolecular C–H activation by $\mathbf{4^{ox}}$ and subsequent rebound to form $\mathbf{4^{reb}}$ followed by the intermolecular reactivity shown in Scheme 5.3.

### 5.2.3 Observation of the $Co^{IV}$ Intermediate $[PhB(^{Ad}Im)_3Co^{IV}O]^+$

The reaction mechanism shown in Scheme 5.3A invokes a key $Co^{IV}$-oxo intermediate. Such high-valent Co complexes are quite rare although they have been invoked as reactive intermediates.[8c,9a,9b,14] While there is one example of a spectroscopically characterized terminal $Co^{IV}$-oxo species, it does not engage in the activation of aliphatic C–H bonds.[9b] Therefore, we set out to observe any transient $Co^{IV}$ complex in order to support the proposed agency of $\mathbf{4^{ox}}$. We first monitored addition of $FcBF_4$ to solutions of **4** by UV-vis spectroscopy at temperatures lower than

–80 °C in the hopes of slowing down the reaction enough to observe **4$^{ox}$**. However, no evidence for an intermediate is discernible in the UV-vis spectra of reactions carried out in THF at –105 °C or in 2-MeTHF at –130 °C (See Appendix 4). We turned to EPR spectroscopy in the hopes of observing an $S = 1/2$ signal in solutions prepared by mixing $FcBF_4$ and **4** at low temperatures (–105 °C in THF or –130 °C in 2-MeTHF) followed by freezing in liquid nitrogen. However, no $S = 1/2$ signal consistent with a $Co^{IV}$ intermediate can be observed in these experiments.

C–H activation reactions mediated by transition metal-oxo and hydroxide complexes frequently have large deuterium kinetic isotope effects (KIEs), especially at low temperatures.[8b,15] Furthermore, deuteration of reactive C–H groups on ligands has previously enabled the characterization of transient oxo intermediates.[16] Therefore, we reasoned that we would be able to observe **4$^{ox}$** by slowing down the reaction through deuteration of the Ad groups on the ligand in **4**. This was achieved on a small scale starting from adamantane-$d_{16}$. The starting material for the first step of the ligand synthesis,[10] 1-bromoadamantane-$d_{15}$, was synthesized by refluxing adamantane-$d_{16}$ in bromine for 3 hours.[17] After work up, 1-bromoadamantane-$d_{15}$ was isolated in 73% yield. With this material in hand, 1-(adamantyl-$d_{15}$)-imidazole and $PhB(^{Ad\text{-}d15}ImH)_3OTf_2$ were made following the reported procedures for the synthesis of the proteo compounds.[10] Finally, following the procedures detailed in Chapter 2.4 and Chapter 5.4, the compounds $PhB(^{Ad\text{-}d15}Im)_3Co^{II}Cl$, **2-*d*$_{45}$**, and **4-*d*$_{45}$** were made. Unfortunately, after this lengthy synthetic route, the obtained **4-*d*$_{45}$** was contaminated with a 29% impurity of **2-*d*$_{45}$** as determined by $^1$H NMR spectroscopy. Fortunately, this impurity can be easily accounted for during subsequent analysis of the reactions as described below.

Oxidation of **4-*d*$_{45}$** with $FcBF_4$ in THF-$d_8$ at –105 °C was initially followed by UV-vis spectroscopy (Figure A4.19). After collection of an initial spectrum, 1 equivalent of $FcBF_4$ was injected into the cuvette and a spectrum was collected beginning ~5 seconds after injection. Additional spectra were collected every 45 seconds. Examination of the spectra > 900 nm shows immediate consumption of **4-*d*$_{45}$** upon addition of oxidant, as evidenced by the disappearance of the trailing absorbance from **4-*d*$_{45}$** in the first scan after injection, followed by no further changes over time. This is in contrast to the oxidation of **4**, where only ~1/2 of **4** is consumed immediately after injection of $FcBF_4$, as the other 1/2 equivalent of $FcBF_4$ is consumed by the rapidly produced **4$^{reb}$**. A slower disappearance of the additional 1/2 equivalent of **4** occurs during the putative proton transfer step, consistent with the mechanism shown in Scheme 5.3. Thus, for the oxidation of **4-*d*$_{45}$**, it is likely that all oxidation equivalents are consumed in the generation of **4$^{ox}$-*d*$_{45}$** without any convolution from the immediate formation of **4$^{reb}$** or **5**. After spectral deconvolution to remove features from the small amount of **3-*d*$_{45}$** generated from the **2-*d*$_{45}$** impurity, we observe a spectrum with features at 492 nm, 552 nm, and 616 nm (Figure A4.20). This spectrum displays generally good agreement with the spectrum predicted by TD-DFT calculations carried out on **4$^{ox}$** (Figure A4.20), even considering the limited accuracy of computational methods in predicting such spectra.[18] This correlation supports that we are indeed observing this proposed $Co^{IV}$ intermediate.

We additionally looked at this reaction by EPR spectroscopy. Fortunately, any **3-*d*$_{45}$**, which is diamagnetic, that would be generated from the **2-*d*$_{45}$** impurity will be silent by EPR spectroscopy, preventing any signal convolution as was seen in UV-vis spectroscopy. Preparation of samples at –105 °C in THF-$d_8$ followed by immediate freezing in liquid nitrogen and collection of data within 5 minutes at 15 K reveals a unique $S = 1/2$ signal (Figure 5.4). Simulation of this signal gives *g*-

values of 2.0439, 2.0238, and 2.0218. There is also an 8-line pattern arising from coupling to the $I = 7/2$ $^{59}$Co nucleus. This pattern can be simulated with hyperfine coupling constants of $A$ = 16.6, 76.2, and –0.2 MHz. These simulated parameters are consistent with an $S = 1/2$ Co complex, as proposed for this $d^5$ $Co^{IV}$-oxo species. These parameters are also in line with those that have been reported previously for other $S = 1/2$ $Co^{IV}$ complexes.[9a,14b,19] In particular, **4$^{ox}$-*d*$_{45}$** displays relatively small hyperfine coupling constants that are more similar to those reported for spin delocalized systems[19a,c] than those reported for systems where the spin is highly localized on the $^{59}$Co nucleus.[14b] This, in addition to the *g*-values near 2, suggests that there is likely a significant amount of O–centered spin density in **4$^{ox}$-*d*$_{45}$**. IBO analysis predicts a population of 0.44 spins on O,[20] consistent with this hypothesis. Regardless, the UV-vis and EPR spectroscopic data for the oxidation of **4-*d*$_{45}$** support the presence of **4$^{ox}$** as an intermediate in the reaction outlined in Scheme 5.3.

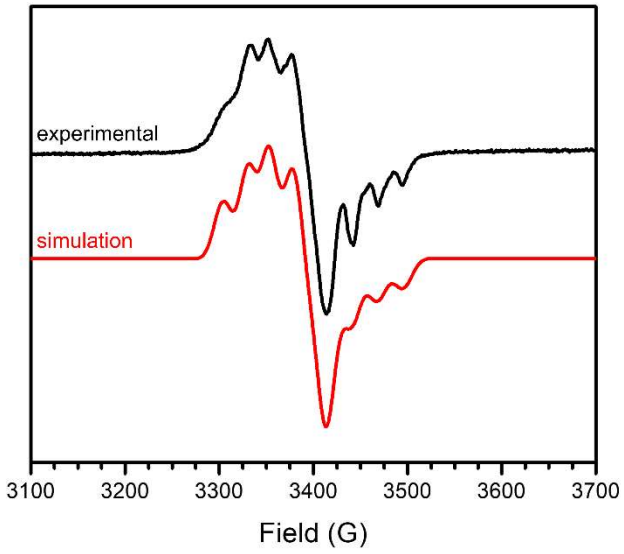


**Figure 5.4.** Perpendicular mode X-band EPR spectrum (15 K) of **4$^{ox}$-*d*$_{45}$** generated in situ at –105 °C in THF-$d_8$. Simulation parameters: $g$ = 2.0439, 2.0238, 2.0218; $A$ = 16.6, 76.2, –0.2 MHz. Experimental conditions: microwave frequency 9.6304 GHz, microwave power 0.2 mW.

### 5.2.4 Analysis of C–H Activation by $[PhB(^{Ad}Im)_3Co^{IV}O]^+$

While the above data from reactions with **4-*d*$_{45}$** support the agency of **4$^{ox}$** in this system, the fleeting nature of this and other intermediates invoked in Scheme 5.3A, namely **4$^{rad}$** and **4$^{reb}$**, prompted us to use density functional theory calculations to optimize these possible intermediates and analyze the free energies of this proposed mechanism (Figure 5.5). These calculations reveal that the initial C–H activation step to produce **4$^{rad}$** is endergonic with ΔG = +3.3 kcal/mol. This result agrees with our experimentally determined thermodynamics; we calculate an upper bound for the $BDFE_{O–H}$ in **3** as 94 kcal/mol (see Chapter 5.2.2), and the $BDE_{C–H}$ for the $CH_2$ groups in free adamantane is 98.5 kcal/mol.[21] Using these as good approximations for the C–H bond broken and the O–H bond formed to give the intermediate **4$^{rad}$**, we would estimate that ΔG = +4.5 kcal/mol for C–H activation.

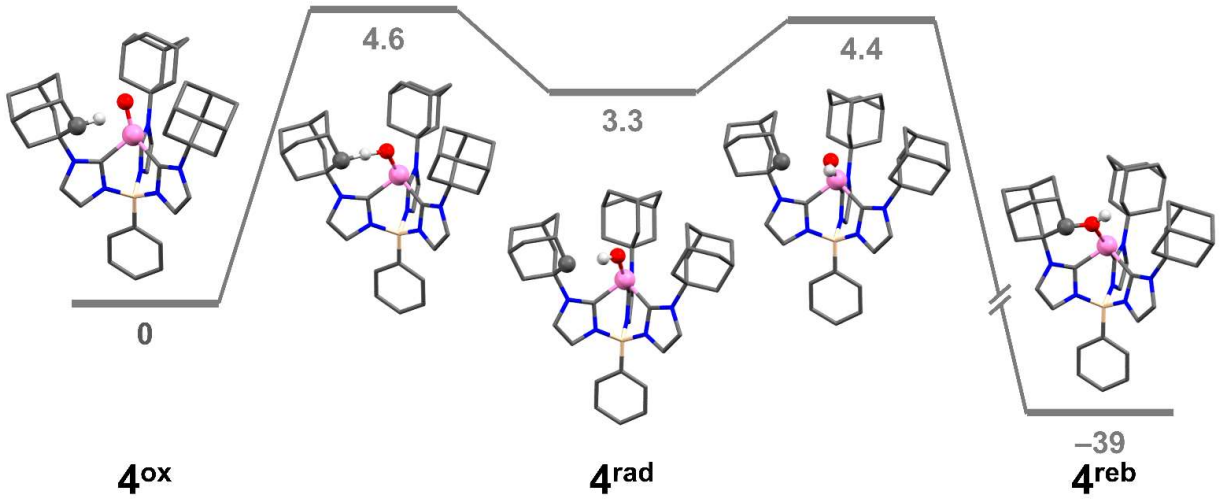


**Figure 5.5.** Reaction coordinate for intramolecular C–H activation and rebound from **4$^{ox}$**. The structures shown are the DFT optimized structures of the intermediates and transition states, shown as sticks except for Co, O, the transferring H–atom, and the involved C–atom. The energies given are the calculated free energies at –80 °C, relative to **4$^{ox}$**, in kcal/mol.

Despite this initial endergonic step, productive reactivity does occur to form **5**, presumably through the intermediate $\mathbf{4^{reb}}$. This must be driven by a favorable secondary reaction, since ground state thermodynamics would predict that for a reaction with $\Delta G > 0$, any equilibrium would heavily favor the reactants in the first step. Indeed, this idea is supported by the very exergonic secondary reaction predicted by DFT to produce $\mathbf{4^{reb}}$ from $\mathbf{4^{rad}}$ (Figure 5.5) with $\Delta G = -42$ kcal/mol. This second step only has a barrier of 1.1 kcal/mol from $\mathbf{4^{rad}}$ and would be expected to proceed very rapidly whenever $\mathbf{4^{rad}}$ is formed. This combination of a very exergonic step with almost no barrier likely contributes to favoring formation of $\mathbf{4^{reb}}$ and ultimately the observed product **5**.

We can contrast this result to the analogous $Co^{III}$ system (complex **4**) which does not engage in this reactivity. Samples of **4** are stable at –35 °C for weeks and can be handled at room temperature over hours, while all attempts at isolating $\mathbf{4^{ox}}$ result in rapid formation of **5**. DFT analysis of the same reaction coordinate for the $Co^{III}$ system (Figure A4.30) reveals that the initial C–H activation step is now 17 kcal/mol uphill from **4** while the rebound step to produce a $Co^{I}$ complex is only 19 kcal/mol downhill from the $Co^{II}$ intermediate. Not only is there less driving force for rebound in this system, but the formation of a $Co^{I}$ complex is essentially thermoneutral from the starting complex **4**. This highlights that by oxidizing to a formally $Co^{IV}$ oxidation state, we are able to engage in more difficult reactivity by a) utilizing a stronger oxidant to enable the initial C–H activation step and b) driving the overall reaction with an extremely favorable secondary rebound step, which is not accessible for a $Co^{III}$ starting material.

We also sought to contextualize the rate of C–H activation by $\mathbf{4^{ox}}$ by comparing to other examples in the literature. Most isolable transition metal-oxo (or related) complexes that engage in uphill reactivity do so at very slow rates.[8f,8g,13] In contrast, cytochrome P450 enzymes are known to react

with the strong C–H bonds in fatty acids with second order rate constants on the order of $10^4$-$10^7$ $M^{-1}s^{-1}$ and a first order rate constant for C–H activation after substrate is bound has been estimated at > 1400 $s^{-1}$ at 4 °C.[3a] We note that care must be taken in comparing the rate constants of these bimolecular reactions in synthetic examples with enzymatic reactions. Nonetheless, we set out to estimate the first order rate constant for C–H activation by **4$^{ox}$** in order to see how the present system compares to one of the most kinetically active oxidants known.

Given our inability to isolate **4$^{ox}$** upon oxidation of **4**, we are unable to directly measure the rate constant for C–H activation. However, the rapid kinetics of the reaction necessitate that the rate of C–H activation must be greater than the rate of oxidation of **4** by $FcBF_4$. Therefore, in order to provide a lower bound on the rate of C–H activation by **4$^{ox}$**, we estimated the rate of oxidation of **4** by the method of initial rates.[22] Unfortunately, the rate of this reaction is at the limit of measurable rates for our experimental apparatus, so we were only able to provide a lower bound for the rate constant for oxidation (See Chapter 5.4 and Appendix 4). Nonetheless, we estimated the lower bound of the second order rate constant for oxidation of **4** by $FcBF_4$ as 440±50 $M^{-1}s^{-1}$ at –80 °C. We carried out this analysis at two additional temperatures, –105 °C and –40 °C, in order to estimate the second order rate constant at 4 °C for direct comparison to P450. This analysis gives us a lower bound on the second order rate constant for oxidation of 1.1(6)•$10^3$ $M^{-1}s^{-1}$ at 4 °C. To convert this oxidation rate constant to a C–H activation rate constant, we used our assumption that the rate of C–H activation by **4$^{ox}$** is greater than the rate of oxidation at any point during the reaction. If we assume that an upper bound for the maximum buildup of [**4$^{ox}$**] is 1% of initial concentration of **4**, then we can use this lower bound for $k_2$ to determine a lower bound for

the first order rate constant for C–H activation by **4$^{ox}$** as 1.3(7)•$10^2$ $s^{-1}$ at 4 °C (See Chapter 5.4, Equation 5.5).

This first order rate constant is large and comparable to that reported for C–H activation by cytochrome P450 enzymes, ~$10^3$ $s^{-1}$ at 4 °C. This large rate constant is also consistent with the relatively low energy of the transition state predicted by DFT (Figure 5.5). In fact, this system has many parallels to the proposed factors that enable the remarkable reactivity of P450. It has been recently argued that the reactivity of P450 is enabled by a thermodynamically favorable rebound immediately following unfavorable C–H activation, exactly the scenario at play in this Co-based system.[3c] These similarities suggest that the C–H activation exhibited by the terminal metal-oxo **4$^{ox}$** is biomimetic, and that the strategy of enabling uphill C–H activation with a rapid and favorable rebound step can be general across synthetic and natural systems.

## 5.3 Conclusions

Oxidation of PhB($^{Ad}$Im)$_3$Co$^{III}$O results in an unusual and highly reactive Co$^{IV}$-oxo intermediate which rapidly activates a C–H bond on the ligand. While this initial C–H activation step is endergonic, an extremely favorable rebound step to form a C–O bond enables the overall reactivity. This mechanistic scenario has been confirmed by the isolation and characterization of the chiral Co$^{III}$-alkoxide compound **5** as well as spectroscopic characterization of the deuterated intermediate **4$^{ox}$-*d*$_{45}$**. DFT calculated reaction energetics as well as spectroscopic parameters also support this picture.

Efforts to measure the kinetics of C–H activation provide a lower bound for the first order rate constant for C–H activation of 130 $s^{-1}$, a value comparable to the 1400 $s^{-1}$ value determined for

C–H activation by compound I in P450 enzymes.[3a] Thus, by oxidizing a terminal $Co^{III}$-oxo complex, we are able to generate a hydroxylating intermediate that is capable of activating strong C–H bonds with similar rate constants and mechanistic features to enzymatic systems. These studies constitute one of the few well-characterized examples of activation of strong C–H bonds by a transition metal-oxo complex. In particular, this well-defined system, where we can measure and determine thermodynamic parameters, validates the proposed importance of rebound in enzymatic and synthetic catalysts.

## 5.4 Experimental

**General Considerations.** All manipulations were performed under a dry nitrogen atmosphere using either standard Schlenk techniques or in an mBraun Unilab Pro glovebox unless otherwise stated. All chemicals were obtained from commercial sources and used as received unless otherwise stated. Adamantane-$d_{16}$ was purchased from CDN Isotopes and used as received. Solvents were dried on a solvent purification system from Pure Process Technologies before storing over 4 Å molecular sieves under $N_2$. Tetrahydrofuran (THF), THF-$d_8$, and diethyl ether ($Et_2O$) were stirred over NaK alloy and passed through a column of activated alumina prior to storing over 4 Å sieves under $N_2$. $NaBAr^F{}_4$ was prepared according to previously reported procedures.[11] $FcBF_4$ and $TBAPF_6$ were recrystallized prior to use. $PhB(^tBuIm)_3Co^{III}O$ and $PhB(^{Ad}Im)_3Co^{III}O$ were prepared according to the methods described in Chapter 2.4. EPR spectra were recorded on a Bruker Elexsys E500 spectrometer with an Oxford ESR 900 X-band cryostat and a Bruker Cold-Edge Stinger. UV-vis spectra were recorded on a Thermo Scientific Evolution 300 spectrometer with the VISIONpro software suite. A standard 1 cm quartz cuvette with an air-tight screw cap with a puncturable Teflon seal was used for all measurements. A Unisoku

CoolSpek cryostat was used for low temperature measurements. $^{1}H$, $^{13}C\{^{1}H\}$, $^{11}B\{^{1}H\}$, and $^{19}F$ NMR spectra were recorded on either Bruker DRX-400 or AVANCE-500 spectrometers. $^{1}H$ and $^{13}C\{^{1}H\}$ spectra were referenced to residual proteo-solvent peaks. $^{11}B\{^{1}H\}$ spectra were baseline corrected to remove the signal from the borosilicate tube. Combustion analysis was performed by Midwest Microlab. IR spectra were recorded on a Bruker Tensor II spectrometer with the OPUS software suite as mulls in Nujol oil pressed between KBr plates or as KBr pellets. Electrochemical measurements were carried out using a BAS Epsilon potentiostat and using BAS Epsilon software version 1.40.67NT. Magnetic moments were determined using the Evans method.[23]

**Synthesis of $Fc^{Bz}BF_4$.** Benzoylferrocene (200 mg, 0.69 mmol) was dissolved in 15 mL of $Et_2O$ at room temperature. $AgBF_4$ (121 mg, 0.62 mmol, 0.9 equiv.) was added as a solid and the reaction allowed to stir for 30 minutes. The $Et_2O$ was removed and the residue dissolved in DCM and filtered to remove gray Ag solid. The solution was concentrated to ~2 mL before addition of excess $Et_2O$ to precipitate out the $Fc^{Bz}BF_4$. The blue solid was collected by filtration. The solid was recrystallized by layering a DCM solution under $Et_2O$ at –35 °C to afford pure $Fc^{Bz}BF_4$ (211 mg, 0.56 mmol, 90% yield). The solid was stored in the freezer to prevent decomposition.

**Synthesis of samples of impure $\mathbf{1^{dim}}$.** To a solution of **1** in THF (12 mL) at room temperature was added 1 equivalent of $Fc^{Bz}BF_4$ dissolved in minimal MeCN. The solution was allowed to stir for ~15 minutes before removal of solvent in vacuo. The orange-brown residue was washed extensively with $Et_2O$, followed by washing with toluene before being dried to afford a dark purple-red residue. This residue was generally redissolved in THF and layered under pentane at –35 °C to give a purple-red powder that was used for subsequent experiments.

**Synthesis of isotopically labeled samples of $\mathbf{1^{dim}}$.** Isotopically labeled samples of $\mathbf{1^{dim}}$ were synthesized as described above, substituting **1-$^{18}$O** to afford fully labeled $\mathbf{1^{dim}}$ or using a 1:1 mixture of **1** and **1-$^{18}$O** to afford partially labeled $\mathbf{1^{dim}}$.

**Synthesis of 1-bromoadamantane-$d_{15}$.** This compound was synthesized following a previously reported procedure.[17] A 50 mL round bottom flask equipped with a stir bar was charged with 2.0 g (13 mmol) of adamantane-$d_{16}$ and 5.0 mL of $Br_2$ (97 mmol). A long reflux condenser was added and loosely capped with a septum equipped with a vent needle. The mixture was heated to reflux (~60 °C) for 3 h before being cooled to room temperature. The mixture was diluted with $CCl_4$ (20 mL) and transferred to a separatory funnel. The solution was washed with saturated sodium bisulfite ($NaHSO_3$) solution in 10 mL portions until the $Br_2$ color was gone. CAUTION: Lots of heat and gas is released during this step. Take appropriate safety precautions. The now pale yellow $CCl_4$ solution was washed twice with $H_2O$ before drying over $MgSO_4$ and filtering to give a clear yellow solution. The solvent was removed *in vacuo* and the residue recrystallized from MeOH to give pure 1-bromoadamantane-$d_{15}$ in 73% yield (2.21 g, 9.5 mmol). $^2$H NMR ($CDCl_3$, 76.8 MHz): δ 2.33 ($6^2$H), 2.06 ($3^2$H), 1.68 ($6^2$H).

**Synthesis of 1-(adamantyl-$d_{15}$)-imidazole.** This compound was synthesized analogously to 1-adamantylimidazole.[10] A 100 mL Schlenk tube with a Kontes valve was charged with 2.21 g (9.5 mmol) 1-bromoadamantane-$d_{15}$, 2.6 g (38 mmol) imidazole, 2.0 mL toluene, and a stir bar. The Schlenk tube was sealed and heated to 150 °C behind a blast shield for 36 hours. CAUTION: Explosion hazard due to heating above the boiling point of toluene in a sealed vessel. After the reaction, the mixture was allowed to cool to room temperature before being unsealed and mixed with 50 mL of 1 M KOH. Dichloromethane (DCM, 50 mL) was added and the mixture transferred

to a separatory funnel. The DCM layer was collected, dried over $MgSO_4$, filtered and pumped down to a brown, sticky residue. Extraction into hot hexanes and removal of the solvent *in vacuo* afforded 1-(adamantyl-$d_{15}$)-imidazole in 55% yield (1.12 g, 5.2 mmol). $^1$H NMR ($CDCl_3$, 500 MHz): δ 7.63 (1H, Im-*H*), 2.06 (2H, Im-*H*). $^2$H NMR ($CDCl_3$, 76.8 MHz): δ 2.19 ($3\,^2$H, Ad-$^2$*H*), 2.05 ($6\,^2$H, Ad-$^2$*H*), 1.70 ($6\,^2$H, Ad-$^2$*H*).

**Synthesis of PhB($^{Ad\text{-}d15}$ImH)$_3$OTf$_2$.** This compound was synthesized analogously to PhB($^{Ad}$ImH)$_3$OTf$_2$.[10] Toluene (7 mL), $PhBCl_2$ (240 μL, 1.8 mmol), 1-(adamantyl-$d_{15}$)-imidazole (1.2 g, 5.5 mmol), and TMSOTf (670 μL, 3.6 mmol) were combined in a 50 mL round bottom Schlenk flask. The flask was equipped with a reflux condenser under active $N_2$ flow and the heterogeneous mixture was heated to 100 °C overnight before being allowed to cool to room temperature. The solvent was decanted and the solid dissolved in boiling DCM. This solution was stored at –35 °C until pure PhB($^{Ad\text{-}d15}$ImH)$_3$OTf$_2$ crystallized as a white solid (714 mg, 0.69 mmol, 37% yield). $^1$H NMR ($CDCl_3$, 500 MHz): δ 8.30 (3H, Im-*H*), 7.42 (6H, Im-*H*, Ph-*H*), 7.27 (3H, Im-*H*), 7.23 (2H, Ph-*H*). $^2$H NMR ($CDCl_3$, 76.8 MHz): δ 2.16 (br, $27\,^2$H, Ad-$^2$*H*), 1.68 ($18\,^2$H, Ad-$^2$*H*).

**Synthesis of PhB($^{Ad\text{-}d15}$Im)$_3$Co$^{II}$Cl.** Isotopically labeled PhB($^{Ad\text{-}d15}$Im)$_3$Co$^{II}$Cl was synthesized following the procedure described in Chapter 2.4, substituting PhB($^{Ad\text{-}d15}$ImH)$_3$OTf$_2$ for PhB($^{Ad}$ImH)$_3$OTf$_2$. The purity of PhB($^{Ad\text{-}d15}$Im)$_3$Co$^{II}$Cl was confirmed by $^1$H NMR spectroscopy.

**Synthesis of 2-*d*$_{45}$.** Isotopically labeled **2** was synthesized following the procedure described in Chapter 2.4, substituting PhB($^{Ad\text{-}d15}$Im)$_3$Co$^{II}$Cl for PhB($^{Ad}$Im)$_3$Co$^{II}$Cl. The purity of **2-*d*$_{45}$** was confirmed by $^1$H NMR spectroscopy.

**Synthesis of 4-*d*$_{45}$.** Isotopically labeled **4** was synthesized following the procedure described in Chapter 2.4, substituting **2-*d*$_{45}$** for **2**. After work-up, this sample of **4-*d*$_{45}$** was contaminated with 29% of **2-*d*$_{45}$** as seen in $^{1}$H NMR spectroscopy. It was used as is and not purified further.

**Synthesis of 5.** A solution of **4** in 12 mL THF (60 mg, 78 μmol) was cooled to –50 °C. A solution of KO$^{t}$Bu in 1.0 mL THF (8.8 mg, 78 μmol) was added prior to addition of a solution of $FcBF_4$ in 0.5 mL MeCN (44 mg, 160 μmol). A color change from purple to red-orange was observed. This reaction was allowed to stir for ~15 minutes at –50 °C before pumping down at room temperature. The red residue was triterated with pentane before being washed with $Et_2O$ to remove Fc. The remaining solid was dissolved in MeCN and layered under $Et_2O$ at –35 °C to give pure **5** as a red powder (43 mg, 50 μmol, 64% yield). $^{1}$H NMR ($CD_3CN$, 400 MHz): δ 7.78 (2H, Ph-*H*), 7.55 (3H, Ph-*H*), 7.53 (1H, Im-*H*), 7.46 (1H, Im-*H*), 7.37 (2H, Im-*H*), 7.31 (1H, Im-*H*), 6.87 (1H, Im-*H*), 3.78 (1H, Ad-*H*), 2.62 (3H, Ad-*H*), 2.53 (1H, Ad-*H*), 2.48 (6H, Ad-*H*), 2.37 (3H, Ad-*H*), 2.30 (7H, Ad-*H*), 2.22 (1H, Ad-*H*), 2.00 (1H, Ad-*H*), 1.89-1.78 (16H, Ad-*H*), 1.72 (3H, Ad-*H*), 1.60 (1H, Ad-*H*), 1.47 (1H, Ad-*H*). $^{13}$C NMR ($CD_3CN$, 100 MHz): δ 134.6, 129.7, 129.5, 127.8, 126.7, 126.5, 123.8, 122.5, 121.4, 80.5, 65.2, 59.5, 59.2, 46.4, 45.7, 43.0, 40.9, 40.0, 37.1, 36.5, 36.3, 36.2, 36.0, 35.7, 31.2, 30.7, 30.5, 30.3, 30.2, 29.9. $^{11}$B NMR ($CD_3CN$, 128 MHz): δ –1.2. $^{19}$F NMR ($CD_3CN$, 471 MHz): δ –151.9. IR (KBr, cm$^{-1}$): 3173 (w), 3134 (m), 2906 (s), 2852 (s), 1626 (br), 1542 (m), 1450 (m), 1430 (s), 1409 (m), 1380 (m), 1363 (w), 1339 (m), 1306 (m), 1248 (m), 1219 (m), 1192 (s), 1172 (m), 1105 (s), 1062 (s), 1029 (s), 933 (m), 903 (w), 891 (s), 832 (s), 816 (w), 801 (w), 785 (m), 764 (m), 725 (s), 697 (s). UV-vis, nm in MeCN (ε, M$^{-1}$cm$^{-1}$): 406 (sh, 799), 492 (736), 526 (695), 648 (sh, 174). Anal. Calc. for $C_{45}H_{55}B_2CoF_4N_6O$: C 63.40, H 6.50, N 9.86, Found: C 63.25, H 6.52, N 9.40.

**Ion Exchange to Produce 5-BAr$^{F}_{4}$.** A solution of 15 mg (18 μmol) NaBAr$^{F}_{4}$ in 1.2 mL $Et_2O$ was added to 15 mg (18 μmol) of solid **5**. The mixture was allowed to stir until all of the red solid had dissolved into solution. This solution was filtered to remove $NaBF_4$ and layered under pentane at –35 °C to afford single crystals of **5-BAr$^{F}_{4}$** suitable for X-ray diffraction.

**Cyclic Voltammetry.** For cyclic voltammetry experiments, 5.0 mL of a 3 mM solution of the complex of interest were prepared in the desired solvent. Tetrabutylammonium hexafluorophosphate ($TBAPF_6$) was used as the supporting electrolyte at a concentration of 0.1 M. A glassy carbon electrode with a 3 mm diameter was used as the working electrode with a platinum wire as the counter electrode. A silver wire was used as the reference electrode and referenced to the $Fc/Fc^+$ couple. Cyclic voltammograms were collected at a standard scan rate of 100 mV/s. Variable scan rate data were collected for **1$^{dim}$** (Figure A4.27) as well.

**Procedure for Oxidations of 4 Monitored by UV-vis Spectroscopy.** In the glovebox, 2.0 mL of a 1.25 mM solution of **4** in THF or 2-MeTHF was transferred to a standard 1 cm cuvette and sealed with a puncturable cap. The cuvette was then transferred to the cryostat and cooled to the desired temperature (–80 °C, –105 °C, or –130 °C). After an initial scan, 50 μL of a 50 mM solution (1 equivalent) of $FcBF_4$ in 2:1 THF/MeCN (100 μL of a 25 mM solution in 1:1 2-MeTHF/EtCN for experiments at –130 °C) was injected into the cuvette. The reaction was monitored by collecting spectra every 45 seconds until the spectrum stopped changing.

**Procedure for Oxidation of 4 in the Presence of Base Monitored by UV-vis Spectroscopy.** In the glovebox, 2.0 mL of a 1.25 mM solution of **4** in THF was transferred to a standard 1 cm cuvette and sealed with a puncturable cap. The cuvette was then transferred to the cryostat and cooled to –80 °C. After an initial scan, 25 μL of a 100 mM solution (1 equivalent) of KO$^{t}$Bu in

THF was injected and a spectrum collected to ensure no side reactions had occurred. Next, 100 μL of a 50 mM solution (2 equivalents) of $FcBF_4$ in 2:1 THF/MeCN was injected into the cuvette. The reaction was monitored by collecting spectra every 45 seconds until the spectrum stopped changing.

**Procedure for Oxidation of 4 Monitored by Low Temperature NMR Spectroscopy.** In a small vial in the glovebox, cooled 700 μL of a 2.0 mM solution of **4** in THF-$d_8$ to –80 °C in the cold well. Next, 14 μL of a 100 mM solution (1 equivalent) of $FcBF_4$ in $CD_3CN$ were added and the mixture allowed to react for ~10 minutes before being transferred to a pre-cooled J. Young NMR tube. The tube was transported to the NMR spectrometer in a –78 °C cold bath before spectra were collected at –30 °C.

**Procedure for Oxidation of 4 in the Presence of Base Monitored by Low Temperature NMR Spectroscopy.** In the glovebox, 500 μL of a solution of 5 mM **4** and 5 mM KO$^t$Bu in THF-$d_8$ was transferred to a standard NMR tube and sealed with a puncturable septum. The tube was removed from the glovebox and cooled to –40 °C in a cold bath. After cooling, 50 μL of a 100 mM solution (2 equivalents) of $FcBF_4$ in $CD_3CN$ was injected through the septum. The solution was thoroughly mixed and allowed to react for ~10 minutes before spectra were collected at –35 °C.

**Estimation of a Lower Bound for the *k* for C–H Activation by $4^{ox}$.** A lower bound for the rate constant for C–H activation by $\mathbf{4^{ox}}$ was found by determining the second order rate constant for oxidation of **4** with $FcBF_4$ by UV-vis spectroscopy where we monitored the consumption of **4** by the disappearance of its trailing absorbance at 940 nm. This reaction is extremely fast and must be carried out stoichiometrically, prompting the use of the method of initial rates.[22] In a typical

experiment, 2.0 mL of a 1.25 mM solution of **4** in THF was transferred to a standard 1 cm cuvette and sealed with a puncturable cap. The cuvette was then transferred to the cryostat and cooled to the desired temperature (–40 °C, –80 °C, or –105 °C). Single wavelength data collection at 940 nm was started. Data was collected every 20 ms with an integration time of 10 ms. After the initial absorbance had stabilized, 50 μL of a 50 mM solution (1 equivalent) of $FcBF_4$ in 2:1 THF/MeCN was injected into the cuvette. Data was collected for at least 30 seconds. At each temperature, absorbance data were converted into a concentration versus time plot using Beer's Law. Due to mixing limitations of our instrument, the first 0.3, 0.4, or 0.5 seconds of data were disregarded (as determined by visual inspection of an anomalous spike in the absorbance data) at –40 °C, –80 °C, and –105 °C, respectively. A linear fit of the first 30% of the concentration versus time profile gave an "initial rate" for the reaction (Figure A4.21-Figure A4.23). Typically, initial rates are performed on the first 5% of the reaction, but mixing limitations precluded this analysis in our case. Therefore, this "initial rate" is an underestimation of the true rate. Nonetheless, we can use this "initial rate" and the initial concentrations of **4** and $FcBF_4$ to calculate a lower bound on the second order rate constant, $k_2$, for this reaction at a given temperature (Equation 5.2). A linear fit of a plot of $\ln(k_2/T)$ versus $1/T$ allows for the extrapolation of this lower bound $k_2$ to other temperatures (Figure A4.24). Assuming Equation 5.3 is true, conversion of this lower bound $k_2$ value to a lower bound first order rate constant, $k$, for C–H activation by $\mathbf{4^{ox}}$ was done using Equation 5.2 and Equation 5.4 to give Equation 5.5, which was evaluated assuming 1% of initial **4** had been converted into $\mathbf{4^{ox}}$. This percentage was chosen with the following justification: a reasonable lower bound for the concentration of $\mathbf{4^{ox}}$ observable by EPR spectroscopy is 1% of the initial concentration of **4**. Since we never observed $\mathbf{4^{ox}}$ by EPR, that puts an upper bound on the

concentration of $\mathbf{4^{ox}}$ as 1% of the initial concentration of **4**. Assuming that during this initial "1%" build-up of $\mathbf{4^{ox}}$ there is no loss of $\mathbf{4^{ox}}$, we can evaluate Equation 5.5 below with [**4**] = [$FcBF_4$] = 0.99*[**4**]$_0$.

Equation 5.2 $$\text{Rate}_{\text{ox}} = \frac{-d[\mathbf{4}]}{dt} = k_2 \cdot [\mathbf{4}] \cdot [FcBF_4]$$

Equation 5.3 $$\text{Rate}_{\text{C-H act}} > \text{Rate}_{\text{ox}}$$

Equation 5.4 $$\text{Rate}_{\text{C-H act}} = \frac{-d[\mathbf{4^{ox}}]}{dt} = k \cdot [\mathbf{4^{ox}}]$$

Equation 5.5 $$k \cdot [\mathbf{4^{ox}}] > k_2 \cdot [\mathbf{4}] \cdot [FcBF_4]$$

**Procedure for Oxidation of 4-*d*$_{45}$ Monitored by UV-vis Spectroscopy.** In the glovebox, 2.0 mL of a solution of **4-*d*$_{45}$** (contaminated with 29% **2-*d*$_{45}$**) in THF (1.25 mM total Co concentration) was transferred to a standard 1 cm cuvette and sealed with a puncturable cap. The cuvette was then transferred to the cryostat and cooled to the desired temperature –105 °C. After an initial scan, 50 µL of a 50 mM solution (1 equivalent relative to total Co) of $FcBF_4$ in 2:1 THF/MeCN was injected into the cuvette. The reaction was monitored by collecting spectra every 45 seconds until the spectrum stopped changing. The spectrum of **4$^{ox}$-*d*$_{45}$** was revealed by subtracting off 29% of the spectrum of **3-*d*$_{45}$** expected to form from oxidation of the **2-*d*$_{45}$** contaminant.

**Procedure for Oxidation of 4-*d*$_{45}$ Monitored by EPR Spectroscopy.** In the glovebox, 150 µL of a solution of **4-*d*$_{45}$** (contaminated with 29% **2-*d*$_{45}$**) in THF-$d_8$ (10 mM total Co concentration) was transferred to an EPR tube and sealed with a puncturable septum. The tube was removed from the glovebox and cooled in an ethanol/liquid nitrogen bath which can reach temperatures as low as –116 °C. After cooling (during which the solution stayed liquid), 15 µL of a 100 mM solution (1 equivalent relative to total Co) of $FcBF_4$ in $CD_3CN$ was injected through the septum. The

solutions were mixed as rapidly and completely as possible before freezing in liquid nitrogen. An EPR spectrum was collected at 15 K within ~5 minutes of freezing the sample. Any **3-*d*$_{45}$** expected to form from oxidation of the **2-*d*$_{45}$** contaminant would be silent ($S = 0$) by EPR spectroscopy and therefore not convolute the spectrum. The EPR spectrum was simulated using the simulation software package in the program SpinCount.[24]

**Computational Methods.** All DFT calculations were performed in ORCA 5.0.0 using the O3LYP functional with default grid settings.[25] The CPCM continuum polarization model with gaussian charges and the dielectric constant of THF was included.[26] The basis sets of Weigend and Ahrlich were employed: cobalt was given def2-TZVPP; all ligands bound to cobalt, the transferring hydrogen, and the carbon donating the transferring hydrogen were given def2-TZVP; the secondary hydrogen also bound to the donating carbon was given def2-SVP; all other atoms were given def2-SV(P).[27] We confirmed the barrier height to C–H activation was unchanged within 0.1 kcal/mol with respect to larger basis sets and integration grids. Frequency calculations were performed numerically. All minima were confirmed to have zero imaginary frequencies and saddle points to have exactly one imaginary frequency, excepting for a few modes with magnitudes less than 40 $cm^{-1}$ which all corresponded to rotating adamantyl groups or cyclopentadienyl ligands. Thermodynamic values were computed using the QRRHO model of Grimme and coworkers;[28] spurious imaginary modes (but not the reactive modes) were included to keep a consistent set of normal modes in all free energy differences. TD-DFT and population analyses of **4$^{ox}$** were calculated at the optimized geometry with a slightly different basis set; Co and O were given def2-QZVPP, the carbene carbons were given def2-TZVPP, and all other atoms given def2-SV(P). TD-DFT was calculated without frozen core orbitals. The delocalization index, which measures the

number of electron pairs shared in a bond and can serve as an estimate of the bond order,[29] was calculated in Becke fuzzy atomic space using the Multiwfn program.[30] Intrinsic atomic populations were calculated in Iboview with exponent 4.[20]

**Crystallographic Details.** The diffraction data for **5** were measured at 100 K on a Bruker D8 VENTURE diffractometer equipped with a microfocus Mo-target X-ray tube ($\lambda$ = 0.71073 Å) and PHOTON 100 CMOS detector. Data reduction and integration were performed with the Bruker APEX3 software package (Bruker AXS, version 2017.3-0, 2018). Data were scaled and corrected for absorption effects using the multi-scan procedure as implemented in SADABS (Bruker AXS, version 2014/5).[31] The structures were solved by SHELXT (Version 2014/5)[32] and refined by a full-matrix least-squares procedure using OLEX2 (XL refinement program version 2018/1).[33] Structure solutions were performed with the use of standard restraints and constraints as implemented in ShelXL. Additional crystallographic and refinement data can be found in the Supporting Information.

**X-ray Absorption Measurements.** Samples were prepared by packing finely ground powder into a PTFE washer (5.3 mm internal diameter) sealed on one side with Kapton tape. The powder was compacted with a PTFE rod and one face of the washer sealed with Kapton tape. All sample preparation was performed under an inert atmosphere. Data were acquired at the Advanced Photon Source at Argonne National Laboratory with a bending magnet source with ring energy at 7.00 GeV. Ni K-edge (8332.8 eV) data were acquired at the MRCAT 10-BM beam line in transmission. The incident, transmitted and reference X-ray intensities were monitored using gas ionization chambers. A metallic cobalt foil standard was used as a reference for energy calibration and was

measured simultaneously with experimental samples. X-ray absorption spectra were collected at room temperature. Data collected was processed using the Demeter software suite.

## 5.5 References


[1] (a) White, M. C.; Zhao, J. "Aliphatic C–H Oxidations for Late-Stage Functionalization." *J. Am. Chem. Soc.* **2018**, *140* (43), 13988–14009. (b) Milan, M.; Salamone, M.; Costas, M.; Bietti, M. "The Quest for Selectivity in Hydrogen Atom Transfer Based Aliphatic C–H Bond Oxygenation." *Acc. Chem. Res.* **2018**, *51* (9), 1984–1995.

[2] (a) Montellano, P. R. O. de. "Hydrocarbon Hydroxylation by Cytochrome P450 Enzymes." *Chem. Rev.* **2009**, *110* (2), 932–948. (b) Hausinger, R. P. "Critical Reviews in Biochemistry and Molecular Biology Fe(II)/α-Ketoglutarate-Dependent Hydroxylases and Related Enzymes Fe(II)/α-Ketoglutarate-Dependent Hydroxylases and Related Enzymes." *Crit. Rev. Biochem. Mol. Biol.* **2004**, *39* (1), 21–68.

[3] (a) Rittle, J.; Green, M. T. "Cytochrome P450 Compound I: Capture, Characterisation, and C-H Bond Activation Kinetics." *Science.* **2010**, *330*, 933–937. (b) Yosca, T. H.; Rittle, J.; Krest, C. M.; Onderko, E. L.; Silakov, A.; Calixto, J. C.; Behan, R. K.; Green, M. T. "Iron(IV)Hydroxide $pK_a$ and the Role of Thiolate Ligation in C-H Bond Activation by Cytochrome P450." *Science.* **2013**, *342* (6160), 825–829. (c) Mittra, K.; Green, M. T. "Reduction Potentials of P450 Compounds I and II: Insight into the Thermodynamics of C–H Bond Activation." *J. Am. Chem. Soc.* **2019**, *141* (13), 5504–5510.

[4] (a) Ortiz de Montellano, P. R.; Stearns, R. A. "Timing of the Radical Recombination Step in Cytochrome P-450 Catalysis with Ring-Strained Probes." *J. Am. Chem. Soc.* **1987**, *109* (11), 3415–3420. (b) Saouma, C. T.; Mayer, J. M. "Do Spin State and Spin Density Affect Hydrogen Atom Transfer Reactivity?" *Chem. Sci.* **2014**, *5* (1), 21–31.

[5] (a) Costas, M. Remote Oxidation of Aliphatic C-H Bonds with Biologically Inspired Catalysts. In *Remote C-H Bond Functionalizations*; Wiley, 2021; pp 383–421. (b) Groves, J. T.; Nemo, T. E.; Myers, R. S. "Hydroxylation and Epoxidation Catalyzed by Iron-Porphine Complexes. Oxygen Transfer from Iodosylbenzene." *J. Am. Chem. Soc.* **1979**, *101* (4), 1032–1033. (c) Groves, J. T.; Nemo, T. E. "Aliphatic Hydroxylation Catalyzed by Iron Porphyrin Complexes." *J. Am. Chem. Soc.* **1983**, *105* (20), 6243–6248. (d) Groves, J. T.; Kruper, W. J.; Haushalter, R. C. "Hydrocarbon Oxidations with Oxometalloporphinates. Isolation and Reactions of a (Porphinato)Manganese(V) Complex." *J. Am. Chem. Soc.* **1980**, *102* (20), 6375–6377. (e) Dantignana, V.; Milan, M.; Cussó, O.; Company, A.; Bietti, M.; Costas, M. "Chemoselective Aliphatic C–H Bond Oxidation Enabled by Polarity Reversal." *ACS Cent. Sci.* **2017**, *3* (12), 1350–1358. (f) Chen, M. S.; White, M. C. "A Predictably Selective Aliphatic C H Oxidation Reaction for Complex Molecule Synthesis." *Science.* **2007**, *318* (5851), 783–787. (g) Leising,

R. A.; Norman, R. E.; Que, L. "Alkane Functionalization by Nonporphyrin Iron Complexes: Mechanistic Insights." *Inorg. Chem.* **1990**, *29* (14), 2553–2555.

[6] (a) Groves, J. T.; Haushalter, R. C.; Nakamura, M.; Nemo, T. E.; Evans, B. J. "High-Valent Iron-Porphyrin Complexes Related to Peroxidase and Cytochrome P-450." *J. Am. Chem. Soc.* **1981**, *103* (10), 2884–2886. (b) Groves, J. T.; Stern, M. K. "Synthesis, Characterization, and Reactivity of Oxomanganese(IV) Porphyrin Complexes." *J. Am. Chem. Soc.* **1988**, *110* (26), 8628–8638. (c) Sorokin, A.; Robert, A.; Meunier, B. "Intramolecular Kinetic Isotope Effects in Alkane Hydroxylations Catalyzed by Manganese and Iron Porphyrin Complexes." *J. Am. Chem. Soc.* **1993**, *115* (16), 7293–7299. (d) Chen, K.; Jr., L. Q. "Evidence for the Participation of a High-Valent Iron–Oxo Species in Stereospecific Alkane Hydroxylation by a Non-Heme Iron Catalyst." *Chem. Commun.* **1999**, *8* (15), 1375–1376.

[7] (a) Baglia, R. A.; Prokop-Prigge, K. A.; Neu, H. M.; Siegler, M. A.; Goldberg, D. P. "Mn(V)(O) versus Cr(V)(O) Porphyrinoid Complexes: Structural Characterization and Implications for Basicity Controlling H-Atom Abstraction." *J. Am. Chem. Soc.* **2015**, *137* (34), 10874–10877. (b) Gupta, R.; Borovik, A. S. "Monomeric $Mn^{III/II}$ and $Fe^{III/II}$ Complexes with Terminal Hydroxo and Oxo Ligands: Probing Reactivity via O-H Bond Dissociation Energies." *J. Am. Chem. Soc.* **2003**, *125* (43), 13234–13242. (c) Yin, G.; Danby, A. M.; Kitko, D.; Carter, J. D.; Scheper, W. M.; Busch, D. H. "Understanding the Selectivity of a Moderate Oxidation Catalyst: Hydrogen Abstraction by a Fully Characterized, Activated Catalyst, the Robust Dihydroxo Manganese(IV) Complex of a Bridged Cyclam." *J. Am. Chem. Soc.* **2007**, *129* (6), 1512–1513. (d) Evans, M. G.; Polanyi, M. "Inertia and Driving Force of Chemical Reactions." *Trans. Faraday Soc.* **1938**, *34*, 11–24.

[8] (a) Thyagarajan, S.; Incarvito, C. D.; Rheingold, A. L.; Theopold, K. H. "Formation and Reactivity of a Cobalt(II) Hydroperoxide Intermediate." *Chem. Commun.* **2001**, 2198–2199. (b) Reinaud, O. M.; Theopold, K. H. "Hydrogen Tunneling in the Activation of Dioxygen by a Tris(Pyrazolyl)Borate Cobalt Complex." *J. Am. Chem. Soc.* **1994**, *116* (15), 6979–6980. (c) Andris, E.; Navrátil, R.; Jašík, J.; Srnec, M.; Rodríguez, M.; Costas, M.; Roithová, J. "M−O Bonding Beyond the Oxo Wall: Spectroscopy and Reactivity of Cobalt(III)-Oxyl and Cobalt(III)-Oxo Complexes." *Angew. Chemie* **2019**, *131* (28), 9721–9726. (d) Hikichi, S.; Komatsuzaki, H.; Akita, M.; Moro-oka, Y. "Aliphatic C−H Bond Oxygenation by the $Co^{II}OOX$ Species with the Hindered Hydrotris(Pyrazolyl)Borate Ligand (X = Co(II), Alkyl, H)." *J. Am. Chem. Soc.* **1998**, *120* (19), 4699–4710. (e) Hikichi, S.; Yoshizawa, M.; Sasakura, Y.; Komatsuzaki, H.; Moro-oka, Y.; Akita, M. "Structural Characterization and Intramolecular Aliphatic C−H Oxidation Ability of $M^{III}(\mu\text{-}O)_2M^{III}$ Complexes of Ni and Co with the Hydrotris(3,5-Dialkyl-4-X-Pyrazolyl)Borate Ligands $Tp^{Me2,X}$ (X=Me, H, Br) and $Tp^{iPr2}$" *Chem. - A Eur. J.* **2001**, *7* (23), 5011–5028. (f) Bryant, J. R.; Mayer, J. M. "Oxidation of C−H Bonds by $[(Bpy)_2(Py)Ru^{IV}O]^{2+}$ Occurs by Hydrogen Atom Abstraction." *J. Am. Chem. Soc.* **2003**, *125* (34), 10351–10361. (g) Cook, G. K.; Mayer, J. M. "C-H Bond Activation by Metal Oxo Species: Oxidation of Cyclohexane by Chromyl Chloride." *J. Am. Chem. Soc* **1994**, *116*, 1855–1868. (h) Gardner, K. A.; Kuehnert, L. L.; Mayer, J. M. "Hydrogen Atom Abstraction by Permanganate: Oxidations of Arylalkanes in Organic Solvents." *Inorg. Chem.* **1997**, *36* (10), 2069–2078. (i) Kaizer, J.; Klinker, E. J.; Oh, N. Y.; Rohde, J.-U.; Song, W. J.; Stubna, A.; Kim, J.; Münck, E.;

Nam, W.; Que, L. "Nonheme $Fe^{IV}O$ Complexes That Can Oxidize the C−H Bonds of Cyclohexane at Room Temperature." *J. Am. Chem. Soc.* **2004**, *126* (2), 472–473.

[9] (a) Hong, S.; Pfaff, F. F.; Kwon, E.; Wang, Y.; Seo, M.-S.; Bill, E.; Ray, K.; Nam, W. "Spectroscopic Capture and Reactivity of a Low-Spin Cobalt(IV)-Oxo Complex Stabilized by Binding Redox-Inactive Metal Ions." *Angew. Chem., Int. Ed.* **2014**, *53* (39), 10403–10407. (b) Wang, B.; Lee, Y.-M.; Tcho, W.-Y.; Tussupbayev, S.; Kim, S.-T.; Kim, Y.; Seo, M. S.; Cho, K.-B.; Dede, Y.; Keegan, B. C.; Ogura, T.; Kim, S. H.; Ohta, T.; Baik, M.-H.; Ray, K.; Shearer, J.; Nam, W. "Synthesis and Reactivity of a Mononuclear Non-Haem Cobalt(IV)-Oxo Complex." *Nat. Commun.* **2017**, *8*, 14839. (c) Goetz, M. K.; Anderson, J. S. "Experimental Evidence for $pK_a$-Driven Asynchronicity in C–H Activation by a Terminal Co(III)–Oxo Complex." *J. Am. Chem. Soc.* **2019**, *141* (9), 4051–4062.

[10] Hill, E. A.; Zhao, N.; Filatov, A. S.; Anderson, J. S. "Nickel(II)-Methyl Complexes Adopting Unusual Seesaw Geometries." *Chem. Commun.* **2020**, *56* (57), 7861–7864.

[11] Zhao, N.; Filatov, A. S.; Xie, J.; Hill, E. A.; Rogachev, A. Y.; Anderson, J. S. "Generation and Reactivity of a $Ni^{III}_2$(μ-1,2-Peroxo) Complex." *J. Am. Chem. Soc.* **2020**, *142* (52), 21634–21639.

[12] Betley, T. A.; Wu, Q.; Van Voorhis, T.; Nocera, D. G. "Electronic Design Criteria for O-O Bond Formation via Metal-Oxo Complexes." *Inorg. Chem.* **2008**, *47* (6), 1849–1861.

[13] Dhar, D.; Tolman, W. B. "Hydrogen Atom Abstraction from Hydrocarbons by a Copper(III)-Hydroxide Complex." *J. Am. Chem. Soc.* **2015**, *137* (3), 1322–1329.

[14] (a) Zhang, L.; Liu, Y.; Deng, L. "Three-Coordinate Cobalt(IV) and Cobalt(V) Imido Complexes with N-Heterocyclic Carbene Ligation: Synthesis, Structure, and Their Distinct Reactivity in C-H Bond Amination." *J. Am. Chem. Soc.* **2014**, *136* (44), 15525–15528. (b) Kwon, Y. M.; Lee, Y.; Evenson, G. E.; Jackson, T. A.; Wang, D. "Crystal Structure and C–H Bond-Cleaving Reactivity of a Mononuclear $Co^{IV}$–Dinitrate Complex." *J. Am. Chem. Soc.* **2020**, *142* (31), 13435–13441.

[15] (a) Donoghue, P. J.; Tehranchi, J.; Cramer, C. J.; Sarangi, R.; Solomon, E. I.; Tolman, W. B. "Rapid C–H Bond Activation by a Monocopper(III)–Hydroxide Complex." *J. Am. Chem. Soc.* **2011**, *133* (44), 17602–17605. (b) Mahapatra, S.; Halfen, J. A.; Tolman, W. B. "Mechanistic Study of the Oxidative N-Dealkylation Reactions of Bis(μ-Oxo)Dicopper Complexes." *J. Am. Chem. Soc.* **1996**, *118* (46), 11575–11586.

[16] England, J.; Guo, Y.; Farquhar, E. R.; Young, V. G.; Münck, E.; Que, L. "The Crystal Structure of a High-Spin Oxoiron(IV) Complex and Characterization of Its Self-Decay Pathway." *J. Am. Chem. Soc.* **2010**, *132* (25), 8635–8644.

[17] Barfield, M.; Marshall, J. L.; Canada, E. D. "Nuclear Spin-Spin Coupling via Nonbonded Interactions. 2. γ-Substituent Effects for Vicinal Coupling Constants Involving $^{13}C$." *J. Am. Chem. Soc.* **1980**, *102* (1), 7–12.

[18] Neese, F. "A Critical Evaluation of DFT, Including Time-Dependent DFT, Applied to Bioinorganic Chemistry." *JBIC J. Biol. Inorg. Chem. 2006 116* **2006**, *11* (6), 702–711.

[19] (a) McAlpin, J. G.; Stich, T. A.; Ohlin, C. A.; Surendranath, Y.; Nocera, D. G.; Casey, W. H.; Britt, R. D. "Electronic Structure Description of a $[Co(III)_3Co(IV)O_4]$ Cluster: A Model for the Paramagnetic Intermediate in Cobalt-Catalyzed Water Oxidation." *J. Am. Chem. Soc.* **2011**, *133* (39), 15444–15452. (b) Stich, T. A.; McAlpin, J. G.; Wall, R. M.; Rigsby, M. L.; David Britt, R. "Electron Paramagnetic Resonance Characterization of Dioxygen-Bridged Cobalt Dimers with Relevance to Water Oxidation." *Inorg. Chem.* **2016**, *55* (24), 12728–12736. (c) Li, Y.; Handunneththige, S.; Farquhar, E. R.; Guo, Y.; Talipov, M. R.; Li, F.; Wang, D. "Highly Reactive $Co^{III,IV}_2(\mu\text{-}O)_2$ Diamond Core Complex That Cleaves C–H Bonds." *J. Am. Chem. Soc.* **2019**, *141* (51), 20127–20136. (d) Zolnhofer, E. M.; Käß, M.; Khusniyarov, M. M.; Heinemann, F. W.; Maron, L.; Van Gastel, M.; Bill, E.; Meyer, K. "An Intermediate Cobalt(IV) Nitrido Complex and Its N-Migratory Insertion Product." *J. Am. Chem. Soc.* **2014**, *136* (42), 15072–15078. (e) Anson, F. C.; Collins, T. J.; Coots, R. J.; Gipson, S. L.; Richmond, T. G. "Synthesis and Characterization of Stable Cobalt(IV) Coordination Complexes: Molecular Structure of Trans-[$\eta^4$-1,2-Bis(3,5-Dichloro-2-Hydroxybenzamido)-4,5-Dichlorobenzene]Bis(4-Tert-Butylpyridine)Cobalt(IV)." *J. Am. Chem. Soc.* **1984**, *106* (17), 5037–5038. (f) Topich, J.; Halpern, J. "Organobis(Dioximato)Cobalt(IV) Complexes: Electron Paramagnetic Resonance Spectra and Electronic Structures." *Inorg. Chem.* **1979**, *18* (5), 1339–1343.

[20] (a) Knizia, G. "Intrinsic Atomic Orbitals: An Unbiased Bridge between Quantum Theory and Chemical Concepts." *J. Chem. Theory Comput.* **2013**, *9* (11), 4834–4843. (b) Klein, J. E. M. N.; Knizia, G. "CPCET versus HAT: A Direct Theoretical Method for Distinguishing X-H Bond-Activation Mechanisms." *Angew. Chem., Int. Ed.* **2018**, *57* (37), 11913–11917.

[21] Luo, Y.-R. "Handbook of Bond Dissociation Energies in Organic Compounds;" CRC Press: Boca Raton, 2003.

[22] Dhar, D.; Yee, G. M.; Markle, T. F.; Mayer, J. M.; Tolman, W. B. "Reactivity of the Copper(III)-Hydroxide Unit with Phenols." *Chem. Sci.* **2017**, *8* (2), 1075–1085.

[23] Jenkins, D. M.; Peters, J. C. "Spin-State Tuning at Pseudotetrahedral $d^7$Ions: Examining the Structural and Magnetic Phenomena of Four-Coordinate $[BP_3]Co^{II}$-X Systems." *J. Am. Chem. Soc.* **2005**, *127* (19), 7148–7165.

[24] Golombek, A. P.; Hendrich, M. P. "Quantitative Analysis of Dinuclear Manganese(II) EPR Spectra." *J. Magn. Reson.* **2003**, *165* (1), 33–48.

[25] (a) Neese, F.; Wennmohs, F.; Becker, U.; Riplinger, C. "The ORCA Quantum Chemistry Program Package." *J. Chem. Phys.* **2020**, *152* (22), 224108. (b) Handy, N. C.; Cohen, A. J. "Left-Right Correlation Energy." *Mol. Phys.* **2001**, *99* (5), 403–412. (c) Cohen, A. J.; Handy, N. C. "Dynamic Correlation." *Mol. Phys.* **2001**, *99* (7), 607–615. (d) Lee, C.; Yang, W.; Parr, R. G. "Development of the Colle-Salvetti Correlation-Energy Formula into a Functional of the Electron Density." *Phys. Rev. B* **1988**, *37* (2), 785–789.

[26] York, D. M.; Karplus, M. "A Smooth Solvation Potential Based on the Conductor-Like Screening Model." *J. Phys. Chem. A* **1999**, *103* (50), 11060–11079.

[27] (a) Weigend, F.; Ahlrichs, R. "Balanced Basis Sets of Split Valence, Triple Zeta Valence and Quadruple Zeta Valence Quality for H to Rn: Design and Assessment of Accuracy." *Phys. Chem. Chem. Phys.* **2005**, *7* (18), 3297. (b) Weigend, F. "Accurate Coulomb-Fitting Basis Sets for H to Rn." *Phys. Chem. Chem. Phys.* **2006**, *8* (9), 1057.

[28] Grimme, S. "Supramolecular Binding Thermodynamics by Dispersion-Corrected Density Functional Theory." *Chem. - A Eur. J.* **2012**, *18* (32), 9955–9964.

[29] (a) Poater, J.; Solà, M.; Duran, M.; Fradera, X. "The Calculation of Electron Localization and Delocalization Indices at the Hartree-Fock, Density Functional and Post-Hartree-Fock Levels of Theory." *Theor. Chem. Accounts Theory, Comput. Model. (Theoretica Chim. Acta)* **2002**, *107* (6), 362–371. (b) Matito, E.; Poater, J.; Solà, M.; Duran, M.; Salvador, P. "Comparison of the AIM Delocalization Index and the Mayer and Fuzzy Atom Bond Orders." *J. Phys. Chem. A* **2005**, *109* (43), 9904–9910. (c) Outeiral, C.; Vincent, M. A.; Martín Pendás, Á.; Popelier, P. L. A. "Revitalizing the Concept of Bond Order through Delocalization Measures in Real Space." *Chem. Sci.* **2018**, *9* (25), 5517–5529.

[30] (a) Becke, A. D. "A Multicenter Numerical Integration Scheme for Polyatomic Molecules." *J. Chem. Phys.* **1988**, *88* (4), 2547–2553. (b) Lu, T.; Chen, F. "Multiwfn: A Multifunctional Wavefunction Analyzer." *J. Comput. Chem.* **2012**, *33* (5), 580–592.

[31] Krause, L.; Herbst-Irmer, R.; Sheldrick, G. M.; Stalke, D. "Comparison of Silver and Molybdenum Microfocus X-Ray Sources for Single-Crystal Structure Determination." *J. Appl. Crystallogr.* **2015**, *48* (1), 3–10.

[32] Sheldrick, G. M. "SHELXT - Integrated Space-Group and Crystal-Structure Determination." *Acta Crystallogr. Sect. A Found. Crystallogr.* **2015**, *71* (1), 3–8.

[33] (a) Dolomanov, O. V; Bourhis, L. J.; Gildea, R. J.; Howard, J. A. K.; Puschmann, H. "OLEX2: A Complete Structure Solution, Refinement and Analysis Program." *J. Appl. Crystallogr.* **2009**, *42* (2), 339–341. (b) Sheldrick, G. M. "Crystal Structure Refinement with SHELXL." *Acta Crystallogr. Sect. C Struct. Chem.* **2015**, *71*, 3–8.

# Appendix 1: Supporting Data for Chapter 2

## A1.1 NMR Spectra and Related Tables and Equations

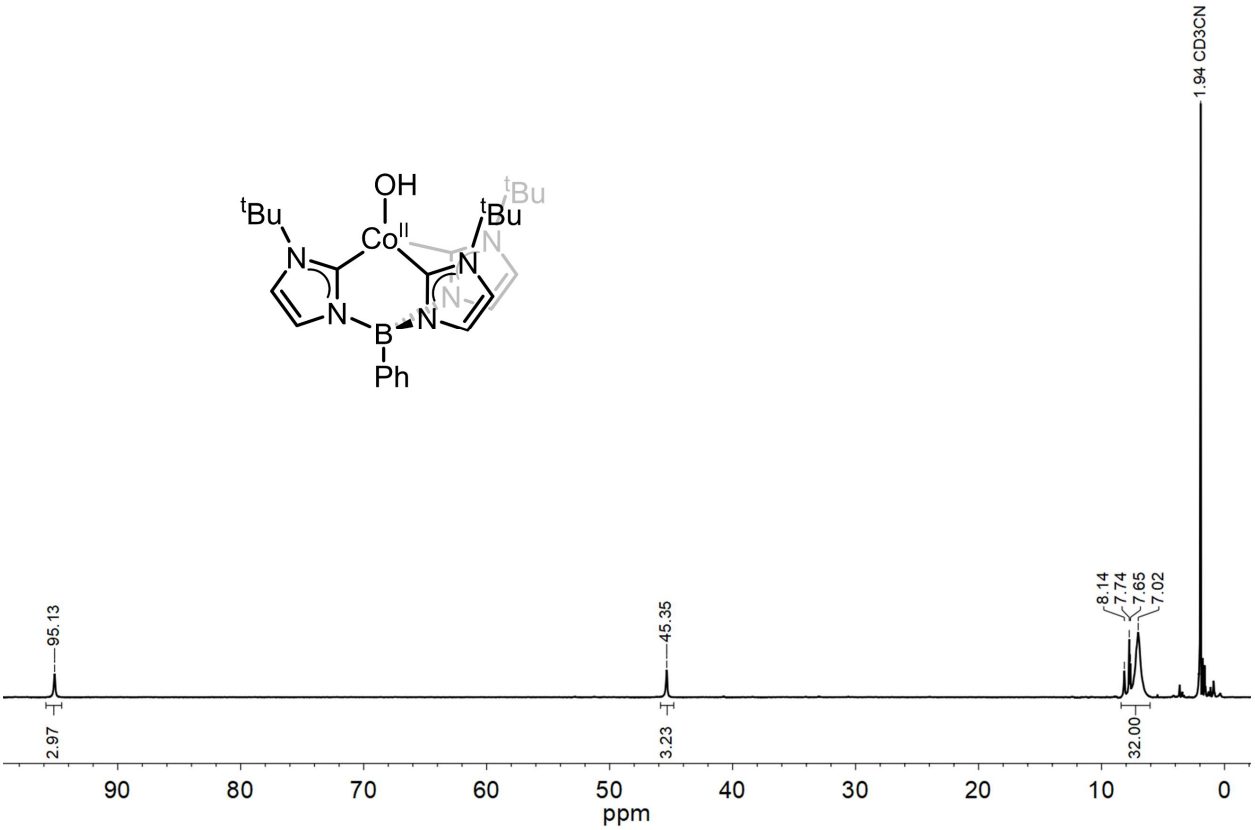


**Figure A1.1.** $^{1}$H NMR spectrum of **1** in $CD_3CN$ at room temperature. Unlabeled peaks are THF, $Et_2O$, and hexanes impurities.

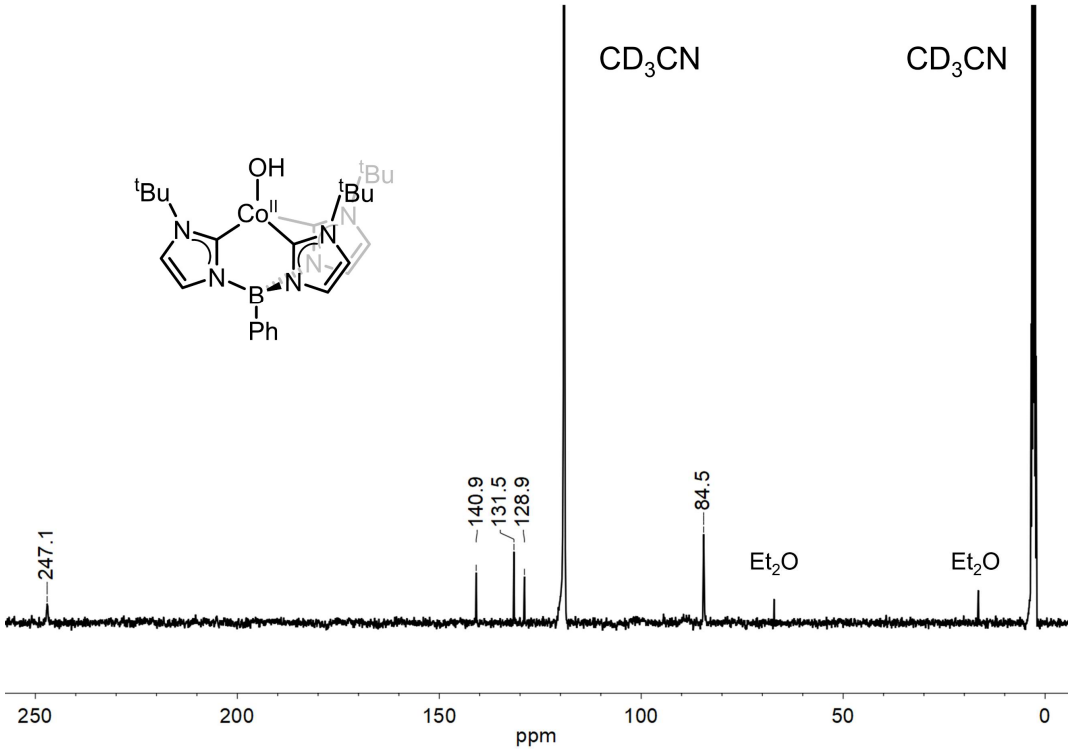


**Figure A1.2.** $^{13}$C NMR spectrum of **1** in $CD_3CN$ at room temperature. Only five of the expected nine resonances were observable.

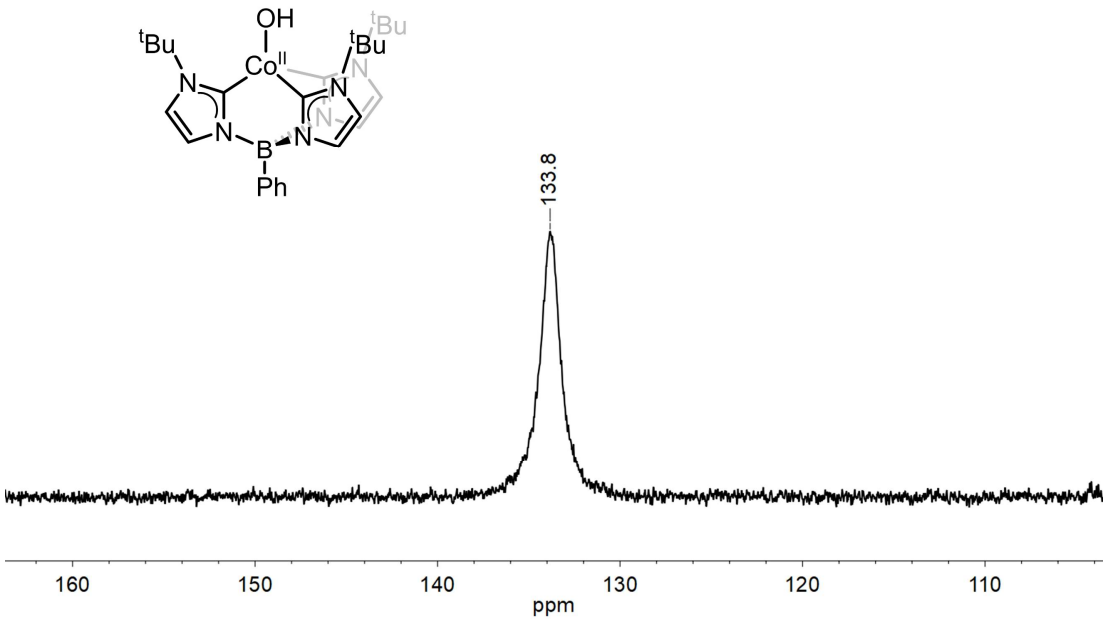


**Figure A1.3.** $^{11}$B NMR spectrum of **1** in $CD_3CN$ at room temperature.

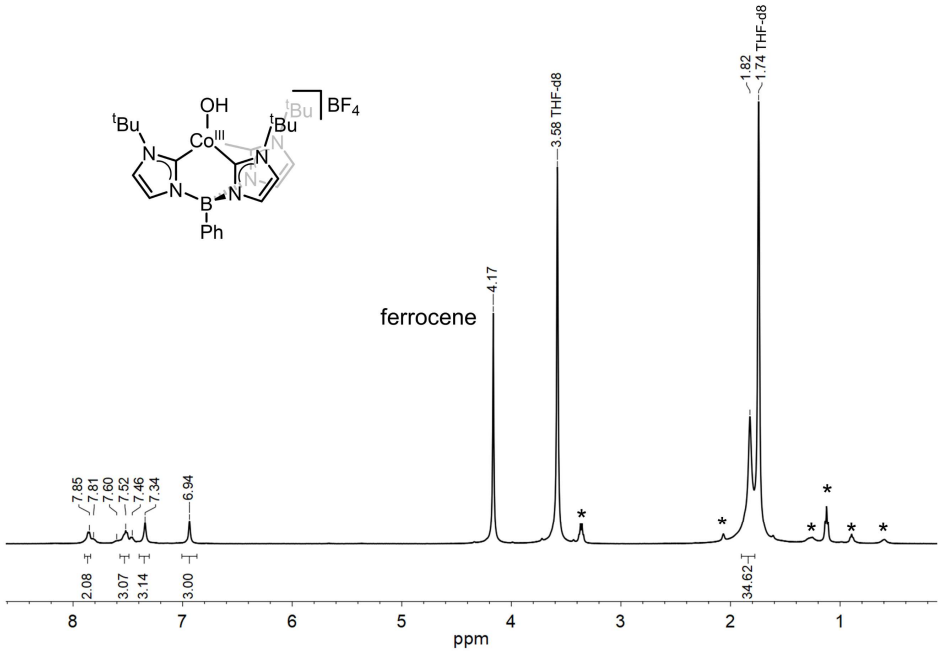


**Figure A1.4.** $^{1}$H NMR spectrum of in situ prepared **2** in THF-$d_8$ at −78 °C. Asterisks indicate $Et_2O$, hexanes, and MeCN impurities.

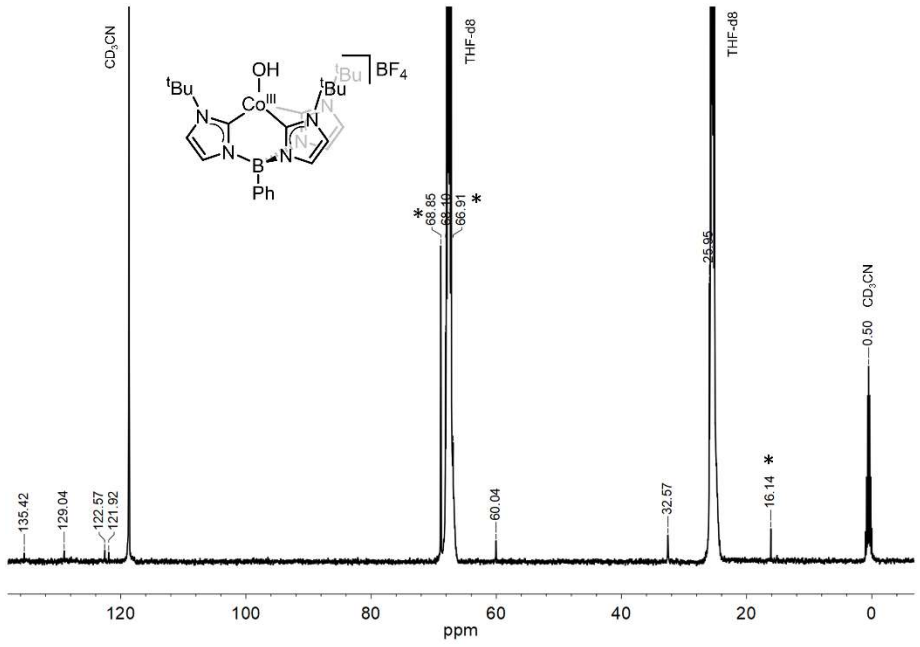


**Figure A1.5.** $^{13}$C NMR spectrum of in situ prepared **2** in THF-$d_8$ at −78 °C. Signals from $CD_3CN$ are visible due to the added $FcBF_4$ solution. Asterisks indicate an $Et_2O$ impurity and ferrocene. The carbene carbon resonance was not observable.

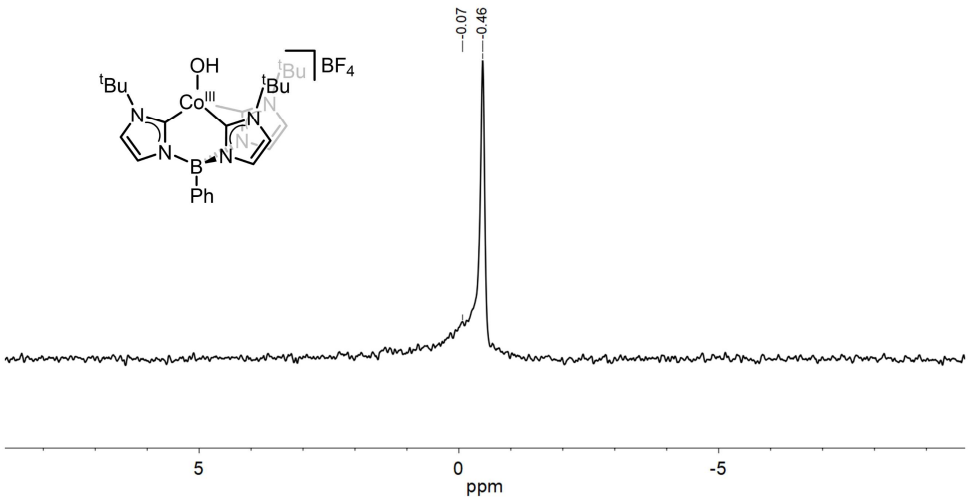


**Figure A1.6.** $^{11}$B NMR spectrum of in situ prepared **2** in $CD_3CN$ at −35 °C. The resonance for the $BF_4^-$ counter-anion gives the sharp signal on top of the broader signal due to the boron in the cobalt complex.

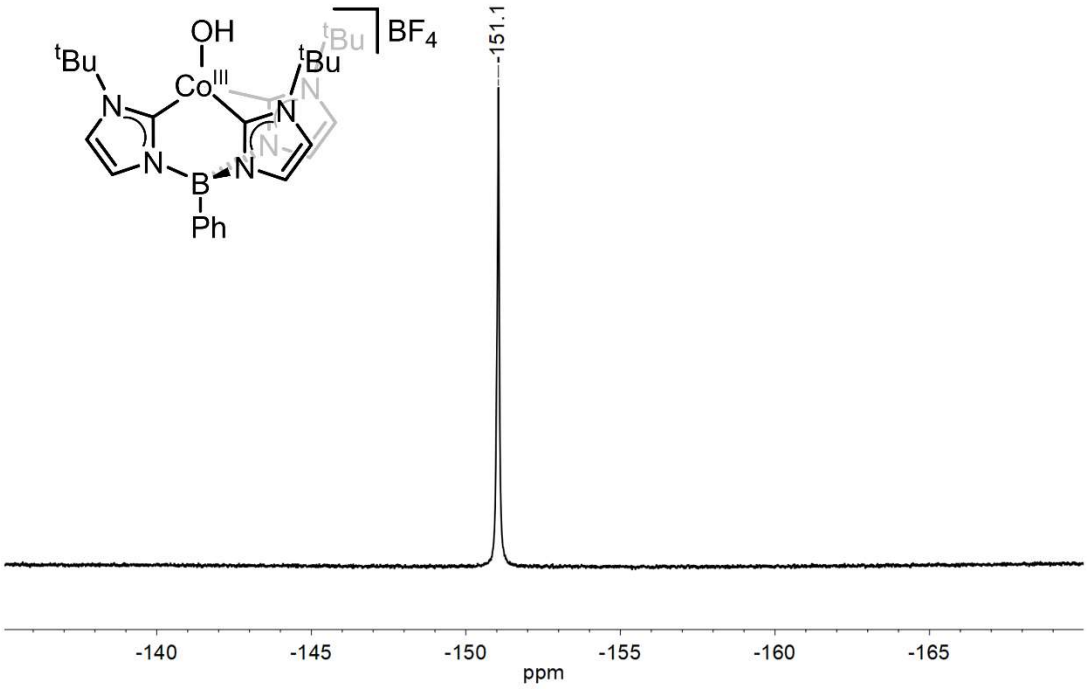


**Figure A1.7.** $^{19}$F NMR spectrum of in situ prepared **2** in $CD_3CN$ at −35 °C.

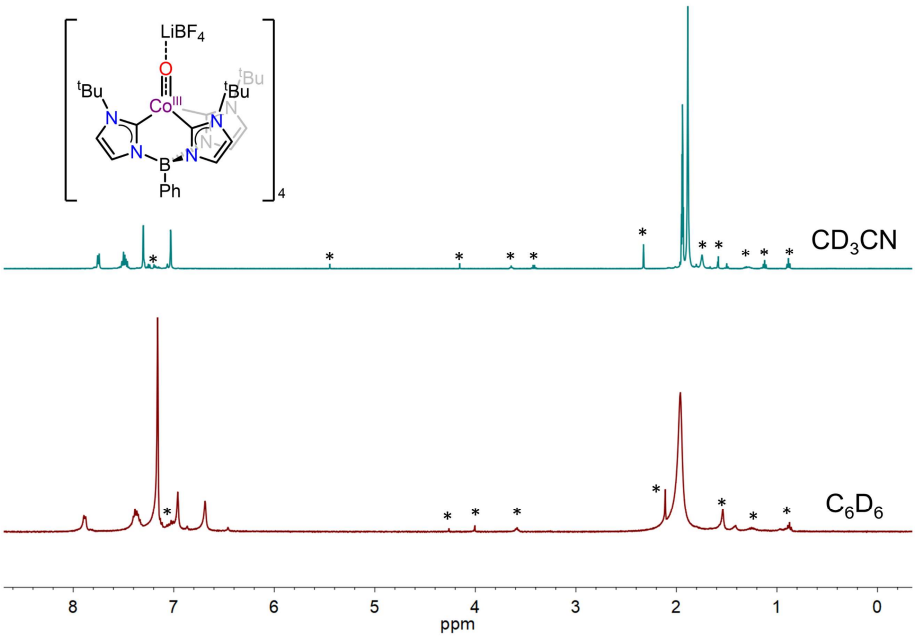


**Figure A1.8.** Representative $^{1}H$ NMR spectra of **3** in $CD_3CN$ and $C_6D_6$ demonstrating the solvent effects on the solution structure of **3**. Asterisks indicate solvent impurities.

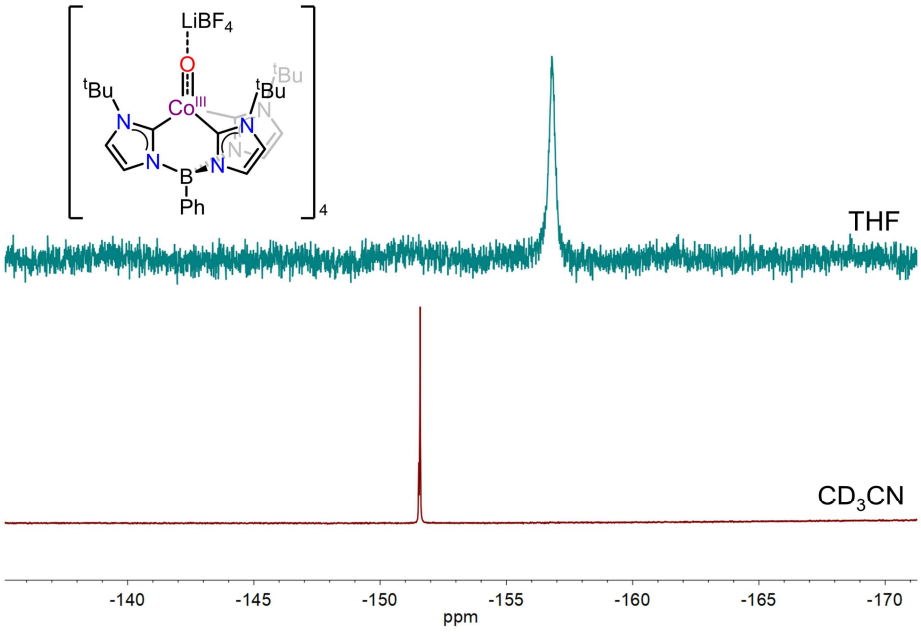


**Figure A1.9.** $^{19}F$ NMR spectra of **3** in THF and $CD_3CN$ showing solvent effects on the solution structure of the complex. The sharpening of the $^{19}F$ $BF_4^-$ resonance in the case of $CD_3CN$ suggests dissociation of $BF_4^-$ from the complex.

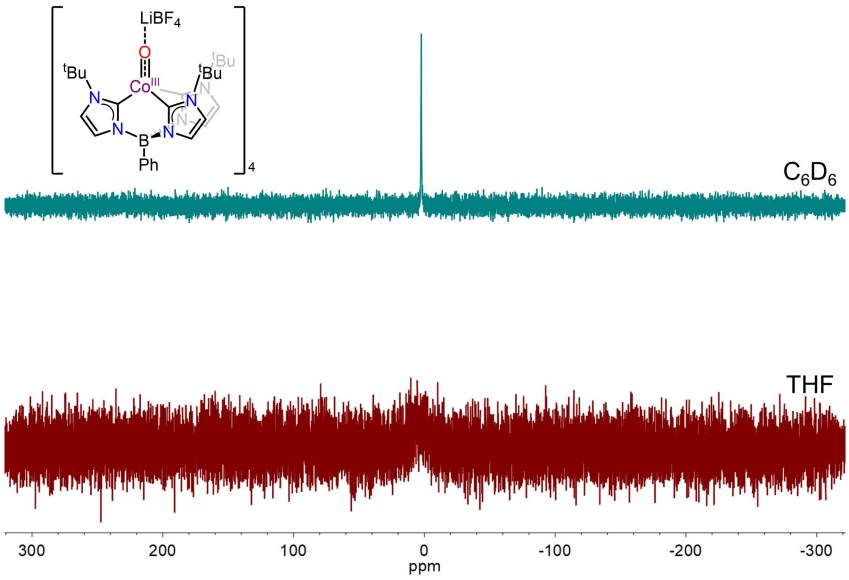


**Figure A1.10.** $^{7}$Li NMR spectra of **3** in $C_6D_6$ and THF showing solvent effects on the solution structure of the complex. The broadening of the $^{7}$Li resonance in the case of THF is attributed to an equilibrium between the tetrameric structure and a fully dissociated $Li^{+}$ ion.

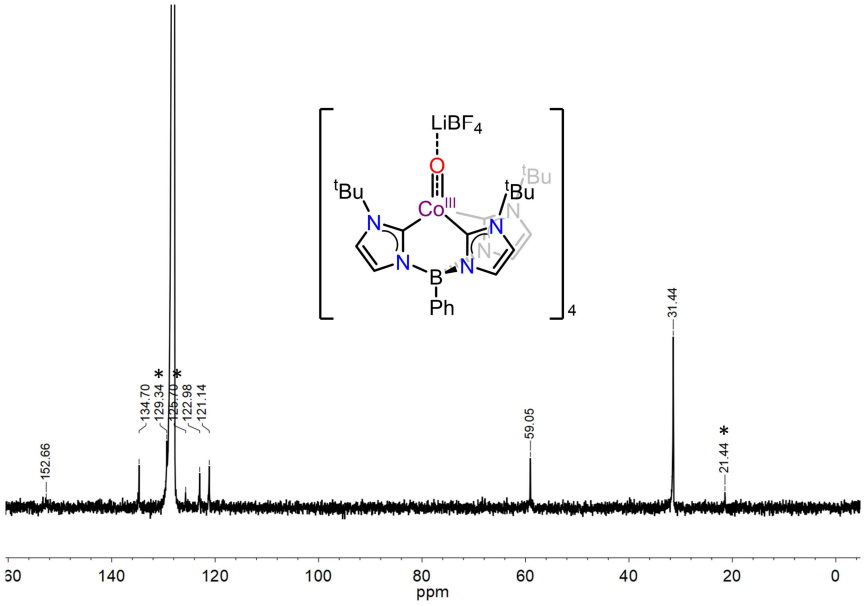


**Figure A1.11.** $^{13}$C NMR spectrum of **3** in $C_6D_6$ at room temperature. Asterisks indicate a toluene impurity. Only six of the expected nine resonances were observable.

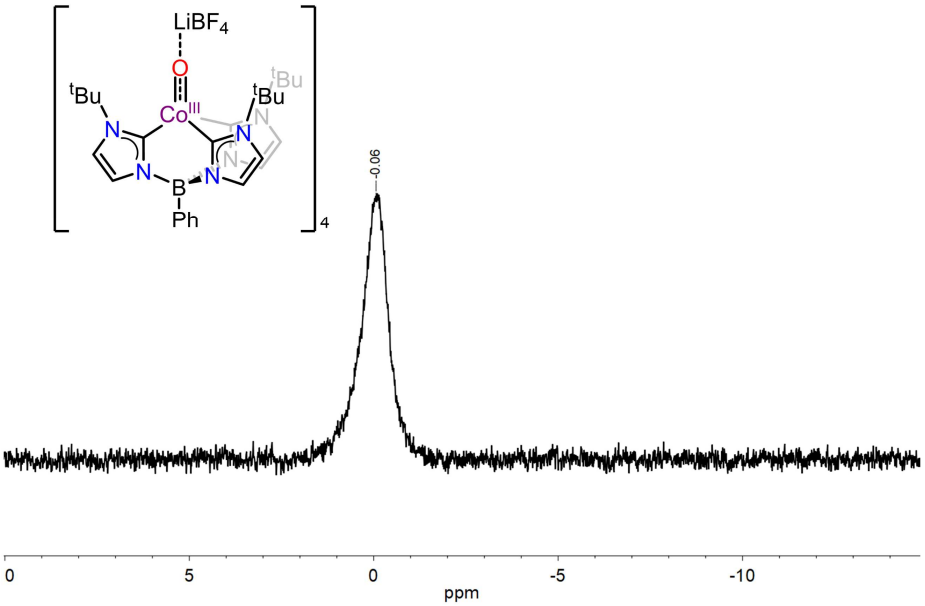


**Figure A1.12.** $^{11}$B NMR spectrum of **3** in $C_6D_6$ at room temperature. The $BF_4^-$ resonance overlaps with that of the ligand.

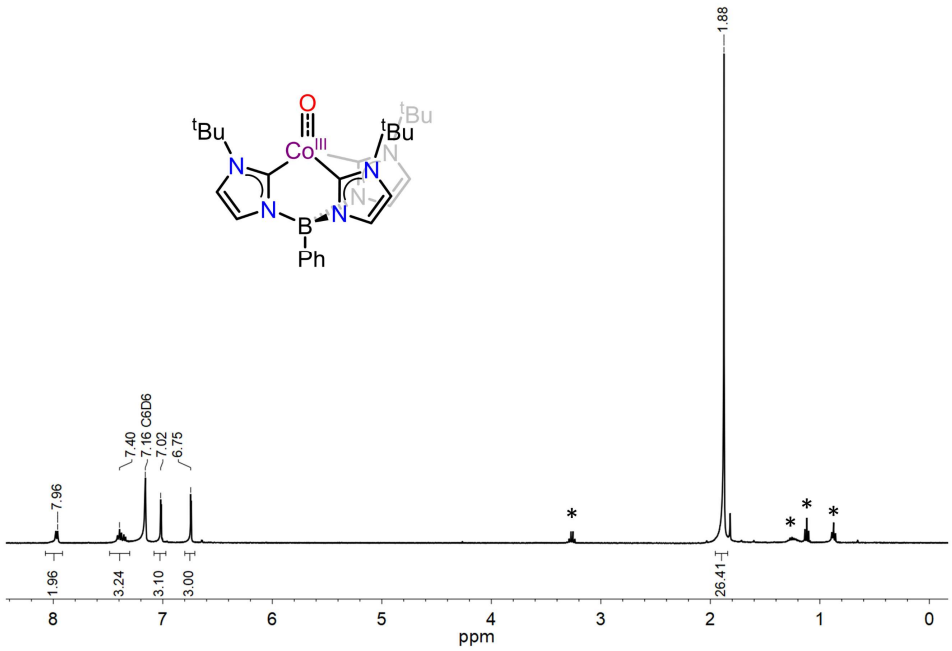


**Figure A1.13.** $^1$H NMR spectrum of **4** in $C_6D_6$ at room temperature. Asterisks indicate $Et_2O$ and pentanes impurities.

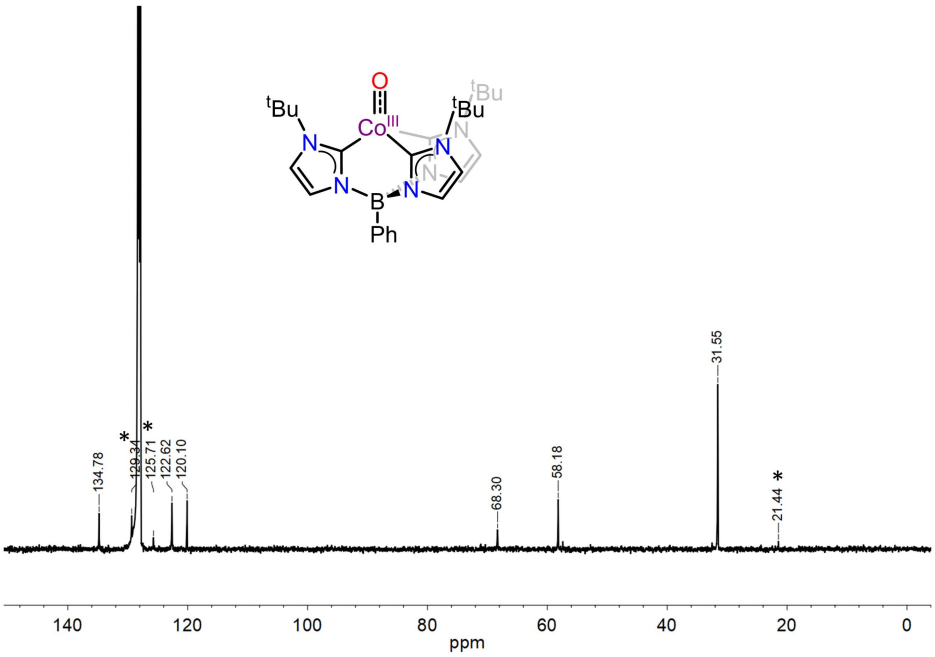


**Figure A1.14.** $^{13}$C NMR spectrum of **4** in $C_6D_6$ at room temperature. Asterisks indicate a toluene impurity. Only five of the expected nine resonances were observable.

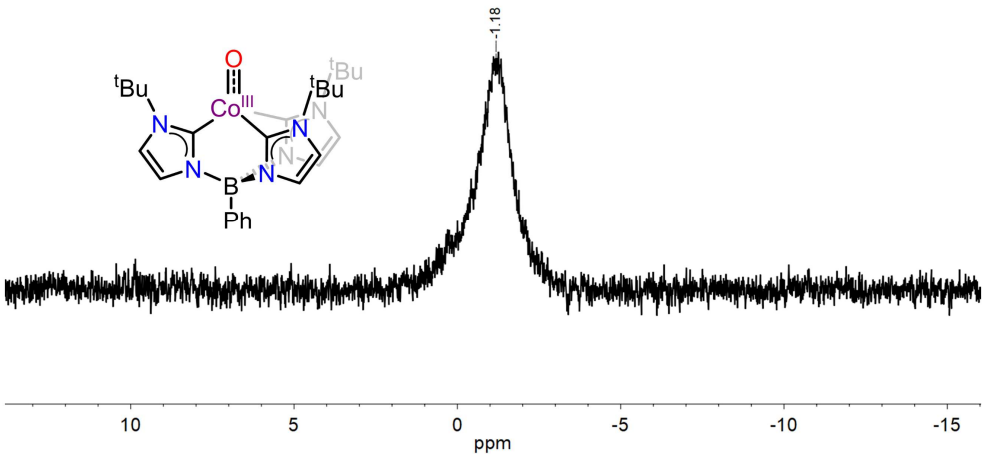


**Figure A1.15.** $^{11}$B NMR spectrum of **4** in $C_6D_6$ at room temperature.

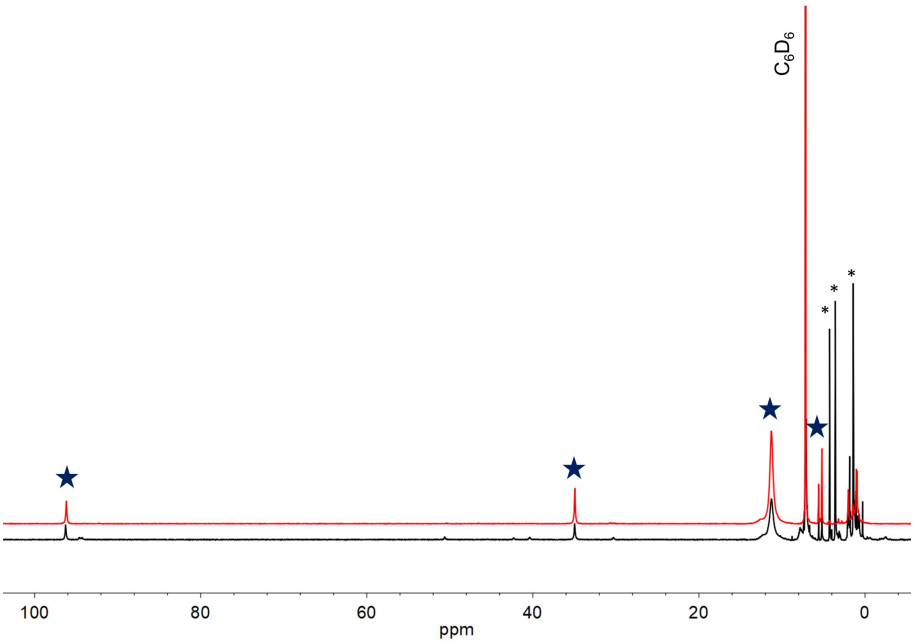


**Figure A1.16.** $^{1}$H NMR spectra of reaction of **3** with $PMe_3$ (black spectrum) demonstrating that the major Co-containing product of the reaction is $PhB(^{t}BuIm)_3Co^{II}Cl$ (red spectrum, resonances indicated by stars). Asterisks indicate DCM and THF impurities in the reaction spectrum.

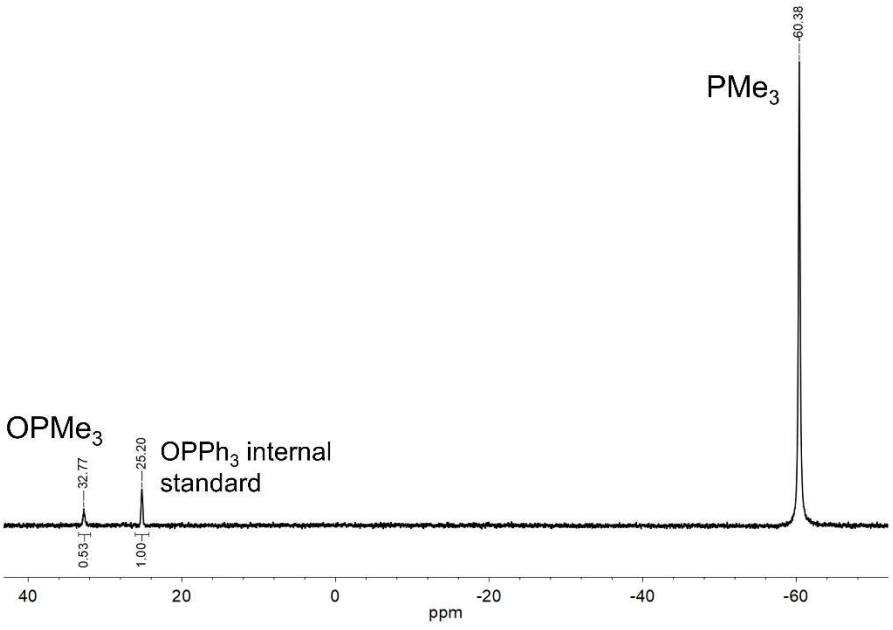


**Figure A1.17.** $^{31}$P NMR spectrum demonstrating the formation of free $OPMe_3$ during the course of the reaction of **4** with excess $PMe_3$ in THF. One equivalent of the $OPPh_3$ internal standard equals one equivalent of **4**.

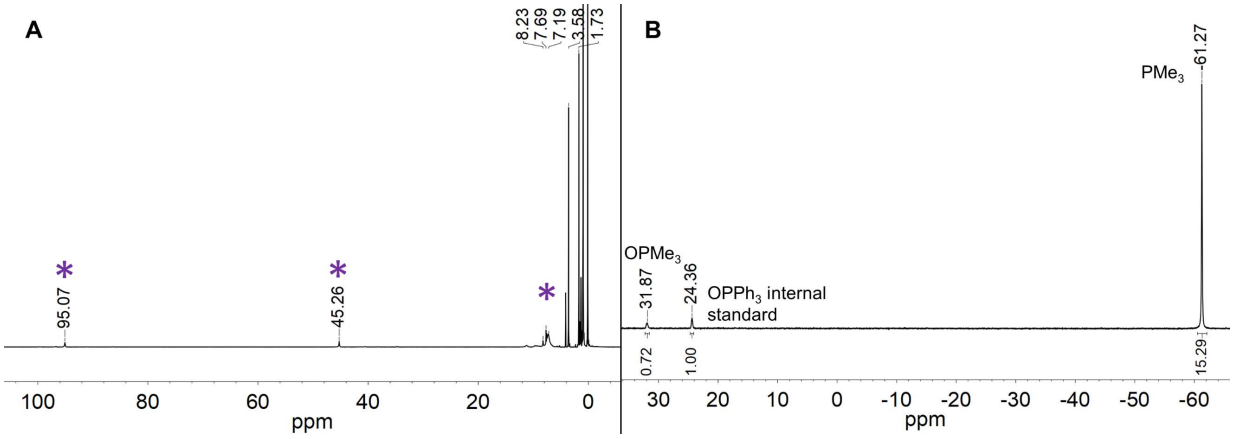


**Figure A1.18.** (A) $^{1}$H NMR spectrum and (B) $^{31}$P NMR spectrum of the reaction between **4** and excess $PMe_3$ in THF-$d_8$ that has been kept rigorously free of DCM. Purple asterisks indicate the major Co-containing product which matches the reported resonances for **1** (see reference 11 in Chapter 2). The resonances between 0 and 5 ppm are from residual THF, $PMe_3$, and $OPMe_3$. One equivalent of the $OPPh_3$ internal standard equals one equivalent of **4**.

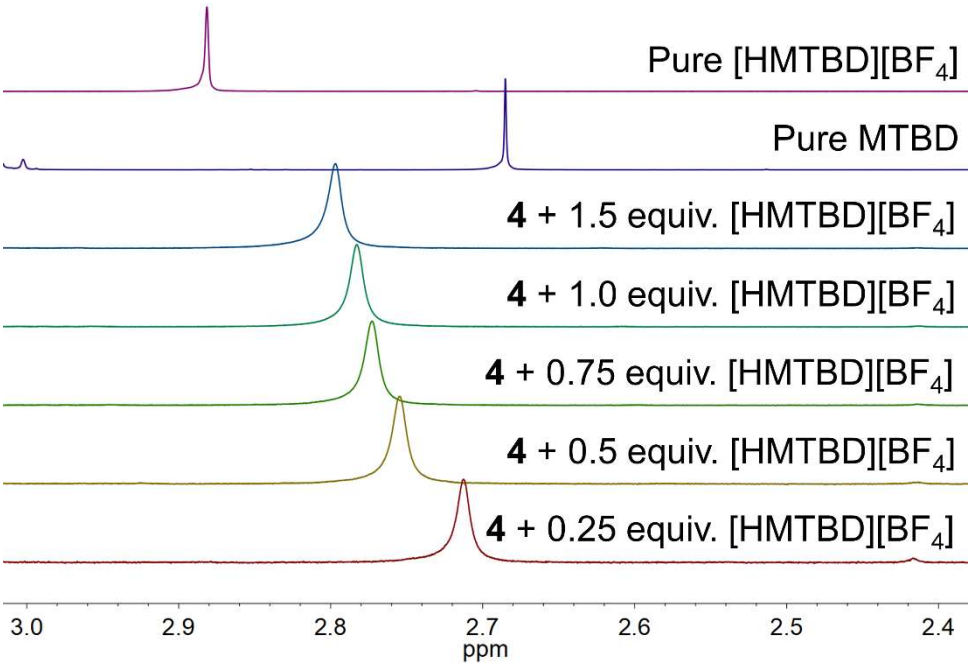


**Figure A1.19.** $^1$H NMR spectra of mixtures of **4** and [HMTBD][$BF_4$] in $CD_3CN$ at −35 °C. These were used to determine the concentrations of **2**, **4**, MTBD, and [HMTBD][$BF_4$] in $CD_3CN$ to calculate $K_{eq}$ (see Experimental in Chapter 2). Only the region between 2.4 and 3.0 ppm is displayed showing the resonance for the methyl group of MTBD/$HMTBD^+$.

| $[4]_i$ (mM) | $[HB^+]_i$ (mM) | $\delta_{obs}$ (ppm) | $[4]_{eq}$ (mM) | $[HB^+]_{eq}$ (mM) | $[2]_{eq}$ (mM) | $[B]_{eq}$ (mM) | $K_{eq}$ |
|---|---|---|---|---|---|---|---|
| 10.0 | 2.50 | 2.72 | 7.89 | 0.39 | 2.11 | 2.11 | 1.42 |
| 10.0 | 5.00 | 2.75 | 6.58 | 1.58 | 3.42 | 3.42 | 1.13 |
| 10.0 | 7.50 | 2.77 | 5.66 | 3.16 | 4.34 | 4.34 | 1.06 |
| 10.0 | 10.0 | 2.78 | 4.74 | 4.74 | 5.26 | 5.26 | 1.23 |
| 10.0 | 15.0 | 2.80 | 3.68 | 8.68 | 6.32 | 6.32 | 1.25 |
| | | | Average (± Std. Dev.) | | | | 1.2(0.1) |

**Table A1.1.** Data used for the determination of $K_{eq}$ values of the equilibrium between **4** and $HMTBD^+$ (denoted $HB^+$ in the table) at various initial concentrations of [HMTBD][$BF_4$]. $\delta_{obs}$ is the observed chemical shift for the methyl group of MTBD/$HMTBD^+$.

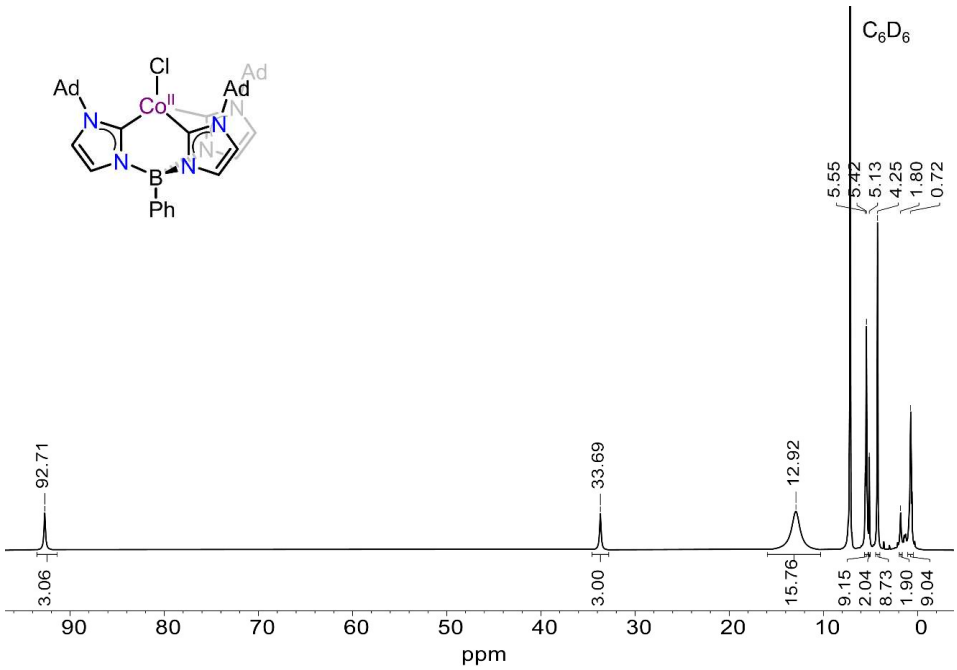


**Figure A1.20.** $^{1}$H NMR spectrum of **5** in $C_6D_6$ at room temperature.

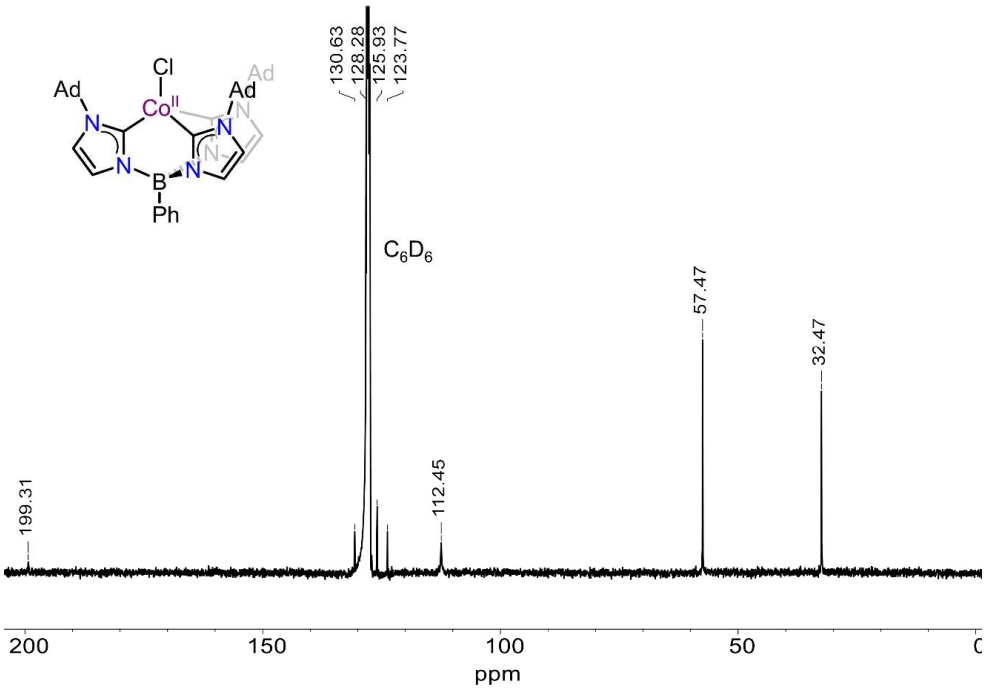


**Figure A1.21.** $^{13}$C NMR spectrum of **5** in $C_6D_6$ at room temperature. Note: not all expected resonances in this paramagnetic compound were observable.

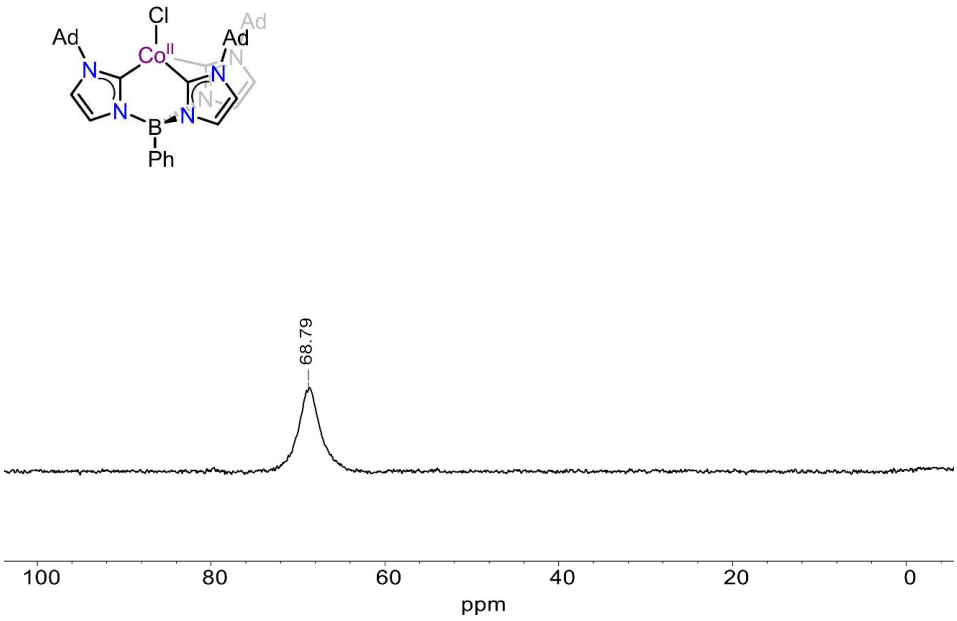


**Figure A1.22.** $^{11}$B NMR spectrum of **5** in $C_6D_6$ at room temperature.

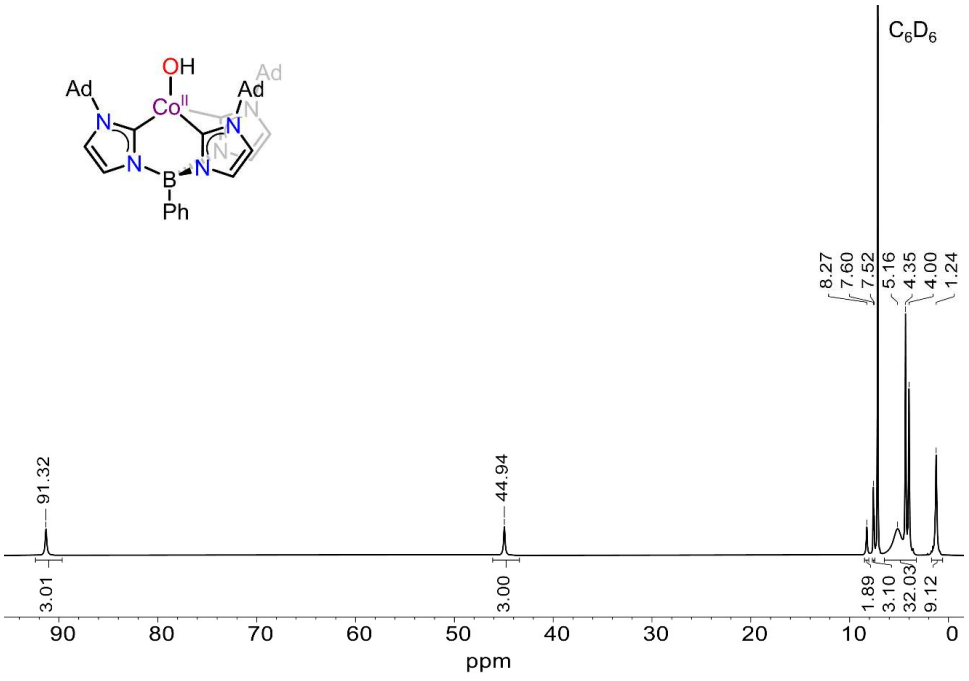


**Figure A1.23.** $^{1}$H NMR spectrum of **6** in $C_6D_6$ at room temperature.

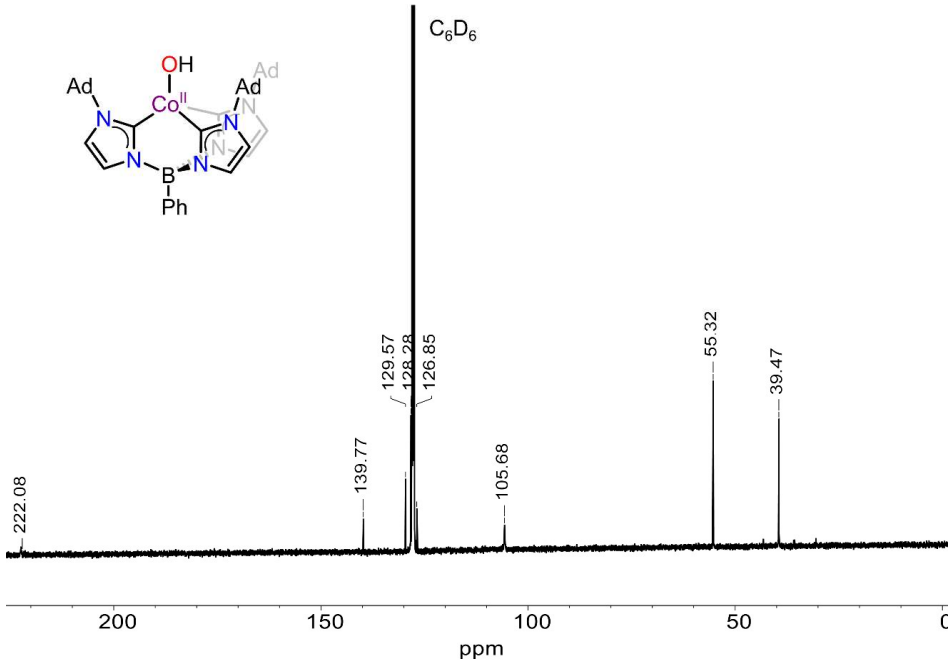


**Figure A1.24.** $^{13}$C NMR spectrum of **6** in $C_6D_6$ at room temperature. Note: not all expected resonances in this paramagnetic compound were observable.

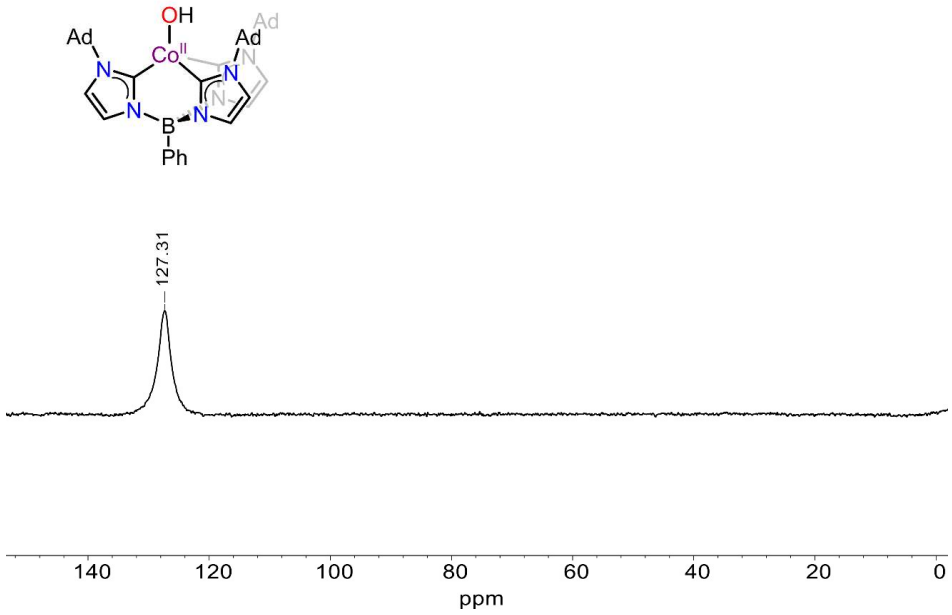


**Figure A1.25.** $^{11}$B NMR spectrum of **6** in $C_6D_6$ at room temperature.

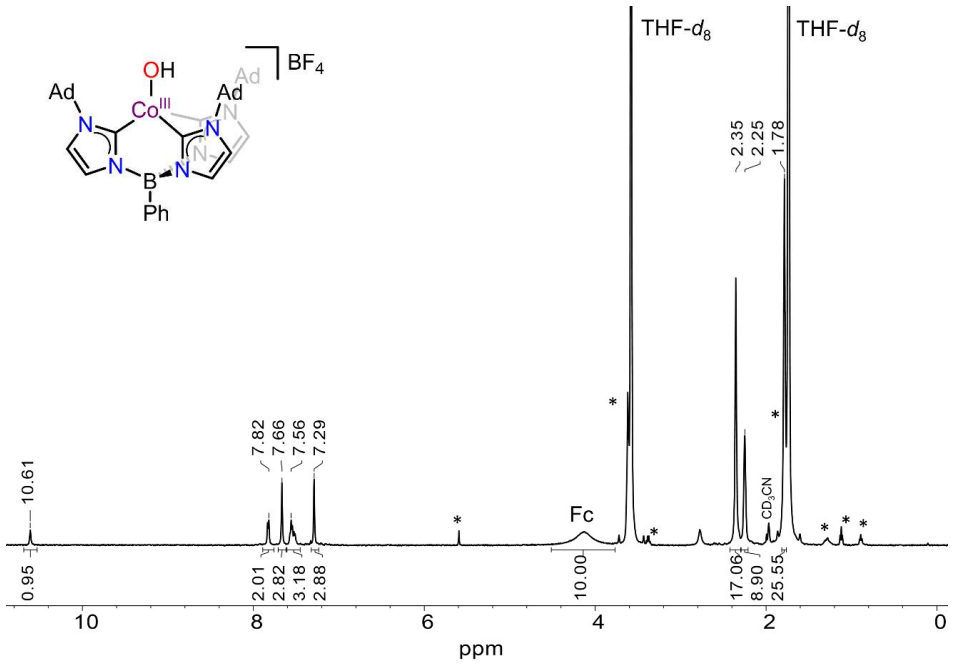


**Figure A1.26.** $^{1}$H NMR spectrum of **7** in THF-$d_8$ at –35 °C. Asterisks indicate solvent impurities (DCM, $Et_2O$, THF, pentane). $CD_3CN$ and Fc are present due to the in situ preparation of **7** from **6**.

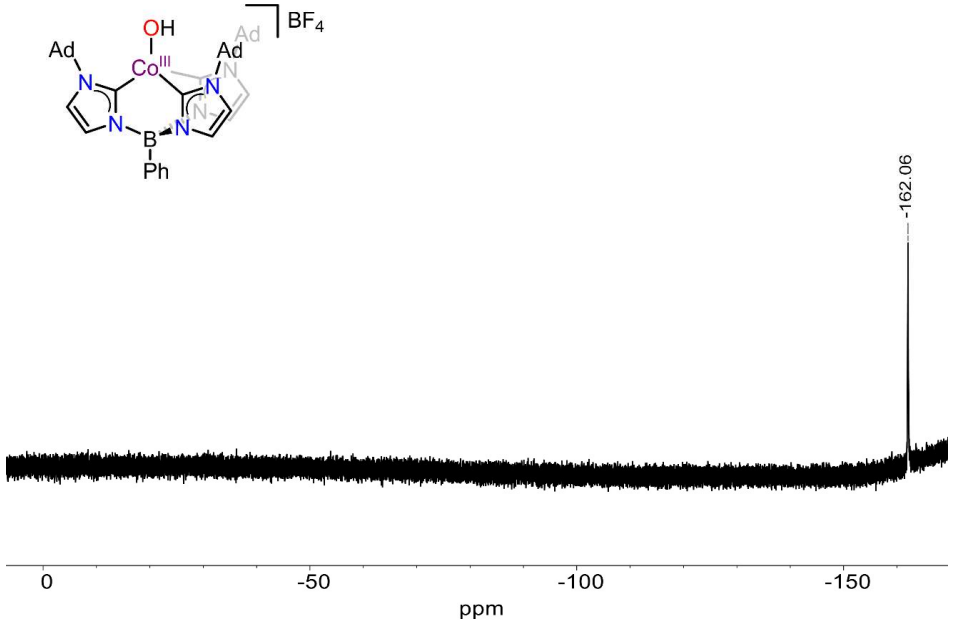


**Figure A1.27.** $^{19}$F NMR spectrum of **7** in THF-$d_8$ at –35 °C.

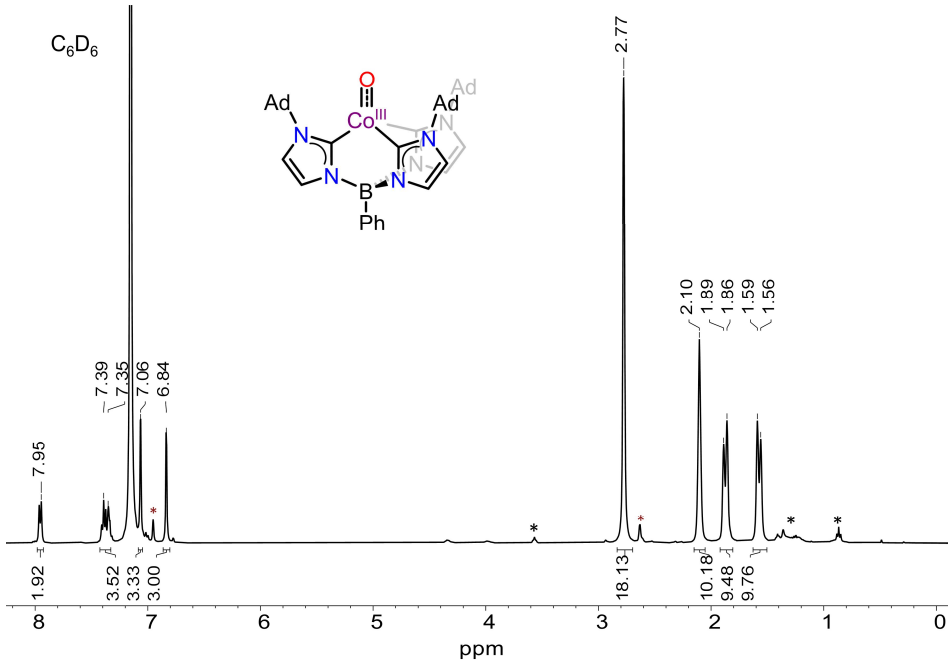


**Figure A1.28.** $^{1}$H NMR spectrum of **8** in $C_6D_6$ at room temperature. Black asterisks indicate solvent impurities. Red asterisks indicate an impurity due to residual water in solvent.

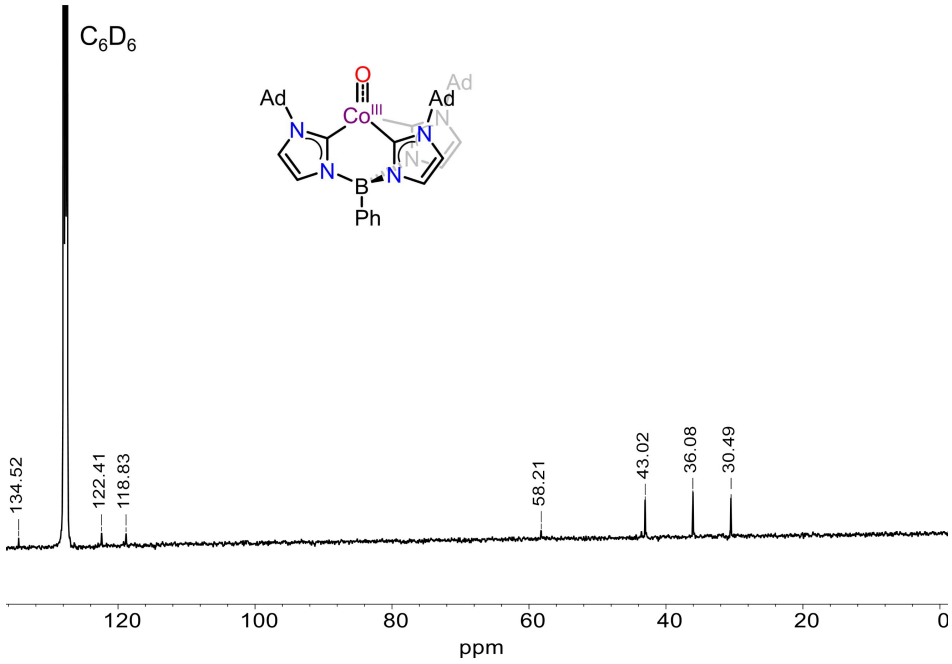


**Figure A1.29.** $^{13}$C NMR spectrum of **8** in $C_6D_6$ at room temperature. Note: not all expected resonances were observable for this inherently unstable compound.

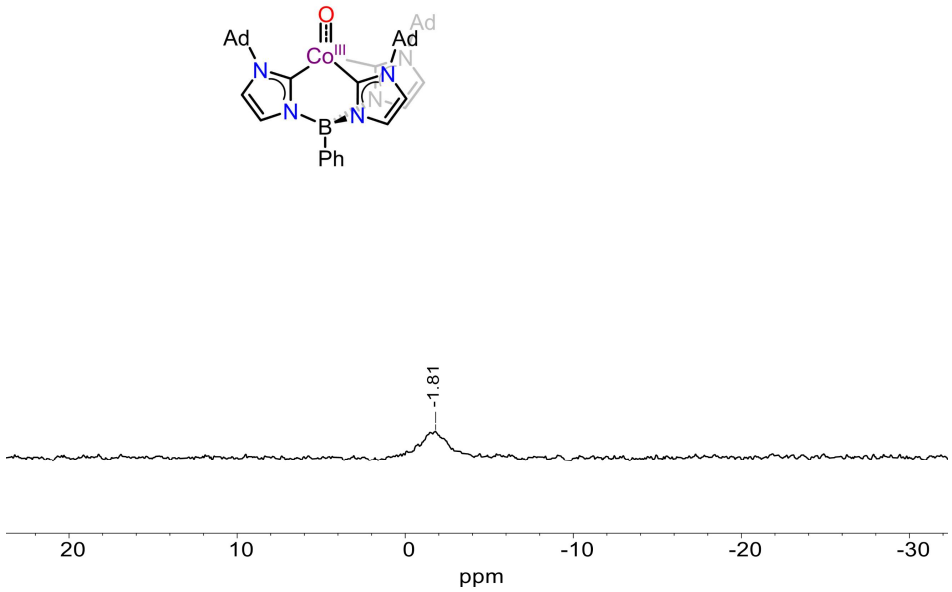


**Figure A1.30.** $^{11}$B NMR spectrum of **8** in $C_6D_6$ at room temperature.

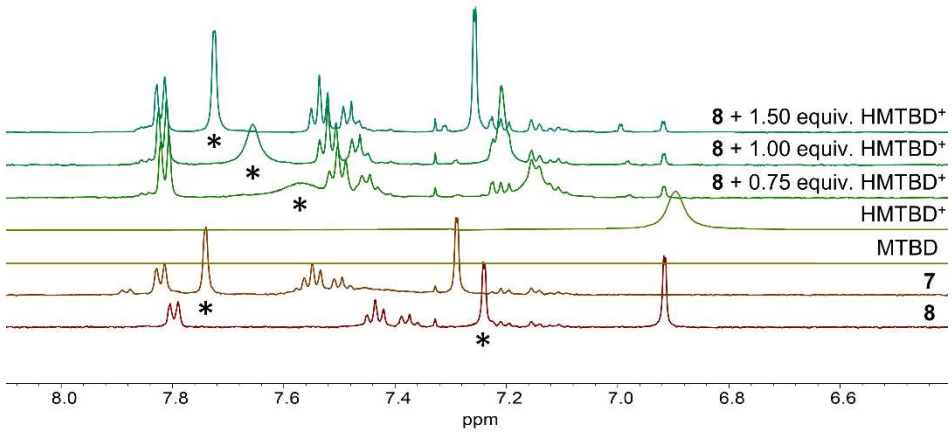


**Figure A1.31.** $^{1}$H NMR spectra (aromatic region) in THF-$d_8$ at –35 °C for the titration of **8** with [HMTBD][$BF_4$]. Asterisks indicate the **7**/**8** Im-*H* peak used for analysis (Table A1.2).

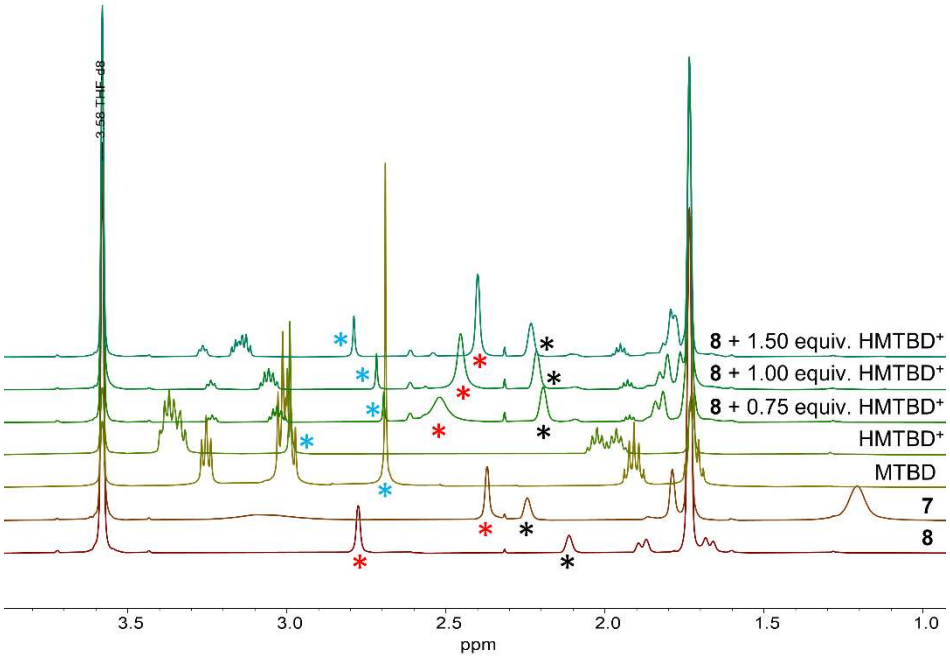


**Figure A1.32.** $^{1}$H NMR spectra (aliphatic region) in THF-$d_8$ at –35 °C for the titration of **8** with [HMTBD][$BF_4$]. Black and red asterisks indicate the two **7**/**8** Ad-*H* peaks used for analysis and blue asterisks indicate the MTBD/HMTBD$^+$ methyl peak used for analysis (Table A1.2).

**Table A1.2.** $^{1}$H NMR spectroscopic data used for calculation of $\Delta pK_{ip}$ between [HMTBD][$BF_4$] and **7**.

| $\delta_{obs}$ (H)MTBD[a] | $\frac{[MTBD]}{[HMTBD]^+}$ [b] | $\delta_{obs}$ Im-*H*[a] | $\frac{[7]}{[8]}$ [c] | $\Delta pK_{ip}$ [d] | $\delta_{obs}$ Ad-*H*[a] | $\frac{[7]}{[8]}$ [c] | $\Delta pK_{ip}$ [d] | $\delta_{obs}$ Ad-*H*[a] | $\frac{[7]}{[8]}$ [c] | $\Delta pK_{ip}$ [d] |
|---|---|---|---|---|---|---|---|---|---|---|
| 2.70 | 29 | 7.57 | 1.94 | 1.75 | 2.52 | 1.67 | 1.68 | 2.19 | 1.33 | 1.59 |
| 2.72 | 9 | 7.66 | 5.25 | 1.67 | 2.45 | 4.00 | 1.56 | 2.22 | 3.67 | 1.52 |
| 2.79 | 2 | 7.73 | 32.3 | 1.81 | 2.40 | 12.3 | 1.39 | 2.23 | 6.00 | 1.08 |
| 2.69 | 74 | 7.57 | 1.94 | 2.16 | 2.53 | 1.50 | 2.05 | 2.19 | 1.33 | 1.99 |
| 2.74 | 9 | 7.67 | 6.14 | 1.74 | 2.45 | 4.00 | 1.56 | 2.22 | 3.67 | 1.52 |
| 2.73 | 6.5 | 7.68 | 7.33 | 1.68 | 2.43 | 5.64 | 1.57 | 2.22 | 3.67 | 1.38 |
| 2.70 | 29 | 7.59 | 2.33 | 1.83 | 2.50 | 2.08 | 1.78 | 2.20 | 1.80 | 1.72 |
| 2.72 | 9 | 7.65 | 4.56 | 1.61 | 2.46 | 3.44 | 1.49 | 2.21 | 2.50 | 1.35 |
| 2.80 | 1.7 | 7.73 | 32.3 | 1.75 | 2.40 | 12.3 | 1.33 | 2.23 | 6.00 | 1.02 |
| Average $\Delta pK_{ip}$ from each **7**/**8** peak analysis | | | | **1.78** | | | **1.60** | | | **1.46** |
| | | | | | | | | Overall Average $\Delta pK_{ip}$ of 3 analyses | | **1.6** |
| | | | | | | | | Standard Deviation | | **0.2** |

[a]From Figure A and Figure A; 3 trials at each concentration. [b]Calculated according to Equation 2.11. [c]Equation 2.10. [d]Calculated according to Equation 2.12 and Equation 2.13, for each $HMTBD^+$/MTBD and **7**/**8** peak analysis pair.

**Table A1.3.** Metrics used for the calculation of $\Delta pK_a$ between $HMTBD^+$ and $\mathbf{7}^+$.

| Relevant Metrics | Value | Species | $K_d$[c] | $\Delta pK_a$[d] |
|---|---|---|---|---|
| r ($\mathbf{7}^+$)[a] / Å | 7.5 | **7** | $2.79 \cdot 10^{-5}$ | **4.6** |
| r ($HMTBD^+$)[b] / Å | 3 | [HMTBD][$BF_4$] | $3.05 \cdot 10^{-8}$ | |
| r ($BF_4$)[b] / Å | 2 | | | |
| N / $mol^{-1}$ | $6.02 \cdot 10^{23}$ | | | |
| e / esu | $4.8 \cdot 10^{-10}$ | | | |
| $\epsilon$ (THF) | 7.6 | | | |
| k / erg•$deg^{-1}$ | $1.38 \cdot 10^{-16}$ | | | |
| T / K | 238 | | | |

[a]Determined by taking the cube root of the molecular volume of the cation determined in Hyperchem. [b]From reference 25 in Chapter 2. [c]Calculated according to Equation A1.1-Equation A1.3. [d]Calculated according to Equation 2.14.

Equation A1.1 $$K_d = \frac{3000 \cdot \exp(b)}{4\pi N a^3}$$

Equation A1.2 $$a = r^+ + r^- \text{ (in cm)}$$

Equation A1.3 $$b = \frac{-e^2}{a\epsilon kT}$$

## A1.2 EPR Spectra

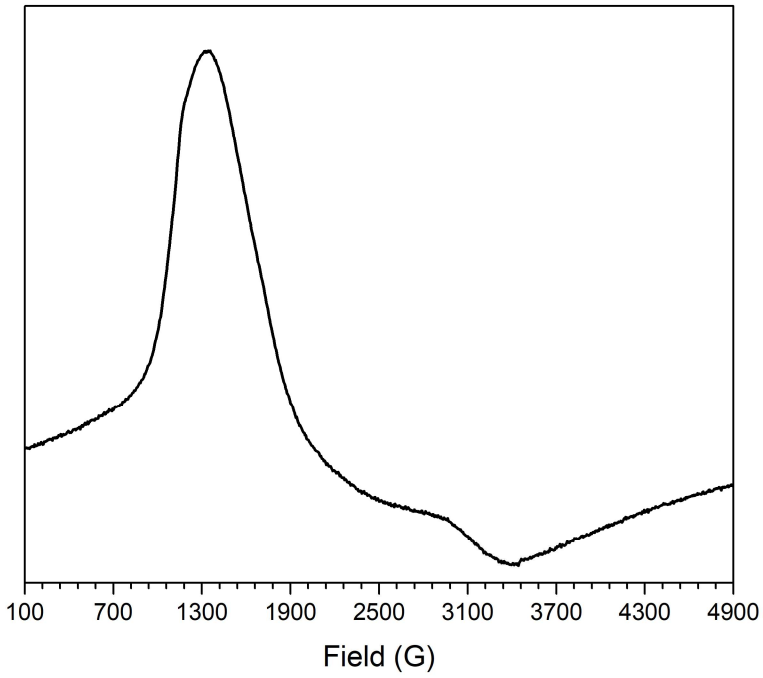


**Figure A1.33.** EPR spectrum of **1** collected on a 15 mM frozen 1,3-difluorobenzene solution at 15 K with a microwave frequency of 9.63 GHz and a microwave power of 0.2 mW.

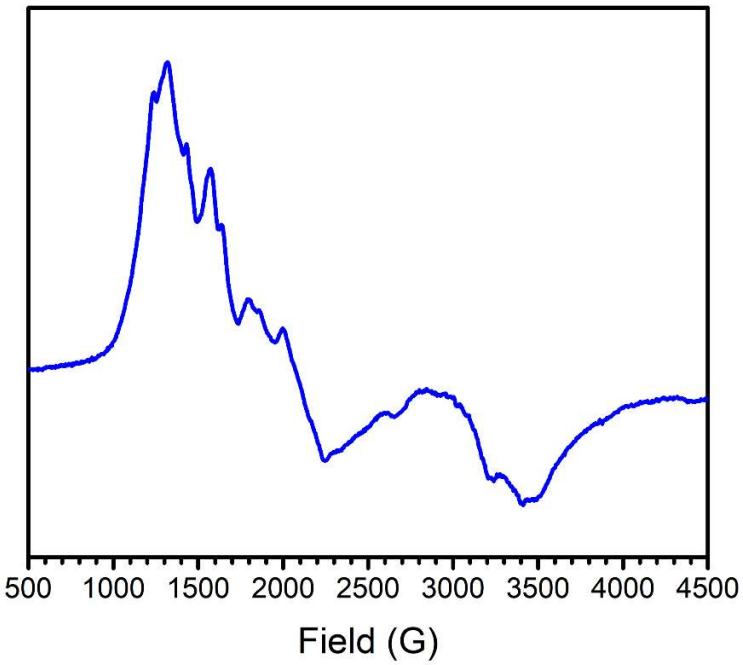


**Figure A1.34.** EPR spectrum of **5** collected on a 5 mM frozen solution in THF at 15 K. Experimental conditions: microwave frequency 9.63 GHz, microwave power 0.02 mW.

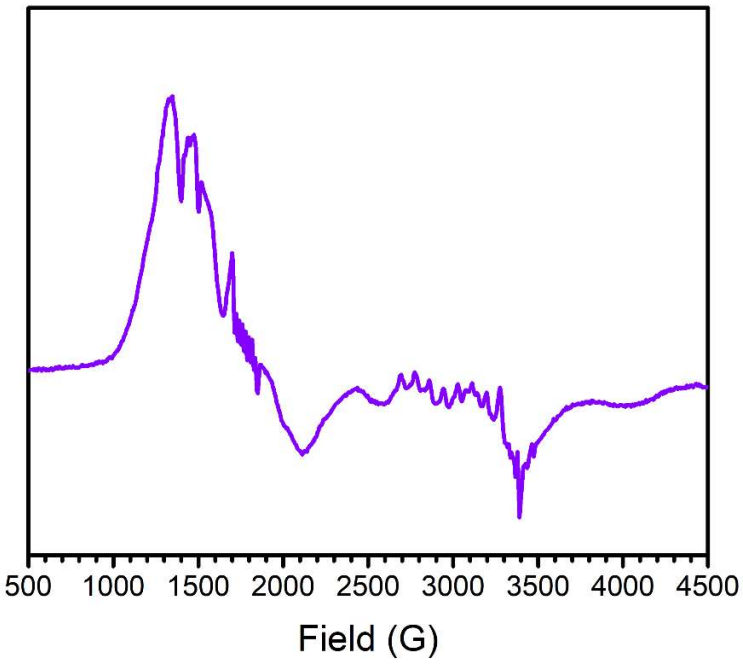


**Figure A1.35.** EPR spectrum of **6** collected on a 5 mM frozen solution in THF at 15 K. Experimental conditions: microwave frequency 9.63 GHz, microwave power 0.02 mW.

## A1.3 IR Spectra

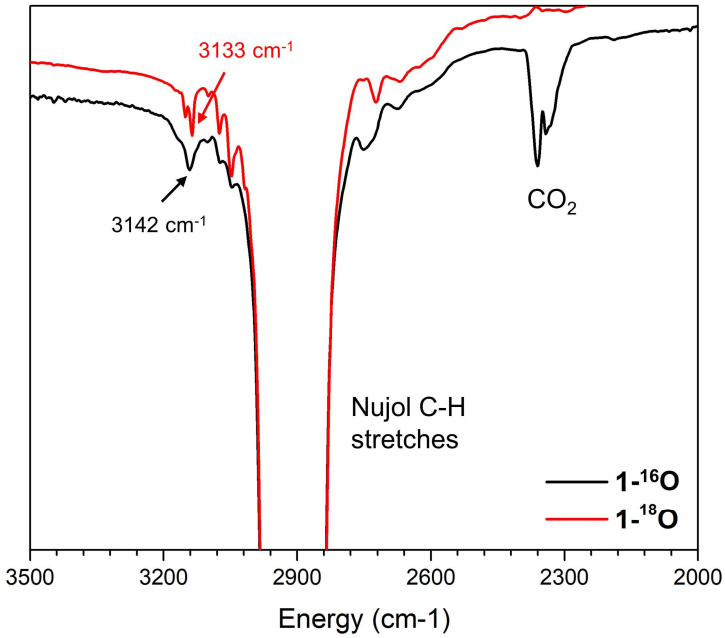


**Figure A1.36.** Overlay of IR spectra of **1-$^{16}$O** and **1-$^{18}$O** demonstrating the isotope dependence of the O–H stretching vibration.

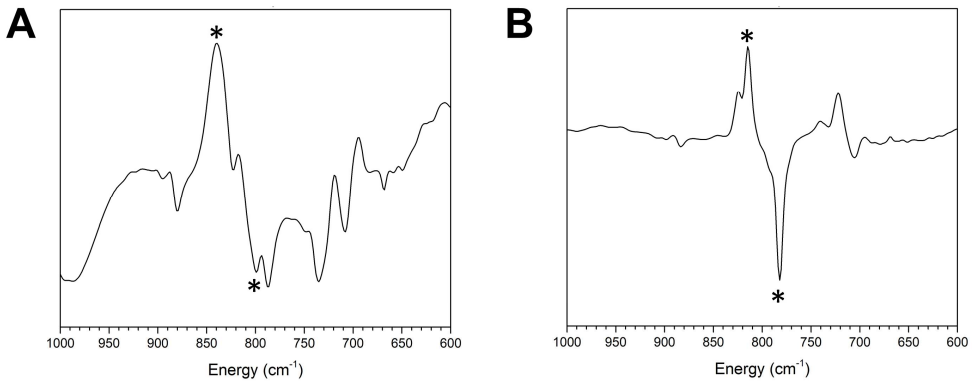


**Figure A1.37.** (A) Difference IR spectrum for **3** and **3-$^{18}$O**. Asterisks indicate the isotope dependent shift. (B) Difference IR spectrum for **4** and **4-$^{18}$O**. Asterisks indicate the isotope dependent shift.

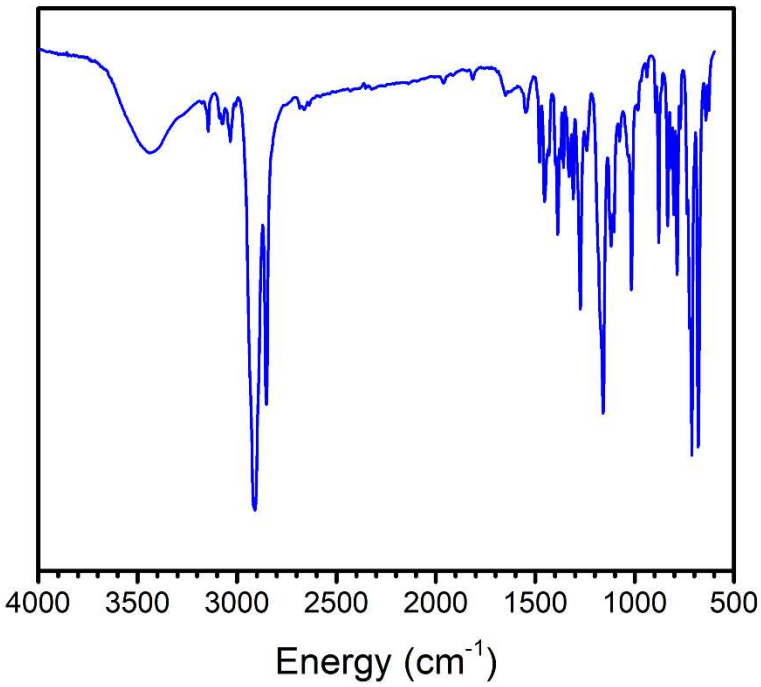


**Figure A1.38.** IR spectrum of **5** collected as a KBr pellet.

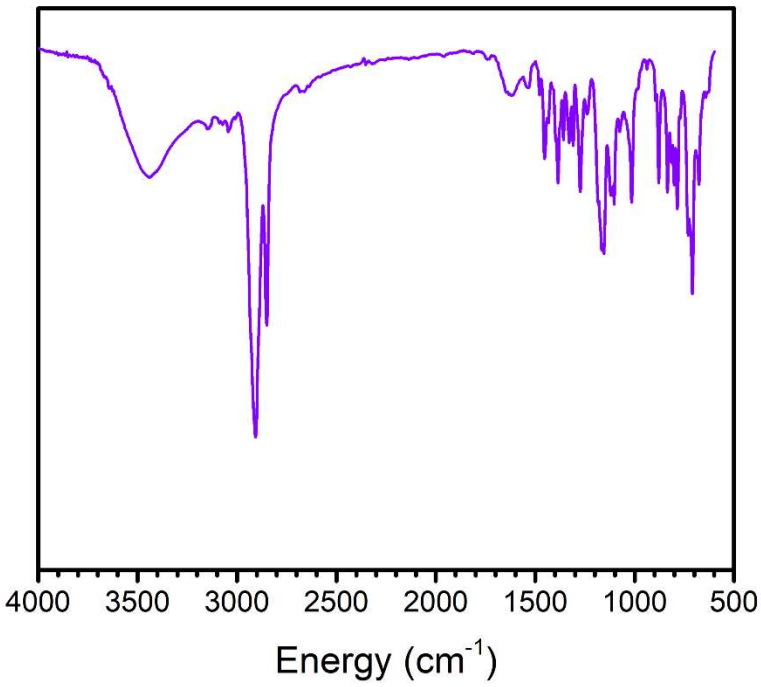


**Figure A1.39.** IR spectrum of **6** collected as a KBr pellet.

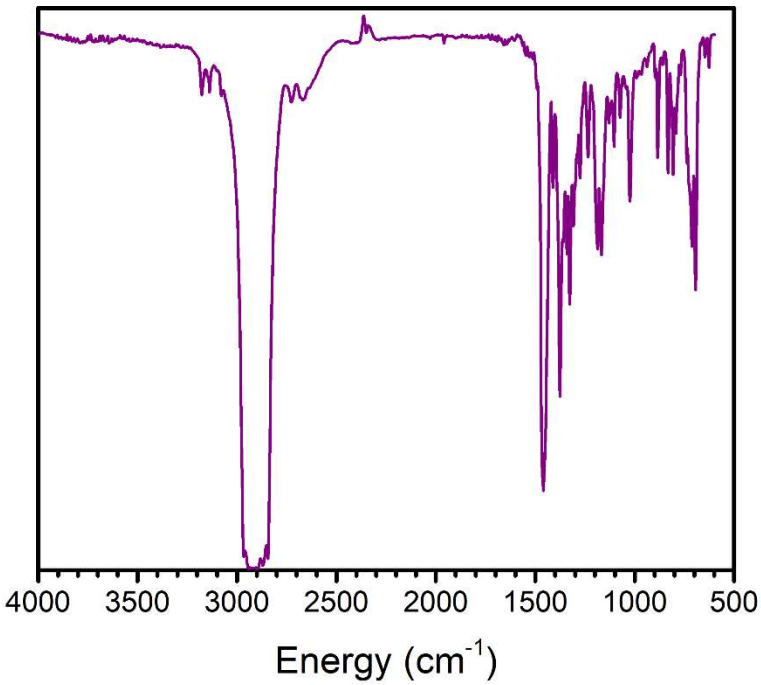


**Figure A1.40.** IR spectrum of **8** collected as a Nujol mull pressed between KBr plates.

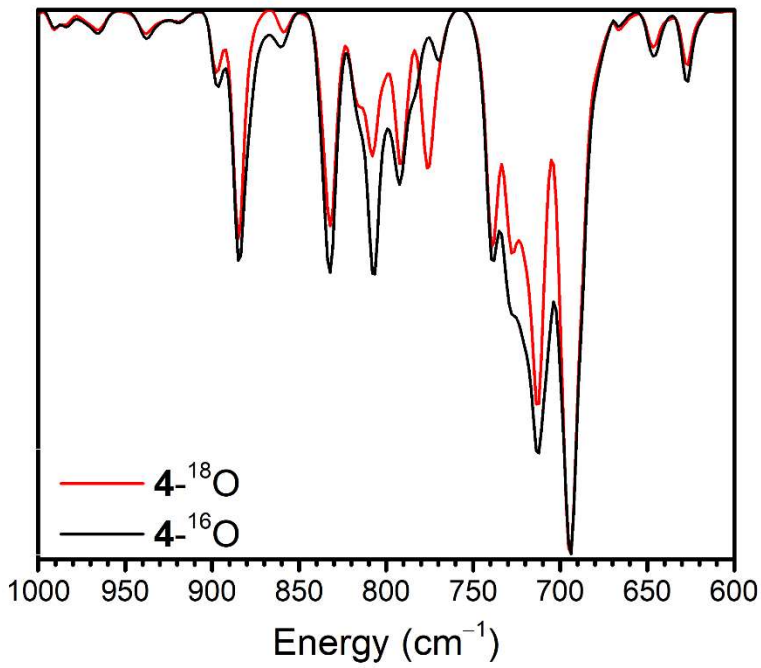


**Figure A1.41.** Overlay of IR spectra of **8-$^{16}$O** and **8-$^{18}$O** showing the Co–O stretch.

## A1.4 UV-vis Spectra

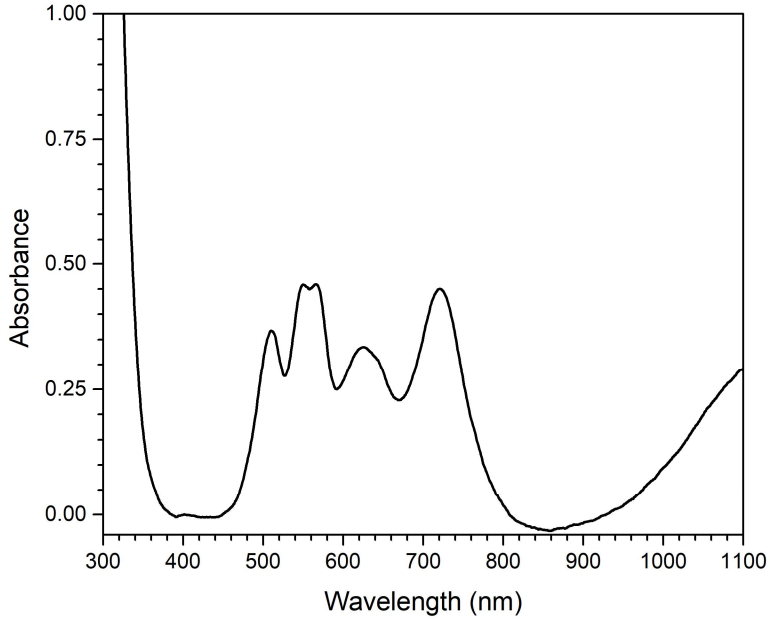


**Figure A1.42.** UV-vis spectrum of **1** in THF (1.25 mM).

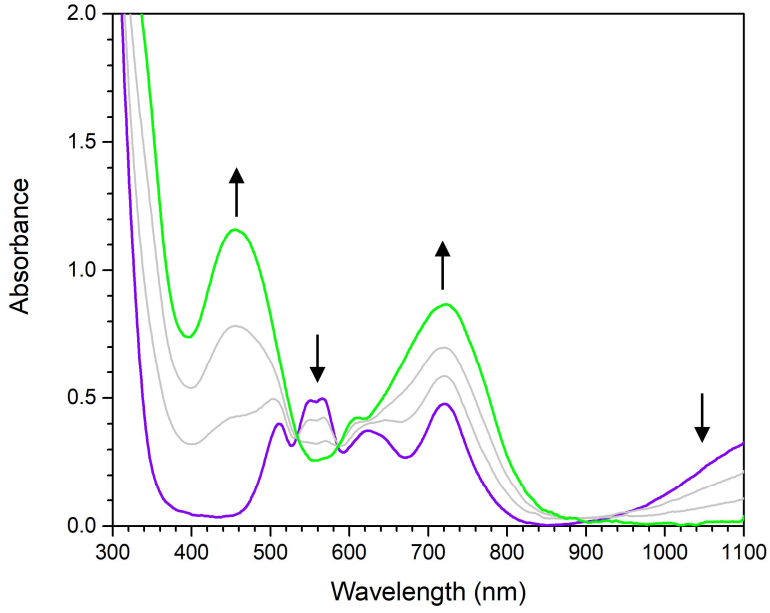


**Figure A1.43.** Generation of **2** (green trace) monitored by UV-vis spectroscopy upon the addition of $FcBF_4$ to **1** (purple trace) in THF at −78 °C. Gray traces indicate partial equivalent additions of $FcBF_4$.

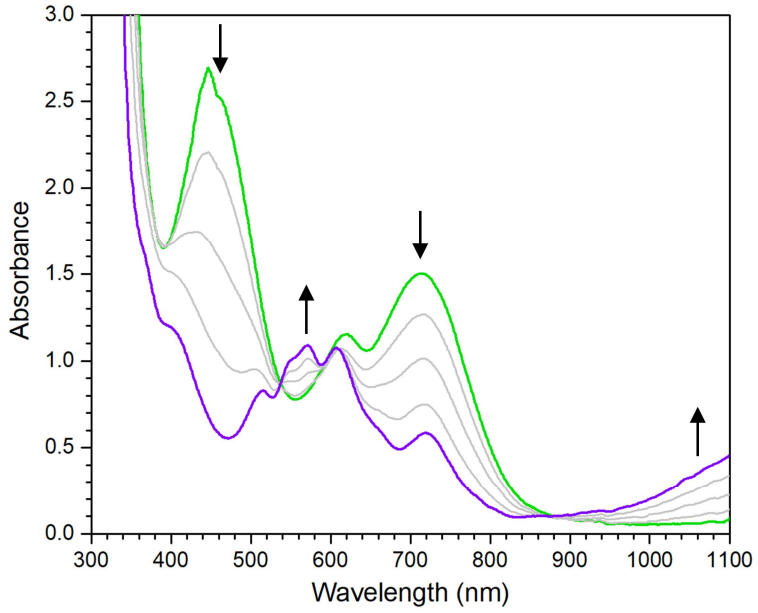


**Figure A1.44.** Reduction of **2** (green trace) monitored by UV-vis spectroscopy. Upon the addition of $CoCp_2$ to a solution of **2** in MeCN at –35 °C, complex **1** (purple trace) is regenerated. Gray traces indicate partial equivalent additions of $CoCp_2$.

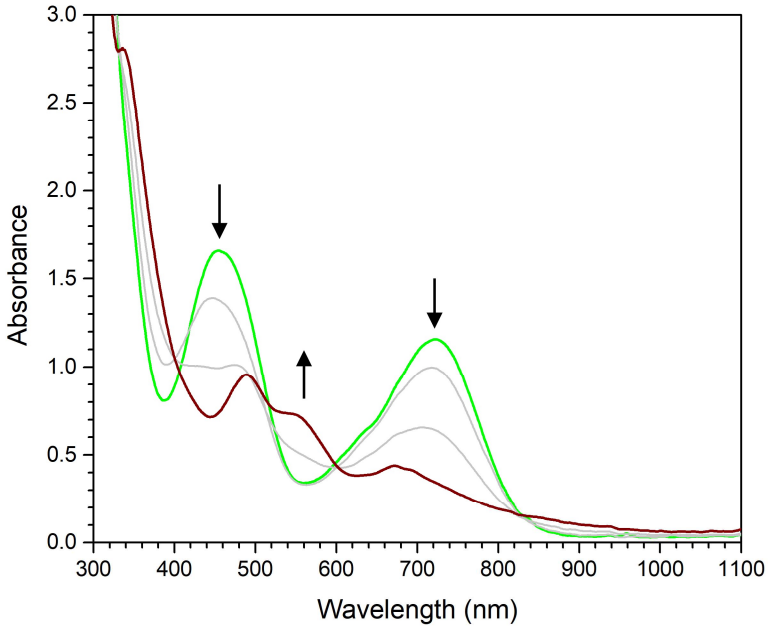


**Figure A1.45.** Generation of **3** by UV-vis spectroscopy. UV-vis spectra demonstrate the generation of **3** (dark red trace) upon addition of LiHMDS to **2** (green trace) in THF at –78 °C. Gray traces indicate partial equivalent additions of LiHMDS.

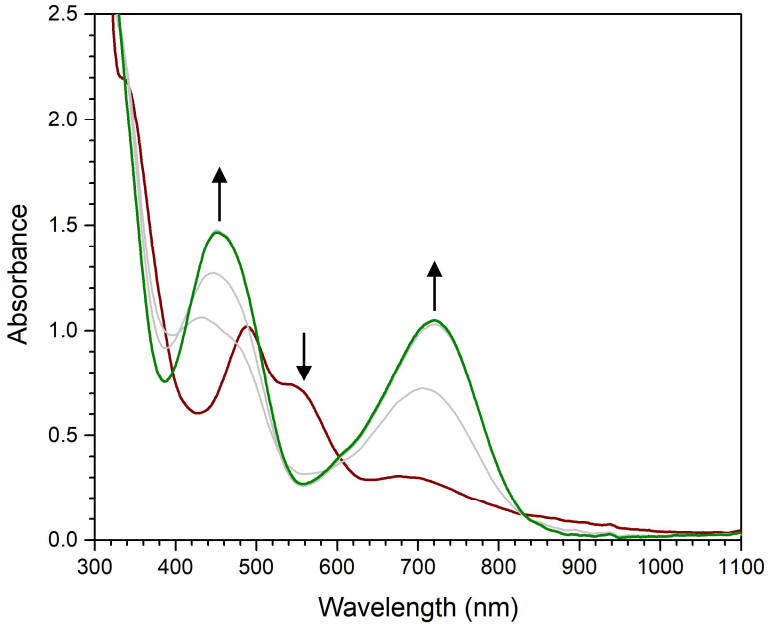


**Figure A1.46.** Protonation of **3** by UV-vis spectroscopy. UV-vis spectra demonstrate the regeneration of **2** (green trace) upon addition of $[HNEt_3][BF_4]$ to **3** (dark red trace) at −78 °C in THF. Gray traces indicate partial equivalent additions of $[HNEt_3][BF_4]$.

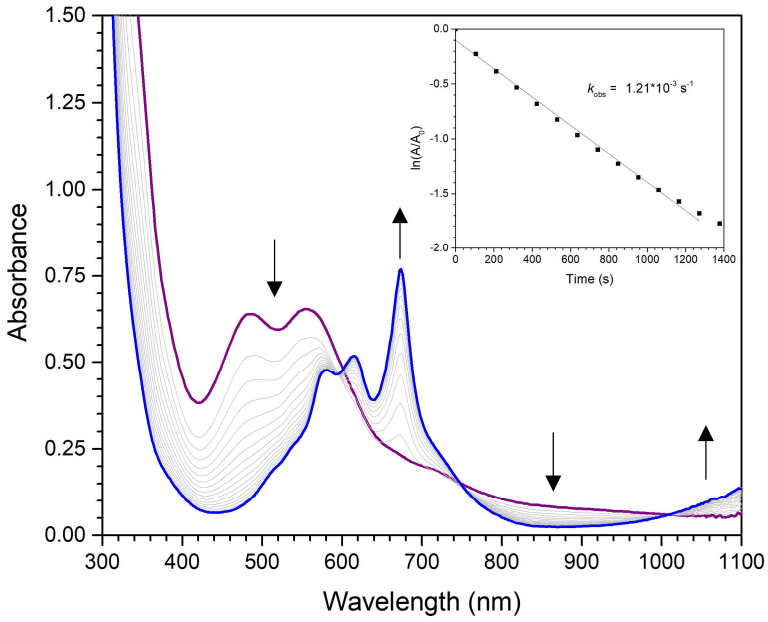


**Figure A1.47.** UV-vis spectra demonstrating the reactivity of **3** (dark purple trace) with excess $PMe_3$ resulting in the formation of $PhB(^tBuIm)_3Co^{II}Cl$ (blue trace). Gray traces indicate two-

minute time intervals during the reaction. Inset: first order kinetic plot of the reaction monitored at 470 nm.

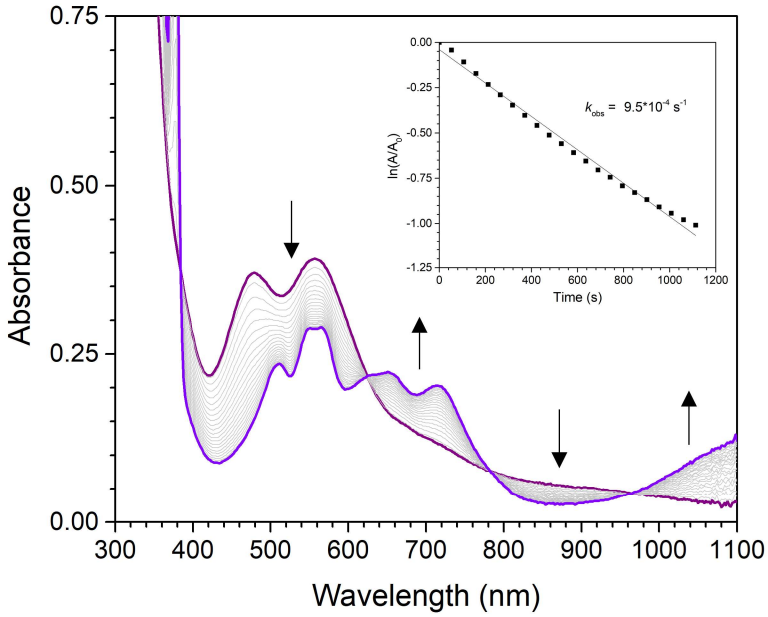


**Figure A1.48.** UV-vis spectra demonstrating the reactivity of **4** (dark purple trace) with excess DHA resulting in the formation of **1** (bright purple trace). Gray traces indicate one-minute time intervals during the reaction. Inset: first order kinetic plot of the reaction monitored at 470 nm.

| | Complex **3** | Complex **4** |
|---|---|---|
| $PMe_3$ | 12.1 ± 0.1 | 11.8 ± 0.04 |
| DHA | 7.7 ± 1.6 | 9.5 ± 0.6 |
| Self-decay | 0.083 | 0.094 |

**Table A1.4.** Rates of reaction ($k_{obs}$, $10^{-4}$ $s^{-1}$) of **3** and **4** with substrates.

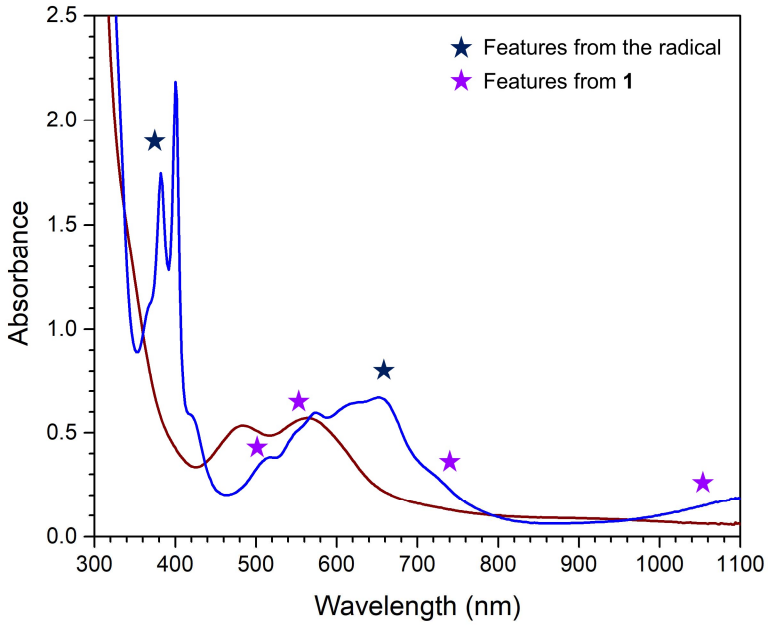


**Figure A1.49.** UV-vis spectra showing the reaction between **4** (dark red trace) and 2,4,6-tri(*tert*-butyl)phenol resulting in a spectrum (blue trace) that is a superposition of the spectrum of **1** and the spectrum of the phenoxyl radical.

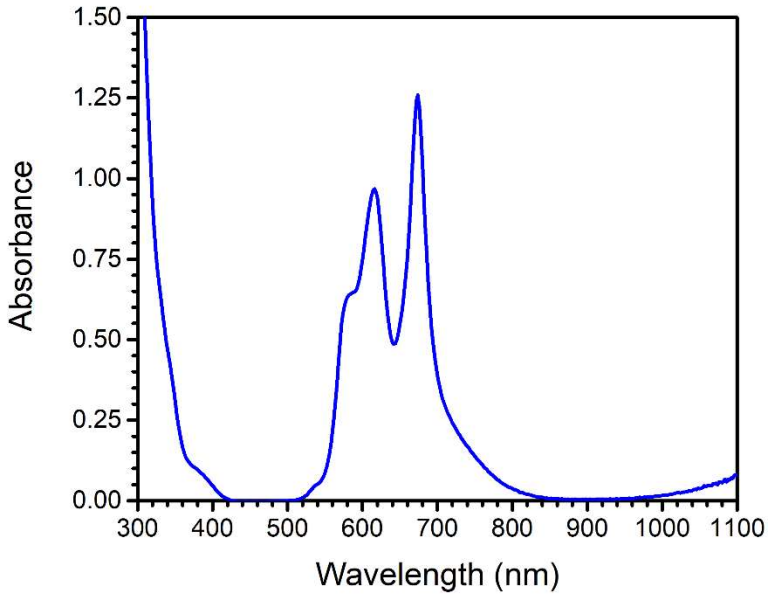


**Figure A1.50.** UV-vis spectrum of **5** in THF (1.25 mM) at room temperature.

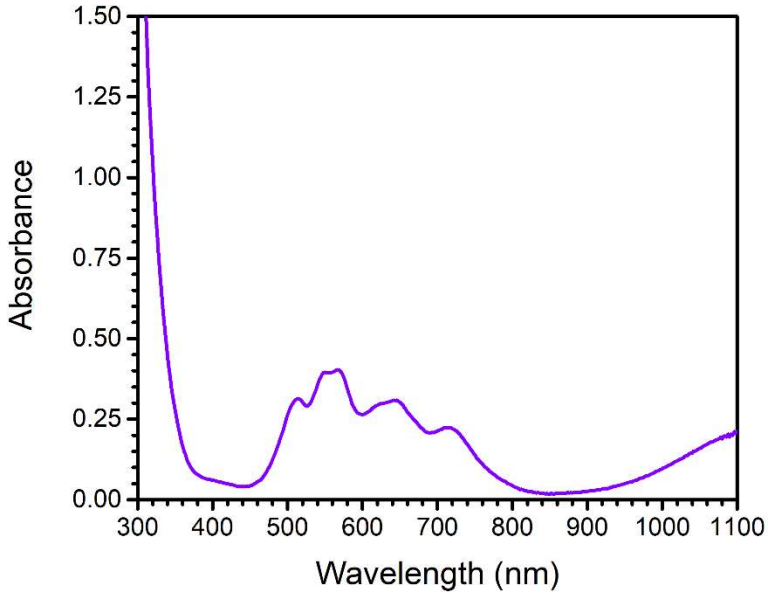


**Figure A1.51**. UV-vis spectrum of **6** in THF (1.25 mM) at room temperature.

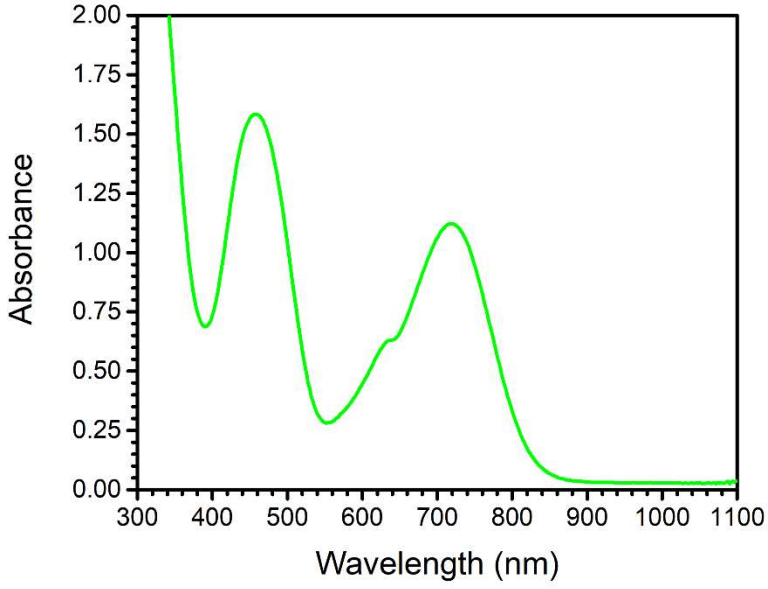


**Figure A1.52.** UV-vis spectrum of in situ prepared **7** in THF (1.25 mM) at –80 °C.

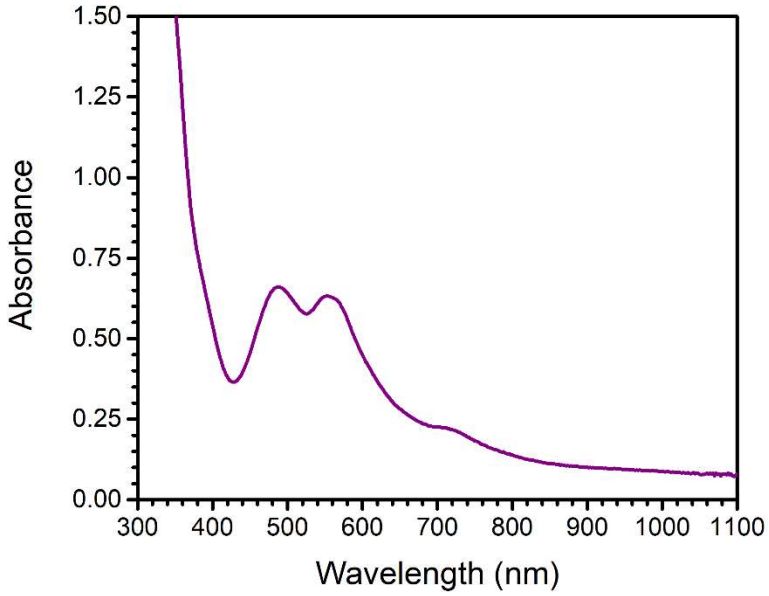


**Figure A1.53.** UV-vis spectrum of **8** in THF (1.25 mM) at room temperature.

## A1.5 Cyclic Voltammetry

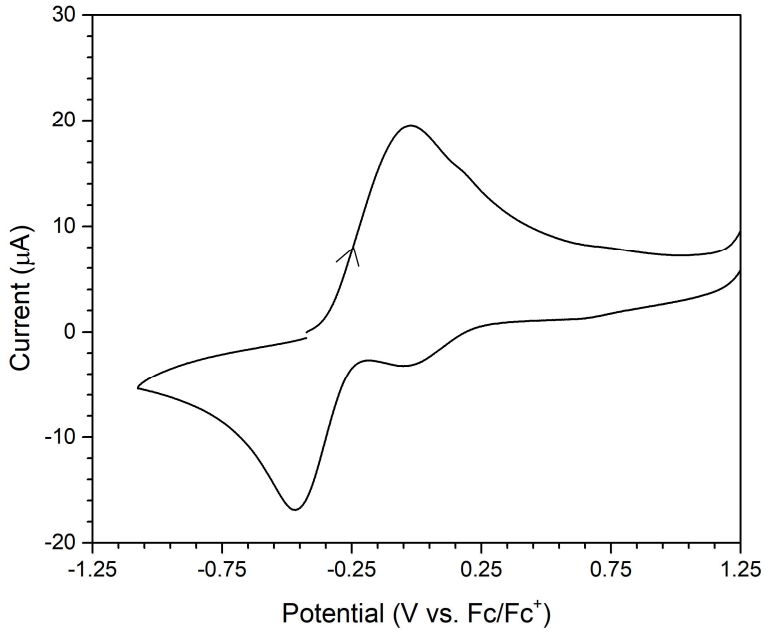


**Figure A1.54.** Cyclic voltammogram of **1** (3 mM) in MeCN with 0.1 M [TBA][$PF_6$] as the supporting electrolyte. See Chapter 2.4 for experimental details.

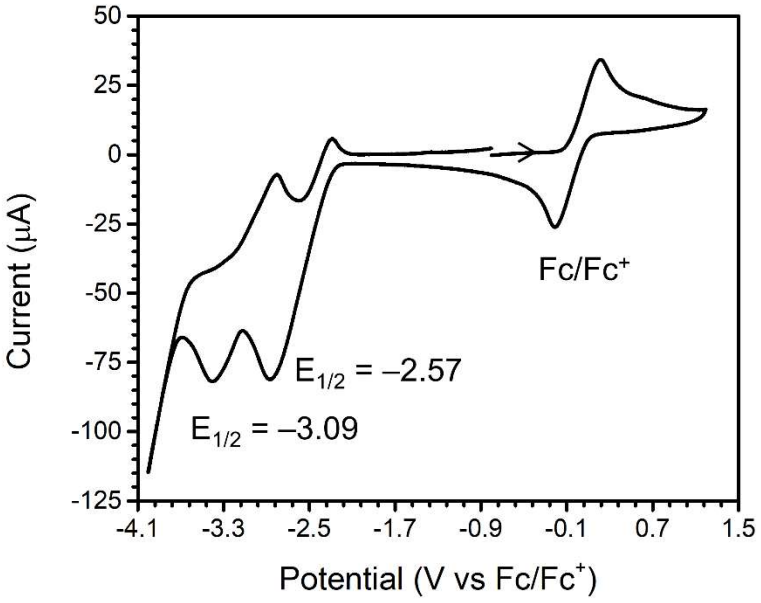


**Figure A1.55.** CV of **5** in THF. Conditions: 3 mM **5**, 0.1 M $TBAPF_6$. Internal reference to $Fc/Fc^+$.

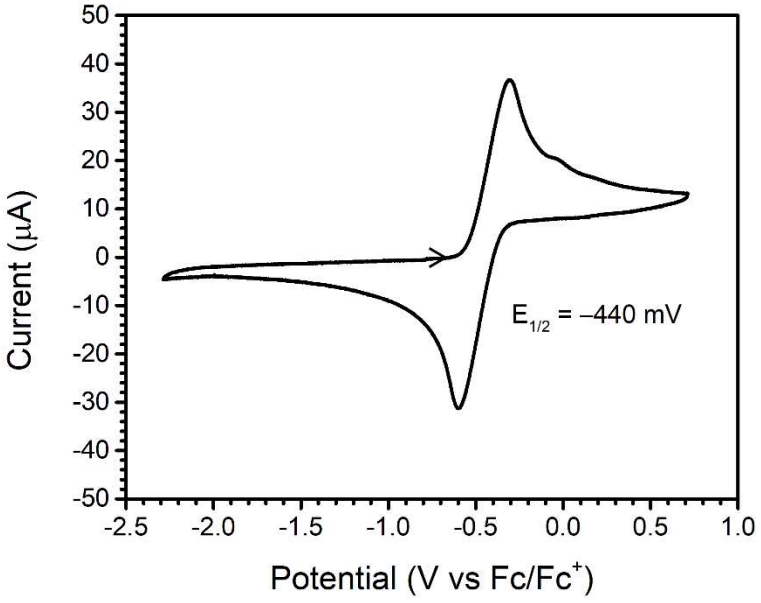


**Figure A1.56.** CV of **6** in THF. Conditions: 3 mM **6**, 0.1 M $TBAPF_6$. Externally referenced to $Fc/Fc^+$.

## A1.6 Schemes

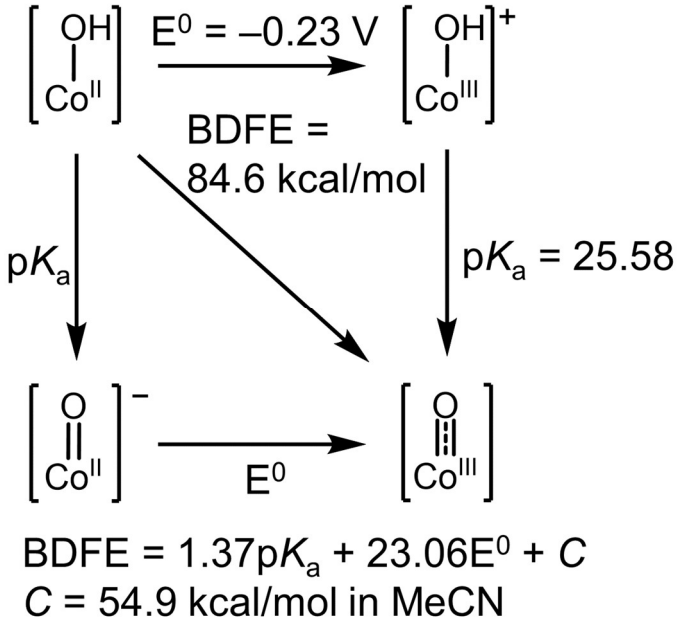


**Scheme A1.1.** Thermodynamic square scheme describing the relationship between p$K_a$, $E^0$, and $BDFE_{O–H}$ for **1**.

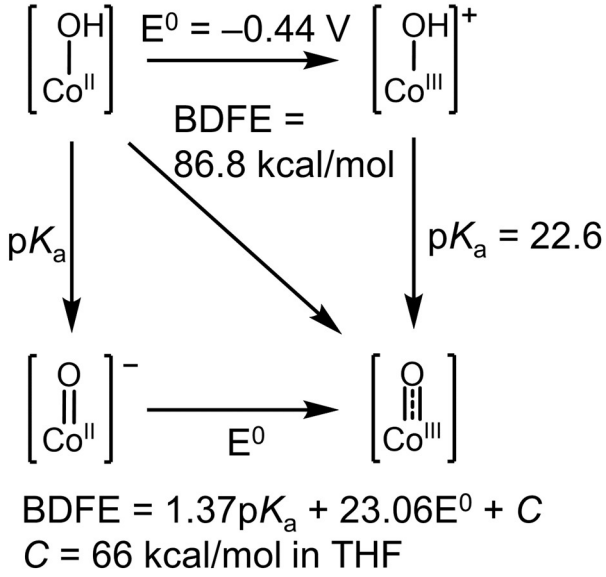


**Scheme A1.2.** Thermodynamic square scheme for the calculation of the $BDFE_{O–H}$ in **6**.

## A1.7 Gas Chromatography-Mass Spectrometry

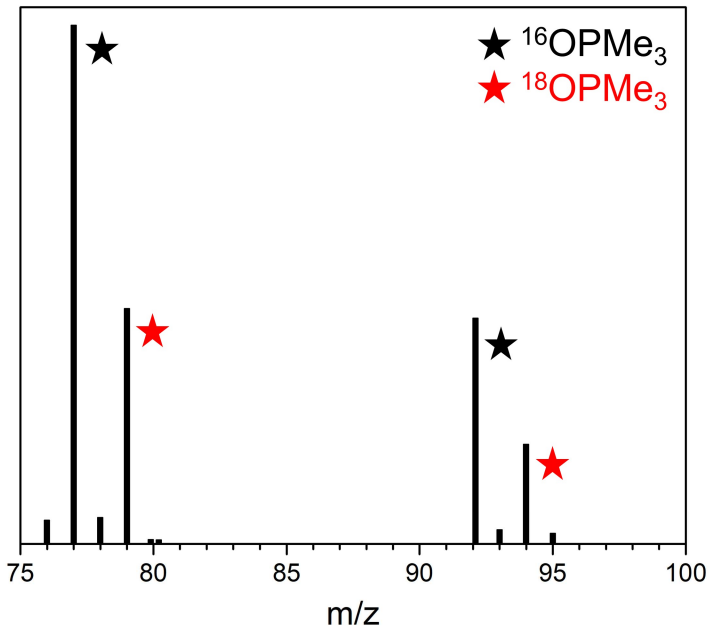


**Figure A1.57.** Mass spectrum of the reaction of **4-$^{18}$O** and $PMe_3$. $^{16}OPMe_3$ has m/z = 92.0 and $^{18}OPMe_3$ has m/z = 94.0. The peaks at m/z = 77.0 and 79.0 are fragments with loss of a methyl group, respectively. The presence of $^{16}OPMe_3$ is likely due to air exposure during the GC-MS experiment.

## A1.8 Crystallographic Data

| | Complex **1** | Complex **2**[a] | Complex **3**[b] | Complex **4** |
|---|---|---|---|---|
| **Bond Lengths (Å)** | | | | |
| Co1–O1 | 1.876(2) | 1.776(7) | 1.657 | 1.682(6) |
| Co–$C_{avg}$ | 2.032 | 1.888 | 1.913 | 1.929 |
| **Bond Angles (°)** | | | | |
| B1–Co1–O1 | 172.65(6) | 135.50(3) | 170.1 | 160.2(3) |
| C1–Co1–O1 | 128.80(6) | 169.98(4) | 118.3 | 114.4(3) |
| C8–Co1–O1 | 117.10(6) | 101.16(4) | 135.2 | 145.9(3) |
| C15–Co1–O1 | 123.86(6) | 99.69(4) | 124.3 | 114.2(3) |
| C1–Co1–C8 | 91.70(6) | 86.54(4) | 87.0 | 88.9(3) |
| C8–Co1–C15 | 93.00(6) | 96.77(4) | 88.9 | 88.9(3) |
| C15–Co1–C1 | 93.08(6) | 85.59(4) | 90.6 | 90.3(3) |

**Table A1.5.** Selected bond lengths and bond angles for complexes **1**-**4**. [a]Average bond lengths and angles of the two molecules in the unit cell. [b]Average bond lengths and angles over the four units of the tetramer.

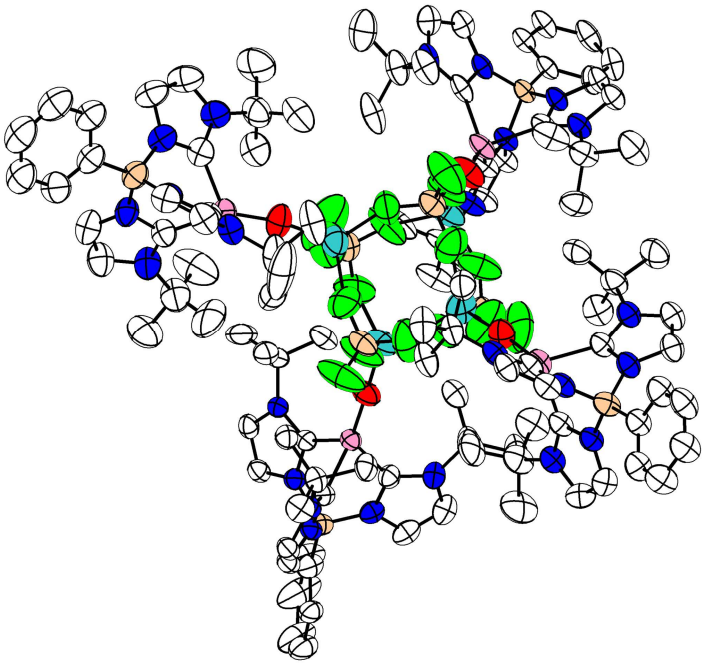

**Figure A1.58.** Crystal structure of **3** depicting the full tetrameric oligomer. Ellipsoids are shown at 50% probability with all H atoms and solvent molecules omitted for clarity. Pink – Co, white – C, blue – N, tan – B, red – O, teal – Li, green – F.

**Table A1.6.** Crystallographic and refinement data for complexes **1**-**8**.

| Complex | **1** | **2** | **3** |
|---|---|---|---|
| Empirical formula | $C_{27}H_{39}BCoN_6O$ | $C_{33}H_{50}B_2CoF_4N_7O_2$ | $C_{108}H_{152}B_8Co_4F_{16}Li_4N_{24}O_4$ |
| Formula weight | 533.38 | 733.35 | 2504.49 |
| Temperature/K | 100(2) | 100(2) | 100(2) |
| Crystal system | monoclinic | monoclinic | triclinic |
| Space group | $P2_1/n$ | Pc | P-1 |
| a/Å | 9.6707(4) | 13.223(2) | 18.430(2) |
| b/Å | 17.7011(6) | 13.700(3) | 21.294(3) |
| c/Å | 16.2742(6) | 20.789(4) | 24.547(3) |
| α/° | 90 | 90 | 108.217(2) |
| β/° | 92.0150(10) | 100.227(3) | 94.643(2) |
| γ/° | 90 | 90 | 115.486(2) |
| Volume/Å$^3$ | 2784.13(18) | 3706.2(12) | 7994.9(16) |
| Z | 4 | 4 | 2 |

**Table A1.6, continued**

| | | | |
|---|---|---|---|
| $\rho_{calc}$g/cm$^3$ | 1.272 | 1.314 | 1.040 |
| μ/mm$^{-1}$ | 0.647 | 0.128 | 0.113 |
| F(000) | 1132.0 | 1544.0 | 2608.0 |
| Crystal size/mm$^3$ | 0.335×0.192×0.172 | 0.003 × 0.002 × 0.002 | 0.003 × 0.003 × 0.002 |
| Radiation | MoKα (λ = 0.71073) | synchrotron (λ = 0.41328) | synchrotron (λ = 0.41328) |
| 2Θ range for data collection/° | 4.802 to 55.108 | 1.728 to 23.778 | 1.862 to 30.408 |
| Index ranges | -12 ≤ h ≤ 12, -22 ≤ k ≤ 23, -21 ≤ l ≤ 21 | -13 ≤ h ≤ 13, -13 ≤ k ≤ 13, -20 ≤ l ≤ 20 | -22 ≤ h ≤ 22, -26 ≤ k ≤ 26, -31 ≤ l ≤ 30 |
| Reflections collected | 34187 | 46054 | 176440 |
| Independent reflections | 6420 [$R_{int}$ = 0.0334, $R_{sigma}$ = 0.0269] | 7683 [$R_{int}$ = 0.1336, $R_{sigma}$ = 0.0829] | 31689 [$R_{int}$ = 0.0640, $R_{sigma}$ = 0.0490] |
| Data/restraints/parameters | 6420/0/358 | 7683/2/905 | 31689/0/1549 |
| Goodness-of-fit on $F^2$ | 1.031 | 1.039 | 1.065 |
| Final R indexes [I>=2σ (I)] | $R_1$ = 0.0345, $wR_2$ = 0.0808 | $R_1$ = 0.0474, $wR_2$ = 0.0883 | $R_1$ = 0.0654, $wR_2$ = 0.1905 |
| Final R indexes [all data] | $R_1$ = 0.0466, $wR_2$ = 0.0862 | $R_1$ = 0.0722, $wR_2$ = 0.0979 | $R_1$ = 0.0948, $wR_2$ = 0.2107 |
| Largest diff. peak/hole / e Å$^{-3}$ | 0.42/-0.38 | 0.22/-0.28 | 0.95/-0.73 |
| Flack parameter | N/A | 0.5 | N/A |

| Compound | **4** | **5** | **6** |
|---|---|---|---|
| Empirical formula | $C_{27}H_{38}BCoN_6O$ | $C_{52}H_{64}BClCoN_6$ | $C_{52}H_{65}BCoN_6O$ |
| Formula weight | 532.37 | 878.28 | 859.84 |
| Temperature/K | 100(2) | 100(2) | 100(2) |
| Crystal system | hexagonal | monoclinic | monoclinic |
| Space group | P6cc | $P2_1/n$ | $P2_1/n$ |
| a/Å | 36.640(6) | 14.2592(9) | 12.272(4) |
| b/Å | 36.640(6) | 17.7464(11) | 12.944(4) |
| c/Å | 10.1573(15) | 17.2825(11) | 28.083(10) |
| α/° | 90 | 90 | 90 |
| β/° | 90 | 97.574(2) | 99.115(6) |
| γ/° | 120 | 90 | 90 |
| Volume/Å$^3$ | 11809(4) | 4335.2(5) | 4405(3) |
| Z | 12 | 4 | 4 |
| $\rho_{calc}$g/cm$^3$ | 0.898 | 1.346 | 1.297 |
| μ/mm$^{-1}$ | 0.109 | 0.503 | 0.436 |
| F(000) | 3384.0 | 1868.0 | 1836.0 |

**Table A1.6, continued**

| | | | |
|---|---|---|---|
| Crystal size/mm$^3$ | 0.003× 0.002 × 0.002 | 0.196 × 0.109 × 0.05 | 0.2 × 0.15 × 0.1 |
| Radiation | synchrotron (λ = 0.41328) | MoKα (λ = 0.71073) | MoKα (λ = 0.71073) |
| 2Θ range for data collection/° | 2.69 to 23.864 | 4.174 to 48.384 | 4.604 to 51.362 |
| Index ranges | -36 ≤ h ≤ 36, -36 ≤ k ≤ 36, -9 ≤ l ≤ 9 | -16 ≤ h ≤ 16, -20 ≤ k ≤ 20, -19 ≤ l ≤ 19 | -14 ≤ h ≤ 14, -15 ≤ k ≤ 15, -34 ≤ l ≤ 34 |
| Reflections collected | 147121 | 46719 | 62681 |
| Independent reflections | 4042 [$R_{int}$ = 0.1872, $R_{sigma}$ = 0.0377] | 6884 [$R_{int}$ = 0.1268, $R_{sigma}$ = 0.0879] | 8323 [$R_{int}$ = 0.1229, $R_{sigma}$ = 0.0659] |
| Data/restraints/parameters | 4042/162/331 | 6884/0/551 | 8323/2/555 |
| Goodness-of-fit on $F^2$ | 1.020 | 1.027 | 1.089 |
| Final R indexes [I>=2σ (I)] | $R_1$ = 0.0448, $wR_2$ = 0.1166 | $R_1$ = 0.0554, $wR_2$ = 0.1073 | $R_1$ = 0.0892, $wR_2$ = 0.2205 |
| Final R indexes [all data] | $R_1$ = 0.0557, $wR_2$ = 0.1236 | $R_1$ = 0.1098, $wR_2$ = 0.1241 | $R_1$ = 0.1215, $wR_2$ = 0.2414 |
| Largest diff. peak/hole / e Å$^{-3}$ | 0.39/-0.29 | 0.51/-0.44 | 1.00/-0.59 |
| Flack parameter | 0.5 | N/A | N/A |

| Compound | **7** | **8** |
|---|---|---|
| Empirical formula | $C_{49}H_{67}B_2CoF_4N_6O_2$ | $C_{45}H_{56}BCl_{0.25}CoN_6O$ |
| Formula weight | 928.69 | 775.56 |
| Temperature/K | 100(2) | 99.99 |
| Crystal system | monoclinic | monoclinic |
| Space group | $P2_1/n$ | $P2_1/n$ |
| a/Å | 12.244(3) | 19.7541(15) |
| b/Å | 14.169(4) | 11.7092(8) |
| c/Å | 26.513(7) | 21.8979(16) |
| α/° | 90 | 90 |
| β/° | 95.082(5) | 108.521(2) |
| γ/° | 90 | 90 |
| Volume/Å$^3$ | 4582(2) | 4802.8(6) |
| Z | 4 | 4 |
| $\rho_{calc}$g/cm$^3$ | 1.3462 | 1.073 |
| μ/mm$^{-1}$ | 0.304 | 0.407 |
| F(000) | 1969.7 | 1649.0 |
| Crystal size/mm$^3$ | 0.2 × 0.1 × 0.1 | 0.187 × 0.063 × 0.015 |
| Radiation | synchrotron (λ = 0.61992) | MoKα (λ = 0.71073) |

**Table A1.6, continued**

| | | |
|---|---|---|
| 2Θ range for data collection/° | 2.7 to 48.48 | 4.238 to 44.094 |
| Index ranges | $-14 \leq h \leq 14$, $0 \leq k \leq 17$, $0 \leq l \leq 28$ | $-20 \leq h \leq 20$, $-12 \leq k \leq 12$, $-23 \leq l \leq 23$ |
| Reflections collected | 8014 | 53576 |
| Independent reflections | 8011 [$R_{int}$ = 0.0000, $R_{sigma}$ = 0.0485] | 5906 [$R_{int}$ = 0.1369, $R_{sigma}$ = 0.0685] |
| Data/restraints/parameters | 8011/3/587 | 5906/0/487 |
| Goodness-of-fit on $F^2$ | 1.150 | 1.073 |
| Final R indexes [I>=2σ (I)] | $R_1$ = 0.1146, $wR_2$ = 0.3002 | $R_1$ = 0.0643, $wR_2$ = 0.1514 |
| Final R indexes [all data] | $R_1$ = 0.1310, $wR_2$ = 0.3058 | $R_1$ = 0.0929, $wR_2$ = 0.1637 |
| Largest diff. peak/hole / e $Å^{-3}$ | 1.75/-0.96 | 1.95/-0.30 |
| Flack parameter | N/A | N/A |

| | Complex **1** | Complex **2** | Complex **3** | Complex **4** |
|---|---|---|---|---|
| **Bond Lengths (Å)** | | | | |
| Co1–Cl1 | 2.245(1) | | | |
| Co1–O1 | | 1.827(5) | 1.875(6) | 1.655(4) |
| Co–$C_{avg}$ | 2.041 | 2.006 | 1.902 | 1.913 |
| **Bond Angles (°)** | | | | |
| B1–Co1–Cl1 | 179.0(9) | | | |
| B1–Co1–O1 | | 173.0(2) | 141.7(3) | 177.0(1) |
| C1–Co1–C4 | 95.6(2) | 92.7(2) | 96.9(4) | 87.0(2) |
| C4–Co1–C7 | 90.9(2) | 90.6(2) | 81.6(3) | 88.5(2) |
| C7–Co1–C1 | 95.3(2) | 90.4(2) | 87.2(4) | 88.6(2) |

**Table A1.7.** Selected bond lengths and angles for complexes **5**-**8**.

## A1.9 Density Functional Theory Calculations

| Species | Free Energy (Hartrees) | Free Energy (kcal/mol) |
|---|---|---|
| **1** | 0 | 0 |
| **4** (straight) | 0.643 (0.640) | 403 (401) |
| H | 0.508 | 319 |
| Difference (BDFE) | 0.135 | 85 |

**Table A1.8.** Computed free energies used for the determination of the $BDFE_{OH}$ of **1**. Note that "straight" indicates the energy of a geometry optimization with a constrained B–Co–O angle of 175°.

**Table A1.9.** Coordinates for the optimized structure of **8** ($S = 0$).

| | | | |
|---|---|---|---|
| Co | 0.03725098540100 | -0.00115732408001 | 0.00950771938706 |
| O | 0.69334699334279 | 0.01341845347968 | 1.52428818436862 |
| C | 0.78344010579972 | -1.33936616270509 | -1.08893752710622 |
| N | 1.35871311956813 | -2.55312664673451 | -0.82809299651631 |
| C | 1.70294561706899 | -3.15722632346845 | 0.48348198772896 |
| C | 2.75635145696057 | -2.29935728786411 | 1.19083864474046 |
| H | 3.64575496619706 | -2.23473464034920 | 0.55352386768597 |
| H | 2.35309744759194 | -1.29512671091018 | 1.32803694969451 |
| C | 0.45537275700591 | -3.28299443034442 | 1.36090973556934 |
| H | 0.01932154851151 | -2.28568347678821 | 1.50551888319993 |
| H | -0.29076754046511 | -3.91356316876063 | 0.84518155396910 |
| C | 2.28973935262478 | -4.56229623151310 | 0.29100236851527 |
| H | 1.56334057595103 | -5.21336345577288 | -0.22568566047098 |
| H | 3.20082532630307 | -4.51541524489680 | -0.32900617523943 |

**Table A1.9, continued**

| | | | |
|---|---|---|---|
| C | 3.11251193117859 | -2.91177513049111 | 2.54360090522020 |
| H | 3.85740549436368 | -2.26412303177567 | 3.03658848190769 |
| C | 0.82110232539034 | -3.88761913209152 | 2.71558705384152 |
| H | -0.09173899050845 | -3.94704780707865 | 3.33422482561078 |
| C | 2.64983129253712 | -5.17919843914293 | 1.64363894895372 |
| H | 3.06532790268020 | -6.18551084845251 | 1.46216168716410 |
| C | 3.69109897233926 | -4.30901564120897 | 2.34294308514234 |
| H | 4.61404384437907 | -4.25922184183532 | 1.73725595340146 |
| H | 3.96465639966831 | -4.75579287984027 | 3.31587932139573 |
| C | 1.85528632013599 | -3.00058085551845 | 3.40826474918877 |
| H | 1.43841347937622 | -1.99276828021908 | 3.57496010579046 |
| H | 2.10737905098317 | -3.42022222647694 | 4.39907243025103 |
| C | 1.39950353312626 | -5.28475485339828 | 2.51226599378600 |
| H | 0.65328121001789 | -5.94024990556307 | 2.02795625301512 |
| H | 1.65208497468777 | -5.74232198145507 | 3.48564065068197 |
| C | 1.62896520341734 | -3.18362537785180 | -2.02667463746162 |
| H | 2.07816355667911 | -4.16645154576976 | -2.09426514800062 |
| C | 1.23603821316286 | -2.35216152612194 | -3.02099487559285 |
| H | 1.26029402776694 | -2.49967813471548 | -4.09609818482534 |
| N | 0.74277776605517 | -1.22078229803187 | -2.43220915290415 |
| C | -1.51678154948339 | -0.08678018302011 | -1.14741024839392 |
| N | -2.83888732969052 | -0.26484815303100 | -0.86641051614052 |
| C | -3.44937249046463 | -0.24501567315972 | 0.47531892378875 |
| C | -3.13931103832076 | 1.08969841734588 | 1.16079329264788 |
| H | -2.04630111798253 | 1.22039768046139 | 1.21671096495343 |
| H | -3.53918484883551 | 1.91526485639879 | 0.54617919012701 |
| C | -4.97139782074917 | -0.40141929891618 | 0.38999837826090 |

**Table A1.9, continued**

| | | | |
|---|---|---|---|
| H | -5.40211553135946 | 0.41090055304897 | -0.22046057060968 |
| H | -5.22801989995020 | -1.35824764678798 | -0.09617100538330 |
| C | -2.89617763845036 | -1.39328897276853 | 1.32380602804836 |
| H | -3.12010489283574 | -2.35393302447606 | 0.82734200980845 |
| H | -1.79941996883345 | -1.30062383209477 | 1.38006756673571 |
| C | -3.74424960304085 | 1.12115648296080 | 2.56287664833610 |
| H | -3.49619752362610 | 2.08746154542351 | 3.03555540716060 |
| C | -5.58239632888449 | -0.36745763817942 | 1.79192567877735 |
| H | -6.67583714504635 | -0.48146218552271 | 1.69617926329914 |
| C | -3.50020234706479 | -1.35764002846212 | 2.72660590071870 |
| H | -3.07443136395514 | -2.18734904226304 | 3.31744860587190 |
| C | -3.16426087539705 | -0.02368975050279 | 3.39326484198801 |
| H | -2.06961878279035 | 0.09032020444289 | 3.48580797423520 |
| H | -3.58075000935628 | 0.00248706092823 | 4.41618011965026 |
| C | -5.25981474198032 | 0.96631358792933 | 2.46217596257983 |
| H | -5.68863795741649 | 1.79952921767104 | 1.87681695421441 |
| H | -5.71707170131554 | 1.00503763049858 | 3.46708347752742 |
| C | -5.01583890790299 | -1.51343775093755 | 2.62797161914475 |
| H | -5.26911575219660 | -2.48422518514795 | 2.16504122709499 |
| H | -5.46836544662476 | -1.50601973314722 | 3.63576633127127 |
| C | -3.53748781315738 | -0.44477702462438 | -2.04331661972723 |
| H | -4.60750441691601 | -0.61440703865737 | -2.08185150147462 |
| C | -2.63726075047149 | -0.35953595084433 | -3.05580099932420 |
| H | -2.79160873473794 | -0.47553707090833 | -4.12412020566072 |
| N | -1.41435247388119 | -0.11203406011709 | -2.48953649597876 |
| C | 0.65340454788606 | 1.39833684509562 | -1.05647206994319 |
| N | 1.19730569133336 | 2.62586709465155 | -0.80004003297551 |

**Table A1.9, continued**

| | | | |
|---|---|---|---|
| C | 1.45105625218458 | 3.27024563278188 | 0.51199220923032 |
| C | 1.90727871637209 | 4.72297728997350 | 0.31613377140247 |
| H | 2.84210302090814 | 4.75594287304137 | -0.26818457080153 |
| H | 1.14156352709361 | 5.29075486193519 | -0.24088139448657 |
| C | 0.16811576179168 | 3.28871805078694 | 1.34852822709023 |
| H | -0.61570241106739 | 3.83859477634592 | 0.79782582280538 |
| H | -0.17736099993236 | 2.25519507606298 | 1.48989212842921 |
| C | 2.55721367659881 | 2.52252515722858 | 1.26606977546726 |
| H | 2.24413828348636 | 1.47442763017697 | 1.40506059843644 |
| H | 3.47905850285511 | 2.53599786923704 | 0.65674189296368 |
| C | 2.15811651610716 | 5.38984791144778 | 1.67017242118936 |
| H | 2.48137564369281 | 6.42925365499408 | 1.48749772884436 |
| C | 0.42670586748700 | 3.94208611947802 | 2.70547672568632 |
| H | -0.50869597301474 | 3.92020820590773 | 3.29176099935805 |
| C | 2.80580412932660 | 3.18643423604460 | 2.62117716735965 |
| H | 3.59309776003529 | 2.62350155147850 | 3.15245264040068 |
| C | 3.25427244500521 | 4.63074046118856 | 2.41436798231904 |
| H | 4.19534958371422 | 4.65819542303169 | 1.83569729536470 |
| H | 3.45716627904610 | 5.11410694503582 | 3.38715287090563 |
| C | 0.87590782461680 | 5.38549788599819 | 2.49793565550029 |
| H | 0.08628397234629 | 5.96092995047907 | 1.98151333135755 |
| H | 1.05187496362486 | 5.87804830768752 | 3.47124440737403 |
| C | 1.51764133366725 | 3.16700179372368 | 3.44484651496567 |
| H | 1.19387131540075 | 2.12572429000069 | 3.61535900502018 |
| H | 1.69663138838890 | 3.62120863862338 | 4.43630361930111 |
| C | 1.52100928597298 | 3.22552616903293 | -2.00317472101261 |
| H | 1.96989357060989 | 4.20854288884312 | -2.07397484610966 |

**Table A1.9, continued**

| | | | |
|---|---|---|---|
| C | 1.17272802428821 | 2.36753445232245 | -2.99168731725915 |
| H | 1.26044428874614 | 2.46621656497520 | -4.06972937426719 |
| N | 0.63988532858218 | 1.25864515717333 | -2.39281114941738 |
| B | 0.02358335499872 | 0.00378353467983 | -3.06861327970346 |
| C | 0.16509527828945 | 0.15162514166761 | -4.66729441107366 |
| C | -0.81519593719197 | 0.78317512363867 | -5.44993057567921 |
| H | -1.74076618989841 | 1.13576148175631 | -4.98807054917650 |
| C | -0.64150239965425 | 1.01759142555806 | -6.81345966054558 |
| H | -1.43566894118741 | 1.50921400931157 | -7.38451353606892 |
| C | 0.54035890814552 | 0.63865544636171 | -7.44382385994554 |
| H | 0.68113554453394 | 0.81827286409963 | -8.51433150004261 |
| C | 1.54956938654340 | 0.04780012554010 | -6.68785525119482 |
| H | 2.49734779530386 | -0.23135582349966 | -7.15933051758918 |
| C | 1.36152411869805 | -0.18040893370745 | -5.32580249986038 |
| H | 2.19310854768475 | -0.61096176598446 | -4.76069585925904 |

**Table A1.10.** Coordinates for the optimized structure of **4** ($S = 0$) used to determine the values shown in Table 2.1.

| | | | |
|---|---|---|---|
| Co | 0.00644078512716 | -0.00204159186536 | 0.00789777150338 |
| O | 0.64258093742352 | -0.00200068026939 | 1.53094974479593 |
| C | 0.76249795310311 | -1.33115002322487 | -1.08852478337605 |
| N | 1.34793902272660 | -2.53717061909516 | -0.82114405027858 |
| C | 1.72634831110565 | -3.11556007092061 | 0.50037454106992 |
| C | 2.78676103453187 | -2.22311985256165 | 1.13469385249890 |
| H | 3.65835058946329 | -2.14506503637074 | 0.47945976115947 |
| H | 2.37916182011111 | -1.23153900417722 | 1.32823079131832 |
| H | 3.11183267535140 | -2.65818545590832 | 2.08254611366548 |

**Table A1.10, continued**

| | | | |
|---|---|---|---|
| C | 0.49264111570350 | -3.23763920479725 | 1.38615984786763 |
| H | 0.07440871335819 | -2.24719022731286 | 1.60886303172988 |
| H | -0.27685462649602 | -3.86051713756895 | 0.89953005782748 |
| H | 0.77316899477527 | -3.71558271147697 | 2.33874010778703 |
| C | 2.31536883455228 | -4.51047171663255 | 0.31035426698261 |
| H | 1.60151353871478 | -5.20749090510501 | -0.15881187957811 |
| H | 3.24818901785414 | -4.50023109627913 | -0.27598469849479 |
| H | 2.56126328221615 | -4.90888444756877 | 1.30693405896067 |
| C | 1.62098955389888 | -3.17414167870617 | -2.01470489554751 |
| H | 2.07740967840122 | -4.15444199592720 | -2.07502756622902 |
| C | 1.22033168006374 | -2.35227352309628 | -3.01445017812844 |
| H | 1.24366259848564 | -2.50684656607901 | -4.08863785575990 |
| N | 0.71960192193454 | -1.22049172874324 | -2.43252710839018 |
| C | -1.54198622877860 | -0.08293171524977 | -1.15794505157203 |
| N | -2.86484916942506 | -0.25574272106949 | -0.88057153905661 |
| C | -3.48133141560853 | -0.24541259293766 | 0.46860930996347 |
| C | -3.15355288061725 | 1.08135454511512 | 1.14579272571835 |
| H | -2.06529442937770 | 1.20768036185671 | 1.25673504223358 |
| H | -3.54639433609039 | 1.92731812083948 | 0.55759609377702 |
| H | -3.60627444476110 | 1.11194123451136 | 2.15013455874356 |
| C | -4.99533257590333 | -0.38271347107204 | 0.35613073272002 |
| H | -5.44347476000887 | 0.44175865541982 | -0.22230593606639 |
| H | -5.29251821789650 | -1.34177065644303 | -0.09857214384140 |
| H | -5.42300058452270 | -0.35043481189384 | 1.37075612839934 |
| C | -2.93342995969999 | -1.41793096640069 | 1.27398321081073 |
| H | -3.16255608996702 | -2.37530279321232 | 0.77709014927802 |
| H | -1.84160886294960 | -1.33374056078112 | 1.38835666751504 |

**Table A1.10, continued**

| | | | |
|---|---|---|---|
| H | -3.38441881140820 | -1.42779583864430 | 2.27959059004051 |
| C | -3.56064942045467 | -0.43338453882445 | -2.05926108238557 |
| H | -4.63119340922639 | -0.59934830087663 | -2.10120402000533 |
| C | -2.65755351061715 | -0.35102025942487 | -3.06961228873310 |
| H | -2.80966882375056 | -0.46586408724577 | -4.13841276516076 |
| N | -1.43539198833494 | -0.10818087350122 | -2.49979902518127 |
| C | 0.63260943888081 | 1.39277009477608 | -1.05780435129333 |
| N | 1.18501955731242 | 2.61358235489085 | -0.79575523613044 |
| C | 1.46675479177423 | 3.23664001905176 | 0.52868368092340 |
| C | 1.92686588486920 | 4.67997564984326 | 0.33806763693552 |
| H | 2.88652035196176 | 4.74943153843649 | -0.19906202846842 |
| H | 1.17469541024078 | 5.29169557857071 | -0.18729336239527 |
| H | 2.07841507082972 | 5.12108116934699 | 1.33576696648781 |
| C | 0.19228010145675 | 3.25011233955334 | 1.36502889836768 |
| H | -0.60492956443944 | 3.81568986385983 | 0.85392461349733 |
| H | -0.15378572471838 | 2.22560409910614 | 1.55897279895969 |
| H | 0.39554119399879 | 3.73544928892327 | 2.33348063802292 |
| C | 2.58028871048211 | 2.45039923424969 | 1.21545109834494 |
| H | 2.25540197214714 | 1.41330384507290 | 1.40033662364525 |
| H | 3.49078842220086 | 2.45076419628960 | 0.59211200524725 |
| H | 2.82394078590733 | 2.92297334208527 | 2.18180559633217 |
| C | 1.51558160311598 | 3.21680086370315 | -1.99467552549559 |
| H | 1.97273130608255 | 4.19688840313186 | -2.05836594557627 |
| C | 1.16166192485648 | 2.36600649398042 | -2.98811134955776 |
| H | 1.25069316505681 | 2.46911522098409 | -4.06572105570409 |
| N | 0.61968429111748 | 1.25805414950591 | -2.39479144007553 |
| B | 0.00420240758912 | 0.00434320455185 | -3.07381982575226 |

**Table A1.10, continued**

| | | | |
|---|---|---|---|
| C | 0.15542997352629 | 0.14940442684919 | -4.67178265721636 |
| C | -0.81987786308625 | 0.77717498967504 | -5.46357891082475 |
| H | -1.74935697629698 | 1.13010605197132 | -5.00991433819947 |
| C | -0.63637832144055 | 1.00715484677383 | -6.82661988516192 |
| H | -1.42694044383397 | 1.49576681188027 | -7.40520220896889 |
| C | 0.55049952972845 | 0.62751768015224 | -7.44704925335578 |
| H | 0.69887172848249 | 0.80362531988728 | -8.51711544497856 |
| C | 1.55486222116033 | 0.04038274151211 | -6.68178059402045 |
| H | 2.50639527544121 | -0.23926099551863 | -7.14534990229526 |
| C | 1.35700894987246 | -0.18358254102972 | -5.32044638786170 |
| H | 2.18474731271658 | -0.61170373854494 | -4.74787314201313 |

# Appendix 2: Supporting Data for Chapter 3

## A2.1 Derivation of expression used to estimate $k_{et}$

The overall reaction is shown in Equation A2.1, where L = $PhB(^tBuIm)_3^-$. This gives the overall rate law shown in Equation A2.2 where $k_2$ is the experimentally measured second order rate constant.

Equation A2.1 $$LCo^{III}O + RH \xrightarrow{k_2} LCo^{II}OH + R^{\cdot}$$

Equation A2.2 $$\text{Rate} = k_2[LCo^{III}O][RH]$$

Equation A2.3 shows the reactions associated with a stepwise mechanism assuming steady state kinetics with a pre-equilibrium proton transfer followed by electron transfer.

Equation A2.3 $$LCo^{III}O + RH \underset{k_{-1}}{\overset{k_1}{\rightleftharpoons}} LCo^{III}OH^+ + R^- \xrightarrow{k_{et}} LCo^{II}OH + R^{\cdot}$$

In this scenario, the rate law is shown in Equation A2.4.

Equation A2.4 $$\text{Rate} = \frac{k_1 k_{et}}{k_{-1}+k_{et}}[LCo^{III}O][RH]$$

We know that $k_{-1}$ must be much larger than $k_1$ due to the p$K_a$ difference between **3** and the substrates. Additionally, we do not spectroscopically observe **2** as an intermediate. This leads to two limiting scenarios: $k_{et} >> k_1, k_{-1}$ or $k_{-1} >> k_1, k_{et}$. For the scenario $k_{et} >> k_1, k_{-1}$, the rate law simplifies to Equation A2.5.

Equation A2.5 $$\text{Rate} = k_1[LCo^{III}O][RH]$$

If this were the case, then $k_1$ must be equal to the $k_2$ value we experimentally determined (~$10^{-1}$ $M^{-1}s^{-1}$ for fluorene). This requires that $k_{-1}$ ~ $10^6$ $M^{-1}s^{-1}$ since $K_{eq}$ ~ $10^7$ from experimentally determined p$K_a$ values for **3** and fluorene. For the assumption that $k_{et}$ >> $k_1$, $k_{-1}$ to hold, $k_{et}$ must therefore be much greater than $10^6$ $M^{-1}s^{-1}$. However, we have determined the upper limit of this value to be ~$10^3$ $M^{-1}s^{-1}$ (without any additional driving force), making this scenario likely not possible.

For the scenario $k_{-1}$ >> $k_1$, $k_{et}$, the rate law (Equation A2.4) simplifies to Equation A2.6.

Equation A2.6 $$\text{Rate} = k_{et}K_{eq}[\text{LCo}^{\text{III}}\text{O}][\text{RH}]$$

Finally, setting Equation A2.6 equal to Equation A2.2 gives the relationship between $k_{et}$, $k_2$, and $K_{eq}$ shown in Equation A2.7.

Equation A2.7 $$k_2 = k_{et}K_{eq}$$

Knowing $K_{eq}$ ~ $10^7$ for **3** and fluorene, $k_{et}$ would have to be ~$10^6$ $M^{-1}s^{-1}$ which is again likely inconsistent with our experimentally measured $k_{et}$ value. This analysis supports a concerted mechanism as shown in Equation A2.1.

## A2.2 Electrochemistry

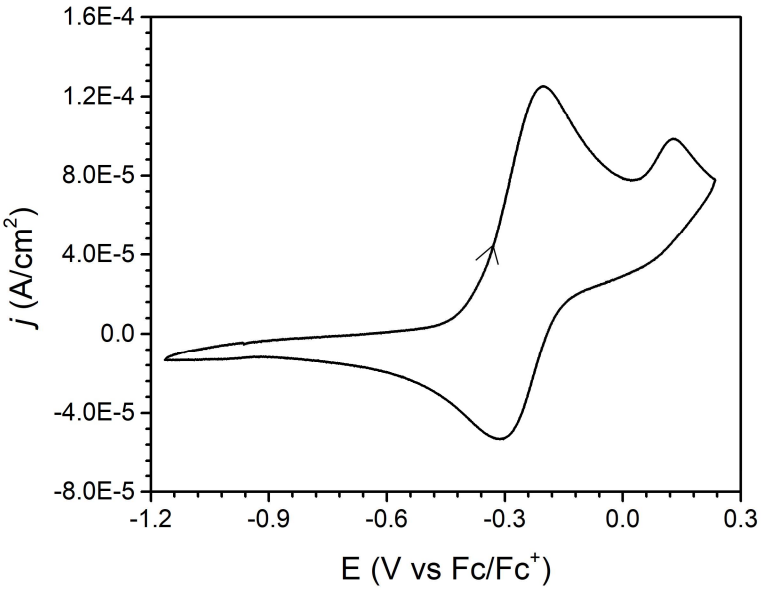


**Figure A2.1.** Cyclic voltammogram of **1** in acetonitrile (0.1 M $TBAPF_6$ as the electrolyte) at room temperature. Working electrode: glassy carbon. Counter electrode: platinum wire. Reference electrode: silver wire referenced externally to $Fc/Fc^+$. Scan rate: 10 mV/s. The arrow indicates the initial scanning direction.

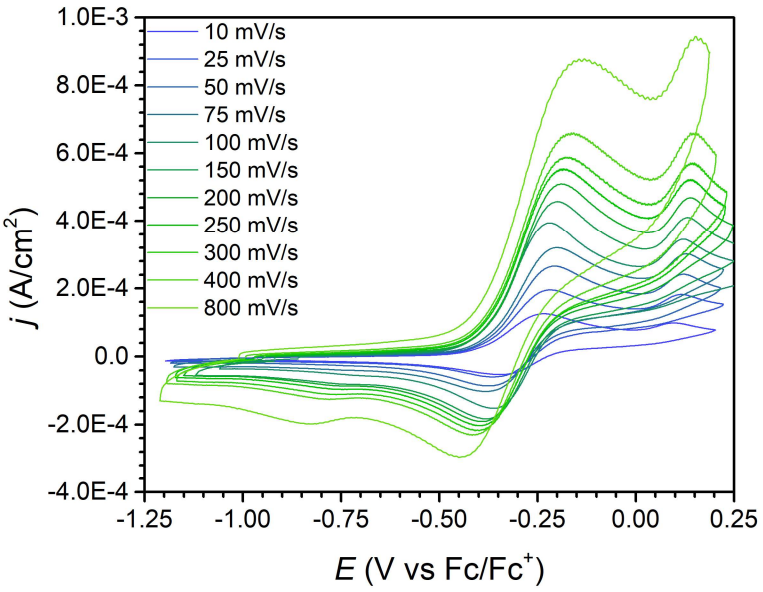


**Figure A2.2.** Overlay of cyclic voltammograms of **1** (3 mM in MeCN, 0.1 M $TBAPF_6$) collected at various scan rates.

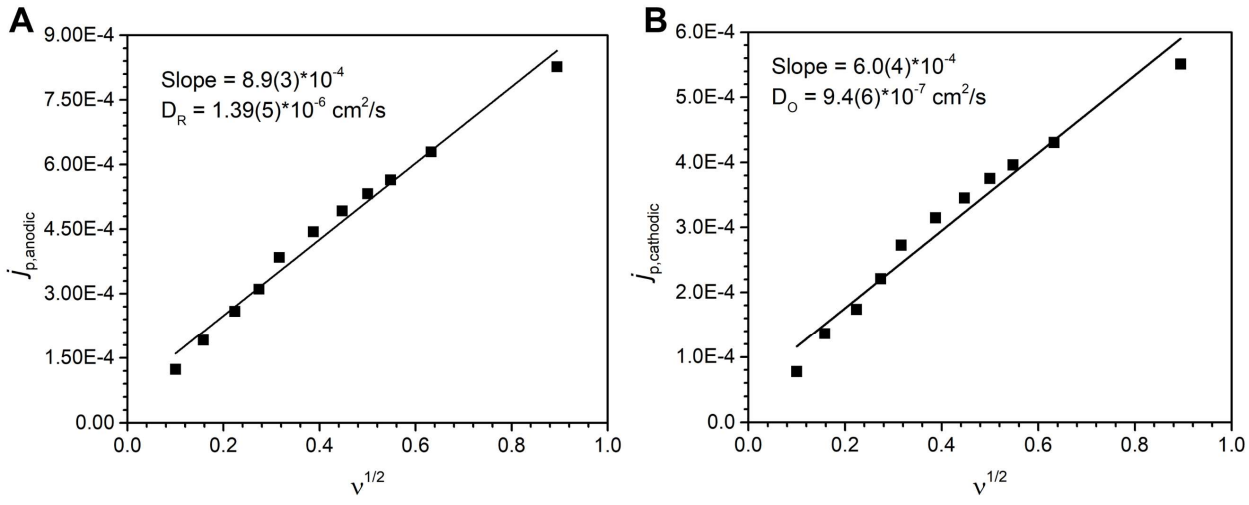


**Figure A2.3.** Plots of (A) anodic peak current density and (B) cathodic peak current density versus the square roots of the scan rates from the CVs in Figure A2.2. $R^2$ = 0.98 (A), 0.96 (B).

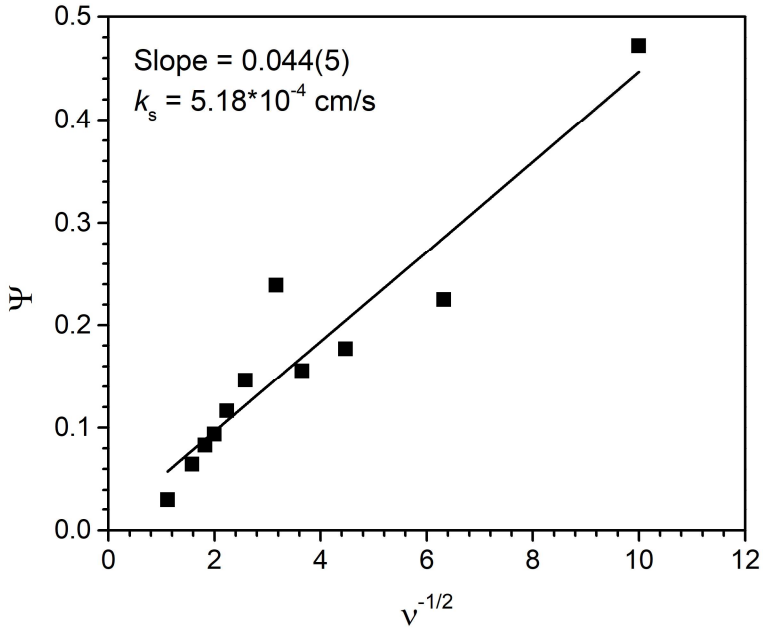


**Figure A2.4.** Plot of the dimensionless parameter Ψ (determined from $\Delta E_p$ at each scan rate in Figure A2.3) versus the inverse of the square roots of the scan rates. $R^2 = 0.88$.

## A2.3 Kinetic Measurements

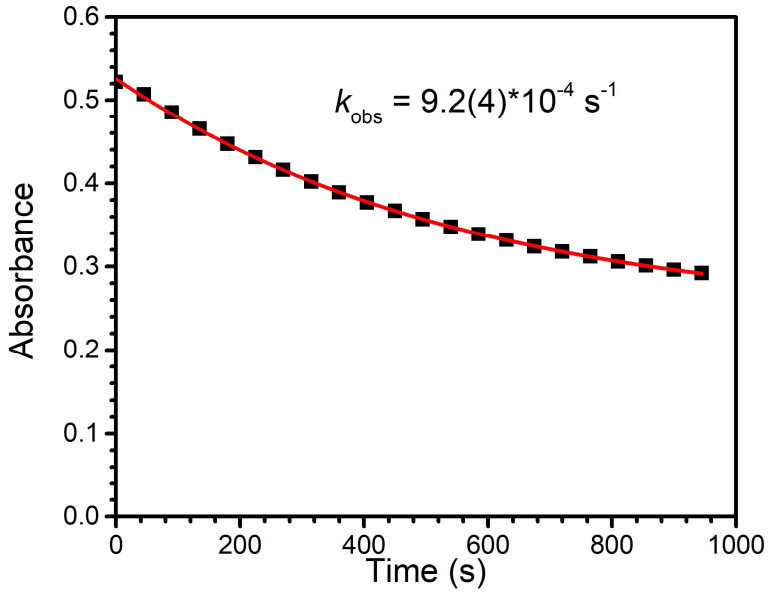


**Figure A2.5.** Representative exponential fit of a plot of A versus time for the reaction between **3** and 10 equivalents of DHA. The average *k* obtained from three trials was taken to be the observed rate constant, $k_{obs}$, for this reaction.

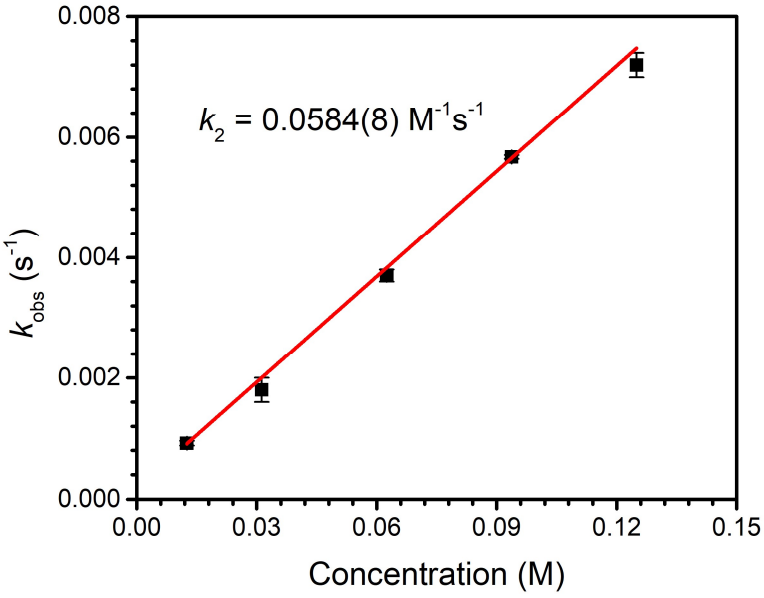


**Figure A2.6.** Plot of $k_{obs}$ versus [DHA] for the reaction between **3** and DHA. The slope of the linear fit is the second order rate constant, $k_2$. $R^2$ = 0.999.

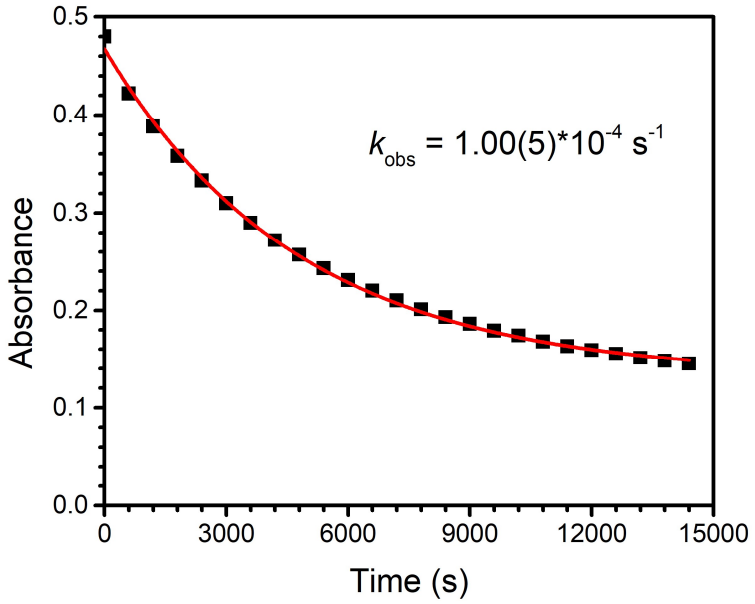


**Figure A2.7.** Representative exponential fit of a plot of A versus time for the reaction between **3** and 10 equivalents of DHA-$d_4$. The average $k$ obtained from three trials was taken to be the observed rate constant, $k_{obs}$, for this reaction at various concentrations.

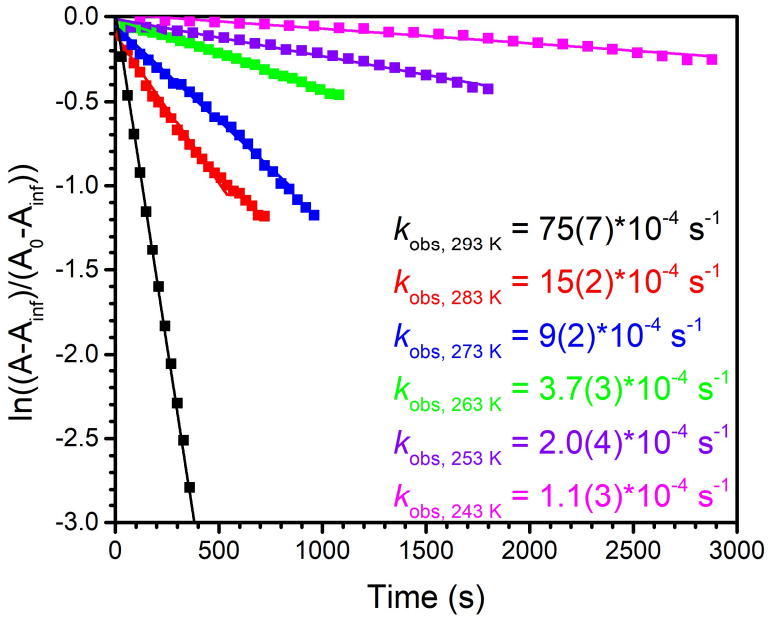


**Figure A2.8.** Representative plots of ln(A-A$_{inf}$/A$_0$-A$_{inf}$) versus time for the reaction between **3** and 50 equivalents of DHA at 293, 283, 273, 263, 253, or 243 K. The slopes of the linear fits of the data were taken to be the rate constants, $k$, at that temperature and the average obtained from

three trials was taken to be the observed rate constant, $k_{obs}$, for these reactions. Black: 293 K. Red: 283 K. Blue: 273 K. Green: 263 K. Purple: 253 K. Pink: 243 K.

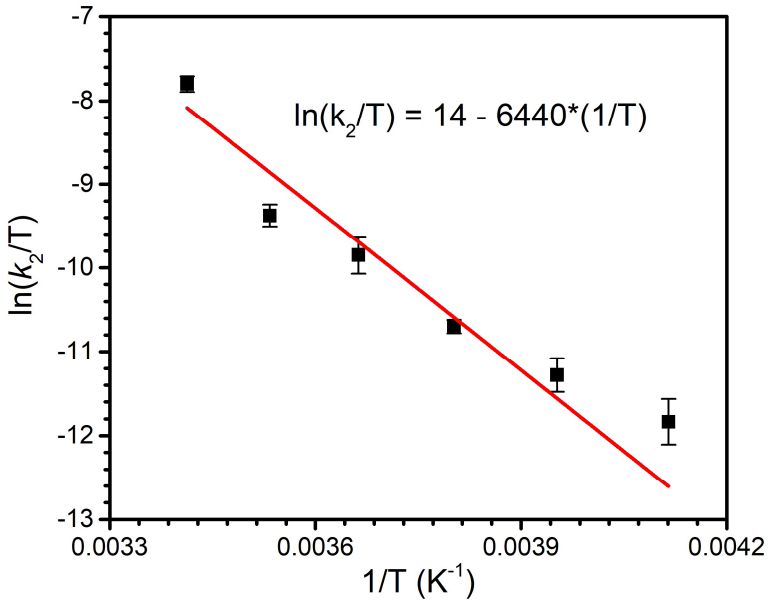


**Figure A2.9.** Plot of ln($k_2$/T) versus 1/T (where $k_2$ = second order rate constant, T = temperature in Kelvin) for the reaction of **3** with DHA. The shown linear fit was used to calculate the activation parameters listed in Table 3.1 of Chapter 3 via the Eyring equation ($R^2$ = 0.93).

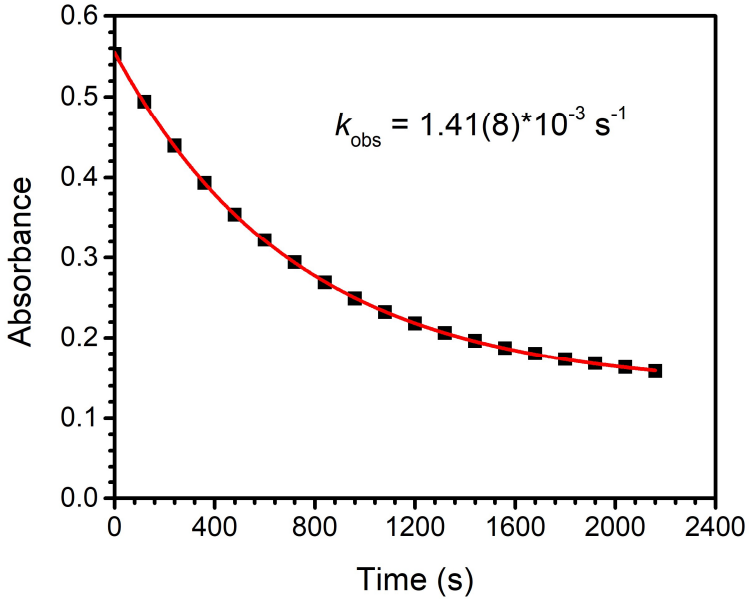


**Figure A2.10.** Representative exponential fit of a plot of A versus time for the reaction between **3** and 10 equivalents of xanthene. The average *k* obtained from three trials was taken to be the observed rate constant, $k_{obs}$, for this reaction.

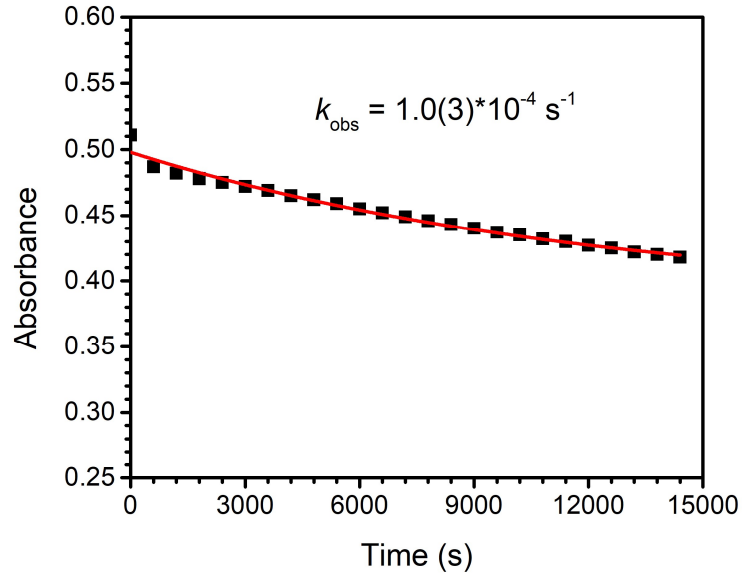


**Figure A2.11.** Representative exponential fit of a plot of A versus time for the reaction between **3** and 10 equivalents of 1,1,3,3-tetraphenylpropene. The average *k* obtained from three trials was taken to be the observed rate constant, $k_{obs}$, for this reaction.

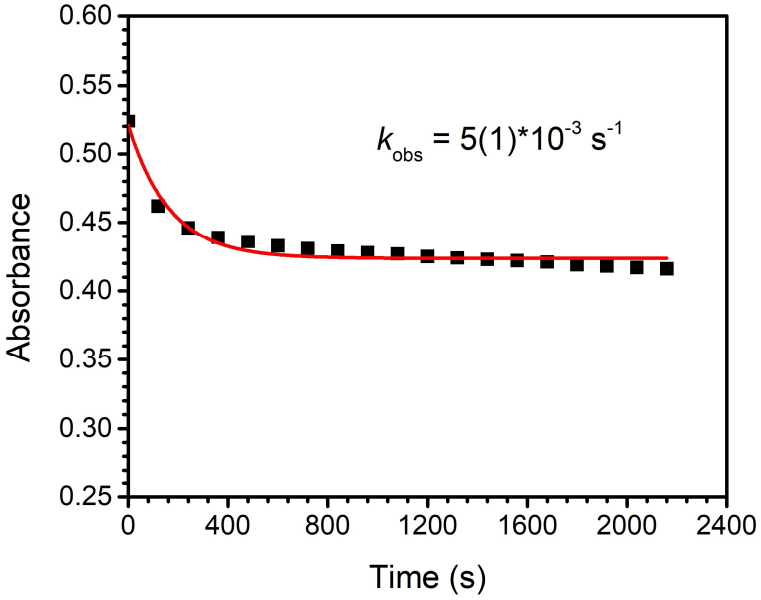


**Figure A2.12.** Representative exponential fit of a plot of A versus time for the reaction between **3** and 100 equivalents of diphenylmethane. The average *k* obtained from three trials was taken to be the observed rate constant, $k_{obs}$, for this reaction at various concentrations.

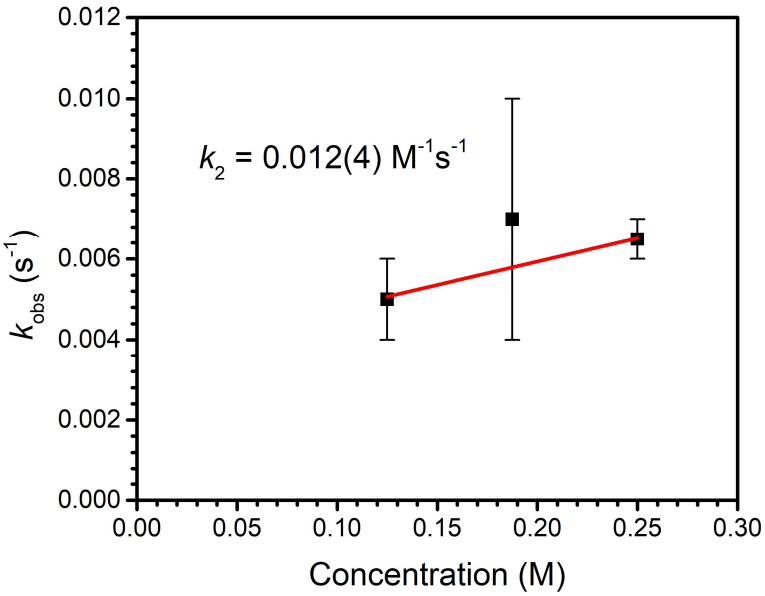


**Figure A2.13.** Plot of $k_{obs}$ versus [$Ph_2CH_2$] for the reaction between **3** and diphenylmethane. The slope of the linear fit is the second order rate constant, $k_2$. $R^2$ = 0.82.

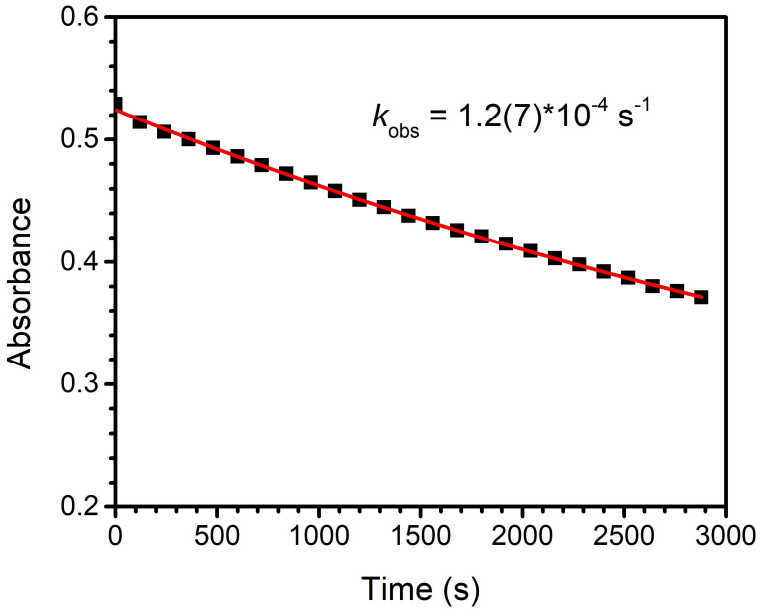


**Figure A2.14.** Representative exponential fit of a plot of A versus time for the reaction between **3** and 100 equivalents of 1,3-cyclohexadiene. The average *k* obtained from three trials was taken to be the observed rate constant, $k_{obs}$, for this reaction at various concentrations.

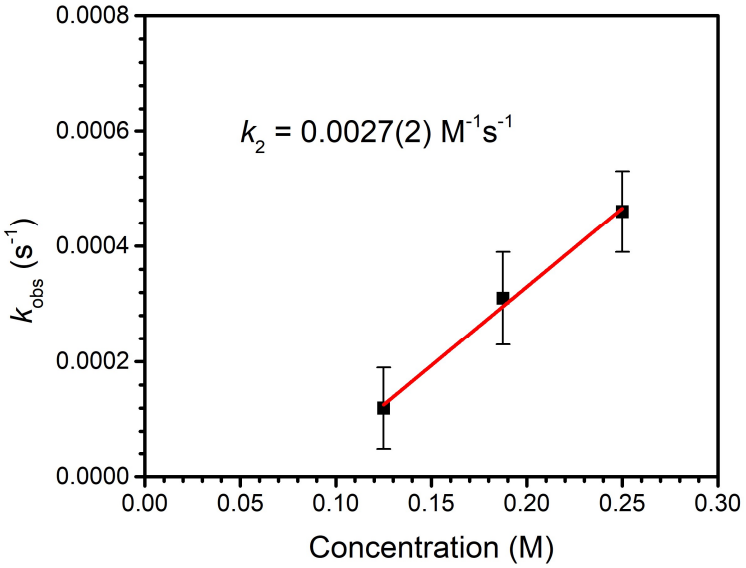


**Figure A2.15.** Plot of $k_{obs}$ versus [1,3-CHD] for the reaction between **3** and 1,3-CHD. The slope of the linear fit is the second order rate constant, $k_2$. $R^2 = 0.99$.

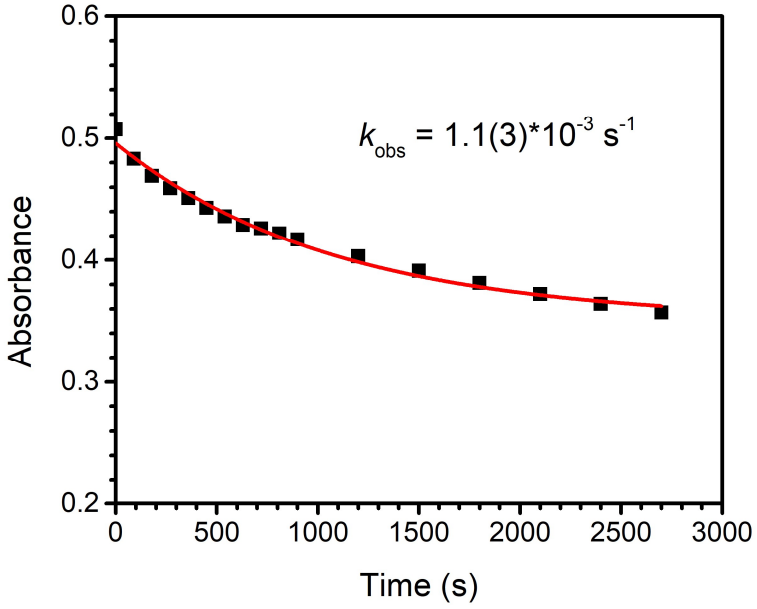


**Figure A2.16.** Representative exponential fit of a plot of A versus time for the reaction between **3** and 10 equivalents of 9-(*tert*-butyl)-9*H*-fluorene. The average *k* obtained from three trials was taken to be the observed rate constant, $k_{obs}$, for this reaction.

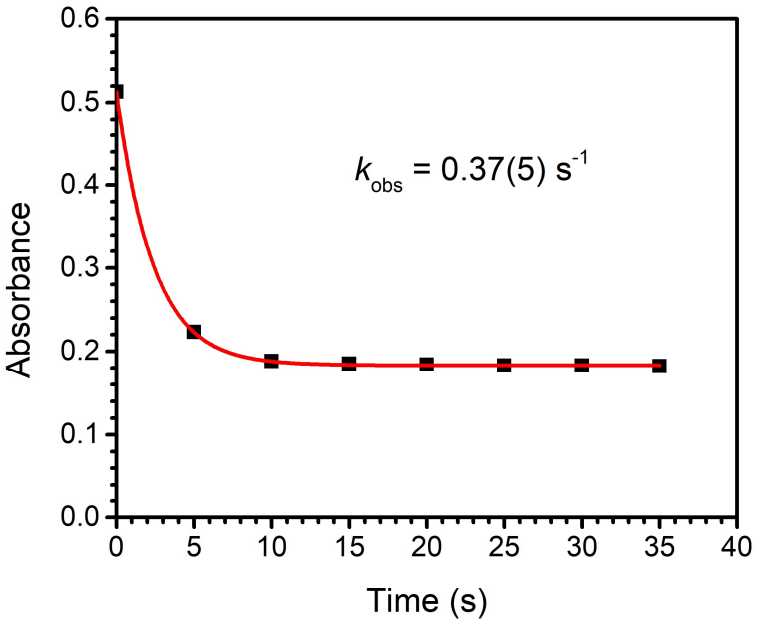


**Figure A2.17.** Representative exponential fit of a plot of A versus time for the reaction between **3** and 10 equivalents of 9-phenyl-9*H*-fluorene. The average *k* obtained from three trials was taken to be the observed rate constant, $k_{obs}$, for this reaction.

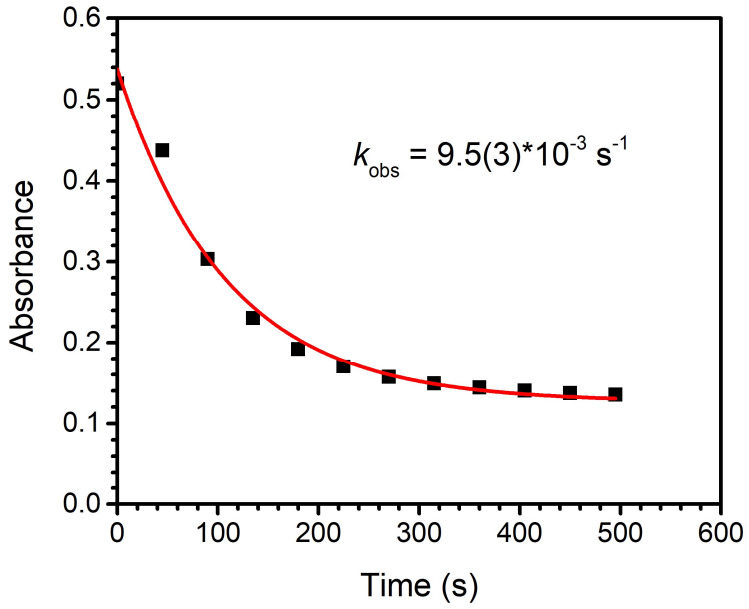


**Figure A2.18.** Representative exponential fit of a plot of A versus time for the reaction between **3** and 10 equivalents of fluorene. The average *k* obtained from three trials was taken to be the observed rate constant, $k_{obs}$, for this reaction at various concentrations.

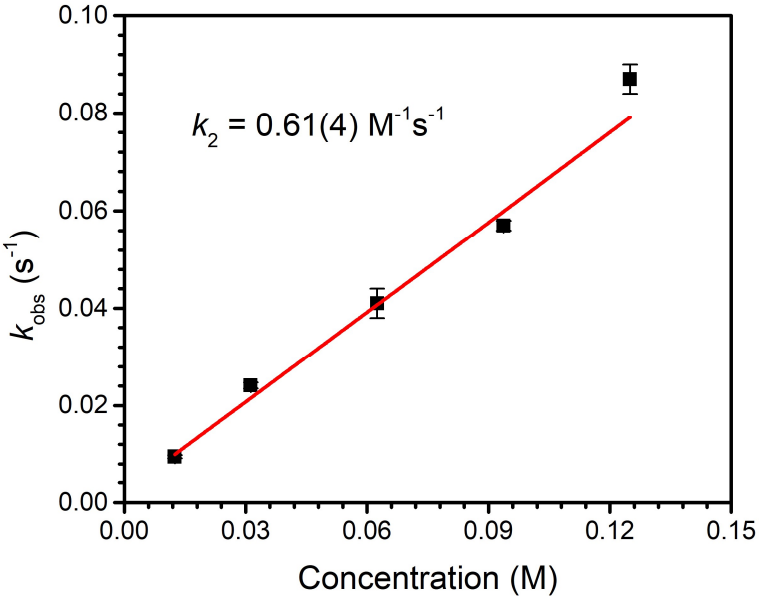


**Figure A2.19.** Plot of $k_{obs}$ versus [fluorene] for the reaction between **3** and fluorene. The slope of the linear fit is the second order rate constant, $k_2$. $R^2 = 0.98$.

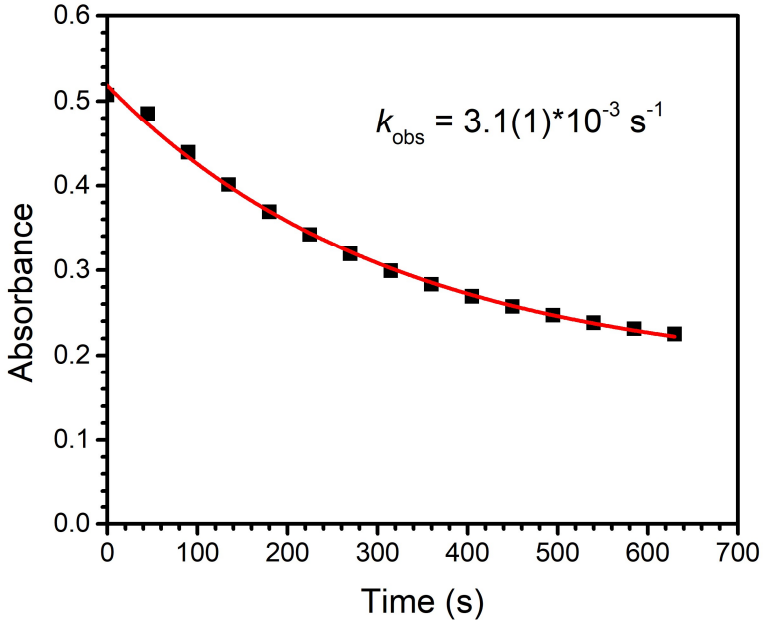


**Figure A2.20.** Representative exponential fit of a plot of A versus time for the reaction between **3** and 10 equivalents of fluorene-$d_2$. The average $k$ obtained from three trials was taken to be the observed rate constant, $k_{obs}$, for this reaction.

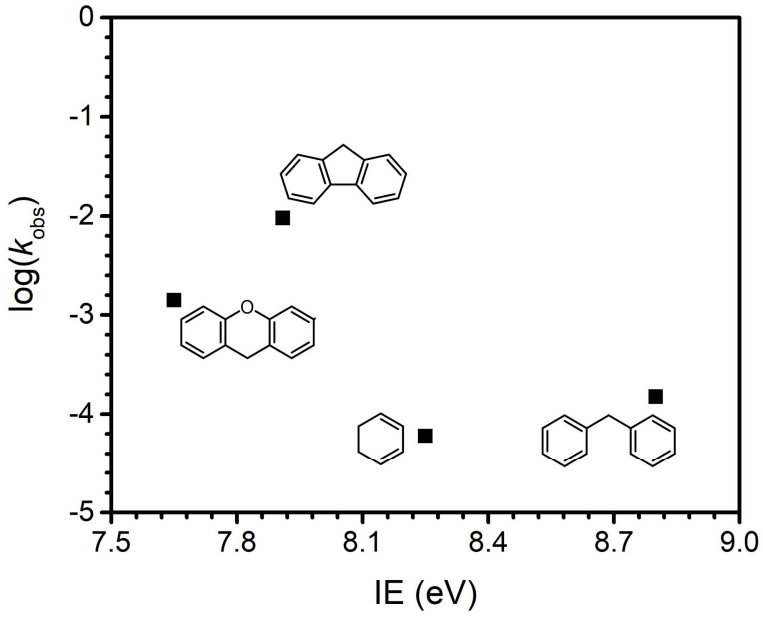


**Figure A2.21.** Plot of log($k_{obs}$) versus gas phase ionization energy for the substrates for which this data is known. The ionization energy data were taken from the NIST database.

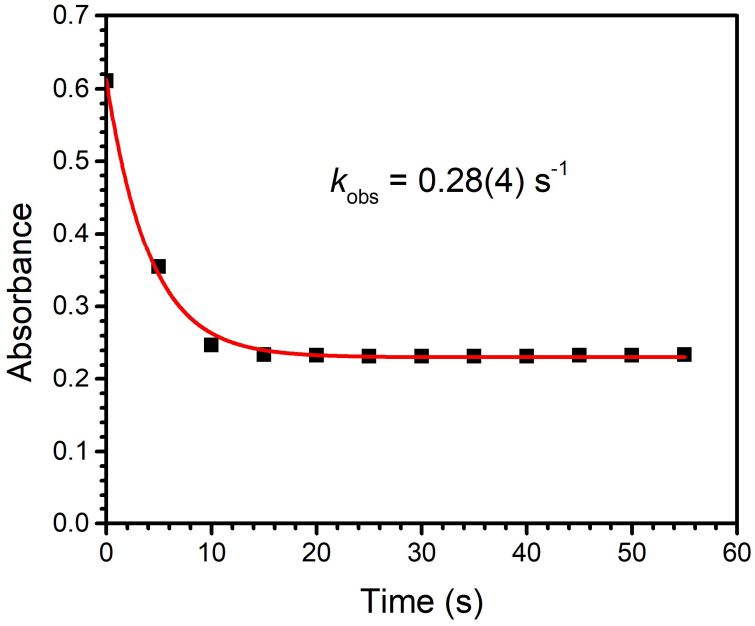


**Figure A2.22.** Representative exponential fit of a plot of A versus time for the reaction between **3** and 10 equivalents of 9-(*p*-tolyl)-9*H*-fluorene. The average *k* obtained from three trials was taken to be the observed rate constant, $k_{obs}$, for this reaction.

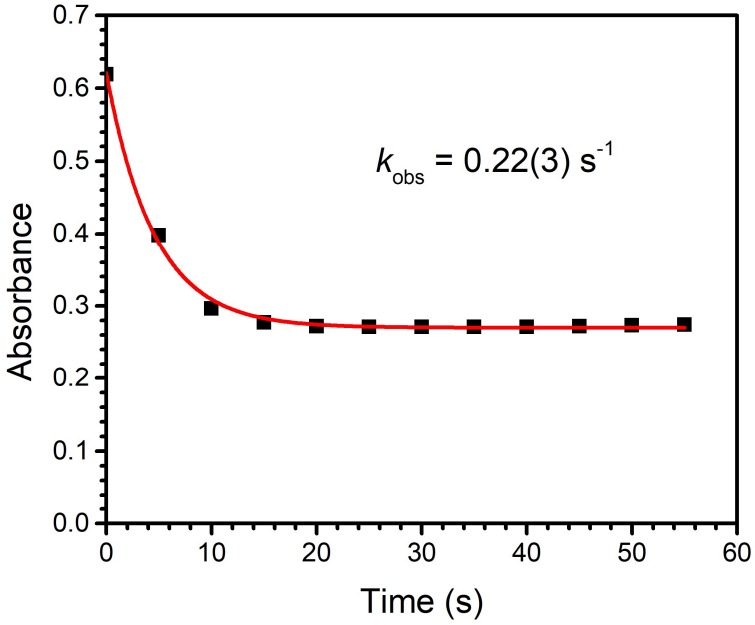


**Figure A2.23.** Representative exponential fit of a plot of A versus time for the reaction between **3** and 10 equivalents of 9-(4-methoxyphenyl)-9*H*-fluorene. The average *k* obtained from three trials was taken to be the observed rate constant, $k_{obs}$, for this reaction.

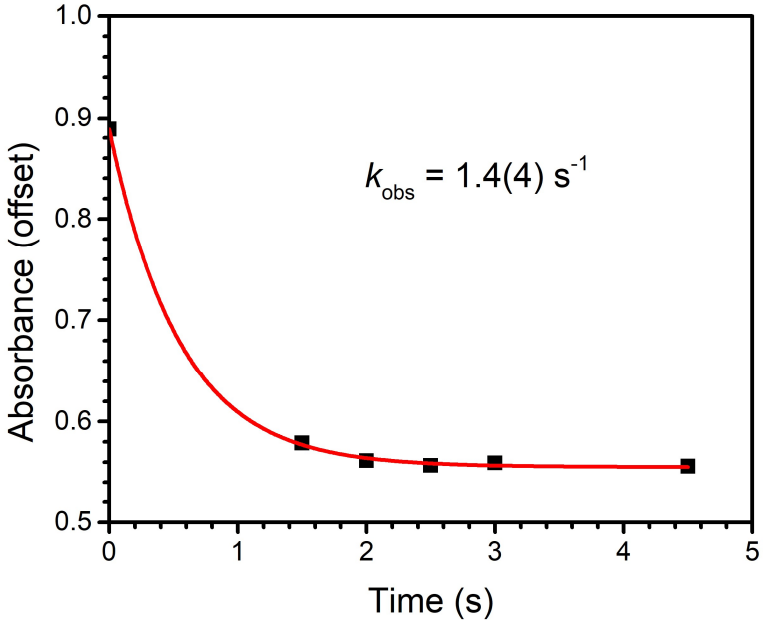


**Figure A2.24.** Representative exponential fit of a plot of A versus time for the reaction between **3** and 10 equivalents of 9-(4-(trifluoromethyl)phenyl)-9*H*-fluorene. The average *k* obtained from three trials was taken to be the observed rate constant, $k_{obs}$, for this reaction.

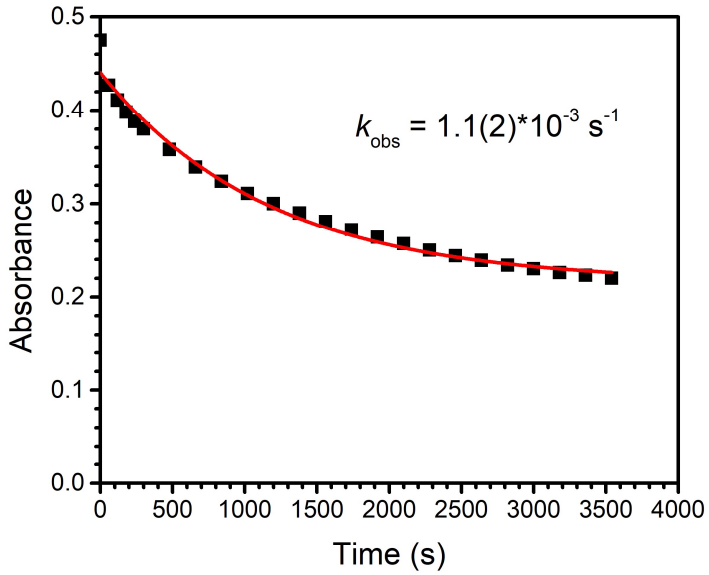


**Figure A2.25.** Representative exponential fit of a plot of A versus time for the reaction between **3** and 10 equivalents of 3-methylxanthene. The average *k* obtained from three trials was taken to be the observed rate constant, $k_{obs}$, for this reaction.

## A2.4 Gas Chromatography-Mass Spectrometry

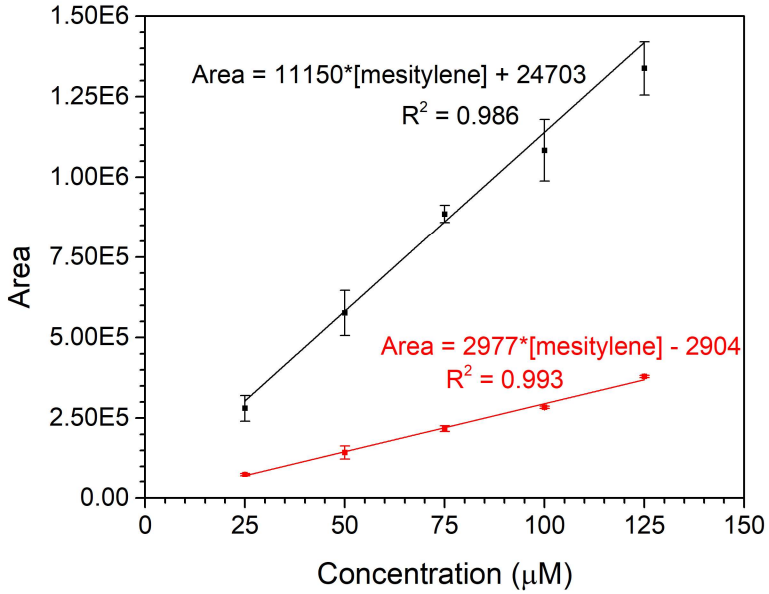


**Figure A2.26.** Calibration curves for the concentration of mesitylene (x-axis) determined from the integrated area (y-axis) from the chromatogram obtained from GC-MS analysis (see Experimental in Chapter 3). The data points and line in black are for the calibration curve determined using PCI-MS. The data points and line in red are for the calibration curve determined using EI-MS.

| Substrate/ Product | Trial | Mes Area | Product Area | [Mes] (μM) | [Product] (μM)[a] | Conversion (%) |
|---|---|---|---|---|---|---|
| DHA/ anthracene | 1 | 196332 | 221171 | 65.9 | 59.3 | 89.9 |
| | 2 | 153323 | 217855 | 52.5 | 58.5 | 111 |
| | 3 | 189674 | 234352 | 64.7 | 63.8 | 99.7 |
| | | Average (± Std. Dev.) | | | | 100(11) |
| fluorene/ 9,9'-bifluorenyl | 1 | 761664 | 519821 | 66.1 | 45.1 | 68.2 |
| | 2 | 691430 | 457503 | 59.8 | 39.6 | 66.2 |
| | 3 | 687786 | 534562 | 59.5 | 46.2 | 77.7 |
| | | Average (± Std. Dev.) | | | | 71(6) |

**Table A2.1.** Relevant data from GC-MS analysis used in determining the reaction conversion percentage for the reactions between **3** and DHA (analyzed by EI-MS) or between **3** and fluorene (analyzed by PCI-MS). Based on stoichiometry, in both of these cases 0.5 equivalents of product would be expected for every 1 equivalent of **3** consumed. [a]In the case of the reaction with DHA, a background concentration of 16.1(6) μM of anthracene that was present in the DHA to begin with was subtracted from the values obtained after the reaction. Mes = mesitylene.

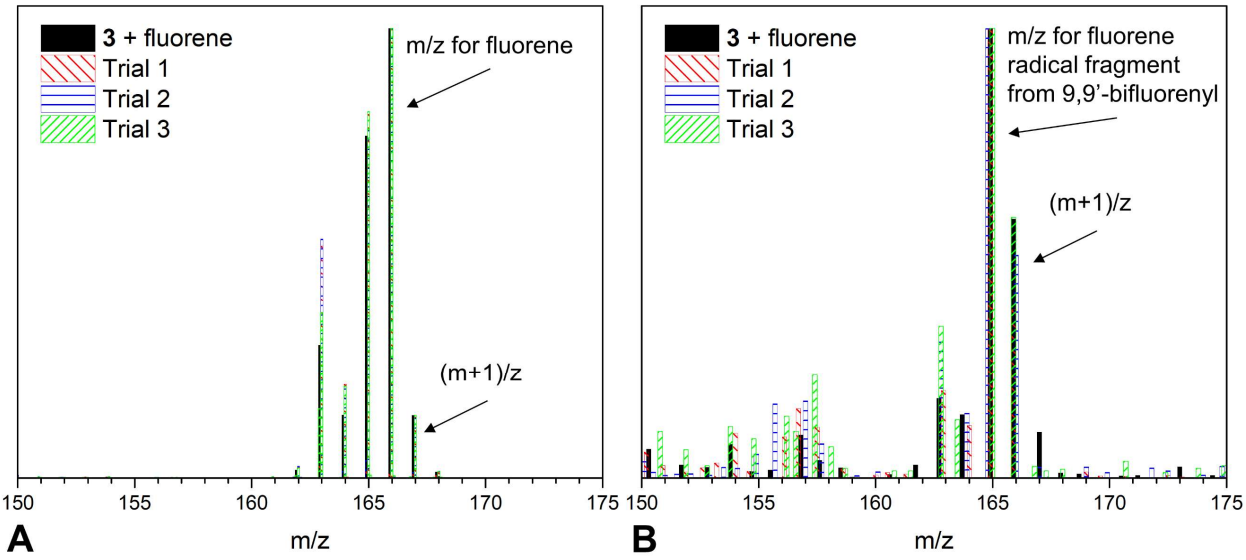


**Figure A2.27.** Overlay of GC-MS data collected for three trials of the reaction of **3** and 10 equivalents of fluorene in the presence of 2 equivalents of [DMTBD][$BF_4$] and 3.2 equivalents of MTBD. In black is the GC-MS data for the reaction of just **3** with 10 equivalents of fluorene. (A) shows the data for the parent fluorene peak and (B) shows the data for the product 9,9'-bifluorenyl peak. The (m+1)/z peak is present in the mass spectra of the deuterium free reaction and shows no enhancement in the mass spectra of the reactions carried out in the presence of deuterium. The intensity is normalized to the largest peak in both cases.

## A2.5 Schemes

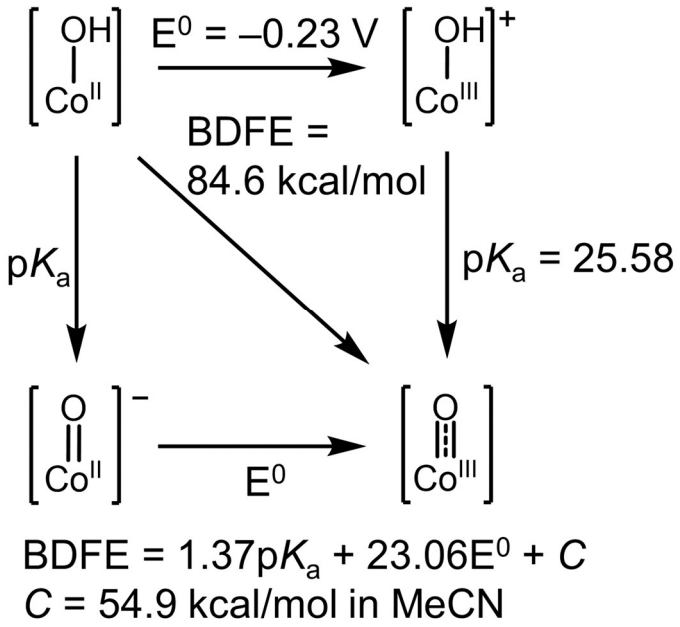


**Scheme A2.1.** Thermodynamic square scheme describing the relationship between p$K_a$, $E^0$, and $BDFE_{O–H}$ for **1**.

## A2.6 Density Functional Theory Calculations

| **Substrate** | **η(mV)** |
|---|---|
| 9,10-dihydroanthracene | –898 |
| fluorene | –1042 |
| 1,3-cyclohexadiene | –492 |

**Table A2.2.** Calculated asynchronicity parameters for the reaction of **3** with DHA, fluorene, or CHD.

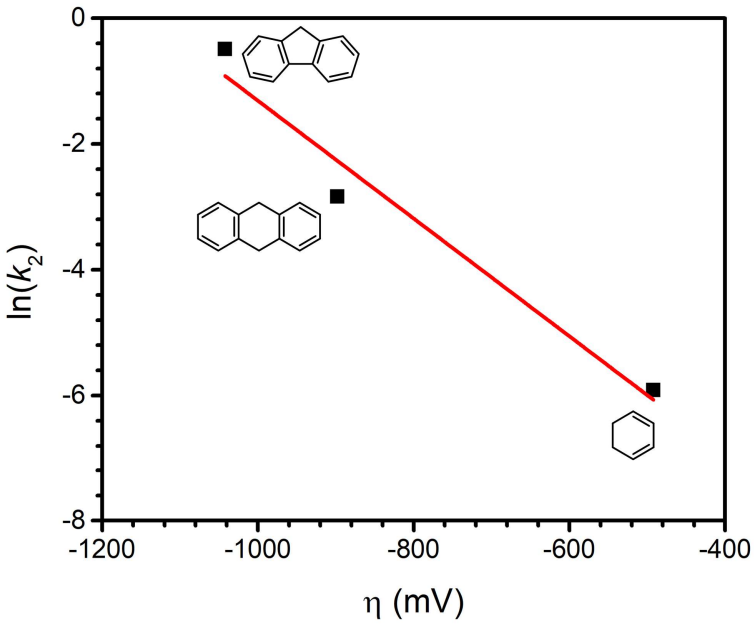


**Figure A2.28.** Plot of ln($k_2$) versus the calculated asynchronicity parameter, η, for the reaction of **3** with fluorene, 9,10-DHA, and 1,3-CHD. Linear fit: ln($k_2$) = –0.009η – 11. $R^2$ = 0.93.

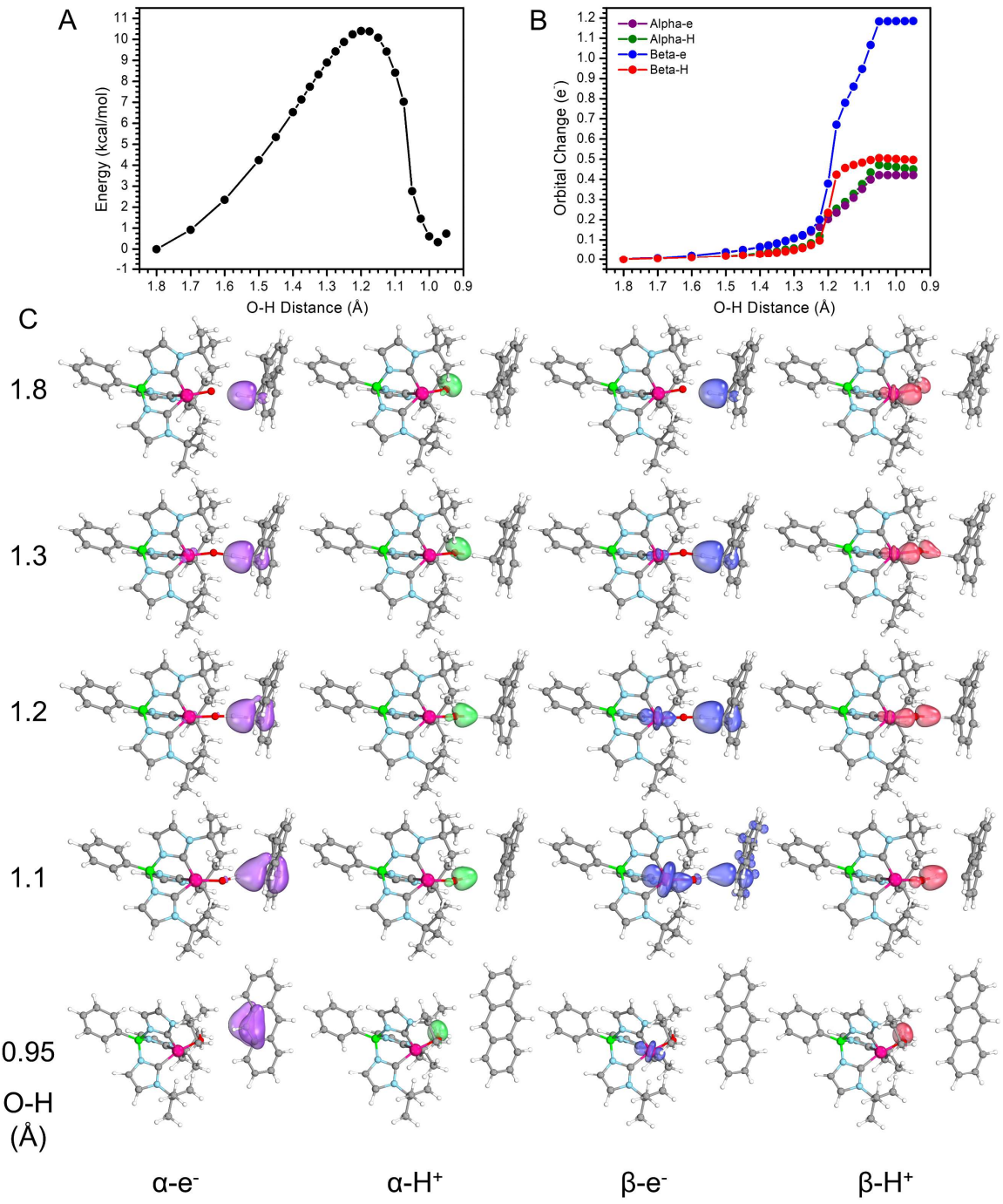


**Figure A2.29.** IBO analysis of the reaction coordinate between **3** and DHA. Each point was optimized by a constrained geometry scan as implemented in ORCA. The BP86 functional was used with TZVPP on Co, N, and O, and 6-31G on all other atoms. A) The single point energies for the reaction coordinate. B) The orbital change of the four orbitals with significant contributions on transferred H. C) Orbital plots along the reaction coordinate.

| Species | G (Hartrees) | G (kcal/mol) |
|---|---|---|
| **1** | –2859.56617 | –1794403 |
| **2** | –2859.41005 | –1794305 |
| **3** | –2858.94445 | –1794013 |
| $PhB(^tBuIm)_3Co^{II}O^-$ | –2859.02541 | –1794064 |
| DHA | –539.01388 | –338236 |
| $DHA^+$ | –538.78192 | –338090 |
| $DHA^-$ | –538.50128 | –337914 |
| $DHA^{rad}$ | –538.40286 | –337852 |
| fluorene | –499.85059 | –313661 |
| $fluorene^+$ | –499.62537 | –313519 |
| $fluorene^-$ | –499.35429 | –313349 |
| $fluorene^{rad}$ | –499.23415 | –313274 |
| CHD | –232.66237 | –145998 |
| $CHD^+$ | –232.44951 | –145864 |
| $CHD^-$ | –232.13476 | –145667 |
| $CHD^{rad}$ | –232.05942 | –145619 |

**Table A2.3.** Computed free energies for the various DFT optimized structures. See Experimental in Chapter 3 for computational details. Note that the "+" designation for a substrate means we optimized the structure that was oxidized by one electron, the "–" designation for a substrate means we optimized the structure after deprotonating the acidic C–H, and the "rad" designation for a substrate means we optimized the structure for the radical product expected from C–H activation.

**Table A2.4.** Coordinates for the optimized structure of **1**.

| | | | |
|---|---|---|---|
| C | -1.90873 | 1.31199 | -0.46034 |
| N | -3.18881 | 1.64390 | -0.74134 |
| C | -3.95121 | 0.50765 | -0.89921 |
| C | -3.11374 | -0.54554 | -0.72124 |

**Table A2.4, continued**

| | | | |
|---|---|---|---|
| N | -1.85982 | -0.03958 | -0.48394 |
| B | -0.55201 | -0.80852 | -0.06982 |
| N | 0.65297 | -0.23147 | -0.89799 |
| C | 1.00178 | 1.07317 | -0.90650 |
| N | 2.08094 | 1.17058 | -1.71172 |
| C | 2.41163 | -0.07042 | -2.21359 |
| C | 1.51246 | -0.94608 | -1.69931 |
| N | -0.35266 | -0.41430 | 1.43636 |
| C | -0.11859 | 0.86965 | 1.79325 |
| N | -0.10588 | 0.88491 | 3.14466 |
| C | -0.38150 | -0.37211 | 3.63672 |
| C | -0.54905 | -1.17984 | 2.55917 |
| Co | -0.20910 | 2.16310 | 0.24156 |
| O | 0.01746 | 3.98119 | 0.59240 |
| C | -3.68164 | 3.03726 | -0.85913 |
| C | -5.15416 | 3.03463 | -1.24411 |
| C | -3.50581 | 3.73660 | 0.48412 |
| C | -2.87553 | 3.74001 | -1.94611 |
| C | 2.77339 | 2.44377 | -2.02050 |
| C | 4.00779 | 2.16875 | -2.86742 |
| C | 1.81215 | 3.33684 | -2.79877 |
| C | 3.18941 | 3.10267 | -0.71038 |
| C | 0.14517 | 2.09506 | 3.96445 |
| C | 1.45262 | 2.72769 | 3.50156 |
| C | -1.0205 | 3.05979 | 3.77799 |
| C | 0.26008 | 1.70924 | 5.43254 |
| H | -5.49287 | 4.07443 | -1.34179 |

**Table A2.4, continued**

| | | | |
|---|---|---|---|
| H | -5.32896 | 2.53880 | -2.20950 |
| H | -4.04189 | 3.19617 | 1.27755 |
| H | -3.91188 | 4.75651 | 0.42970 |
| H | -2.44333 | 3.80568 | 0.75423 |
| H | -2.99705 | 3.23288 | -2.91414 |
| H | -1.80861 | 3.74723 | -1.69052 |
| H | -3.21365 | 4.78014 | -2.05557 |
| H | 3.75490 | 1.71821 | -3.83737 |
| H | 4.72278 | 1.51517 | -2.34740 |
| H | 4.51506 | 3.12095 | -3.07119 |
| H | 1.50354 | 2.85605 | -3.73803 |
| H | 2.29274 | 4.29432 | -3.04328 |
| H | 3.85436 | 2.44005 | -0.13804 |
| H | 3.72882 | 4.03813 | -0.91670 |
| H | 2.31133 | 3.33796 | -0.09419 |
| H | 1.66926 | 3.62003 | 4.10581 |
| H | 2.28774 | 2.02145 | 3.61634 |
| H | -0.87101 | 3.95487 | 4.39806 |
| H | -1.09467 | 3.37912 | 2.73109 |
| H | 1.07012 | 0.98637 | 5.60663 |
| H | -0.67670 | 1.29287 | 5.82837 |
| H | 0.48666 | 2.61217 | 6.01509 |
| H | -5.78140 | 2.55490 | -0.47937 |
| H | -1.96790 | 2.58917 | 4.07978 |
| H | 0.91046 | 3.54553 | -2.20800 |
| C | -0.59373 | -2.40125 | -0.35804 |
| C | -1.23764 | -2.92333 | -1.49259 |

**Table A2.4, continued**

| | | | |
|---|---|---|---|
| C | -1.16795 | -4.27242 | -1.83455 |
| C | -0.43076 | -5.15573 | -1.05110 |
| C | 0.25152 | -4.66468 | 0.05799 |
| C | 0.17456 | -3.31217 | 0.38561 |
| H | -1.79398 | -2.25730 | -2.15542 |
| H | -1.68535 | -4.63336 | -2.72750 |
| H | -0.37381 | -6.21545 | -1.31333 |
| H | 0.85836 | -5.33676 | 0.67071 |
| H | 0.75820 | -2.96111 | 1.23888 |
| H | -5.00878 | 0.52092 | -1.12757 |
| H | -3.33480 | -1.60620 | -0.73801 |
| H | 3.24295 | -0.24439 | -2.88471 |
| H | 1.42803 | -2.01601 | -1.84903 |
| H | -0.43773 | -0.60573 | 4.69234 |
| H | -0.80524 | -2.23168 | 2.52530 |
| H | 1.38689 | 3.03462 | 2.45023 |
| H | 0.06809 | 4.52657 | -0.19986 |

**Table A2.5.** Coordinates for the optimized structure of **2**.

| | | | |
|---|---|---|---|
| C | -1.77841 | 1.20867 | -0.31931 |
| N | -3.02792 | 1.66623 | -0.61913 |
| C | -3.83618 | 0.58376 | -0.87726 |
| C | -3.08016 | -0.53273 | -0.74995 |
| N | -1.81941 | -0.12960 | -0.42850 |
| B | -0.57597 | -0.98920 | -0.05333 |
| N | 0.60514 | -0.33772 | -0.82217 |
| C | 0.88667 | 0.96347 | -0.70444 |

**Table A2.5, continued**

| | | | |
|---|---|---|---|
| N | 1.99847 | 1.20187 | -1.45122 |
| C | 2.38341 | 0.01788 | -2.04015 |
| C | 1.50849 | -0.93952 | -1.64704 |
| N | -0.34418 | -0.58821 | 1.42989 |
| C | -0.14654 | 0.71440 | 1.66080 |
| N | -0.02796 | 0.86515 | 3.00256 |
| C | -0.19347 | -0.35990 | 3.60414 |
| C | -0.40301 | -1.26616 | 2.61376 |
| Co | -0.22107 | 2.04746 | 0.32083 |
| O | -0.18211 | 3.75834 | -0.04227 |
| C | -3.52792 | 3.07059 | -0.76527 |
| C | -5.02840 | 3.05887 | -1.03939 |
| C | -3.30378 | 3.83678 | 0.53114 |
| C | -2.83048 | 3.69751 | -1.96761 |
| C | 2.72445 | 2.48599 | -1.69770 |
| C | 4.06993 | 2.19164 | -2.35323 |
| C | 1.88653 | 3.33298 | -2.64810 |
| C | 2.99227 | 3.18668 | -0.37389 |
| C | 0.22064 | 2.14029 | 3.72486 |
| C | 1.46182 | 2.79332 | 3.13478 |
| C | -1.00480 | 3.02989 | 3.56720 |
| C | 0.45961 | 1.85934 | 5.20097 |
| H | -5.35928 | 4.10159 | -1.12791 |
| H | -5.28468 | 2.56000 | -1.98359 |
| H | -3.79214 | 3.32268 | 1.37049 |
| H | -3.74818 | 4.83701 | 0.44242 |
| H | -2.24184 | 3.96488 | 0.75498 |

**Table A2.5, continued**

| | | | |
|---|---|---|---|
| H | -3.12820 | 3.18383 | -2.89268 |
| H | -1.74071 | 3.63385 | -1.88572 |
| H | -3.11511 | 4.75488 | -2.05936 |
| H | 3.97059 | 1.75439 | -3.35570 |
| H | 4.69538 | 1.53483 | -1.73242 |
| H | 4.60327 | 3.14335 | -2.47157 |
| H | 1.75266 | 2.81809 | -3.60962 |
| H | 2.38934 | 4.29068 | -2.84003 |
| H | 3.52887 | 2.52258 | 0.31802 |
| H | 3.62009 | 4.06999 | -0.55294 |
| H | 2.06914 | 3.53835 | 0.09545 |
| H | 1.67743 | 3.73371 | 3.65955 |
| H | 2.33646 | 2.13472 | 3.22497 |
| H | -0.86314 | 3.97101 | 4.11503 |
| H | -1.18167 | 3.28734 | 2.51473 |
| H | 1.31575 | 1.18844 | 5.35778 |
| H | -0.42495 | 1.43234 | 5.69243 |
| H | 0.68429 | 2.80958 | 5.70240 |
| H | -5.59937 | 2.60118 | -0.21962 |
| H | -1.90459 | 2.53394 | 3.95665 |
| H | 0.89790 | 3.54303 | -2.22750 |
| C | -0.65789 | -2.55044 | -0.40580 |
| C | -1.28113 | -2.99446 | -1.58463 |
| C | -1.26776 | -4.33320 | -1.96868 |
| C | -0.61306 | -5.27861 | -1.18424 |
| C | 0.04505 | -4.86423 | -0.03052 |
| C | 0.02752 | -3.52148 | 0.34144 |

**Table A2.5, continued**

| | | | |
|---|---|---|---|
| H | -1.77685 | -2.27967 | -2.24515 |
| H | -1.76478 | -4.63791 | -2.89303 |
| H | -0.60203 | -6.33075 | -1.47992 |
| H | 0.58533 | -5.58904 | 0.58347 |
| H | 0.59287 | -3.23438 | 1.22936 |
| H | -4.88045 | 0.67825 | -1.13684 |
| H | -3.35854 | -1.57432 | -0.85322 |
| H | 3.24446 | -0.06038 | -2.68876 |
| H | 1.46543 | -1.99524 | -1.88871 |
| H | -0.14849 | -0.50404 | 4.67579 |
| H | -0.60262 | -2.32858 | 2.68520 |
| H | 1.32704 | 3.04590 | 2.07469 |
| H | -0.36069 | 4.40839 | -0.72863 |

**Table A2.6.** Coordinates for the optimized structure of **3**.

| | | | |
|---|---|---|---|
| C | -1.76428 | 1.219607 | -0.44748 |
| N | -2.98673 | 1.678265 | -0.8435 |
| C | -3.82036 | 0.603212 | -1.06373 |
| C | -3.10238 | -0.52008 | -0.8246 |
| N | -1.83919 | -0.12604 | -0.48368 |
| B | -0.59887 | -0.96122 | -0.05064 |
| N | 0.586478 | -0.37941 | -0.85552 |
| C | 0.819198 | 0.936795 | -0.78692 |
| N | 1.896213 | 1.171168 | -1.58412 |
| C | 2.320476 | -0.01878 | -2.14072 |
| C | 1.492469 | -0.9899 | -1.67993 |
| N | -0.37519 | -0.49098 | 1.415964 |

**Table A2.6, continued**

| | | | |
|---|---|---|---|
| C | -0.13811 | 0.814496 | 1.656334 |
| N | -0.00556 | 0.933439 | 3.009135 |
| C | -0.22501 | -0.29596 | 3.591558 |
| C | -0.46863 | -1.17819 | 2.593355 |
| Co | -0.26161 | 2.089016 | 0.279492 |
| O | -0.53956 | 3.628658 | 0.811104 |
| C | -3.4417 | 3.090783 | -1.00568 |
| C | -4.77679 | 3.115823 | -1.74378 |
| C | -3.61856 | 3.709426 | 0.376077 |
| C | -2.42216 | 3.85643 | -1.83831 |
| C | 2.528356 | 2.491931 | -1.82349 |
| C | 3.691276 | 2.343305 | -2.79437 |
| C | 1.488231 | 3.429532 | -2.42374 |
| C | 3.046412 | 3.029368 | -0.49459 |
| C | 0.301743 | 2.154092 | 3.810777 |
| C | 1.507261 | 2.862108 | 3.207334 |
| C | -0.92976 | 3.051375 | 3.829345 |
| C | 0.653314 | 1.7522 | 5.239783 |
| H | -5.05354 | 4.165122 | -1.9095 |
| H | -4.71806 | 2.628422 | -2.72739 |
| H | -4.3598 | 3.143178 | 0.958994 |
| H | -3.9804 | 4.743218 | 0.275288 |
| H | -2.65644 | 3.724074 | 0.906112 |
| H | -2.26997 | 3.37308 | -2.8141 |
| H | -1.46459 | 3.92328 | -1.31239 |
| H | -2.78858 | 4.876964 | -2.01495 |
| H | 3.369017 | 1.958587 | -3.77189 |

**Table A2.6, continued**

| | | | |
|---|---|---|---|
| H | 4.48287 | 1.692209 | -2.3974 |
| H | 4.13337 | 3.334402 | -2.96134 |
| H | 1.093132 | 3.024276 | -3.36586 |
| H | 1.938443 | 4.410061 | -2.6303 |
| H | 3.782543 | 2.341087 | -0.05483 |
| H | 3.529406 | 4.005172 | -0.64344 |
| H | 2.220914 | 3.163926 | 0.216639 |
| H | 1.771671 | 3.729421 | 3.828479 |
| H | 2.376101 | 2.189286 | 3.167512 |
| H | -0.73571 | 3.936638 | 4.451857 |
| H | -1.16845 | 3.384331 | 2.809478 |
| H | 1.505233 | 1.057738 | 5.277808 |
| H | -0.19477 | 1.307944 | 5.778337 |
| H | 0.939575 | 2.660845 | 5.785545 |
| H | -5.59063 | 2.657573 | -1.16486 |
| H | -1.7897 | 2.515944 | 4.258663 |
| H | 0.652981 | 3.579753 | -1.72739 |
| C | -0.67213 | -2.55036 | -0.30582 |
| C | -1.33267 | -3.08235 | -1.42608 |
| C | -1.29866 | -4.44114 | -1.73352 |
| C | -0.582 | -5.3228 | -0.92969 |
| C | 0.117817 | -4.82216 | 0.16403 |
| C | 0.077091 | -3.46051 | 0.458124 |
| H | -1.87549 | -2.42049 | -2.10368 |
| H | -1.82915 | -4.81118 | -2.61496 |
| H | -0.55456 | -6.39015 | -1.16449 |
| H | 0.709235 | -5.49405 | 0.791704 |

**Table A2.6, continued**

| | | | |
|---|---|---|---|
| H | 0.672681 | -3.10467 | 1.300949 |
| H | -4.8496 | 0.705831 | -1.37619 |
| H | -3.41061 | -1.55771 | -0.86539 |
| H | 3.165408 | -0.09166 | -2.81244 |
| H | 1.482763 | -2.05576 | -1.88056 |
| H | -0.19405 | -0.45819 | 4.660218 |
| H | -0.71404 | -2.23162 | 2.648592 |
| H | 1.279362 | 3.222261 | 2.198999 |

**Table A2.7.** Coordinates for the optimized structure of $PhB(^{t}BuIm)_3Co^{II}O^{-}$.

| | | | |
|---|---|---|---|
| C | -1.881 | 1.288012 | -0.46978 |
| N | -3.16162 | 1.628234 | -0.77116 |
| C | -3.94124 | 0.499079 | -0.92149 |
| C | -3.11715 | -0.56308 | -0.73393 |
| N | -1.85565 | -0.07154 | -0.49419 |
| B | -0.55346 | -0.83277 | -0.06866 |
| N | 0.646102 | -0.26204 | -0.89753 |
| C | 0.965739 | 1.057098 | -0.9016 |
| N | 2.04158 | 1.168093 | -1.71986 |
| C | 2.396262 | -0.06829 | -2.22506 |
| C | 1.515259 | -0.96036 | -1.70581 |
| N | -0.35508 | -0.43281 | 1.433283 |
| C | -0.12744 | 0.866471 | 1.763093 |
| N | -0.10935 | 0.895084 | 3.121686 |
| C | -0.38646 | -0.35554 | 3.636229 |
| C | -0.553 | -1.17979 | 2.570618 |
| Co | -0.21543 | 2.170185 | 0.238722 |

**Table A2.7, continued**

| | | | |
|---|---|---|---|
| O | -0.05681 | 3.872837 | 0.434301 |
| C | -3.63859 | 3.025448 | -0.85009 |
| C | -5.06177 | 3.056945 | -1.39063 |
| C | -3.59569 | 3.63082 | 0.549697 |
| C | -2.7139 | 3.801275 | -1.7809 |
| C | 2.713445 | 2.455243 | -1.99351 |
| C | 3.864649 | 2.244631 | -2.96582 |
| C | 1.69037 | 3.415684 | -2.59095 |
| C | 3.236529 | 3.012626 | -0.67287 |
| C | 0.158011 | 2.118497 | 3.908098 |
| C | 1.491806 | 2.699045 | 3.449551 |
| C | -0.95897 | 3.123237 | 3.647959 |
| C | 0.222903 | 1.778714 | 5.390219 |
| H | -5.38087 | 4.103734 | -1.48518 |
| H | -5.1315 | 2.595042 | -2.38625 |
| H | -4.22168 | 3.052418 | 1.245401 |
| H | -3.97 | 4.664998 | 0.5257 |
| H | -2.55682 | 3.64087 | 0.911571 |
| H | -2.7056 | 3.354299 | -2.78602 |
| H | -1.69188 | 3.802887 | -1.37146 |
| H | -3.06212 | 4.841204 | -1.86777 |
| H | 3.521872 | 1.840762 | -3.9293 |
| H | 4.635022 | 1.574197 | -2.55691 |
| H | 4.341848 | 3.213812 | -3.16551 |
| H | 1.268713 | 3.007626 | -3.52166 |
| H | 2.166672 | 4.37994 | -2.82149 |
| H | 3.936421 | 2.30671 | -0.20085 |

**Table A2.7, continued**

| | | | |
|---|---|---|---|
| H | 3.765331 | 3.961796 | -0.84564 |
| H | 2.389356 | 3.195803 | 0.00552 |
| H | 1.723179 | 3.609809 | 4.021371 |
| H | 2.307364 | 1.976248 | 3.602253 |
| H | -0.80232 | 4.025541 | 4.257431 |
| H | -0.9516 | 3.410586 | 2.583431 |
| H | 1.008397 | 1.041071 | 5.611203 |
| H | -0.73501 | 1.395583 | 5.770337 |
| H | 0.455333 | 2.693371 | 5.952567 |
| H | -5.77544 | 2.556519 | -0.71992 |
| H | -1.93858 | 2.696225 | 3.911452 |
| H | 0.88043 | 3.585372 | -1.86441 |
| C | -0.5911 | -2.43294 | -0.34434 |
| C | -1.23573 | -2.96998 | -1.47136 |
| C | -1.16453 | -4.32278 | -1.79983 |
| C | -0.42468 | -5.19738 | -1.00866 |
| C | 0.256797 | -4.69284 | 0.095238 |
| C | 0.177317 | -3.33662 | 0.4081 |
| H | -1.79667 | -2.31001 | -2.13649 |
| H | -1.68323 | -4.69407 | -2.6882 |
| H | -0.36607 | -6.25993 | -1.25997 |
| H | 0.864493 | -5.3577 | 0.715577 |
| H | 0.755888 | -2.97348 | 1.259969 |
| H | -4.99751 | 0.523066 | -1.15784 |
| H | -3.35364 | -1.62115 | -0.75089 |
| H | 3.226395 | -0.22837 | -2.90222 |
| H | 1.448637 | -2.03166 | -1.86077 |

**Table A2.7, continued**

| | | | |
|---|---|---|---|
| H | -0.444 | -0.57487 | 4.69558 |
| H | -0.80979 | -2.23272 | 2.556668 |
| H | 1.430004 | 2.959637 | 2.382887 |

**Table A2.8.** Coordinates for the optimized structure of DHA.

| | | | |
|---|---|---|---|
| C | -3.57113 | 1.060913 | 0.571932 |
| C | -3.63762 | -0.32931 | 0.516503 |
| C | -2.39696 | 1.712072 | 0.203287 |
| C | -1.28668 | 0.986784 | -0.22914 |
| C | -1.35169 | -0.41252 | -0.28456 |
| C | -2.52947 | -1.05883 | 0.093789 |
| C | -0.01317 | 1.656443 | -0.65012 |
| C | 1.200183 | 0.874415 | -0.24525 |
| C | 1.138227 | -0.52506 | -0.29892 |
| C | -0.14087 | -1.16485 | -0.75588 |
| C | 2.376515 | 1.497305 | 0.172024 |
| C | 3.491463 | 0.743516 | 0.528507 |
| C | 3.431548 | -0.64713 | 0.475772 |
| C | 2.25724 | -1.2744 | 0.067507 |
| H | -4.43427 | 1.639605 | 0.910257 |
| H | -4.55317 | -0.84817 | 0.811386 |
| H | -2.33875 | 2.803094 | 0.253993 |
| H | -2.57809 | -2.15126 | 0.057253 |
| H | 0.036451 | 2.676459 | -0.26314 |
| H | -0.01632 | 1.752933 | -1.74718 |
| H | 2.417393 | 2.58931 | 0.220557 |
| H | 4.407006 | 1.24263 | 0.855851 |

**Table A2.8, continued**

| | | | |
|---|---|---|---|
| H | 4.299972 | -1.24588 | 0.761408 |
| H | 2.206516 | -2.36669 | 0.033273 |
| H | -0.18758 | -2.21711 | -0.44131 |
| H | -0.14776 | -1.18227 | -1.86378 |

**Table A2.9.** Coordinates for the optimized structure of $DHA^{+}$.

| | | | |
|---|---|---|---|
| C | -3.72083 | 1.097405 | 0.044228 |
| C | -3.78673 | -0.31032 | -0.01221 |
| C | -2.49634 | 1.734625 | 0.062178 |
| C | -1.31173 | 0.987603 | 0.024687 |
| C | -1.3771 | -0.4322 | -0.03145 |
| C | -2.6281 | -1.06157 | -0.04937 |
| C | -0.00841 | 1.674497 | 0.043226 |
| C | 1.22764 | 0.873322 | 0.00991 |
| C | 1.165093 | -0.54663 | -0.04592 |
| C | -0.13983 | -1.2379 | -0.07014 |
| C | 2.474882 | 1.510715 | 0.03246 |
| C | 3.636788 | 0.766013 | 0.000115 |
| C | 3.576125 | -0.64196 | -0.05581 |
| C | 2.354232 | -1.28597 | -0.07831 |
| H | -4.64326 | 1.681172 | 0.073979 |
| H | -4.75999 | -0.80568 | -0.02628 |
| H | -2.44123 | 2.824671 | 0.106509 |
| H | -2.68124 | -2.15196 | -0.0932 |
| H | 0.027298 | 2.353536 | 0.914957 |
| H | 0.019938 | 2.408272 | -0.78401 |
| H | 2.52015 | 2.601335 | 0.076443 |

**Table A2.9, continued**

| | | | |
|---|---|---|---|
| H | 4.607928 | 1.265377 | 0.017865 |
| H | 4.501032 | -1.22201 | -0.08146 |
| H | 2.307145 | -2.37652 | -0.1221 |
| H | -0.16941 | -1.98439 | 0.753065 |
| H | -0.17504 | -1.90945 | -0.95537 |

**Table A2.10.** Coordinates for the optimized structure of $DHA^-$.

| | | | |
|---|---|---|---|
| C | -3.66941 | 1.044609 | 0.418545 |
| C | -3.72904 | -0.35269 | 0.414671 |
| C | -2.47477 | 1.706801 | 0.175504 |
| C | -1.26943 | 1.003975 | -0.09293 |
| C | -1.35837 | -0.42345 | -0.15074 |
| C | -2.55781 | -1.0647 | 0.124166 |
| C | -0.01192 | 1.633957 | -0.24082 |
| C | 1.185543 | 0.893336 | -0.10782 |
| C | 1.145327 | -0.53633 | -0.16484 |
| C | -0.13983 | -1.15987 | -0.62863 |
| C | 2.45256 | 1.484867 | 0.144171 |
| C | 3.585483 | 0.717973 | 0.374412 |
| C | 3.519254 | -0.67899 | 0.372957 |
| C | 2.285249 | -1.28282 | 0.097456 |
| H | -4.57252 | 1.627056 | 0.628968 |
| H | -4.6662 | -0.87652 | 0.617882 |
| H | -2.4448 | 2.800991 | 0.211624 |
| H | -2.58854 | -2.16001 | 0.083294 |
| H | 0.03843 | 2.717604 | -0.15534 |
| H | 2.522964 | 2.577393 | 0.17739 |

**Table A2.10, continued**

| | | | |
|---|---|---|---|
| H | 4.53961 | 1.217518 | 0.572935 |
| H | 4.408041 | -1.28448 | 0.565741 |
| H | 2.215974 | -2.37634 | 0.058784 |
| H | -0.18748 | -2.22777 | -0.36082 |
| H | -0.1443 | -1.1291 | -1.74356 |

**Table A2.11.** Coordinates for the optimized structure of $DHA^{rad}$.

| | | | |
|---|---|---|---|
| C | -3.71252 | 1.118945 | 0.166853 |
| C | -3.80174 | -0.26739 | 0.005274 |
| C | -2.47171 | 1.724838 | 0.238696 |
| C | -1.28156 | 0.964614 | 0.151075 |
| C | -1.37889 | -0.44275 | -0.01148 |
| C | -2.63908 | -1.03033 | -0.08145 |
| C | -0.01153 | 1.581298 | 0.222825 |
| C | 1.197014 | 0.852906 | 0.13624 |
| C | 1.165936 | -0.55756 | -0.02539 |
| C | -0.14231 | -1.28467 | -0.10379 |
| C | 2.451518 | 1.503168 | 0.208125 |
| C | 3.63187 | 0.788149 | 0.122166 |
| C | 3.59483 | -0.60081 | -0.03779 |
| C | 2.367307 | -1.2562 | -0.10927 |
| H | -4.62101 | 1.722043 | 0.236665 |
| H | -4.7787 | -0.75295 | -0.0529 |
| H | -2.3934 | 2.80777 | 0.366156 |
| H | -2.71453 | -2.11441 | -0.2083 |
| H | 0.038807 | 2.658753 | 0.350772 |
| H | 2.473308 | 2.588845 | 0.334938 |

**Table A2.11, continued**

| | | | |
|---|---|---|---|
| H | 4.591437 | 1.307963 | 0.179549 |
| H | 4.523776 | -1.17145 | -0.10698 |
| H | 2.342227 | -2.34253 | -0.23557 |
| H | -0.17347 | -2.05614 | 0.688568 |
| H | -0.17358 | -1.86909 | -1.04198 |

**Table A2.12.** Coordinates for the optimized structure of fluorene.

| | | | |
|---|---|---|---|
| C | -3.69153 | 0.547121 | 0.069847 |
| C | -3.32949 | -0.80063 | 0.136895 |
| C | -2.71643 | 1.542772 | -0.00123 |
| C | -1.37793 | 1.174266 | -0.00466 |
| C | -1.01143 | -0.18329 | 0.062534 |
| C | -1.98809 | -1.17637 | 0.133756 |
| C | -0.15136 | 2.031414 | -0.07249 |
| C | 0.96713 | 1.035754 | -0.03958 |
| C | 0.445831 | -0.26936 | 0.040764 |
| C | 2.339031 | 1.244544 | -0.07762 |
| C | 3.192382 | 0.14115 | -0.03475 |
| C | 2.676503 | -1.1547 | 0.045507 |
| C | 1.301 | -1.37037 | 0.084 |
| H | -4.74874 | 0.824193 | 0.073394 |
| H | -4.10633 | -1.56716 | 0.192728 |
| H | -3.00677 | 2.595171 | -0.05389 |
| H | -1.71149 | -2.23243 | 0.187227 |
| H | -0.09741 | 2.737765 | 0.765475 |
| H | -0.12887 | 2.644284 | -0.98199 |
| H | 2.749489 | 2.255683 | -0.14133 |

**Table A2.12, continued**

| | | | |
|---|---|---|---|
| H | 4.274601 | 0.292365 | -0.06477 |
| H | 3.358894 | -2.00751 | 0.078169 |
| H | 0.90403 | -2.38667 | 0.147022 |

**Table A2.13.** Coordinates for the optimized structure of fluorene$^{+}$.

| | | | |
|---|---|---|---|
| C | -3.65509 | 0.534063 | 0.070485 |
| C | -3.28981 | -0.82945 | 0.137375 |
| C | -2.69988 | 1.556705 | -0.00168 |
| C | -1.36774 | 1.206291 | -0.00647 |
| C | -0.98991 | -0.17282 | 0.061216 |
| C | -1.9635 | -1.19598 | 0.133559 |
| C | -0.1495 | 2.064506 | -0.07462 |
| C | 0.960683 | 1.068895 | -0.04164 |
| C | 0.425756 | -0.25632 | 0.040378 |
| C | 2.32428 | 1.260249 | -0.07877 |
| C | 3.154552 | 0.132361 | -0.03356 |
| C | 2.633758 | -1.17868 | 0.048228 |
| C | 1.274272 | -1.38691 | 0.085923 |
| H | -4.71605 | 0.796587 | 0.075424 |
| H | -4.07135 | -1.58946 | 0.192554 |
| H | -3.01481 | 2.600349 | -0.05289 |
| H | -1.66861 | -2.24569 | 0.185399 |
| H | -0.09548 | 2.769481 | 0.76367 |
| H | -0.12734 | 2.675509 | -0.98462 |
| H | 2.758361 | 2.259756 | -0.14238 |
| H | 4.238814 | 0.268762 | -0.06256 |
| H | 3.321664 | -2.02543 | 0.080877 |

**Table A2.13, continued**

| | | | |
|---|---|---|---|
| H | 0.859925 | -2.39476 | 0.149099 |

**Table A2.14.** Coordinates for the optimized structure of fluorene$^{-}$.

| | | | |
|---|---|---|---|
| C | -3.68385 | 0.555112 | 0.121391 |
| C | -3.34447 | -0.81547 | 0.121601 |
| C | -2.70919 | 1.538606 | 0.103154 |
| C | -1.34196 | 1.178006 | 0.084064 |
| C | -1.00008 | -0.22913 | 0.084374 |
| C | -2.00845 | -1.19951 | 0.103283 |
| C | -0.15494 | 1.938467 | 0.063502 |
| C | 0.934309 | 1.043416 | 0.049718 |
| C | 0.429698 | -0.31353 | 0.062728 |
| C | 2.334089 | 1.241218 | 0.02682 |
| C | 3.187129 | 0.150285 | 0.01679 |
| C | 2.689146 | -1.17078 | 0.029546 |
| C | 1.317551 | -1.39544 | 0.052468 |
| H | -4.73943 | 0.844968 | 0.136563 |
| H | -4.13356 | -1.5721 | 0.136432 |
| H | -2.99871 | 2.594386 | 0.103742 |
| H | -1.74819 | -2.26376 | 0.103844 |
| H | -0.0911 | 3.020547 | 0.056758 |
| H | 2.745627 | 2.255763 | 0.016576 |
| H | 4.269566 | 0.314645 | -0.00171 |
| H | 3.38356 | -2.01515 | 0.020985 |
| H | 0.934252 | -2.42155 | 0.062371 |

**Table A2.15.** Coordinates for the optimized structure of fluorene$^{rad}$.

| | | | |
|---|---|---|---|
| C | -3.68801 | 0.561844 | 0.122416 |
| C | -3.34757 | -0.79524 | 0.121936 |
| C | -2.7013 | 1.543475 | 0.103336 |
| C | -1.35689 | 1.150667 | 0.083686 |
| C | -1.01352 | -0.2369 | 0.083739 |
| C | -2.00748 | -1.20223 | 0.102599 |
| C | -0.15657 | 1.910459 | 0.062258 |
| C | 0.945889 | 1.014408 | 0.048738 |
| C | 0.441996 | -0.32294 | 0.061687 |
| C | 2.326844 | 1.246993 | 0.026709 |
| C | 3.192057 | 0.156537 | 0.017408 |
| C | 2.694567 | -1.15104 | 0.029971 |
| C | 1.316203 | -1.39811 | 0.052284 |
| H | -4.74104 | 0.853071 | 0.138336 |
| H | -4.13813 | -1.5493 | 0.137036 |
| H | -2.97097 | 2.602388 | 0.103891 |
| H | -1.75973 | -2.26712 | 0.102619 |
| H | -0.09256 | 2.991955 | 0.055801 |
| H | 2.718726 | 2.267017 | 0.016905 |
| H | 4.272179 | 0.32242 | -0.00016 |
| H | 3.39085 | -1.99297 | 0.02204 |
| H | 0.945463 | -2.42638 | 0.061766 |

**Table A2.16.** Coordinates for the optimized structure of CHD.

| | | | |
|---|---|---|---|
| C | -1.70216 | 1.036686 | -0.01552 |
| C | -1.65178 | -0.45931 | 0.257918 |

**Table A2.16, continued**

| | | | |
|---|---|---|---|
| C | -0.37859 | 1.692646 | 0.226453 |
| C | 0.76227 | 1.00746 | 0.031991 |
| C | 0.725323 | -0.38913 | -0.38075 |
| C | -0.41608 | -1.09415 | -0.29637 |
| H | -2.49288 | 1.509456 | 0.585656 |
| H | -1.98758 | 1.214025 | -1.07184 |
| H | -2.54921 | -0.94574 | -0.13353 |
| H | -1.67155 | -0.63881 | 1.345204 |
| H | -0.35189 | 2.751807 | 0.49878 |
| H | 1.733193 | 1.495898 | 0.15564 |
| H | 1.646799 | -0.85931 | -0.73552 |
| H | -0.44187 | -2.15353 | -0.56612 |

**Table A2.17.** Coordinates for the optimized structure of $CHD^+$.

| | | | |
|---|---|---|---|
| C | -1.68963 | 1.045743 | 0.124504 |
| C | -1.67358 | -0.4691 | 0.11653 |
| C | -0.38297 | 1.696199 | 0.128007 |
| C | 0.797237 | 1.007165 | -0.07781 |
| C | 0.785037 | -0.38759 | -0.28177 |
| C | -0.3974 | -1.09737 | -0.19865 |
| H | -2.30885 | 1.45581 | 0.942432 |
| H | -2.21754 | 1.441376 | -0.77189 |
| H | -2.45883 | -0.89165 | -0.52404 |
| H | -1.96211 | -0.86862 | 1.107605 |
| H | -0.35166 | 2.78251 | 0.25781 |
| H | 1.746272 | 1.547874 | -0.09695 |
| H | 1.720217 | -0.91092 | -0.49256 |

**Table A2.17, continued**

| | | | |
|---|---|---|---|
| H | -0.38219 | -2.18343 | -0.33122 |

**Table A2.18.** Coordinates for the optimized structure of $CHD^{-}$.

| | | | |
|---|---|---|---|
| C | -1.71894 | 1.06893 | -0.12987 |
| C | -1.62668 | -0.42851 | -0.02189 |
| C | -0.39378 | 1.651186 | 0.283477 |
| C | 0.762557 | 0.985705 | -0.0392 |
| C | 0.763164 | -0.3529 | -0.50868 |
| C | -0.45192 | -1.05875 | -0.33905 |
| H | -2.54151 | 1.463246 | 0.495781 |
| H | -2.00304 | 1.389351 | -1.17583 |
| H | -2.52147 | -1.0051 | 0.203338 |
| H | -0.35721 | 2.650854 | 0.729823 |
| H | 1.72668 | 1.480061 | 0.149079 |
| H | 1.699912 | -0.87955 | -0.70896 |
| H | -0.44221 | -2.15771 | -0.38123 |

**Table A2.19.** Coordinates for the optimized structure of $CHD^{rad}$.

| | | | |
|---|---|---|---|
| C | -1.69947 | 1.0425 | 0.00741 |
| C | -1.62625 | -0.42505 | -0.20962 |
| C | -0.36953 | 1.703426 | 0.085529 |
| C | 0.795117 | 0.999135 | -0.03641 |
| C | 0.792318 | -0.39879 | -0.24296 |
| C | -0.44318 | -1.0842 | -0.32486 |
| H | -2.2962 | 1.264975 | 0.920131 |
| H | -2.31918 | 1.516273 | -0.78639 |

**Table A2.19, continued**

| | | | |
|---|---|---|---|
| H | -2.56251 | -0.97117 | -0.2763 |
| H | -0.34397 | 2.784613 | 0.248043 |
| H | 1.75159 | 1.526533 | 0.027567 |
| H | 1.733008 | -0.94407 | -0.3396 |
| H | -0.44574 | -2.16617 | -0.48654 |

# Appendix 3: Supporting Data for Chapter 4

## A3.1 Kinetic Measurements

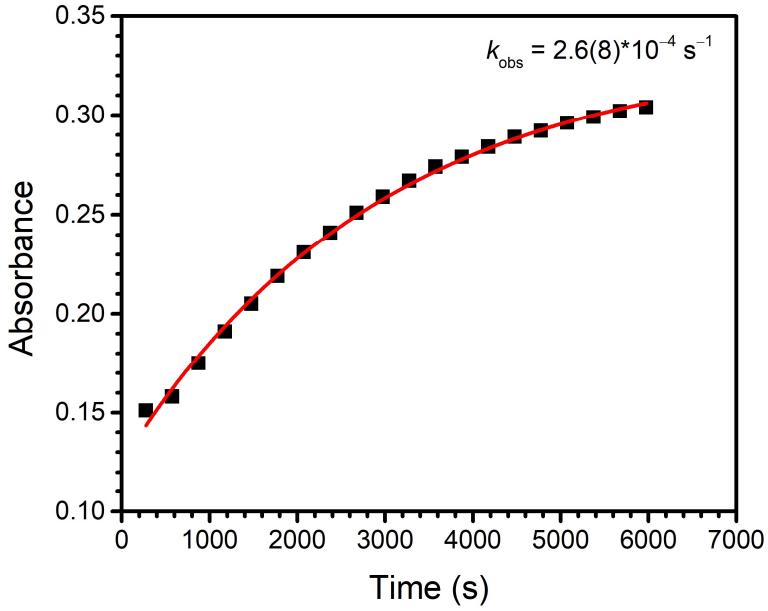


**Figure A3.1.** Representative exponential fit of a plot of A versus time for the reaction between **3$^{Ad}$** and 10 equivalents of 9-phenyl-9*H*-fluorene. The average *k* obtained from three trials was taken to be the observed rate constant, $k_{obs}$, for this reaction.

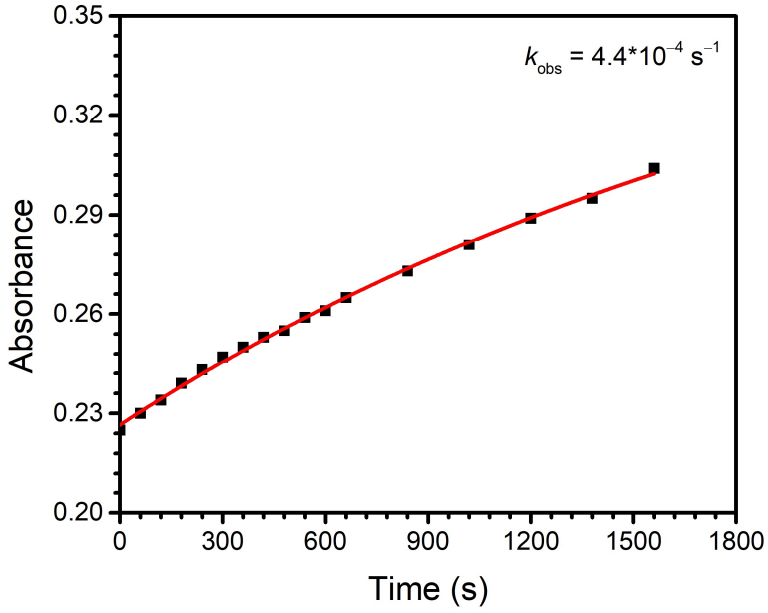


**Figure A3.2.** Representative exponential fit of a plot of A versus time for the reaction between $\mathbf{3^{Ad}}$ and 10 equivalents of indene. The average *k* obtained from three trials was taken to be the observed rate constant, $k_{obs}$, for this reaction.

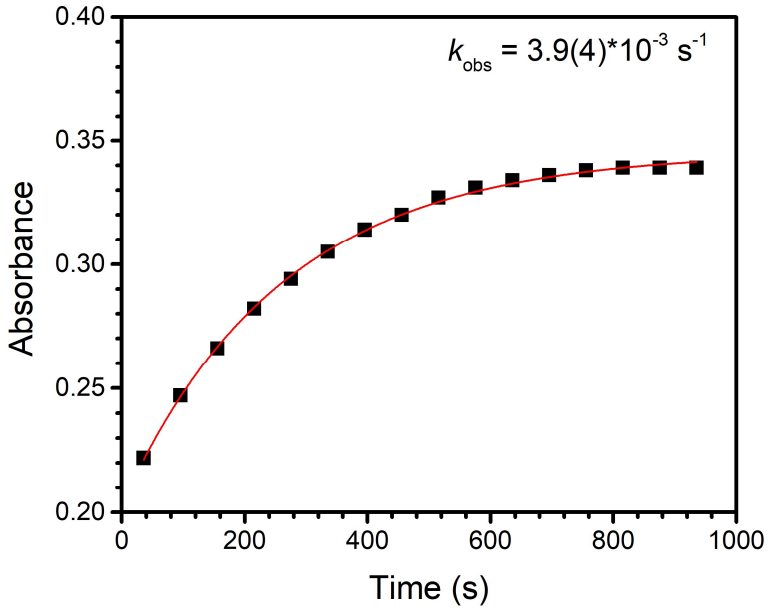


**Figure A3.3.** Representative exponential fit of a plot of A versus time for the reaction between $\mathbf{3^{Ad}}$ and 10 equivalents of 9-(4-(trifluoromethyl)phenyl)-9*H*-fluorene. The average *k* obtained from three trials was taken to be the observed rate constant, $k_{obs}$, for this reaction.

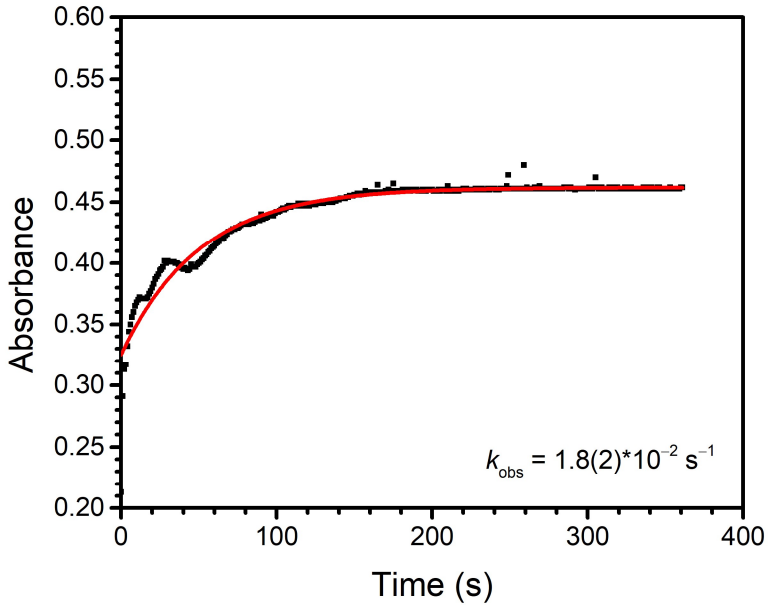


**Figure A3.4.** Representative exponential fit of a plot of A versus time for the reaction between **3**$^{\mathbf{Ad}}$ and 10 equivalents of 4-methoxy-2,6-di(*tert*-butyl)phenol at –100 °C in THF. The average *k* obtained from three trials was taken to be the observed rate constant, $k_{obs}$, for this reaction.

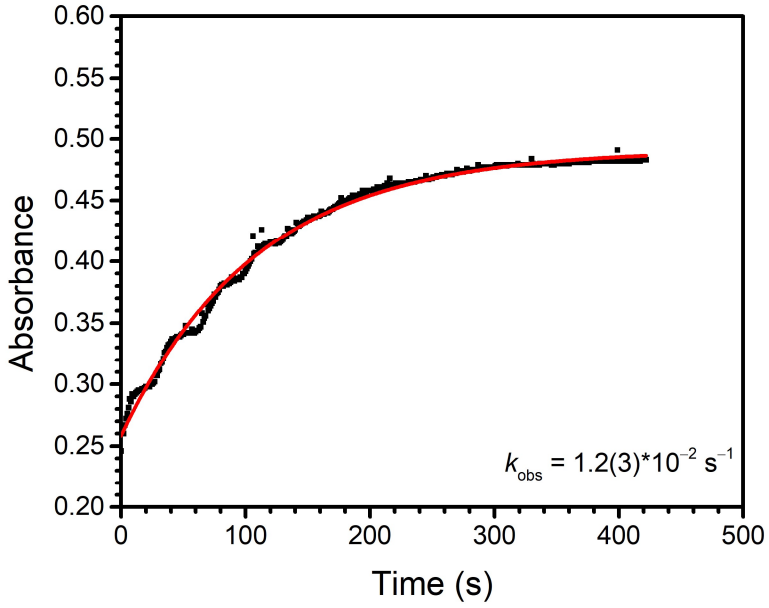


**Figure A3.5.** Representative exponential fit of a plot of A versus time for the reaction between **3**$^{\mathbf{Ad}}$ and 10 equivalents of 4-methyl-2,6-di(*tert*-butyl)phenol at –100 °C in THF. The average *k* obtained from three trials was taken to be the observed rate constant, $k_{obs}$, for this reaction.

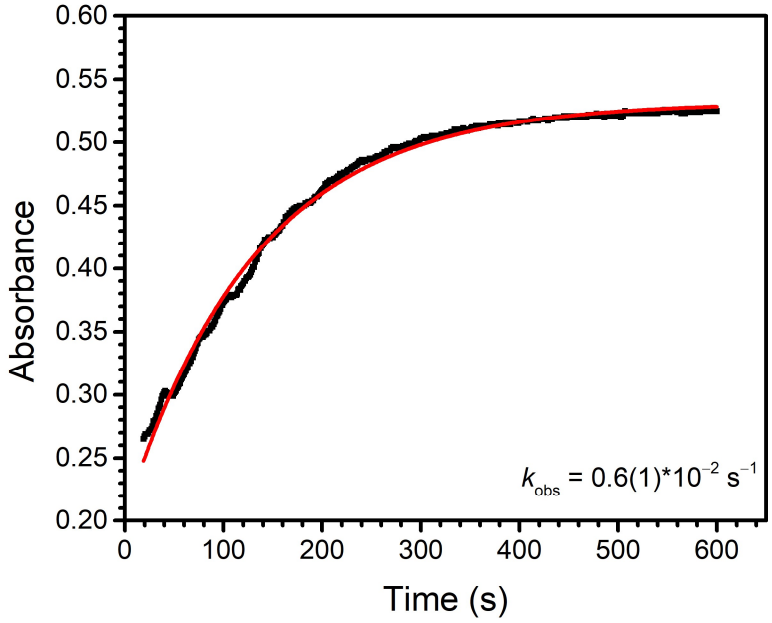


**Figure A3.6.** Representative exponential fit of a plot of A versus time for the reaction between **3**$^{\mathbf{Ad}}$ and 10 equivalents of 2,4,6-tri(*tert*-butyl)phenol at –100 °C in THF. The average *k* obtained from three trials was taken to be the observed rate constant, $k_{obs}$, for this reaction.

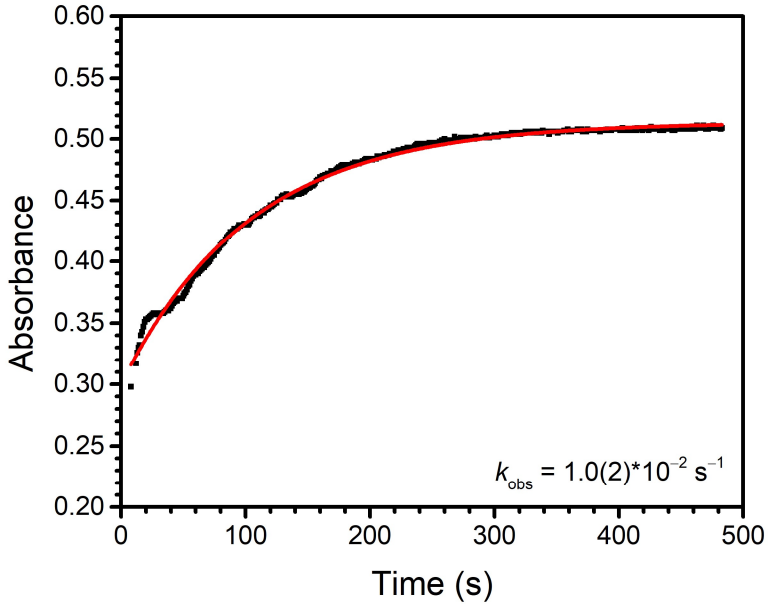


**Figure A3.7.** Representative exponential fit of a plot of A versus time for the reaction between **3**$^{\mathbf{Ad}}$ and 10 equivalents of 2,6-di(*tert*-butyl)phenol at –100 °C in THF. The average *k* obtained from three trials was taken to be the observed rate constant, $k_{obs}$, for this reaction.

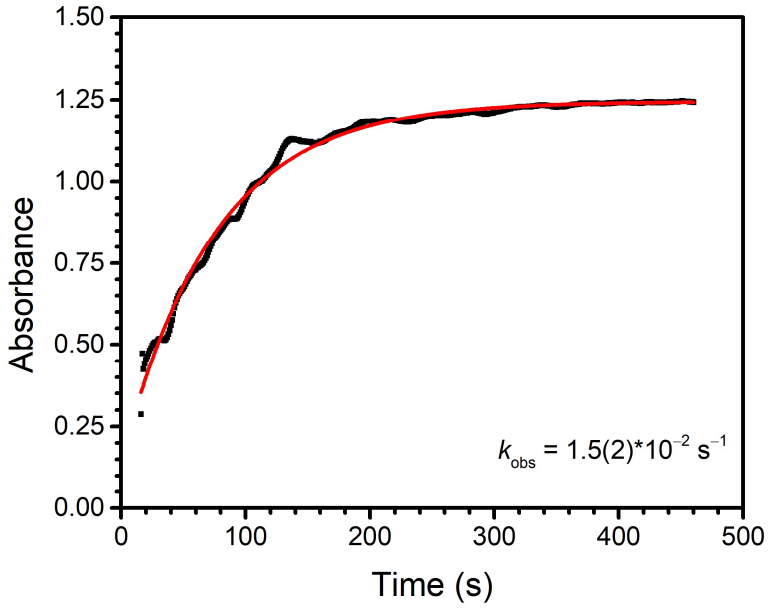


**Figure A3.8.** Representative exponential fit of a plot of A versus time for the reaction between $\mathbf{3^{Ad}}$ and 10 equivalents of 4-bromo-2,6-di(*tert*-butyl)phenol at –100 °C in THF. The average *k* obtained from three trials was taken to be the observed rate constant, $k_{obs}$, for this reaction.

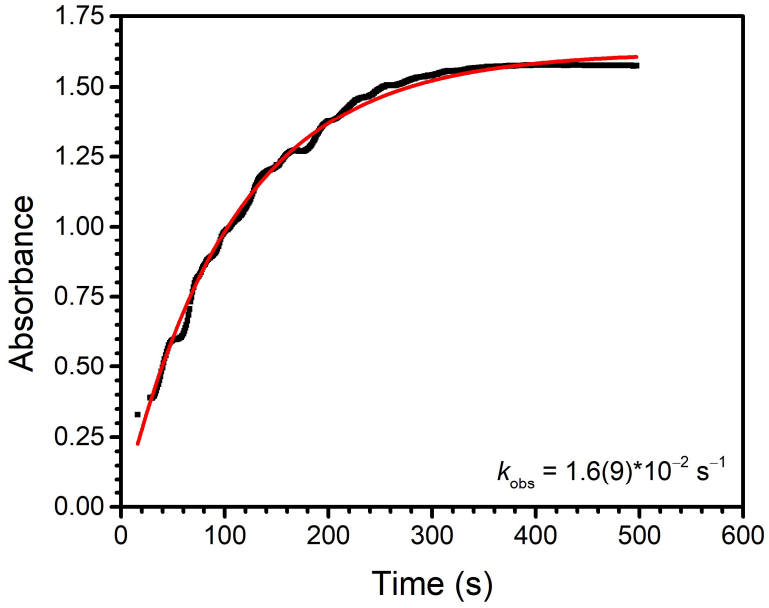


**Figure A3.9.** Representative exponential fit of a plot of A versus time for the reaction between $\mathbf{3^{Ad}}$ and 10 equivalents of methyl 4-hydroxy-3,5-di(*tert*-butyl)benzoate at –100 °C in THF. The average *k* obtained from three trials was taken to be the observed rate constant, $k_{obs}$, for this reaction.

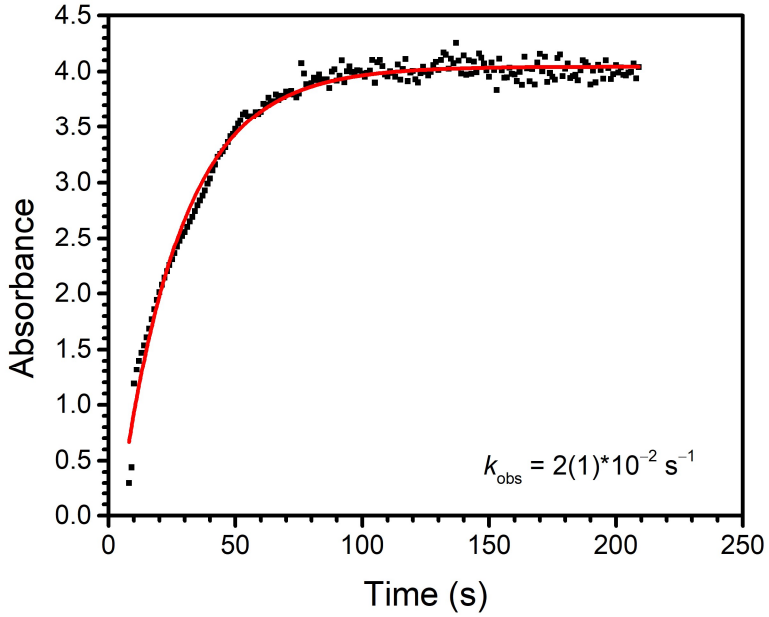


**Figure A3.10.** Representative exponential fit of a plot of A versus time for the reaction between **3**$^{\mathbf{Ad}}$ and 10 equivalents of 4-nitro-2,6-di(*tert*-butyl)phenol at –100 °C in THF. The average *k* obtained from three trials was taken to be the observed rate constant, $k_{obs}$, for this reaction.

## A3.2 UV-vis Spectra

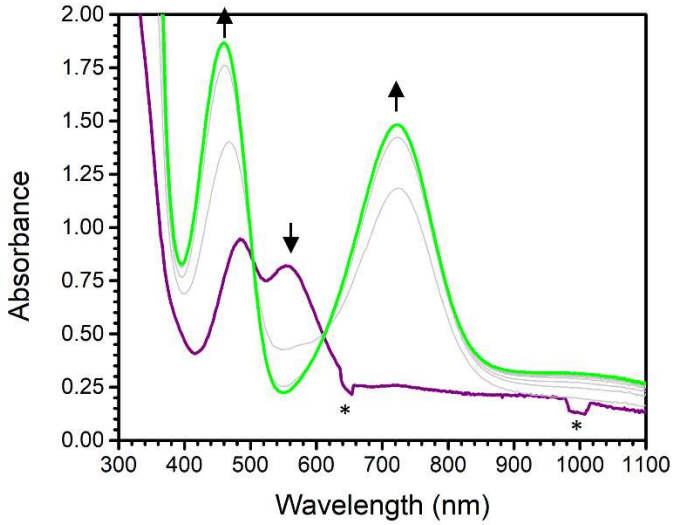


**Figure A3.11.** Representative UV-vis spectra for the reaction between **3**$^{\mathbf{Ad}}$ and 10 equivalents of methyl 4-hydroxy-3,5-di(*tert*-butyl)benzoate at –80 °C in THF showing the formation of **2**$^{\mathbf{Ad}}$ (green spectrum). Asterisks indicate a baseline error.

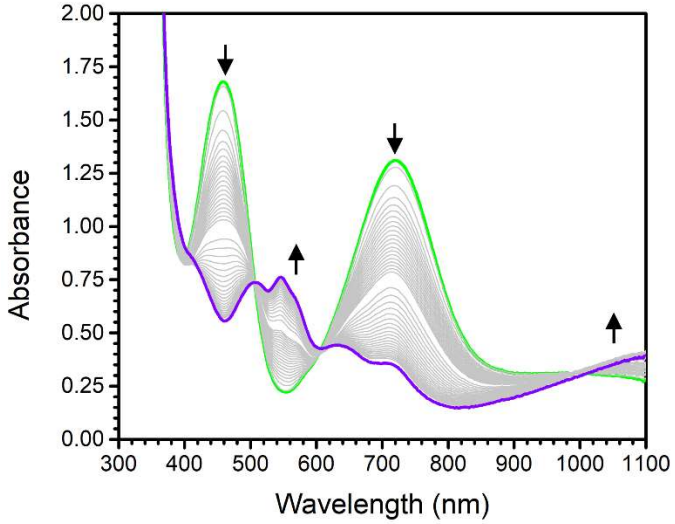


**Figure A3.12.** Representative UV-vis spectra showing the formation of **1**$^{\mathbf{Ad}}$ (violet spectrum) after the reaction between **3**$^{\mathbf{Ad}}$ and 10 equivalents of methyl 4-hydroxy-3,5-di(*tert*-butyl)benzoate that produced **2**$^{\mathbf{Ad}}$ (green spectrum) is warmed to 0 °C.

## A3.3 Additional Thermodynamic Data for Substituted Phenols

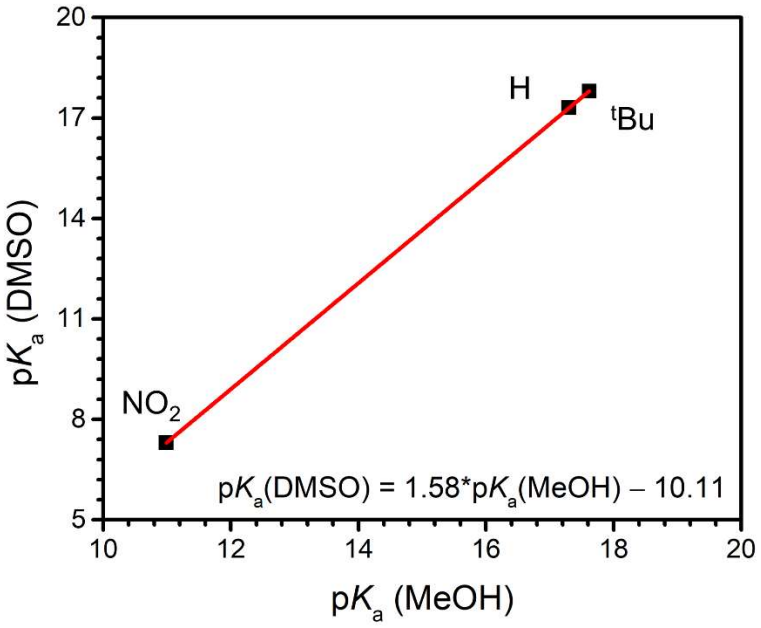


**Figure A3.13.** Plot of p$K_a$ values reported in DMSO and MeOH for some 4-X-2,6-di(*tert*-butyl)phenols used to estimate the p$K_a$ of 4-bromo-2,6-di(*tert*-butyl)phenol in DMSO.

# Appendix 4: Supporting Data for Chapter 5

## A4.1 NMR Spectra

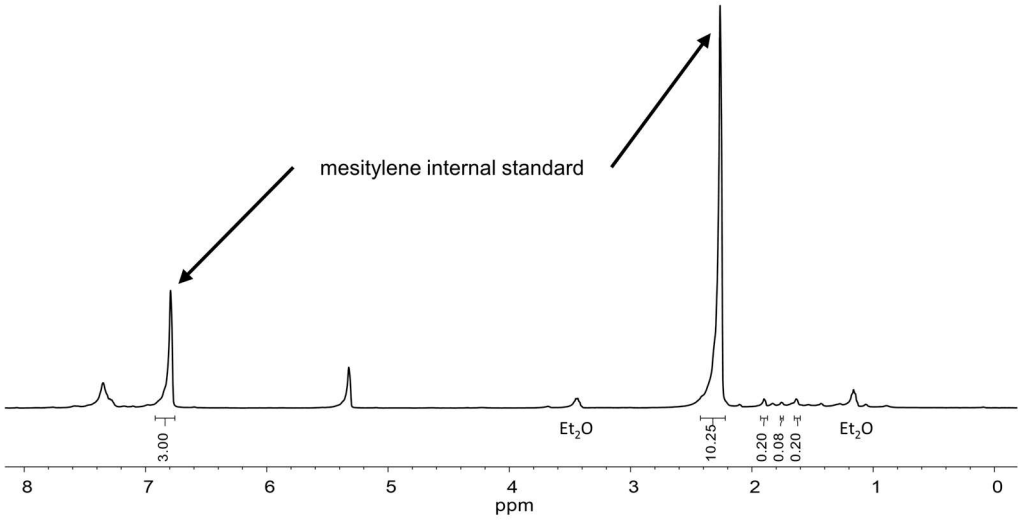


**Figure A4.1.** $^{1}$H NMR spectrum of $\mathbf{1^{dim}}$ in $CD_2Cl_2$ at room temperature. Mesitylene was added as an internal standard (1:1 assuming the molecular weight of $\mathbf{1^{dim}}$ as drawn in Scheme 5.1).

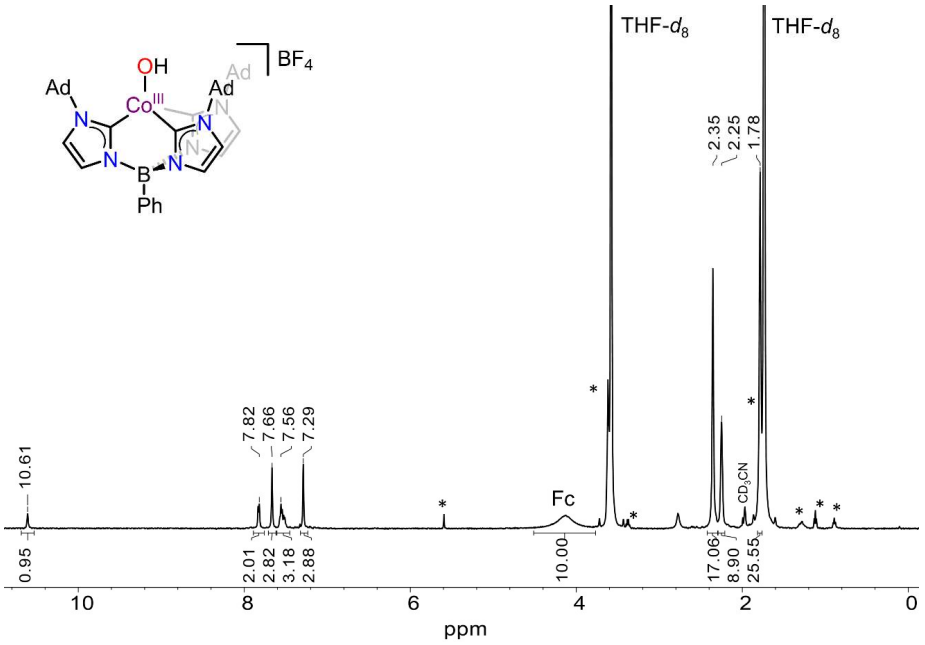


**Figure A4.2.** $^{1}$H NMR spectrum of **3** in THF-$d_8$ at –35 °C. Asterisks indicate solvent impurities (DCM, $Et_2O$, THF, pentane). $CD_3CN$ and Fc are present due to the in situ preparation of **3** from **2**.

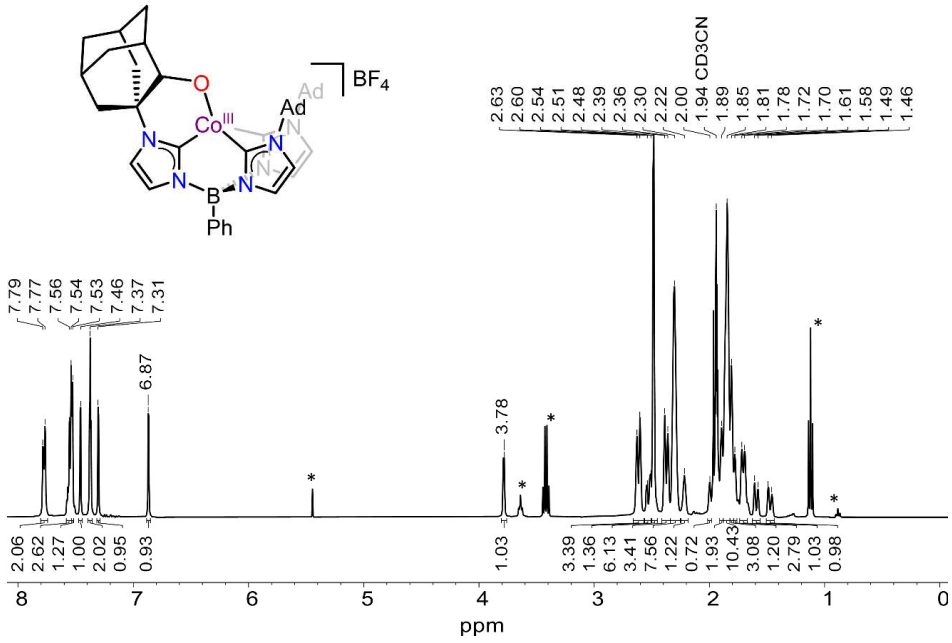


**Figure A4.3.** $^{1}$H NMR spectrum of **5** in $CD_3CN$ at room temperature. Asterisks indicate solvent impurities (DCM, $Et_2O$, pentane).

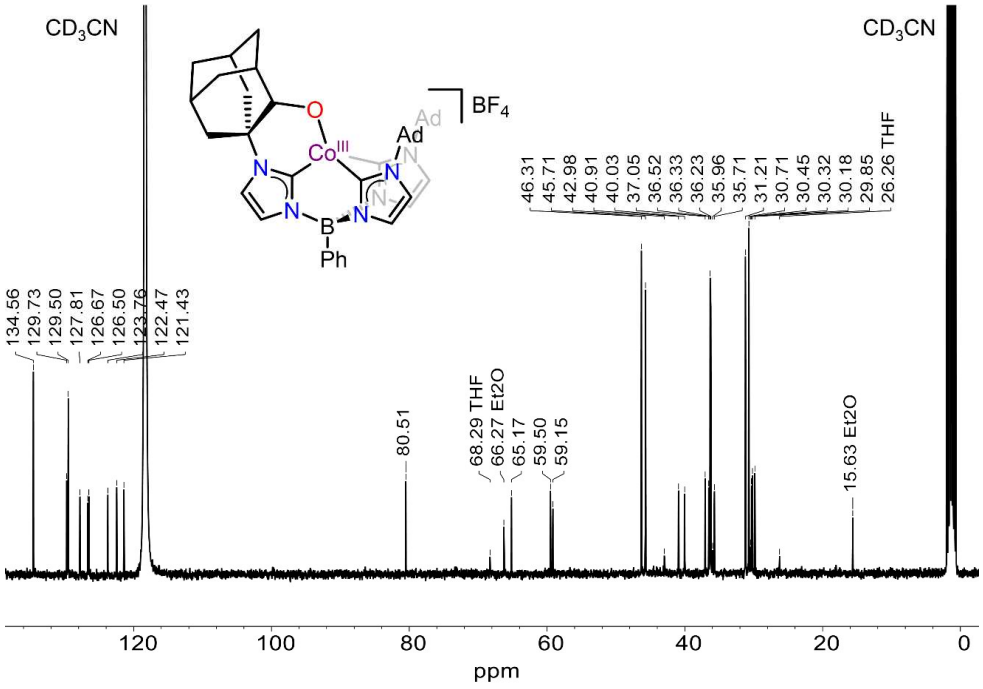


**Figure A4.4.** $^{13}C$ NMR spectrum of **5** in $CD_3CN$ at room temperature.

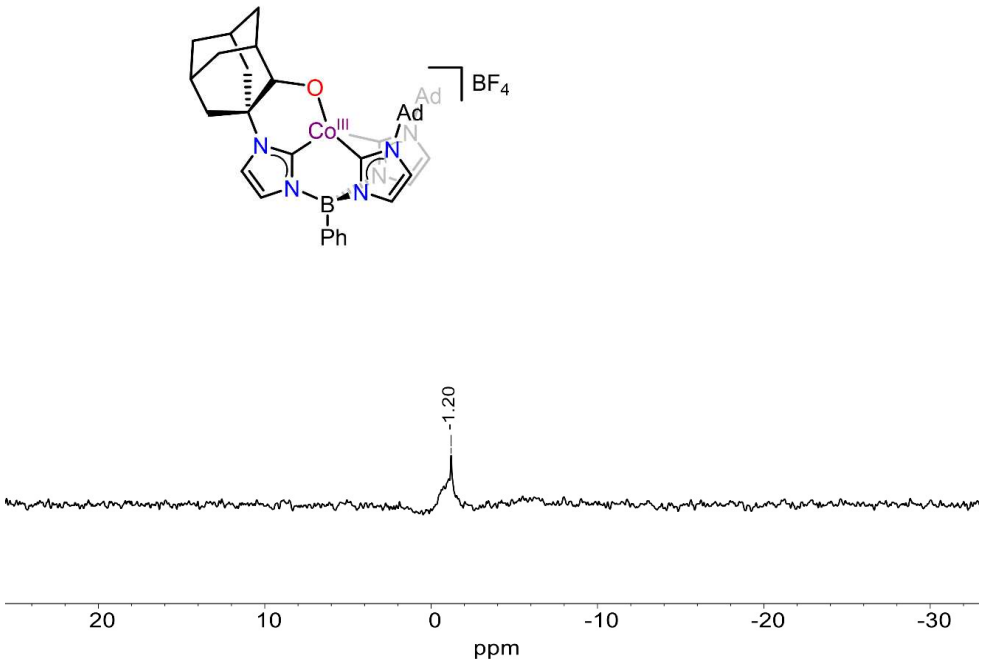


**Figure A4.5.** $^{11}B$ NMR spectrum of **5** in $CD_3CN$ at room temperature. The signals from $BF_4^-$ and the ligand overlap.

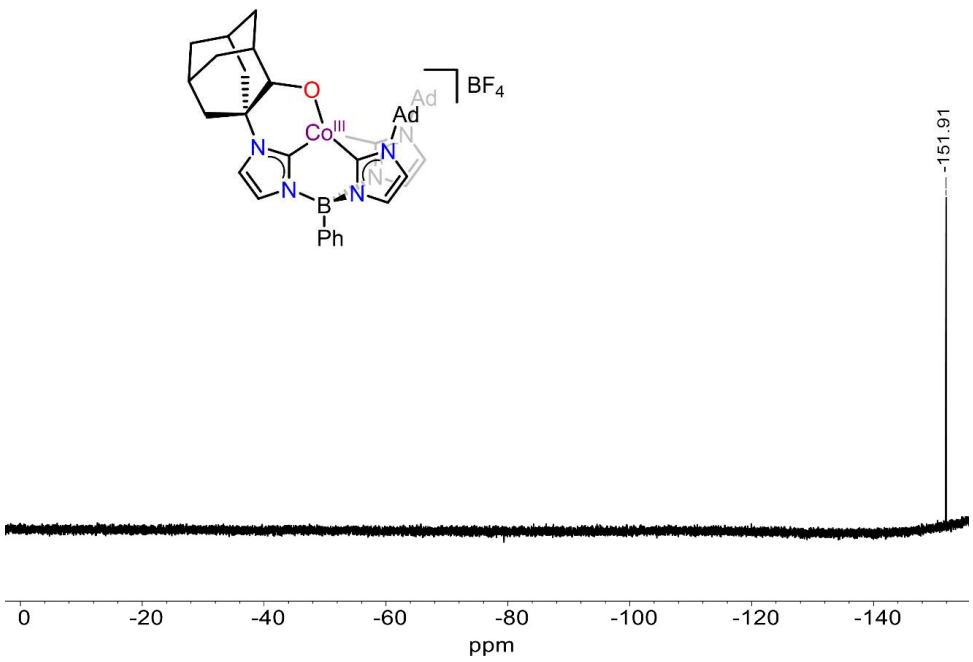


**Figure A4.6.** $^{19}F$ NMR spectrum of **5** in $CD_3CN$ at room temperature.

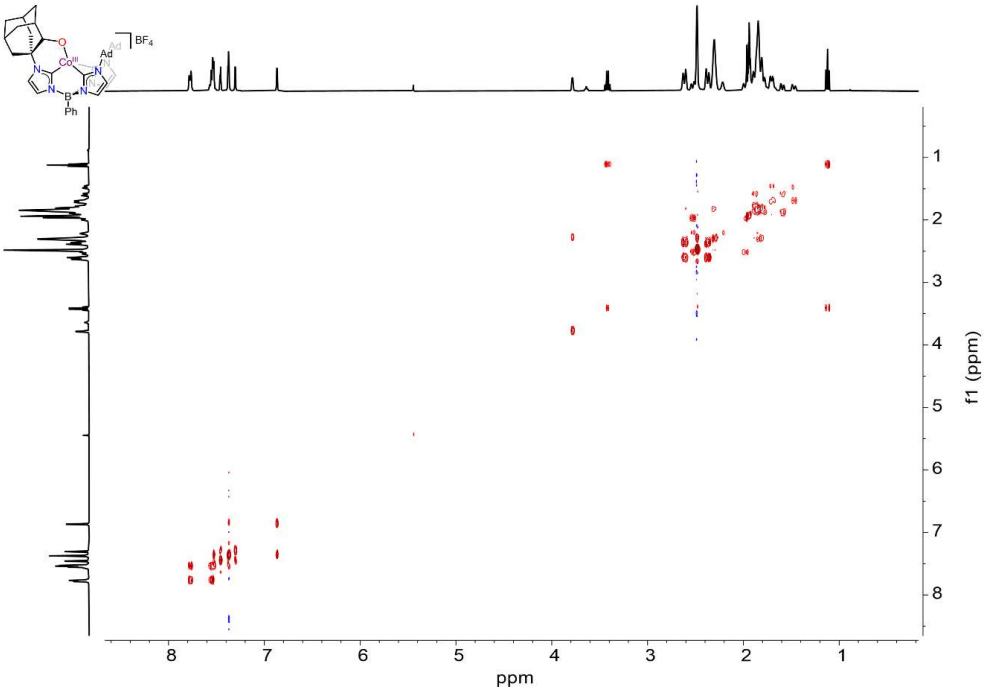


**Figure A4.7.** $^{1}H/^{1}H$ COSY NMR spectrum of **5** in $CD_3CN$ at room temperature.

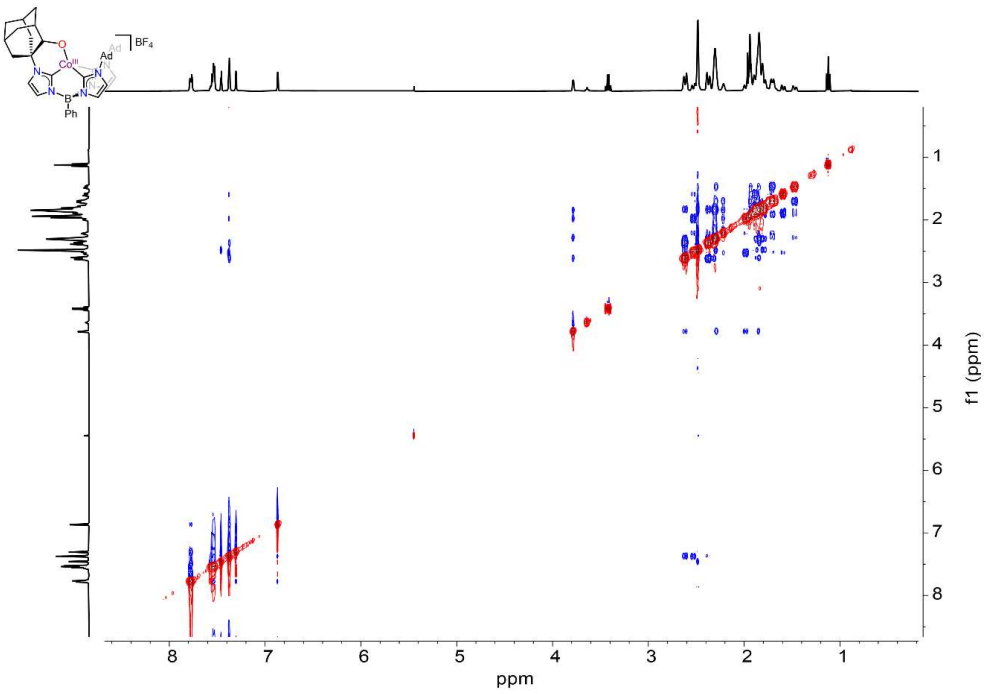


**Figure A4.8.** $^{1}H/^{1}H$ NOESY NMR spectrum of **5** in $CD_3CN$ at room temperature.

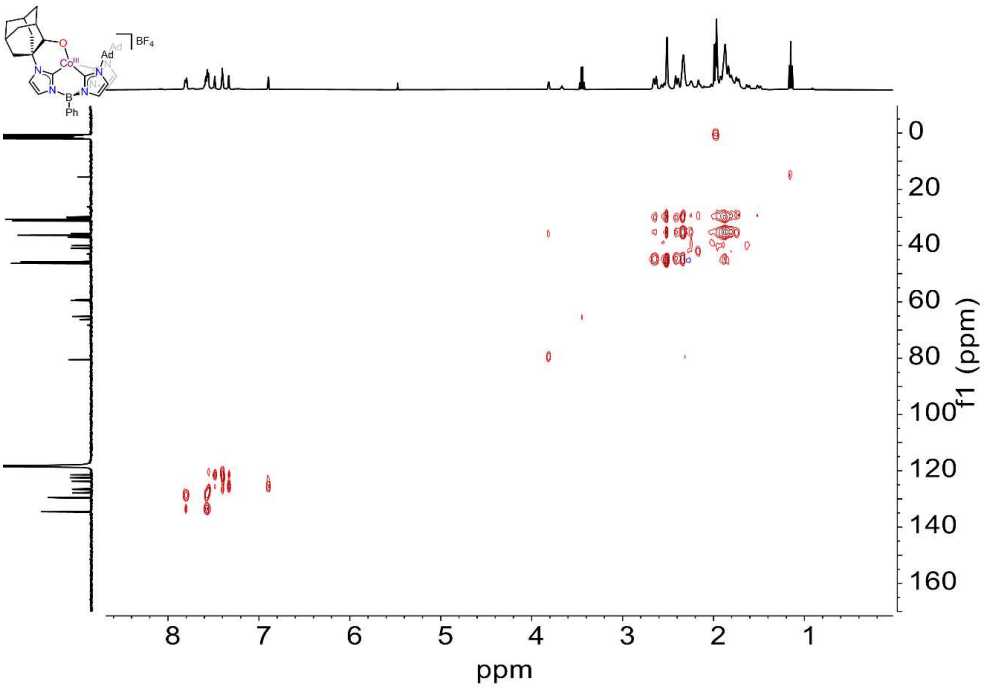


**Figure A4.9.** $^{1}H/^{13}C$ HSQC NMR spectrum of **5** in $CD_3CN$ at room temperature.

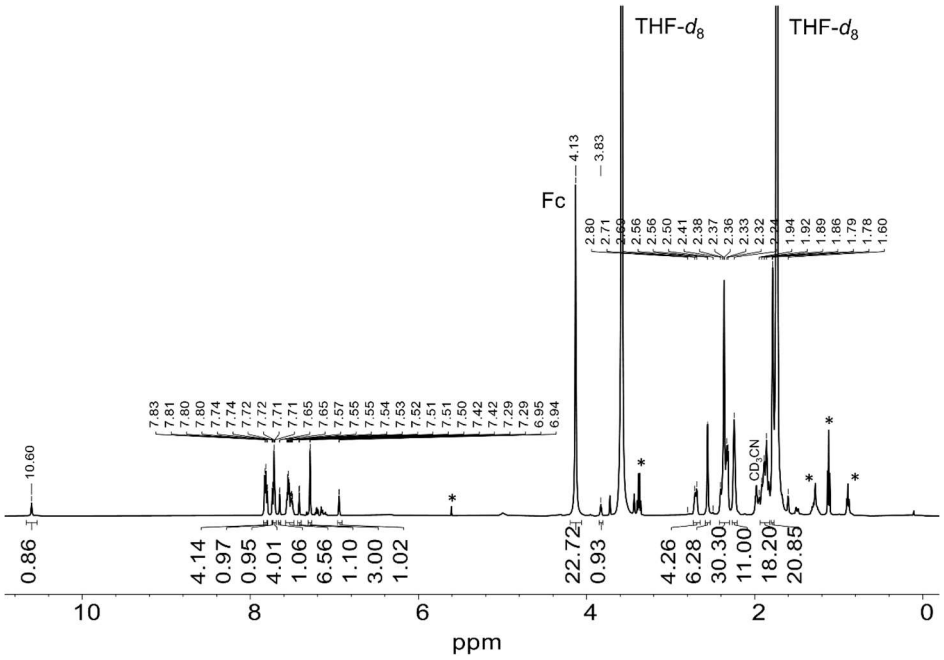


**Figure A4.10.** $^1$H NMR spectrum of **4** reacted with 1 equivalent $FcBF_4$ in THF-$d_8$ collected at –30 °C. Asterisks indicate solvent impurities (DCM, $Et_2O$, pentane).

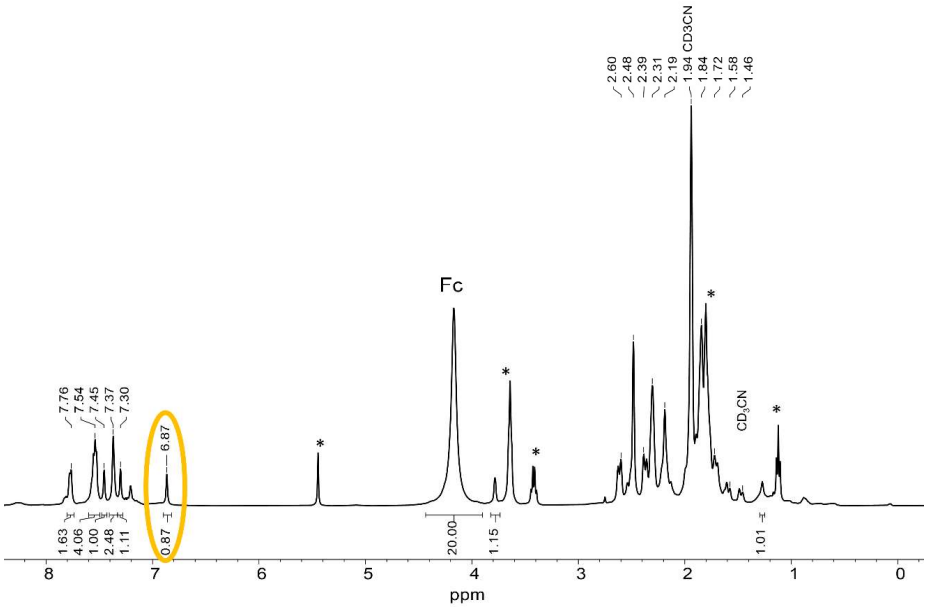


**Figure A4.11.** $^1$H NMR spectrum of the reaction mixture of **4** + KO$^t$Bu + 2 $FcBF_4$ collected at room temperature in $CD_3CN$ showing ~90% yield of **5** (yellow circle, expected 1H) relative to 2 Fc (20H).

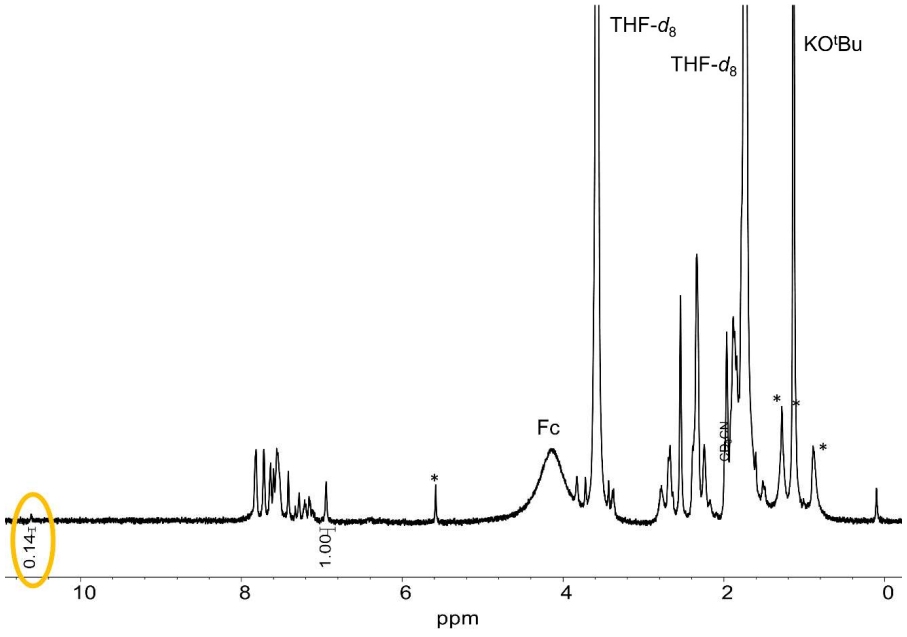


**Figure A4.12.** $^1$H NMR spectrum of the reaction mixture of **4** + KO$^t$Bu + 2 $FcBF_4$ collected at –35 °C in THF-$d_8$ showing very little formation of **3** (yellow circle, expected 1H) relative to **5** (1H).

## A4.2 UV-vis Spectra

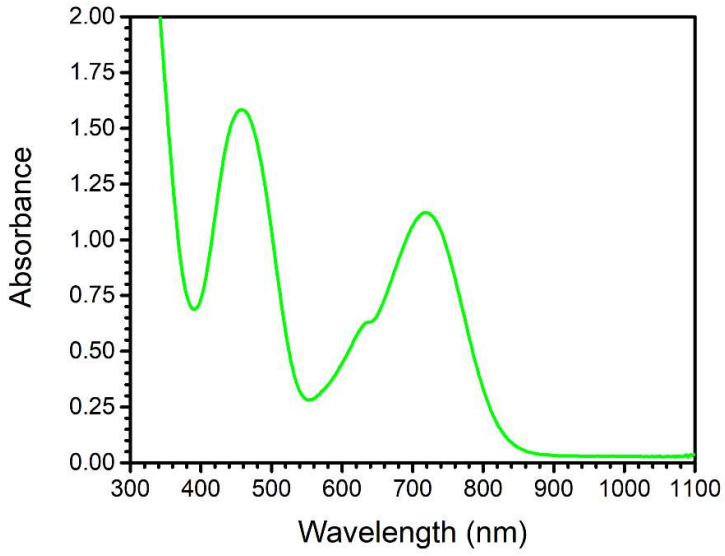


**Figure A4.13.** UV-vis spectrum of in situ prepared **3** in THF (1.25 mM) at –80 °C.

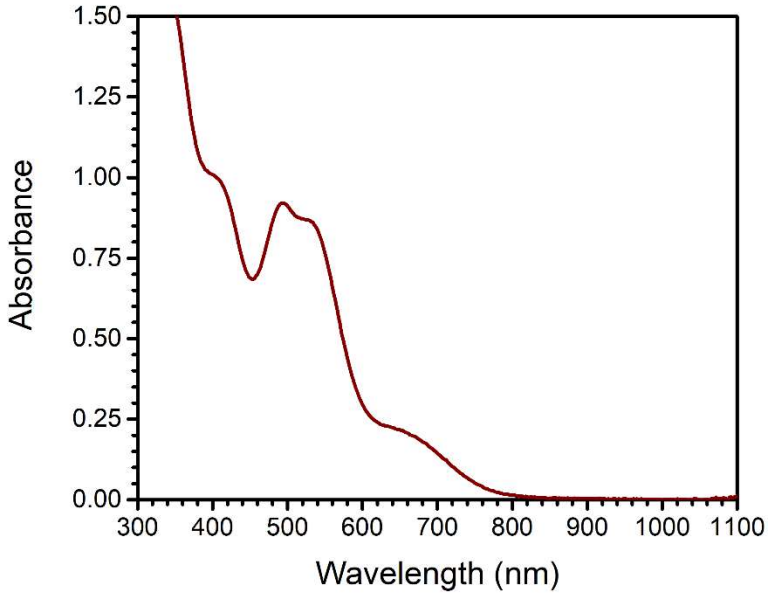


**Figure A4.14.** UV-vis spectrum of **5** in MeCN (1.25 mM) at room temperature.

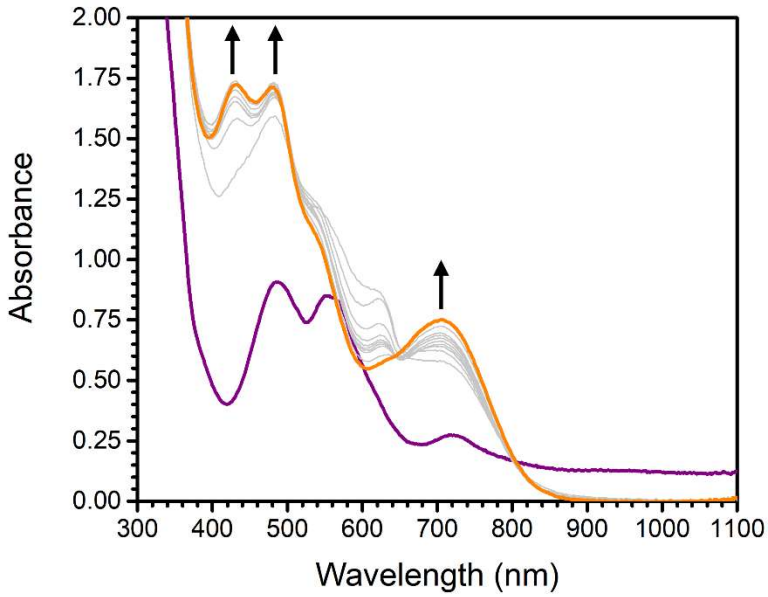


**Figure A4.15.** Oxidation of **4** (purple) with 1 equivalent $FcBF_4$ carried out at –80 °C (1.25 mM in THF) to produce a mixture of **3** and **5** (orange). Each spectrum was collected at 45 second intervals.

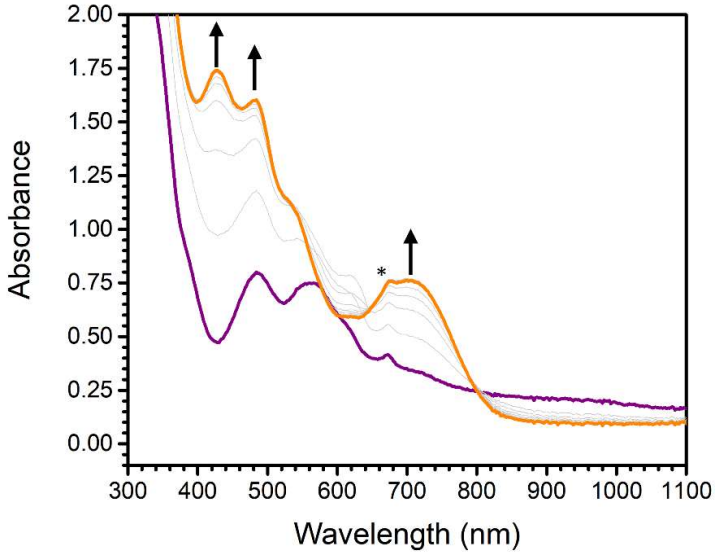


**Figure A4.16.** Oxidation of **4** (purple) with 1 equivalent $FcBF_4$ carried out at –105 °C (1.25 mM in THF) to produce a mixture of **3** and **5** (orange). Each spectrum was collected at 45 second intervals. The asterisk indicates a small impurity of $PhB(^{Ad}Im)_3Co^{II}Cl$.

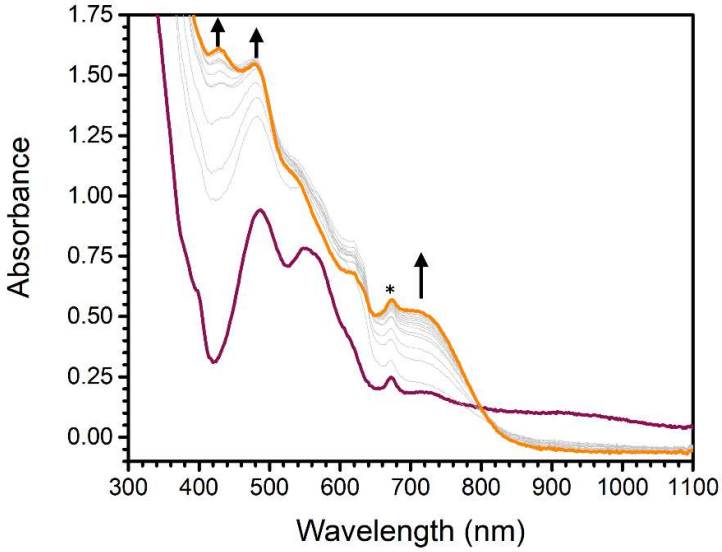


**Figure A4.17.** Oxidation of **4** (purple) with 1 equivalent $FcBF_4$ carried out at –130 °C (1.25 mM in 2-MeTHF) to produce a mixture of **3** and **5** (orange). Each spectrum was collected at 45 second intervals. The asterisk indicates a small impurity of $PhB(^{Ad}Im)_3Co^{II}Cl$.

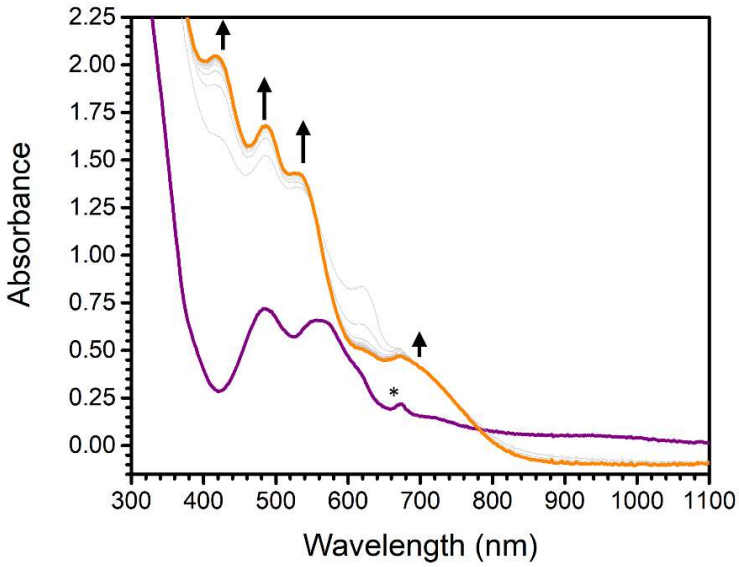


**Figure A4.18.** Oxidation of **4** (purple) with 2 equivalents of $FcBF_4$ in the presence of 1 equivalent of $KO^tBu$ at –80 °C (1.25 mM in THF) to produce majority **5** (orange). Spectra were collected at 45 second intervals. The asterisk indicates a small impurity of $PhB(^{Ad}Im)_3Co^{II}Cl$.

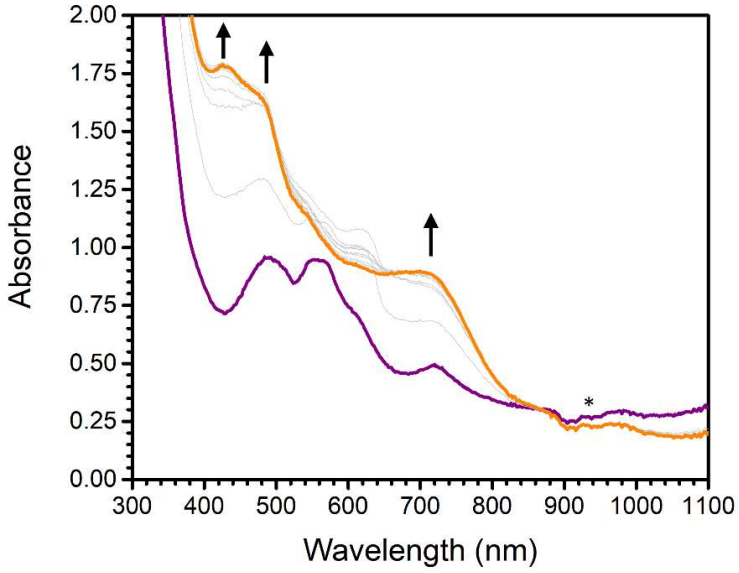


**Figure A4.19.** Oxidation of **4-*d*$_{45}$** (purple) with 1 equivalent (relative to total Co) $FcBF_4$ at –105 °C (1.25 mM Co in THF-$d_8$). Spectra were collected at 45 second intervals. The asterisk indicates a baseline error.

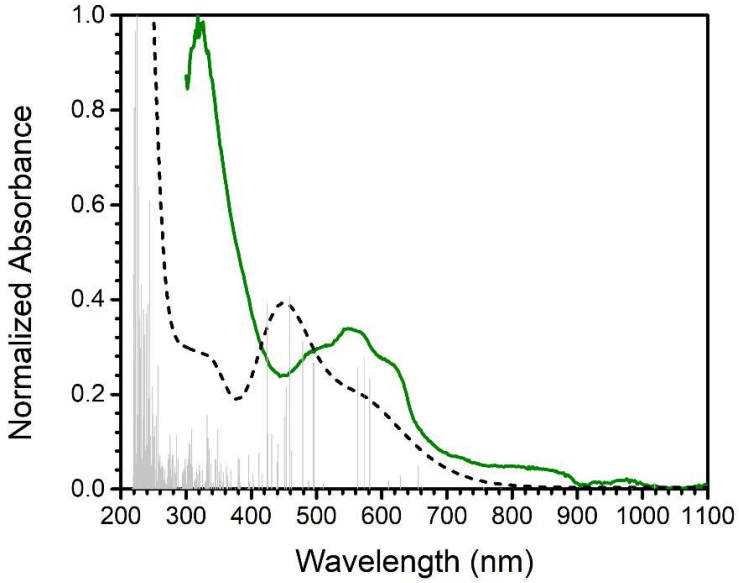


**Figure A4.20.** Overlay of predicted $\mathbf{4^{ox}}$ spectrum (black dashed line) and experimental $\mathbf{4^{ox}}$-$\boldsymbol{d_{45}}$ spectrum (green) obtained by subtracting 29% of a 1.25 mM spectrum of **3** from the first spectrum collected after addition of $FcBF_4$ to **4**-$\boldsymbol{d_{45}}$. The gray bars show the TD-DFT predicted transitions.

## A4.3 Kinetic Data

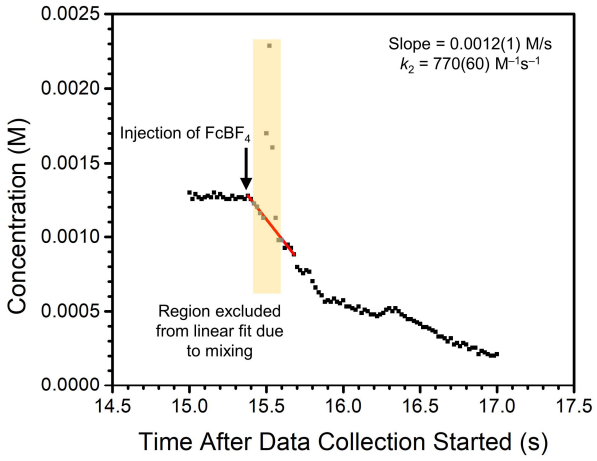


**Figure A4.21.** Representative linear fit of the concentration versus time profile for the oxidation of **4** with $FcBF_4$ at –40 °C monitored at 940 nm. The $k_2$ value was computed by dividing the slope of the linear fit by the product of the initial concentrations of $FcBF_4$ and **4**, 1.25 mM each.

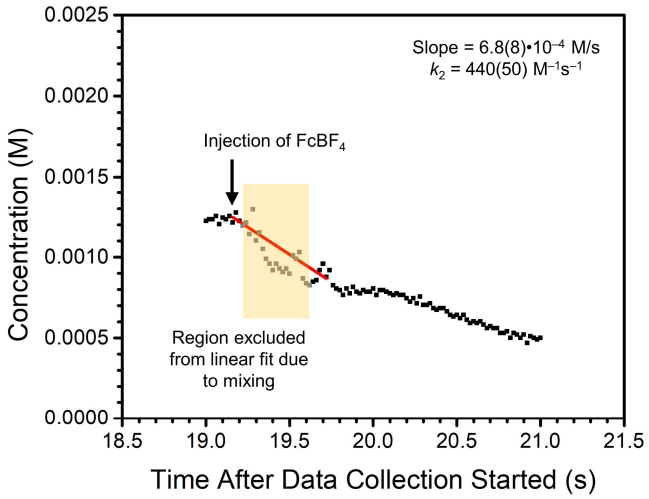


**Figure A 4.22.** Representative linear fit of the concentration versus time profile for the oxidation of **4** with $FcBF_4$ at –80 °C monitored at 940 nm. The $k_2$ value was computed by dividing the slope of the linear fit by the product of the initial concentrations of $FcBF_4$ and **4**, 1.25 mM each.

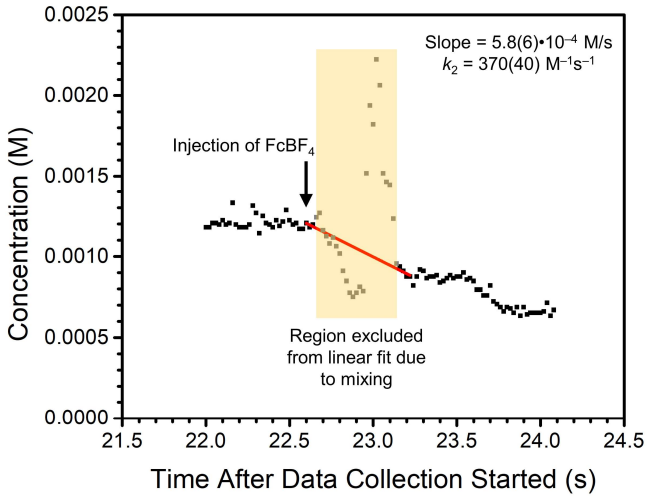


**Figure A4.23.** Representative linear fit of the concentration versus time profile for the oxidation of **4** with $FcBF_4$ at –105 °C monitored at 940 nm. The $k_2$ value was computed by dividing the slope of the linear fit by the product of the initial concentrations of $FcBF_4$ and **4**, 1.25 mM each.

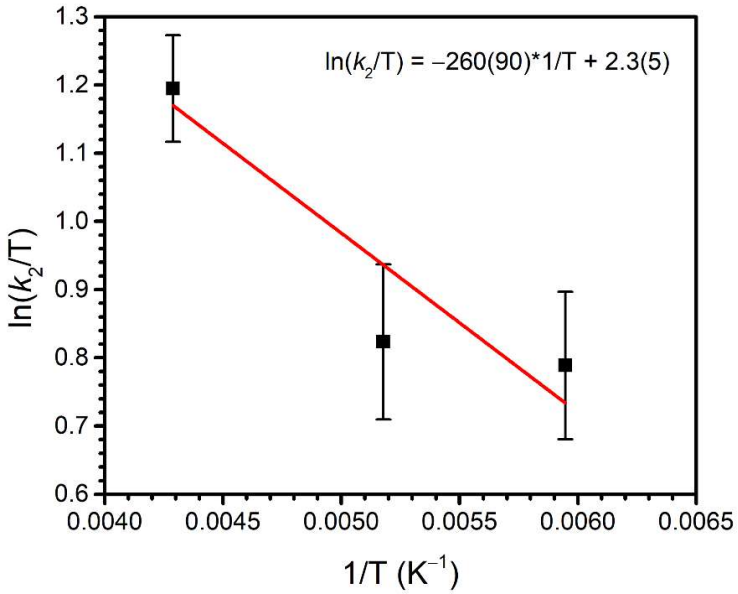


**Figure A4.24.** Eyring analysis plot of the oxidation of **4** with $FcBF_4$.

## A4.4 IR Spectra

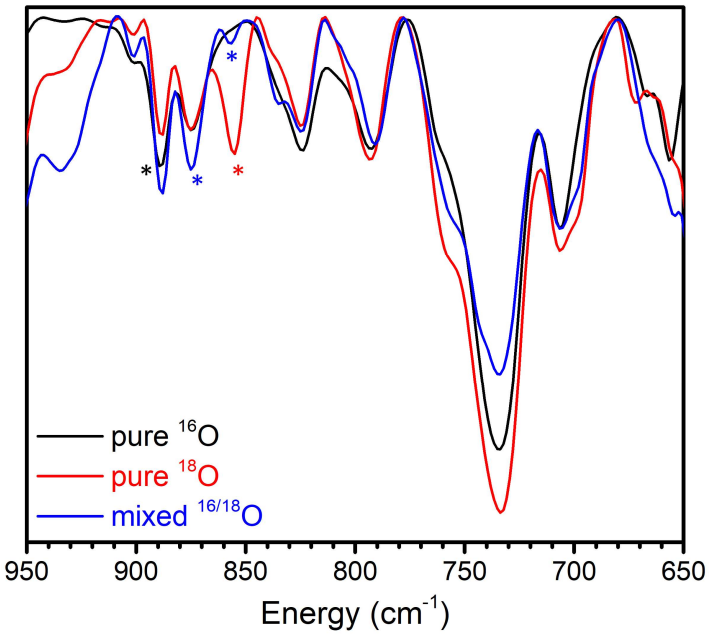


**Figure A4.25.** IR spectra of $\mathbf{1}^{\mathbf{dim}}$ and its isotopologues collected as KBr pellets.

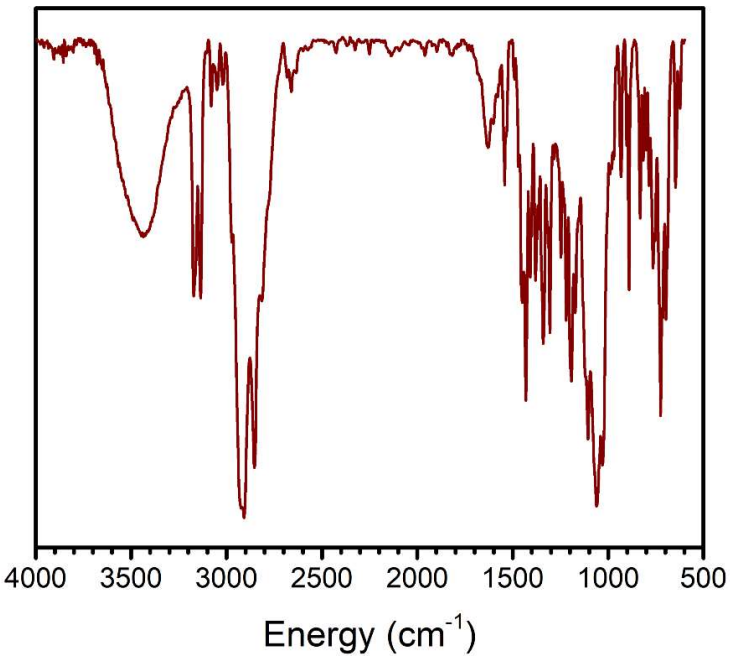


**Figure A4.26.** IR spectrum of **5** collected as a KBr pellet.

## A4.5 Cyclic Voltammograms

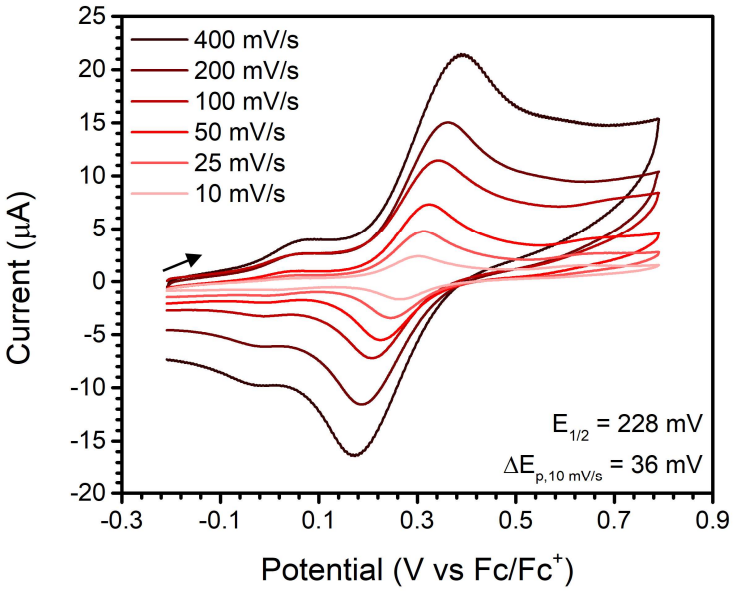


**Figure A4.27.** CV of $\mathbf{1}^{\mathbf{dim}}$ collected in MeCN at variable scan rates. Conditions: 3 mM $\mathbf{1}^{\mathbf{dim}}$, 0.1 M $TBAPF_6$.

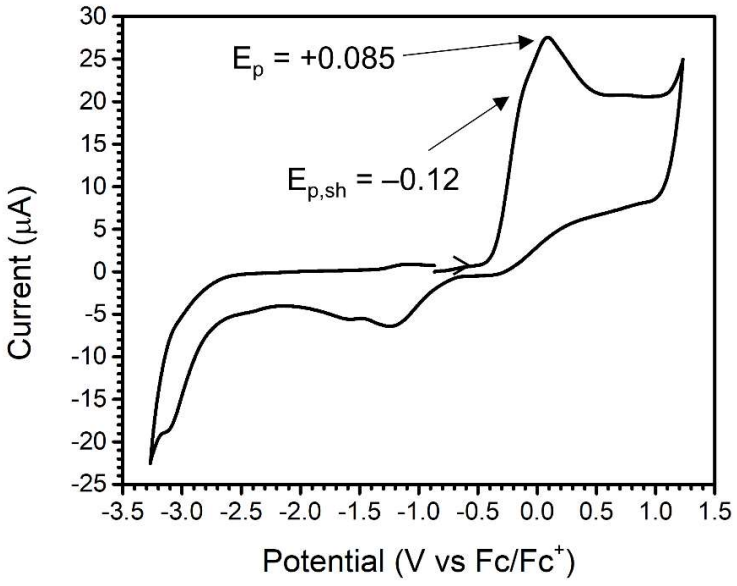


**Figure A4.28.** CV of **4** in THF. Conditions: 3 mM **4**, 0.1 M $TBAPF_6$. Externally referenced to $Fc/Fc^+$.

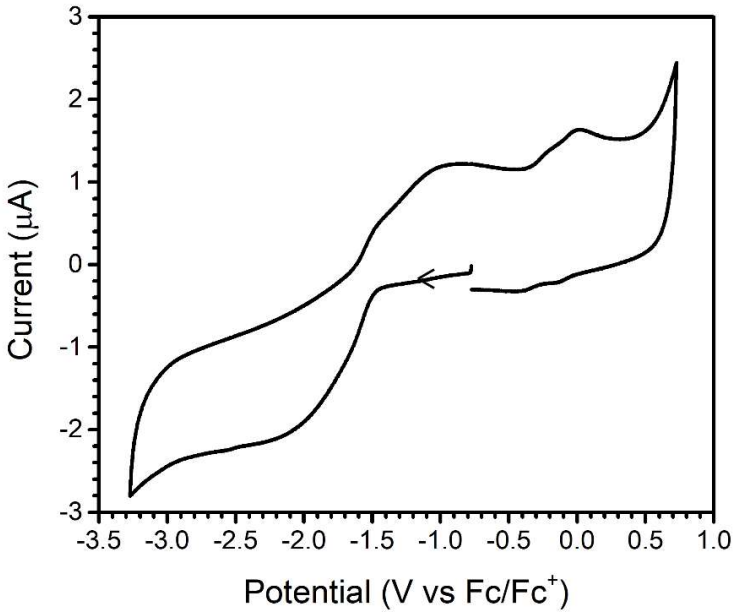


**Figure A4.29.** CV of **5** in THF. Conditions: 3 mM **5**, 0.1 M $TBAPF_6$. Externally referenced to $Fc/Fc^+$.

## A4.6 Thermodynamic Square Schemes and Reaction Coordinates

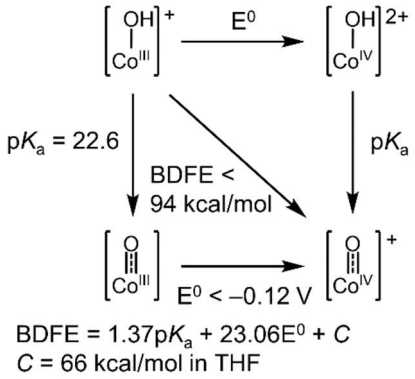


**Scheme A4.1.** Thermodynamic square scheme used to upper bound the $BDFE_{O–H}$ in **3**.

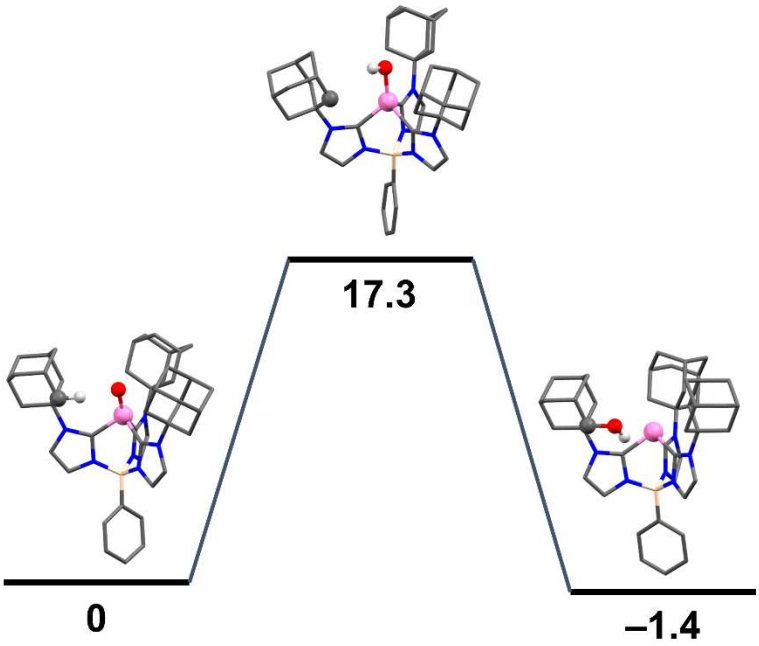


**Figure A4.30.** Ground state reaction coordinate for intramolecular C–H activation and rebound from **4**. The structures shown are the DFT optimized structures of the intermediates, shown as sticks except for Co, O, the transferring H–atom, and the involved C–atom. The energies given are the calculated free energies at –80 °C, relative to **4**, in kcal/mol.

## A4.7 Crystallographic Data

**Table A4.1.** Selected bond lengths and angles for complex **5**.

| | Complex **5** |
|---|---|
| **Bond Lengths (Å)** | |
| Co1–Cl1 | |
| Co1–O1 | 1.784 |
| Co–$C_{avg}$ | 1.859 |
| | |
| **Bond Angles (°)** | |
| B1–Co1–Cl1 | |
| B1–Co1–O1 | 142.6 |
| C1–Co1–C4 | 87.4 |
| C4–Co1–C7 | 90.4 |
| C7–Co1–C1 | 87.2 |

**Table A4.2.** Crystallographic and refinement data for complex **5**.

| Compound | **5** |
|---|---|
| Empirical formula | $C_{77}H_{66.5}B_2CoF_{24}N_6O$ |
| Formula weight | 1628.41 |
| Temperature/K | 100(2) |
| Crystal system | orthorhombic |
| Space group | Pbca |
| a/Å | 27.810(3) |
| b/Å | 16.6399(18) |
| c/Å | 34.619(4) |
| α/° | 90 |
| β/° | 90 |
| γ/° | 90 |
| Volume/$Å^3$ | 16020(3) |
| Z | 8 |
| $\rho_{calc}g/cm^3$ | 1.350 |
| $\mu/mm^{-1}$ | 0.316 |
| F(000) | 6652.0 |
| Crystal size/$mm^3$ | 0.272 × 0.065 × 0.052 |
| Radiation | MoKα (λ = 0.71073) |
| 2Θ range for data collection/° | 4.484 to 41.682 |
| Index ranges | $-27 \leq h \leq 27$, $-16 \leq k \leq 16$, $-31 \leq l \leq 34$ |
| Reflections collected | 80545 |

**Table A4.2, continued**

| | |
|---|---|
| Independent reflections | 8410 [$R_{int}$ = 0.3253, $R_{sigma}$ = 0.1573] |
| Data/restraints/parameters | 8410/727/809 |
| Goodness-of-fit on $F^2$ | 1.025 |
| Final R indexes [I>=2σ (I)] | $R_1$ = 0.0935, $wR_2$ = 0.2213 |
| Final R indexes [all data] | $R_1$ = 0.1871, $wR_2$ = 0.2693 |
| Largest diff. peak/hole / e $Å^{-3}$ | 1.12/-0.45 |

## A4.8 Density Functional Theory Calculations

**Table A4.3.** Coordinates for the optimized structure of $PhB(^{Ad}Im)_3Co^{III}O$ (*S* = 0, **4**).

| | | | |
|---|---|---|---|
| Co | 0.03725098540100 | -0.00115732408001 | 0.00950771938706 |
| O | 0.69334699334279 | 0.01341845347968 | 1.52428818436862 |
| C | 0.78344010579972 | -1.33936616270509 | -1.08893752710622 |
| N | 1.35871311956813 | -2.55312664673451 | -0.82809299651631 |
| C | 1.70294561706899 | -3.15722632346845 | 0.48348198772896 |
| C | 2.75635145696057 | -2.29935728786411 | 1.19083864474046 |
| H | 3.64575496619706 | -2.23473464034920 | 0.55352386768597 |
| H | 2.35309744759194 | -1.29512671091018 | 1.32803694969451 |
| C | 0.45537275700591 | -3.28299443034442 | 1.36090973556934 |
| H | 0.01932154851151 | -2.28568347678821 | 1.50551888319993 |
| H | -0.29076754046511 | -3.91356316876063 | 0.84518155396910 |
| C | 2.28973935262478 | -4.56229623151310 | 0.29100236851527 |
| H | 1.56334057595103 | -5.21336345577288 | -0.22568566047098 |
| H | 3.20082532630307 | -4.51541524489680 | -0.32900617523943 |
| C | 3.11251193117859 | -2.91177513049111 | 2.54360090522020 |
| H | 3.85740549436368 | -2.26412303177567 | 3.03658848190769 |
| C | 0.82110232539034 | -3.88761913209152 | 2.71558705384152 |
| H | -0.09173899050845 | -3.94704780707865 | 3.33422482561078 |
| C | 2.64983129253712 | -5.17919843914293 | 1.64363894895372 |

**Table A4.3, continued**

| | | | |
|---|---|---|---|
| H | 3.06532790268020 | -6.18551084845251 | 1.46216168716410 |
| C | 3.69109897233926 | -4.30901564120897 | 2.34294308514234 |
| H | 4.61404384437907 | -4.25922184183532 | 1.73725595340146 |
| H | 3.96465639966831 | -4.75579287984027 | 3.31587932139573 |
| C | 1.85528632013599 | -3.00058085551845 | 3.40826474918877 |
| H | 1.43841347937622 | -1.99276828021908 | 3.57496010579046 |
| H | 2.10737905098317 | -3.42022222647694 | 4.39907243025103 |
| C | 1.39950353312626 | -5.28475485339828 | 2.51226599378600 |
| H | 0.65328121001789 | -5.94024990556307 | 2.02795625301512 |
| H | 1.65208497468777 | -5.74232198145507 | 3.48564065068197 |
| C | 1.62896520341734 | -3.18362537785180 | -2.02667463746162 |
| H | 2.07816355667911 | -4.16645154576976 | -2.09426514800062 |
| C | 1.23603821316286 | -2.35216152612194 | -3.02099487559285 |
| H | 1.26029402776694 | -2.49967813471548 | -4.09609818482534 |
| N | 0.74277776605517 | -1.22078229803187 | -2.43220915290415 |
| C | -1.51678154948339 | -0.08678018302011 | -1.14741024839392 |
| N | -2.83888732969052 | -0.26484815303100 | -0.86641051614052 |
| C | -3.44937249046463 | -0.24501567315972 | 0.47531892378875 |
| C | -3.13931103832076 | 1.08969841734588 | 1.16079329264788 |
| H | -2.04630111798253 | 1.22039768046139 | 1.21671096495343 |
| H | -3.53918484883551 | 1.91526485639879 | 0.54617919012701 |
| C | -4.97139782074917 | -0.40141929891618 | 0.38999837826090 |
| H | -5.40211553135946 | 0.41090055304897 | -0.22046057060968 |
| H | -5.22801989995020 | -1.35824764678798 | -0.09617100538330 |
| C | -2.89617763845036 | -1.39328897276853 | 1.32380602804836 |
| H | -3.12010489283574 | -2.35393302447606 | 0.82734200980845 |
| H | -1.79941996883345 | -1.30062383209477 | 1.38006756673571 |

**Table A4.3, continued**

| | | | |
|---|---|---|---|
| C | -3.74424960304085 | 1.12115648296080 | 2.56287664833610 |
| H | -3.49619752362610 | 2.08746154542351 | 3.03555540716060 |
| C | -5.58239632888449 | -0.36745763817942 | 1.79192567877735 |
| H | -6.67583714504635 | -0.48146218552271 | 1.69617926329914 |
| C | -3.50020234706479 | -1.35764002846212 | 2.72660590071870 |
| H | -3.07443136395514 | -2.18734904226304 | 3.31744860587190 |
| C | -3.16426087539705 | -0.02368975050279 | 3.39326484198801 |
| H | -2.06961878279035 | 0.09032020444289 | 3.48580797423520 |
| H | -3.58075000935628 | 0.00248706092823 | 4.41618011965026 |
| C | -5.25981474198032 | 0.96631358792933 | 2.46217596257983 |
| H | -5.68863795741649 | 1.79952921767104 | 1.87681695421441 |
| H | -5.71707170131554 | 1.00503763049858 | 3.46708347752742 |
| C | -5.01583890790299 | -1.51343775093755 | 2.62797161914475 |
| H | -5.26911575219660 | -2.48422518514795 | 2.16504122709499 |
| H | -5.46836544662476 | -1.50601973314722 | 3.63576633127127 |
| C | -3.53748781315738 | -0.44477702462438 | -2.04331661972723 |
| H | -4.60750441691601 | -0.61440703865737 | -2.08185150147462 |
| C | -2.63726075047149 | -0.35953595084433 | -3.05580099932420 |
| H | -2.79160873473794 | -0.47553707090833 | -4.12412020566072 |
| N | -1.41435247388119 | -0.11203406011709 | -2.48953649597876 |
| C | 0.65340454788606 | 1.39833684509562 | -1.05647206994319 |
| N | 1.19730569133336 | 2.62586709465155 | -0.80004003297551 |
| C | 1.45105625218458 | 3.27024563278188 | 0.51199220923032 |
| C | 1.90727871637209 | 4.72297728997350 | 0.31613377140247 |
| H | 2.84210302090814 | 4.75594287304137 | -0.26818457080153 |
| H | 1.14156352709361 | 5.29075486193519 | -0.24088139448657 |
| C | 0.16811576179168 | 3.28871805078694 | 1.34852822709023 |

**Table A4.3, continued**

| | | | |
|---|---|---|---|
| H | -0.61570241106739 | 3.83859477634592 | 0.79782582280538 |
| H | -0.17736099993236 | 2.25519507606298 | 1.48989212842921 |
| C | 2.55721367659881 | 2.52252515722858 | 1.26606977546726 |
| H | 2.24413828348636 | 1.47442763017697 | 1.40506059843644 |
| H | 3.47905850285511 | 2.53599786923704 | 0.65674189296368 |
| C | 2.15811651610716 | 5.38984791144778 | 1.67017242118936 |
| H | 2.48137564369281 | 6.42925365499408 | 1.48749772884436 |
| C | 0.42670586748700 | 3.94208611947802 | 2.70547672568632 |
| H | -0.50869597301474 | 3.92020820590773 | 3.29176099935805 |
| C | 2.80580412932660 | 3.18643423604460 | 2.62117716735965 |
| H | 3.59309776003529 | 2.62350155147850 | 3.15245264040068 |
| C | 3.25427244500521 | 4.63074046118856 | 2.41436798231904 |
| H | 4.19534958371422 | 4.65819542303169 | 1.83569729536470 |
| H | 3.45716627904610 | 5.11410694503582 | 3.38715287090563 |
| C | 0.87590782461680 | 5.38549788599819 | 2.49793565550029 |
| H | 0.08628397234629 | 5.96092995047907 | 1.98151333135755 |
| H | 1.05187496362486 | 5.87804830768752 | 3.47124440737403 |
| C | 1.51764133366725 | 3.16700179372368 | 3.44484651496567 |
| H | 1.19387131540075 | 2.12572429000069 | 3.61535900502018 |
| H | 1.69663138838890 | 3.62120863862338 | 4.43630361930111 |
| C | 1.52100928597298 | 3.22552616903293 | -2.00317472101261 |
| H | 1.96989357060989 | 4.20854288884312 | -2.07397484610966 |
| C | 1.17272802428821 | 2.36753445232245 | -2.99168731725915 |
| H | 1.26044428874614 | 2.46621656497520 | -4.06972937426719 |
| N | 0.63988532858218 | 1.25864515717333 | -2.39281114941738 |
| B | 0.02358335499872 | 0.00378353467983 | -3.06861327970346 |
| C | 0.16509527828945 | 0.15162514166761 | -4.66729441107366 |

**Table A4.3, continued**

| | | | |
|---|---|---|---|
| C | -0.81519593719197 | 0.78317512363867 | -5.44993057567921 |
| H | -1.74076618989841 | 1.13576148175631 | -4.98807054917650 |
| C | -0.64150239965425 | 1.01759142555806 | -6.81345966054558 |
| H | -1.43566894118741 | 1.50921400931157 | -7.38451353606892 |
| C | 0.54035890814552 | 0.63865544636171 | -7.44382385994554 |
| H | 0.68113554453394 | 0.81827286409963 | -8.51433150004261 |
| C | 1.54956938654340 | 0.04780012554010 | -6.68785525119482 |
| H | 2.49734779530386 | -0.23135582349966 | -7.15933051758918 |
| C | 1.36152411869805 | -0.18040893370745 | -5.32580249986038 |
| H | 2.19310854768475 | -0.61096176598446 | -4.76069585925904 |

**Table A4.4.** Coordinates for the optimized structure of $[PhB(^{Ad}Im)_3Co^{III}OH]^+$ ($S = 0$, **3**).

| | | | |
|---|---|---|---|
| Co | 0.47951921871899 | -0.04464361984126 | -0.00743652140624 |
| O | 1.78367358538686 | -0.27469204778137 | 1.18164678929066 |
| H | 2.66787156132664 | -0.43006026496915 | 0.83605697557005 |
| C | 0.79049354506871 | -1.50540866936386 | -1.09220382510474 |
| N | 1.06467597082957 | -2.81485626924967 | -0.85018027805862 |
| C | 1.02052073616237 | -3.57769506543173 | 0.42324801444572 |
| C | 2.39159545187580 | -3.58544688618997 | 1.10653915792924 |
| H | 3.12884541477715 | -4.03391991781140 | 0.43249365415995 |
| H | 2.70365769857708 | -2.56071116237605 | 1.30672764633809 |
| C | -0.02563409918846 | -2.97491577278292 | 1.35789407794096 |
| H | 0.24576313983199 | -1.93328038649314 | 1.58086131427793 |
| H | -1.00994518566424 | -2.98444403320822 | 0.85942656598765 |
| C | 0.61649473578946 | -5.03453666760469 | 0.14428895359697 |
| H | -0.35356200026647 | -5.05733176187772 | -0.38200529613801 |

**Table A4.4, continued**

| | | | |
|---|---|---|---|
| H | 1.36003532699620 | -5.52742373582588 | -0.50140121964345 |
| C | 2.31636197721432 | -4.37310638855830 | 2.41390365341919 |
| H | 3.31068812669173 | -4.35344274478659 | 2.89020818716339 |
| C | -0.08661470274189 | -3.75456963347280 | 2.67044413429484 |
| H | -0.83354202708049 | -3.27459596475674 | 3.32609953560608 |
| C | 0.53684053998391 | -5.82238039044794 | 1.45208730372456 |
| H | 0.24446718879457 | -6.85856533628921 | 1.21139239169764 |
| C | 1.90766697046214 | -5.81541445749766 | 2.12549862060583 |
| H | 2.65484031411293 | -6.30207198823993 | 1.47334072874917 |
| H | 1.87076160161783 | -6.39388800228792 | 3.06549336792225 |
| C | 1.28673743162600 | -3.72716817025935 | 3.33985151646896 |
| H | 1.57739700557862 | -2.68634814356309 | 3.56790786439518 |
| H | 1.24901927771035 | -4.27131707959975 | 4.30015482175793 |
| C | -0.49682609333115 | -5.19460628157477 | 2.38105771219295 |
| H | -1.49695674303434 | -5.21792142361879 | 1.91267390901700 |
| H | -0.56358235027980 | -5.77114673280782 | 3.32055889818401 |
| C | 1.30763419932762 | -3.42704850984528 | -2.06558115014484 |
| H | 1.57020006293337 | -4.47487183999421 | -2.15041494178398 |
| C | 1.14426943150937 | -2.49567953938968 | -3.03589379940102 |
| H | 1.22962331653306 | -2.57965797805241 | -4.11540495281855 |
| N | 0.80910495112034 | -1.32408699995402 | -2.41476218456803 |
| C | -1.11601753745030 | 0.25087258797314 | -1.01494906097485 |
| N | -2.37513555051249 | 0.59818080484401 | -0.65709305296576 |
| C | -2.95716742803961 | 0.64841755118069 | 0.69198973909567 |
| C | -3.44696821842240 | 2.06955796649392 | 1.00441017801457 |
| H | -2.59657950701883 | 2.77091104018617 | 0.93699263449530 |
| H | -4.19358243167150 | 2.38330558728831 | 0.25555076967081 |

**Table A4.4, continued**

| | | | |
|---|---|---|---|
| C | -4.14108801861065 | -0.32781914119019 | 0.77650113507390 |
| H | -4.90234781537883 | -0.06247905683608 | 0.02409113779336 |
| H | -3.78706050140234 | -1.34753970508975 | 0.54314802920184 |
| C | -1.92745343568010 | 0.24013832331367 | 1.73852350822142 |
| H | -1.58145559944799 | -0.78426978932480 | 1.52983398421432 |
| H | -1.06276314371858 | 0.92478076144363 | 1.69952014064622 |
| C | -4.06768136984244 | 2.10953778050476 | 2.40119568910277 |
| H | -4.41783440921045 | 3.13620996176610 | 2.60262697193023 |
| C | -4.75921043303020 | -0.27902633745487 | 2.17350921596041 |
| H | -5.61003748105237 | -0.98049068008475 | 2.20819513255407 |
| C | -2.53767652190517 | 0.28931584375854 | 3.14086984843311 |
| H | -1.76335013326209 | -0.00543786322713 | 3.86890807106902 |
| C | -3.02142723703357 | 1.70671628197019 | 3.43836973427430 |
| H | -2.17118036241263 | 2.41250840424931 | 3.42175679690540 |
| H | -3.45731908666735 | 1.74839573324499 | 4.45202607932687 |
| C | -5.24796519667908 | 1.14029245233718 | 2.46147243356524 |
| H | -6.01811745220624 | 1.43333643217888 | 1.72558938906202 |
| H | -5.72086691764492 | 1.18265756449903 | 3.45846518063845 |
| C | -3.71335350012923 | -0.68273767628502 | 3.21039313475245 |
| H | -3.36597297181954 | -1.71486263501950 | 3.02267207970952 |
| H | -4.15489101214080 | -0.66796638635055 | 4.22241577689414 |
| C | -3.10557337667191 | 0.88480670723777 | -1.79002049677561 |
| H | -4.14626301169254 | 1.19418574620256 | -1.75625158911090 |
| C | -2.28015904994831 | 0.69491857312625 | -2.85237814302802 |
| H | -2.47535745970175 | 0.84268974107633 | -3.91005126999102 |
| N | -1.07160896177721 | 0.28007959328106 | -2.36139616430311 |
| C | 1.25299732258668 | 1.24763328433456 | -1.10510430716773 |

**Table A4.4, continued**

| | | | |
|---|---|---|---|
| N | 1.83492406650654 | 2.44678098968406 | -0.82883667444493 |
| C | 2.05842249362704 | 3.12169318880014 | 0.47599474518531 |
| C | 2.15650831901411 | 4.64206535814261 | 0.26911123646440 |
| H | 3.02053571264437 | 4.89020479683171 | -0.36773118265556 |
| H | 1.24730317288245 | 5.01005770697679 | -0.23706938210502 |
| C | 0.87745590267637 | 2.85456114597999 | 1.40746534386816 |
| H | -0.05431432356051 | 3.20173575183110 | 0.92977499317016 |
| H | 0.79708615009865 | 1.77199596793305 | 1.58525635333059 |
| C | 3.36286413146004 | 2.64766408626434 | 1.13081750713284 |
| H | 3.32210642478838 | 1.55928203077435 | 1.28468447088318 |
| H | 4.20813450666144 | 2.86386883719586 | 0.45420967548676 |
| C | 2.34587069175489 | 5.35241589611257 | 1.61005388593688 |
| H | 2.40804424169057 | 6.43682620380042 | 1.41701822962539 |
| C | 1.08327197449672 | 3.55019909109767 | 2.75219605210732 |
| H | 0.22418544320055 | 3.31185107016796 | 3.40276017153484 |
| C | 3.55667743692788 | 3.35758895086475 | 2.47285249024743 |
| H | 4.49188008928112 | 2.99248160149659 | 2.93066283665478 |
| C | 3.64270849997292 | 4.86595694170909 | 2.25382766373181 |
| H | 4.50337294119964 | 5.10878049409843 | 1.60511945873466 |
| H | 3.80692860871566 | 5.38172005373772 | 3.21647268474214 |
| C | 1.16688585168402 | 5.05672744100689 | 2.53084531201356 |
| H | 0.22852060821478 | 5.42855346928161 | 2.08180066547728 |
| H | 1.29608957323982 | 5.57926905844701 | 3.49521199661692 |
| C | 2.37606250652803 | 3.04457265494235 | 3.39214445567965 |
| H | 2.31141915112591 | 1.95686945588281 | 3.57229600376616 |
| H | 2.52463781479225 | 3.52779633011466 | 4.37402915544627 |
| C | 2.15620377756493 | 3.05085987850694 | -2.02804514844740 |

**Table A4.4, continued**

| | | | |
|---|---|---|---|
| H | 2.64537387532507 | 4.01522656296098 | -2.08838496646291 |
| C | 1.75052455920892 | 2.22860413736222 | -3.02453631227521 |
| H | 1.79610711696746 | 2.36922032556648 | -4.09965793594383 |
| N | 1.20286053560095 | 1.12075351268227 | -2.43932099061443 |
| B | 0.31017140956546 | 0.00115433916649 | -3.04885114379828 |
| C | 0.32039987551628 | -0.13366476999673 | -4.64729410858929 |
| C | 1.48977654876664 | 0.09801067274625 | -5.39081660893043 |
| H | 2.40136135657278 | 0.43464415143439 | -4.88901251793267 |
| C | 1.54746337634581 | -0.11686615449883 | -6.76660788322205 |
| H | 2.47739080672785 | 0.08244975624766 | -7.30831776649352 |
| C | 0.42975311089488 | -0.59226625144958 | -7.44727360513356 |
| H | 0.46828264833988 | -0.75899206507356 | -8.52821195981678 |
| C | -0.73017987425686 | -0.87412071796615 | -6.73115703200645 |
| H | -1.60897070804424 | -1.27675996056456 | -7.24457135754047 |
| C | -0.77473969191057 | -0.65493357537738 | -5.35534310428487 |
| H | -1.69052848218433 | -0.93064400074654 | -4.82628003909597 |

**Table A4.5.** Coordinates for the optimized structure of $[PhB(^{Ad}Im)_3Co^{IV}O]^+$ ($S = 1/2$, **4$^{ox}$**).

| | | | |
|---|---|---|---|
| Co | -0.00080135345815 | 0.00102658213544 | -0.00868451950696 |
| O | -0.31607012995222 | 0.25556741774745 | 1.52854178030195 |
| C | 1.14215358576667 | -1.09010465874425 | -1.12004194845411 |
| N | 2.01384116737322 | -2.08060343600541 | -0.83326747507701 |
| C | 2.48565689711296 | -2.48110992769146 | 0.51043647616000 |
| C | 3.06871062087917 | -1.26266287660608 | 1.22716968975479 |
| H | 3.89387755492825 | -0.85657524858451 | 0.63353529161241 |
| H | 2.31007913139808 | -0.48178833811876 | 1.30159914114376 |

**Table A4.5, continued**

| | | | |
|---|---|---|---|
| C | 1.32412808605091 | -3.05618186288028 | 1.32382432460800 |
| H | 0.51861568783892 | -2.30824887098309 | 1.40370674395830 |
| H | 0.90775674440836 | -3.93285319542058 | 0.79792104171221 |
| C | 3.57973777358865 | -3.54723569357840 | 0.40159627602111 |
| H | 3.18788258682916 | -4.44370754692545 | -0.10766386949619 |
| H | 4.42538371565545 | -3.16116371777936 | -0.19243092791392 |
| C | 3.54332576694512 | -1.65008051052463 | 2.62405174451802 |
| H | 3.94315463091383 | -0.75050000193395 | 3.12090666896338 |
| C | 1.80840054888346 | -3.44166914314685 | 2.72068514967977 |
| H | 0.95421333103799 | -3.84273554842846 | 3.29250406197453 |
| C | 4.06640369881301 | -3.93616421372855 | 1.79836600696605 |
| H | 4.85240384547413 | -4.70226525563340 | 1.68911064665310 |
| C | 4.63565065681379 | -2.70948805077039 | 2.50675483784500 |
| H | 5.49681312887428 | -2.30934744074664 | 1.94256028105126 |
| H | 5.00550316091833 | -2.98818553849060 | 3.50927370439600 |
| C | 2.36711860281435 | -2.20631290383348 | 3.42525689534579 |
| H | 1.57980783170689 | -1.43894857483414 | 3.53257547667724 |
| H | 2.69949909409316 | -2.47292328838502 | 4.44404263944811 |
| C | 2.89986253215576 | -4.50303812441657 | 2.60460412708266 |
| H | 2.50068983056688 | -5.40869777803305 | 2.11406191011187 |
| H | 3.24535513977249 | -4.80363802200339 | 3.60935977093213 |
| C | 2.40879453526145 | -2.66732758046548 | -2.01587433894021 |
| H | 3.10829275052734 | -3.49420023289150 | -2.06128758504941 |
| C | 1.77313900596069 | -2.01321471401305 | -3.02313073920051 |
| H | 1.80320303509066 | -2.19818389424290 | -4.09217411546047 |
| N | 1.01610333122749 | -1.02541829582318 | -2.45215289447147 |
| C | -1.49605900504325 | -0.48338650660789 | -1.05926936650455 |

**Table A4.5, continued**

| | | | |
|---|---|---|---|
| N | -2.72181755099705 | -0.98506913215137 | -0.77977779902026 |
| C | -3.39284381134912 | -1.14821940850266 | 0.54134162760074 |
| C | -3.54429191861909 | 0.21935035429408 | 1.21951611588107 |
| H | -2.55772048470690 | 0.68639002639605 | 1.35091935584586 |
| H | -4.14340689001141 | 0.87696818033652 | 0.56556124212254 |
| C | -4.79660516563474 | -1.73763563075445 | 0.34936883808864 |
| H | -5.40394537789002 | -1.07379438878479 | -0.28865906542806 |
| H | -4.73362216862580 | -2.72164212013430 | -0.14567998929408 |
| C | -2.59917134586773 | -2.11143782536625 | 1.42941187060051 |
| H | -2.53008575181071 | -3.09140227894930 | 0.92590614784346 |
| H | -1.57739772559504 | -1.73675560548425 | 1.57504493926390 |
| C | -4.22679383434293 | 0.05102238750124 | 2.57752069927103 |
| H | -4.30255548498179 | 1.04231141160426 | 3.05628195002218 |
| C | -5.49232504075480 | -1.89977534537872 | 1.70275795682380 |
| H | -6.49438366016306 | -2.32423228293617 | 1.52209719616969 |
| C | -3.28794339124581 | -2.25570661101072 | 2.78708238058658 |
| H | -2.68216289752376 | -2.93035417706393 | 3.41623829957621 |
| C | -3.39495828477764 | -0.88453859730744 | 3.45516437073480 |
| H | -2.38808107061528 | -0.46055244654151 | 3.61640284814313 |
| H | -3.86655047111116 | -0.98673121806763 | 4.44866978007342 |
| C | -5.62067890495908 | -0.53745747327432 | 2.37887620671402 |
| H | -6.23547668819436 | 0.13974864520900 | 1.75930052065663 |
| H | -6.13420625252894 | -0.64367618509200 | 3.35080645990890 |
| C | -4.68231436353894 | -2.84161570138519 | 2.58920591822459 |
| H | -4.61349062251433 | -3.84089874157075 | 2.12306993365564 |
| H | -5.18565448348378 | -2.97182420594086 | 3.56356673293149 |
| C | -3.32797576421693 | -1.30068907253174 | -1.97703509972044 |

**Table A4.5, continued**

| | | | |
|---|---|---|---|
| H | -4.32033359114306 | -1.72974230127978 | -2.04078117772255 |
| C | -2.46735498049262 | -0.97443521579612 | -2.97416831263391 |
| H | -2.57177705232622 | -1.09585074791211 | -4.04778318787188 |
| N | -1.34963184263236 | -0.44581475932505 | -2.39167390122016 |
| C | 0.42788152993063 | 1.51176833169035 | -1.02791321450756 |
| N | 0.77837595981651 | 2.78815431858876 | -0.75443484666355 |
| C | 0.96124745311746 | 3.44268286586956 | 0.56978443442605 |
| C | 1.48433180770025 | 4.87246851416553 | 0.38194511507915 |
| H | 2.44399602117391 | 4.85743613597903 | -0.16252121433869 |
| H | 0.76730955152618 | 5.46686025128789 | -0.20868031625960 |
| C | -0.38148409125695 | 3.52096166885797 | 1.30750570395682 |
| H | -1.09306527483801 | 4.10057985965793 | 0.69360048794173 |
| H | -0.79624409079501 | 2.51091626103843 | 1.43870910419954 |
| C | 1.99034132249525 | 2.67061044531219 | 1.40084626721565 |
| H | 1.66231880760094 | 1.63094800258169 | 1.53934102567308 |
| H | 2.95017525995224 | 2.64889029700721 | 0.85601906743413 |
| C | 1.67826420348992 | 5.54642101802183 | 1.74209373269289 |
| H | 2.05481249631550 | 6.56832914658192 | 1.56655259009657 |
| C | -0.18403117937121 | 4.18610439336895 | 2.67054309586478 |
| H | -1.15648607496599 | 4.21346063209102 | 3.19129628238198 |
| C | 2.16457456808655 | 3.33732920293890 | 2.76547597075861 |
| H | 2.88876976695368 | 2.74746614364565 | 3.35323216249094 |
| C | 2.68710115290127 | 4.75748155629492 | 2.57157077673915 |
| H | 3.66741754876176 | 4.73631127918334 | 2.06262565088166 |
| H | 2.83968066915563 | 5.24672645908920 | 3.54988340007360 |
| C | 0.34078653878371 | 5.60602295366512 | 2.47592690232372 |
| H | -0.38536148398424 | 6.20519388455845 | 1.89776192637107 |

**Table A4.5, continued**

| | | | |
|---|---|---|---|
| H | 0.46655201628512 | 6.10489536086073 | 3.45315214176084 |
| C | 0.81982440941944 | 3.37705258764597 | 3.49226305633255 |
| H | 0.44262393495841 | 2.35137437711035 | 3.65191997520869 |
| H | 0.94578012773523 | 3.83489865190528 | 4.48943396777799 |
| C | 0.93222724419170 | 3.44482926027495 | -1.95859335376319 |
| H | 1.21660804501461 | 4.48780268001367 | -2.02818857182922 |
| C | 0.66899689593497 | 2.55588975143056 | -2.94980949389624 |
| H | 0.68235163573094 | 2.68068806190450 | -4.02865025503907 |
| N | 0.35862334599125 | 1.36501439927182 | -2.35364641231442 |
| B | 0.00271992951312 | 0.00563889353128 | -3.03853142240367 |
| C | -0.01160222563407 | 0.20766310698731 | -4.62834741227756 |
| C | -1.13869778954738 | 0.73431762082300 | -5.28203839499461 |
| H | -2.04803785064642 | 0.95657237306452 | -4.71657235362296 |
| C | -1.13594290002129 | 1.02151633165630 | -6.64541008940581 |
| H | -2.03749895102520 | 1.42554838875828 | -7.11624423968553 |
| C | 0.01193078477958 | 0.80525709927755 | -7.40307615511432 |
| H | 0.01821773602298 | 1.02569826906641 | -8.47497613904709 |
| C | 1.15833475367988 | 0.32723084362054 | -6.77508613078532 |
| H | 2.07874654326638 | 0.17989459783399 | -7.34860665152684 |
| C | 1.14327277359753 | 0.04395380887505 | -5.41045488154969 |
| H | 2.07785642963039 | -0.28688262579972 | -4.95112105332627 |

**Table A4.6.** Coordinates for the optimized transition state between $[PhB(^{Ad}Im)_3Co^{IV}O]^+$ (**4$^{ox}$**) and $[PhB(^{Ad}Im)_2(^{\bullet Ad}Im)Co^{III}OH]^+$ (**4$^{rad}$**) ($S$ = 1/2).

| | | | |
|---|---|---|---|
| Co | -0.10950308428583 | -0.00566837295412 | -0.03235708562241 |
| O | 0.66940439395673 | -0.14072560137004 | 1.46069826876940 |
| H | 1.83309996944328 | -0.54907997099450 | 1.59160725809164 |

**Table A4.6, continued**

| | | | |
|---|---|---|---|
| C | 1.11845503239661 | -0.95353632532034 | -1.08393749604411 |
| N | 2.20942949743048 | -1.71660054496108 | -0.80133505842365 |
| C | 2.64844030257235 | -2.26478230354658 | 0.50559578376202 |
| C | 2.92083376010173 | -1.14909916260742 | 1.48593749233451 |
| H | 3.58906989655373 | -0.38407006834163 | 1.08053782896080 |
| C | 1.58451204411954 | -3.22501493887797 | 1.05601147930989 |
| H | 0.61929328734931 | -2.70399043819407 | 1.14119871605065 |
| H | 1.45385924400328 | -4.05503231293067 | 0.34076704025276 |
| C | 3.96390340492758 | -3.05495845284795 | 0.36014129449306 |
| H | 3.81848798451062 | -3.90046073873925 | -0.33349558738105 |
| H | 4.75475548752499 | -2.40609559921583 | -0.05218972112903 |
| C | 3.30778111271230 | -1.66192248213926 | 2.84775154627805 |
| H | 3.45685275891793 | -0.80910127229076 | 3.52983405777947 |
| C | 2.01976308959094 | -3.75801545809763 | 2.42093829080466 |
| H | 1.22983270532745 | -4.42616676013658 | 2.80411104593737 |
| C | 4.39938040050689 | -3.59426042808714 | 1.72346879689050 |
| H | 5.34337807789746 | -4.14795866729482 | 1.58399810578693 |
| C | 4.62345505516151 | -2.43983090439837 | 2.69460687479572 |
| H | 5.42039998974312 | -1.77142630637227 | 2.32471810607380 |
| H | 4.94549552444927 | -2.82109302067857 | 3.67997124413081 |
| C | 2.22180082267227 | -2.59295749613797 | 3.38834476005929 |
| H | 1.27671224318294 | -2.03826476622716 | 3.52084794399190 |
| H | 2.51863652969585 | -2.97247540827908 | 4.38143128316813 |
| C | 3.32643649884135 | -4.53179425966723 | 2.27136080695012 |
| H | 3.18608312835730 | -5.38894622176678 | 1.58926166137689 |
| H | 3.64341952529912 | -4.94000183479083 | 3.24700461246548 |
| C | 2.84523381071942 | -2.01813138278333 | -1.98553951690707 |

**Table A4.6, continued**

| | | | |
|---|---|---|---|
| H | 3.75158343630679 | -2.60907585873111 | -2.03789205716608 |
| C | 2.13038670629555 | -1.44894071019598 | -2.98772323890688 |
| H | 2.32355035344663 | -1.43762921244038 | -4.05562472955789 |
| N | 1.05661940156542 | -0.82386885988994 | -2.42107439281640 |
| C | -1.54210917182950 | -0.52837126189878 | -1.14587096993023 |
| N | -2.76240523564838 | -1.04754256288513 | -0.86803160287862 |
| C | -3.30226892735567 | -1.35467050933667 | 0.46782081426139 |
| C | -2.83881280442732 | -0.29805911588943 | 1.46617830353221 |
| H | -1.73202966290166 | -0.28487874192982 | 1.50131958051120 |
| H | -3.17894574926744 | 0.69845433132246 | 1.14020278562255 |
| C | -4.83589686569362 | -1.36126878249251 | 0.45362237078047 |
| H | -5.20952855445680 | -0.38262038236576 | 0.10498227865135 |
| H | -5.21201784670331 | -2.12972507607304 | -0.24099697086087 |
| C | -2.80543694513037 | -2.73503808590686 | 0.91814730774261 |
| H | -3.13910175607444 | -3.49662927354567 | 0.19212022586577 |
| H | -1.70145513142137 | -2.74385799283022 | 0.92050886638049 |
| C | -3.35615841416692 | -0.61815180581355 | 2.86695417018669 |
| H | -2.99034942218490 | 0.15617408878138 | 3.56270103005577 |
| C | -5.36683681221996 | -1.67332218492417 | 1.85439370034241 |
| H | -6.46922083222842 | -1.67192485674031 | 1.81576711490250 |
| C | -3.33985035687778 | -3.05105620018301 | 2.31481429149985 |
| H | -2.97125532334743 | -4.04530322031266 | 2.61992791835288 |
| C | -2.84433434985048 | -1.99173386835099 | 3.29878266730818 |
| H | -1.73953062799586 | -1.99155421376189 | 3.33635264412529 |
| H | -3.20313964740318 | -2.22288629944595 | 4.31705671584675 |
| C | -4.88304240930881 | -0.61666697525630 | 2.84338293254440 |
| H | -5.25941074966989 | 0.38067124020276 | 2.55391365517385 |

**Table A4.6, continued**

| | | | |
|---|---|---|---|
| H | -5.27640472494700 | -0.83308688892273 | 3.85223615035656 |
| C | -4.86743342127155 | -3.05067723578140 | 2.28851620795928 |
| H | -5.23699903193481 | -3.82616209160873 | 1.59384373491352 |
| H | -5.26383477486214 | -3.29724299950106 | 3.28923774781730 |
| C | -3.37869476214823 | -1.38354081596355 | -2.05664389272851 |
| H | -4.36968633230023 | -1.82254227308983 | -2.10114450004123 |
| C | -2.52310025809667 | -1.05387011362155 | -3.05941896570625 |
| H | -2.62990816619984 | -1.14998755435714 | -4.13651147466486 |
| N | -1.40457117983904 | -0.52624375053281 | -2.47334152545568 |
| C | 0.00963028191949 | 1.51449957822353 | -1.12543081229378 |
| N | 0.25494731065417 | 2.80674033639782 | -0.79457011571467 |
| C | 0.24427991285491 | 3.41954162309488 | 0.55220323398806 |
| C | 0.06739637921644 | 4.94058833469462 | 0.44797418517388 |
| H | 0.90643486897293 | 5.38869587750141 | -0.10854063300368 |
| H | -0.86246180918351 | 5.17406615167161 | -0.09954251016018 |
| C | -0.92756796821235 | 2.86432759302934 | 1.36087967377847 |
| H | -1.87226267475053 | 3.07325719565582 | 0.83070154452713 |
| H | -0.83384332652543 | 1.77001246391965 | 1.44889136899586 |
| C | 1.56605637158115 | 3.13311898353909 | 1.27619027456083 |
| H | 1.71904374339067 | 2.04468137750349 | 1.34549547592588 |
| H | 2.39840209547900 | 3.55509198010051 | 0.68607276147510 |
| C | 0.03436810492060 | 5.56127820714834 | 1.84571527707684 |
| H | -0.09406447297514 | 6.65138280093517 | 1.73534811464062 |
| C | -0.94498797372347 | 3.47169058524367 | 2.76260177196190 |
| H | -1.78584920068178 | 3.03121938827057 | 3.32549554639038 |
| C | 1.53444740790743 | 3.75400232710645 | 2.67370629030968 |
| H | 2.48799763265134 | 3.52998288477066 | 3.18193349350348 |

**Table A4.6, continued**

| | | | |
|---|---|---|---|
| C | 1.35299380132272 | 5.26589933440523 | 2.55823513305155 |
| H | 2.19536945022483 | 5.70824955353352 | 1.99682182146527 |
| H | 1.35250912011433 | 5.72829604986273 | 3.56116696053926 |
| C | -1.12684904744261 | 4.98264328472412 | 2.64903892314750 |
| H | -2.08792062735305 | 5.21650087489091 | 2.15702960992485 |
| H | -1.15661991561051 | 5.43905835038818 | 3.65418503926526 |
| C | 0.37324456099711 | 3.16073118367502 | 3.47126310549304 |
| H | 0.50080193619071 | 2.06908515987699 | 3.57723010862618 |
| H | 0.35959599169991 | 3.58567651941004 | 4.49048023541222 |
| C | 0.56432538945076 | 3.49698285912299 | -1.94761322865375 |
| H | 0.80603413189792 | 4.55357809247860 | -1.95440245355538 |
| C | 0.48523389191168 | 2.61985905298388 | -2.97995473870030 |
| H | 0.68067914179607 | 2.77758528956682 | -4.03576472844999 |
| N | 0.10839220824643 | 1.41212822663257 | -2.45872018763270 |
| B | -0.08866791178601 | 0.00713221281242 | -3.09807098616804 |
| C | -0.18506668981381 | -0.08165435946615 | -4.69733723915509 |
| C | -0.70106819656673 | 0.96988250750740 | -5.47202996707307 |
| H | -0.99154893161985 | 1.91106876931562 | -4.99892558197475 |
| C | -0.89638109045386 | 0.85044406150597 | -6.84712962712459 |
| H | -1.29503400170652 | 1.69825084411930 | -7.41297780827071 |
| C | -0.59638946100404 | -0.34389256558645 | -7.49577940222359 |
| H | -0.74468807314282 | -0.44139771460471 | -8.57567406865286 |
| C | -0.12774924281345 | -1.42075046828433 | -6.74799719572358 |
| H | 0.08474959092059 | -2.37761293762585 | -7.23505635717533 |
| C | 0.06334306034871 | -1.28819466533141 | -5.37412070027359 |
| H | 0.39477208716490 | -2.17045559039831 | -4.81939033428020 |

**Table A4.7.** Coordinates for the optimized structure of ferrocene.

| | | | |
|---|---|---|---|
| Fe | -1.79944323474640 | -1.29598752605293 | 6.35775222175814 |
| C | -3.28414373082313 | -2.63833003281004 | 6.05681698565858 |
| C | -3.73040322201122 | -1.58141272423272 | 6.89353944317155 |
| C | -2.89540097144500 | -1.54739712904209 | 8.04121184670085 |
| C | -1.93255957548268 | -2.58332057349235 | 7.91341039077672 |
| C | -2.17363783995536 | -3.25843119687112 | 6.68785302002333 |
| C | -0.14576698075117 | -1.20248274530156 | 5.19344904510314 |
| C | 0.06242060560350 | -0.50232258422029 | 6.41102982036989 |
| C | -0.91830475924825 | 0.52063922382048 | 6.50295047289317 |
| C | -1.73214980535911 | 0.45286428169053 | 5.34151106646277 |
| C | -1.25490347421414 | -0.61189109209578 | 4.53247023654552 |
| H | -2.96541235309494 | -0.84247147344434 | 8.85672711284641 |
| H | -4.54696866783171 | -0.90657845561830 | 6.68189887397573 |
| H | -1.14226121482407 | -2.80575524913601 | 8.61553119528325 |
| H | -1.59889190957565 | -4.08347353314516 | 6.29287839562759 |
| H | -3.70291365372880 | -2.90820592112729 | 5.09826307199735 |
| H | -1.03858066136308 | 1.21436808129660 | 7.32215202864222 |
| H | -2.58129121381534 | 1.08388391339569 | 5.12324023811401 |
| H | 0.81972254793009 | -0.72419860118923 | 7.14875383976081 |
| H | 0.42482096637688 | -2.04934812600276 | 4.84099061406304 |
| H | -1.67685172975473 | -0.93094608044586 | 3.59053951690229 |

**Table A4.8.** Coordinates for the optimized structure of ferrocenium cation.

| | | | |
|---|---|---|---|
| Fe | -1.79519611969266 | -1.29295326774769 | 6.36624964577413 |
| C | -3.29072338828578 | -2.64408240118029 | 6.05982388892846 |
| C | -3.74030685555145 | -1.59062912863768 | 6.90426387176218 |

**Table A4.8, continued**

| | | | |
|---|---|---|---|
| C | -2.94818492478770 | -1.61196011190925 | 8.08101753224579 |
| C | -2.02102755772712 | -2.66896804303402 | 7.96591691677376 |
| C | -2.22614993726116 | -3.30588786809881 | 6.72408782388734 |
| C | -0.09929722034987 | -1.14908444435705 | 5.16224437350803 |
| C | 0.13541228559238 | -0.41295407769205 | 6.34300044365560 |
| C | -0.86137236040033 | 0.57867638084044 | 6.45307523896649 |
| C | -1.72204540902347 | 0.46544661375525 | 5.33190054931451 |
| C | -1.24813194773958 | -0.60851061326854 | 4.52754696881746 |
| H | -3.01618178860509 | -0.91639627788930 | 8.90508437794669 |
| H | -4.53448632943434 | -0.89206014146510 | 6.68532528817278 |
| H | -1.24609718528367 | -2.91081269535124 | 8.67967845877529 |
| H | -1.64527859237965 | -4.12777037873927 | 6.33073161416018 |
| H | -3.68178915029361 | -2.89065601767577 | 5.08363832003790 |
| H | -0.97662989395742 | 1.27363370734947 | 7.27242752253953 |
| H | -2.58896243754500 | 1.07733062181569 | 5.12968945058333 |
| H | 0.90881648124910 | -0.61578036489364 | 7.07040401911187 |
| H | 0.47295350876969 | -2.00011047802116 | 4.82196397458573 |
| H | -1.68824205540759 | -0.95726855782453 | 3.60489915712934 |

**Table A4.9.** Coordinates for the optimized structure of $[PhB(^{Ad}Im)_2(^{OAd}Im)Co^{III}]^+$ ($S = 0$, **5**).

| | | | |
|---|---|---|---|
| Co | 0.01668854506516 | -0.00883792559231 | -0.00162753599638 |
| O | 1.02951696890258 | 0.06862868204680 | 1.43322215822683 |
| C | 1.44955191869306 | -0.38090863830978 | -1.06932259919888 |
| N | 2.71430451537644 | -0.63918905369708 | -0.68730323917841 |
| C | 3.13684393484148 | -0.89032883258168 | 0.69526338109015 |
| C | 2.40330537385919 | 0.11299493268902 | 1.60214716715109 |

**Table A4.9, continued**

| | | | |
|---|---|---|---|
| H | 2.75958487081171 | 1.12032129023526 | 1.33235784678511 |
| C | 2.77624217868311 | -2.32521099423032 | 1.09025799445756 |
| H | 1.69726131902816 | -2.48809122090830 | 0.95192169850045 |
| H | 3.30017467488776 | -3.02302496882942 | 0.41841692011725 |
| C | 4.64025086233692 | -0.67749488820545 | 0.86860850491058 |
| H | 5.19702790198717 | -1.37384732437807 | 0.22379341480759 |
| H | 4.91153991843581 | 0.34521930202865 | 0.56261539457118 |
| C | 2.77929588960037 | -0.16303662044308 | 3.06079268341245 |
| H | 2.22044990596830 | 0.55321728438125 | 3.68277525906847 |
| C | 3.16939211893689 | -2.56998952792551 | 2.54490477254492 |
| H | 2.90624622060825 | -3.60490340037317 | 2.81487001879304 |
| C | 5.02840491587999 | -0.92434437815434 | 2.32547535939040 |
| H | 6.11376223194376 | -0.76908152045166 | 2.42758184271262 |
| C | 4.27975499379853 | 0.05176674488194 | 3.22736283763003 |
| H | 4.55028844628061 | 1.08990507542127 | 2.97553879757807 |
| H | 4.56586599401604 | -0.10668333495869 | 4.27918600088742 |
| C | 2.40877082051858 | -1.59384085157294 | 3.43912471900584 |
| H | 1.32380569722365 | -1.74870719326778 | 3.33665877817962 |
| H | 2.65849886665867 | -1.77269222148685 | 4.49680497074270 |
| C | 4.67216903065435 | -2.35824812738479 | 2.71052065968754 |
| H | 5.22850958512182 | -3.07012519583541 | 2.07925874420428 |
| H | 4.97028532421739 | -2.55234278498020 | 3.75318430674434 |
| C | 3.49432593135753 | -0.76417532024234 | -1.81431596074769 |
| H | 4.55727279657139 | -0.97487920632914 | -1.77470622541302 |
| C | 2.67722677121050 | -0.57144054789511 | -2.88568680929049 |
| H | 2.92393902703966 | -0.55329179763537 | -3.94165356666681 |
| N | 1.41112532711543 | -0.35720578023812 | -2.40795113541617 |

**Table A4.9, continued**

| | | | |
|---|---|---|---|
| C | -1.11385918361733 | -1.03605777981218 | -1.08757465831259 |
| N | -2.02878326170553 | -1.98947131067365 | -0.79039396941685 |
| C | -2.51070526188893 | -2.40150972868786 | 0.53632184189787 |
| C | -2.12005061384701 | -1.36440910066615 | 1.58121116853895 |
| H | -1.02079794302406 | -1.27182663565052 | 1.61969894652103 |
| H | -2.54951391882232 | -0.39051376668633 | 1.30927067088624 |
| C | -4.04099970381936 | -2.52419478635191 | 0.52565882364360 |
| H | -4.48243025618865 | -1.55897760718927 | 0.23076860235083 |
| H | -4.35837958049815 | -3.27025252854763 | -0.21736921746021 |
| C | -1.89983480138683 | -3.75610049871581 | 0.92122533027489 |
| H | -2.17529681411457 | -4.51148224090304 | 0.16888662775796 |
| H | -0.80105580527242 | -3.67423108377924 | 0.91680297799541 |
| C | -2.61390899758071 | -1.78443911538868 | 2.96561354414163 |
| H | -2.30777994643480 | -1.01622453677415 | 3.69322665850313 |
| C | -4.53875086868260 | -2.94784387194850 | 1.90666458307074 |
| H | -5.63619856992407 | -3.03424735736345 | 1.87209665132688 |
| C | -2.40371160020531 | -4.17660704676098 | 2.30143949810769 |
| H | -1.95614907261760 | -5.14948048476345 | 2.55937255723396 |
| C | -1.99552921878258 | -3.13026878604694 | 3.33632845334467 |
| H | -0.89740836358937 | -3.04438818951136 | 3.38179363413798 |
| H | -2.33378669641718 | -3.43730251146334 | 4.33882146339952 |
| C | -4.13537837196322 | -1.90118467509241 | 2.94110612307166 |
| H | -4.58720085127979 | -0.92697210366294 | 2.69334451166673 |
| H | -4.50929768121144 | -2.18575099234892 | 3.93758329929537 |
| C | -3.92617459980329 | -4.29869365647698 | 2.27260673243137 |
| H | -4.23204023857029 | -5.06441498243875 | 1.54127776763655 |
| H | -4.29750897641874 | -4.62851160324882 | 3.25598157122550 |

**Table A4.9, continued**

| | | | |
|---|---|---|---|
| C | -2.43276962701669 | -2.59874037035927 | -1.96156661165408 |
| H | -3.15832788832321 | -3.40474486766018 | -1.98091715353577 |
| C | -1.76534945127449 | -1.99388385513753 | -2.97775911215165 |
| H | -1.80364629792283 | -2.17440458377106 | -4.04768769992827 |
| N | -0.96775528048377 | -1.03258145754691 | -2.41833144961988 |
| C | -0.45441875049448 | 1.40947153987560 | -1.11219831595568 |
| N | -0.72918834216174 | 2.69972954770448 | -0.79919440983015 |
| C | -0.93213001700882 | 3.27614997159878 | 0.54405311408523 |
| C | -1.79597493192903 | 4.54072259135038 | 0.45749275371135 |
| H | -1.30150664118872 | 5.30073652196690 | -0.16424400766159 |
| H | -2.76032630799235 | 4.29885770435390 | -0.01659777938850 |
| C | -1.65496673979970 | 2.26996170936753 | 1.43620172945508 |
| H | -2.61864669721377 | 1.99846860061225 | 0.97978184266483 |
| H | -1.05230795034770 | 1.35264119179007 | 1.52532326789269 |
| C | 0.41917513996862 | 3.64454088633614 | 1.16922768809304 |
| H | 1.05332752098463 | 2.74790998374210 | 1.22456463584312 |
| H | 0.93155246062249 | 4.37181957818914 | 0.51982409055944 |
| C | -2.01307350331724 | 5.12270417157123 | 1.85451518947455 |
| H | -2.63400651434629 | 6.02726663411336 | 1.75868358668003 |
| C | -1.85848576552771 | 2.84695905687425 | 2.83608764842690 |
| H | -2.36303998490706 | 2.08963950773171 | 3.45701401044941 |
| C | 0.20118784981650 | 4.22992380274755 | 2.56448382359026 |
| H | 1.18134885996334 | 4.48335491568190 | 2.99871613125461 |
| C | -0.66087043147404 | 5.48587335702721 | 2.46466207806600 |
| H | -0.15701149750011 | 6.24614935033777 | 1.84592000094912 |
| H | -0.80379253819448 | 5.92810466164862 | 3.46348889936479 |
| C | -2.72169684305985 | 4.10101247448604 | 2.73793943151563 |

**Table A4.9, continued**

| | | | |
|---|---|---|---|
| H | -3.70900410230187 | 3.85187415950993 | 2.31641795691920 |
| H | -2.89650449358611 | 4.52110363084749 | 3.74131332542633 |
| C | -0.50179270998004 | 3.19817920460008 | 3.44505524100210 |
| H | 0.11909580828220 | 2.29284493556956 | 3.53918751331345 |
| H | -0.63957102778412 | 3.59989376707434 | 4.46154752603830 |
| C | -0.72336256748607 | 3.44237996248504 | -1.96227678905890 |
| H | -0.90967278766350 | 4.50947161400993 | -1.98020628507352 |
| C | -0.46578331186396 | 2.58852795793737 | -2.98492097712874 |
| H | -0.36784085114859 | 2.79084644492872 | -4.04605955682277 |
| N | -0.33419065326342 | 1.33631458220734 | -2.44727254204969 |
| B | 0.02908411805524 | -0.03999055660867 | -3.08076496377713 |
| C | -0.05947060451322 | -0.15015501614594 | -4.67615114003973 |
| C | -1.03497477929405 | 0.55889729407731 | -5.39643821156472 |
| H | -1.70566824634883 | 1.24628739636965 | -4.87671483803561 |
| C | -1.20175431945948 | 0.39839798412458 | -6.76994597522303 |
| H | -1.96988918397068 | 0.97330066456775 | -7.29362272795977 |
| C | -0.39995775612672 | -0.49733511841672 | -7.47145953546842 |
| H | -0.52475688738874 | -0.62452385079343 | -8.54973512471601 |
| C | 0.54859101859320 | -1.24376169621952 | -6.77903410434351 |
| H | 1.16839631639552 | -1.97106885786659 | -7.30969394960948 |
| C | 0.70577395647708 | -1.07474705167450 | -5.40488492315195 |
| H | 1.43359155454061 | -1.70811475003975 | -4.89440465358912 |

**Table A4.10.** Coordinates for the optimized structure of $[PhB(^{Ad}Im)_2(^{HOAd}Im)Co^{II}]^+$ ($S$ = ½, **4**$^{reb}$).

| | | | |
|---|---|---|---|
| Co | 0.13597251671351 | -0.07404649761255 | 0.01439241893496 |
| O | 1.57336406397120 | -0.04429372734062 | 1.41648574192566 |

**Table A4.10, continued**

| | | | |
|---|---|---|---|
| H | 1.61234496576407 | 0.70957501238990 | 2.01723287016040 |
| C | 1.26311357754316 | -1.09346047182977 | -1.08263938543832 |
| N | 2.43466499609834 | -1.68895617443391 | -0.76639771456265 |
| C | 2.84701607271618 | -1.96900656278367 | 0.61019563090559 |
| C | 2.86928088473860 | -0.66642122631868 | 1.42022097060917 |
| H | 3.57308325714137 | 0.02768105595256 | 0.94584529401103 |
| C | 1.90597748471523 | -2.98429382562060 | 1.26732407297646 |
| H | 0.87216394829405 | -2.60452668162893 | 1.24901943091769 |
| H | 1.92094924945637 | -3.91235314824135 | 0.67157105887945 |
| C | 4.27253652903792 | -2.53236694485227 | 0.63556566228774 |
| H | 4.29645777225408 | -3.46344730481869 | 0.04579626944752 |
| H | 4.96940810266980 | -1.82068215249517 | 0.16168509936598 |
| C | 3.28567999901032 | -0.95021055964959 | 2.86053801181423 |
| H | 3.26642952305663 | 0.00731673496289 | 3.41087984071256 |
| C | 2.34840489184942 | -3.25491052137086 | 2.70512125460018 |
| H | 1.65075989329482 | -3.97882263787186 | 3.15886900419790 |
| C | 4.71477928714565 | -2.81745913346197 | 2.06751171325612 |
| H | 5.73762951978637 | -3.22861065622124 | 2.04190055368135 |
| C | 4.70331562629202 | -1.51392193244155 | 2.85940116249443 |
| H | 5.40616157074900 | -0.78819910497738 | 2.41360462730612 |
| H | 5.03226088485142 | -1.68761723821210 | 3.89832456655931 |
| C | 2.32350022773625 | -1.95068934129254 | 3.49946751144930 |
| H | 1.29976205423369 | -1.54065551678892 | 3.53091328026465 |
| H | 2.62848026265279 | -2.13330839960511 | 4.54396653998463 |
| C | 3.76388945966093 | -3.82681655771978 | 2.70642785010664 |
| H | 3.79025065023525 | -4.77889769157618 | 2.14755643564725 |
| H | 4.08419798002405 | -4.04681798340737 | 3.73988283232617 |

**Table A4.10, continued**

| | | | |
|---|---|---|---|
| C | 3.16254187290632 | -1.91112871898696 | -1.92029804261238 |
| H | 4.13622583461410 | -2.38909572494903 | -1.93320120102367 |
| C | 2.40657919530225 | -1.44286362198786 | -2.94838415714419 |
| H | 2.63379380758973 | -1.41678800749648 | -4.01040259486573 |
| N | 1.23295841954287 | -0.96311963944674 | -2.42081617246452 |
| C | -1.26993818946600 | -0.54597780640369 | -1.03675602560939 |
| N | -2.51421519007433 | -0.94988629080847 | -0.69636496005948 |
| C | -3.00400567220143 | -1.09233771869607 | 0.67168952343431 |
| C | -1.86803659866994 | -0.77045623340061 | 1.64240030075646 |
| H | -1.02818462994229 | -1.47170387262396 | 1.47186670249662 |
| H | -1.52591365851850 | 0.27208217452475 | 1.47045902528333 |
| C | -4.16364164536859 | -0.12168922268901 | 0.93343458485969 |
| H | -3.82568953560742 | 0.91062035055859 | 0.73316541268428 |
| H | -4.99297533359216 | -0.33760120362626 | 0.23812611889132 |
| C | -3.47617879193903 | -2.52878780569702 | 0.93339372780920 |
| H | -4.29284754944462 | -2.78689430435795 | 0.23773161306024 |
| H | -2.64322365775916 | -3.22651290888730 | 0.73628803616498 |
| C | -2.34230750985466 | -0.90167032385189 | 3.08985700231043 |
| H | -1.49859795907022 | -0.66417241200334 | 3.75976080082230 |
| C | -4.64291940065256 | -0.26070488737423 | 2.37838365173541 |
| H | -5.47836154650434 | 0.44046791010349 | 2.54445899517198 |
| C | -3.95870885756714 | -2.66166291480117 | 2.37783858769070 |
| H | -4.29815021365595 | -3.69800928261522 | 2.54490101616790 |
| C | -2.81042110473640 | -2.33597098371586 | 3.33134357560819 |
| H | -1.97331613280458 | -3.04015994713705 | 3.17519376684260 |
| H | -3.14066807222937 | -2.45231546680070 | 4.37865153209808 |
| C | -3.49581733386281 | 0.06973196192470 | 3.33212599452041 |

**Table A4.10, continued**

| | | | |
|---|---|---|---|
| H | -3.15617615711811 | 1.11009267642676 | 3.17682936617373 |
| H | -3.83791298150377 | -0.00640874006705 | 4.37923971179169 |
| C | -5.11600328000698 | -1.69352553535364 | 2.62168399755226 |
| H | -5.96101875625449 | -1.93370188483730 | 1.95189025252531 |
| H | -5.48417086533308 | -1.79902356661974 | 3.65742043870821 |
| C | -3.24228866770637 | -1.18436412482584 | -1.84909435692755 |
| H | -4.27594078696134 | -1.51976429489116 | -1.83143007339119 |
| C | -2.41520660977835 | -0.91797119476166 | -2.89475304649518 |
| H | -2.59584392704867 | -0.97700789344605 | -3.96499857971336 |
| N | -1.20641818058841 | -0.52720349136617 | -2.37211382362162 |
| C | 0.27183105649216 | 1.57494735956078 | -1.06524181149922 |
| N | 0.57721496121402 | 2.88470480643585 | -0.86849747321036 |
| C | 0.50797776334049 | 3.64683686248753 | 0.39024150234612 |
| C | -0.10005498846231 | 5.03606495853586 | 0.13029118332580 |
| H | 0.50912735879969 | 5.59460037666549 | -0.59778575360543 |
| H | -1.10744599386617 | 4.91657739335845 | -0.30561676156275 |
| C | -0.38421792757835 | 2.94021079269006 | 1.41008418938064 |
| H | -1.39374152063722 | 2.80443388484736 | 0.98775536625844 |
| H | 0.01005484087842 | 1.93404699288217 | 1.62144217673851 |
| C | 1.91423053042136 | 3.83017759870243 | 0.97800532587600 |
| H | 2.36995509197122 | 2.83998914711170 | 1.15682726261461 |
| H | 2.55322575241091 | 4.35201377409458 | 0.24437755314153 |
| C | -0.16849650447562 | 5.83926691472803 | 1.42913467210780 |
| H | -0.59865912575990 | 6.83018851566237 | 1.20469279531914 |
| C | -0.44730865471568 | 3.73463695187139 | 2.71388554649966 |
| H | -1.08389427576986 | 3.18312595206313 | 3.42732179391465 |
| C | 1.84033313726488 | 4.62897090191736 | 2.27918037748744 |

**Table A4.10, continued**

| | | | |
|---|---|---|---|
| H | 2.85964506171290 | 4.74265428327520 | 2.68639113370293 |
| C | 1.24015606986239 | 6.00590136073897 | 1.99762251832080 |
| H | 1.87634712824316 | 6.55911925880257 | 1.28356367240003 |
| H | 1.20408404552695 | 6.60033909340988 | 2.92761499249933 |
| C | -1.04716806970281 | 5.11065214052858 | 2.44095837358563 |
| H | -2.07497633350872 | 5.00690054833218 | 2.04949551584854 |
| H | -1.11304797659389 | 5.69173869635195 | 3.37789126337704 |
| C | 0.96179570546285 | 3.88625746360250 | 3.28464567345329 |
| H | 1.39257794148673 | 2.89126651588750 | 3.50399325344308 |
| H | 0.92688770597427 | 4.43908497894027 | 4.24006830687977 |
| C | 0.97514889029759 | 3.45596640261377 | -2.06070449126713 |
| H | 1.29601214507451 | 4.48923118507595 | -2.14829514507689 |
| C | 0.86654957405347 | 2.49344577528809 | -3.01093853800882 |
| H | 1.09234923113537 | 2.54176968583809 | -4.07251522218136 |
| N | 0.40088712765245 | 1.36069237600336 | -2.39825149357998 |
| B | 0.11394593078028 | -0.05331451575310 | -3.02863601787254 |
| C | -0.03917155806767 | -0.09425966512555 | -4.62820830171533 |
| C | -0.65407650009386 | 0.95230683133801 | -5.33519601266965 |
| H | -0.97390431202532 | 1.85408679651716 | -4.80485719244963 |
| C | -0.89768792471499 | 0.87775056403079 | -6.70554113263813 |
| H | -1.37485209814888 | 1.71844484129349 | -7.21923156773624 |
| C | -0.54305285055200 | -0.26537410333849 | -7.41756324831195 |
| H | -0.72911482023912 | -0.32781395995541 | -8.49433491001014 |
| C | 0.03472818879503 | -1.33462555451106 | -6.73850739680223 |
| H | 0.29800810048147 | -2.25020656578174 | -7.27774051827726 |
| C | 0.27222598054310 | -1.24678415142375 | -5.36745985030558 |
| H | 0.69586652921006 | -2.12052932533931 | -4.86421491579311 |

**Table A4.11.** Coordinates for the optimized structure of [PhB($^{Ad}$Im)$_2$($^{HOAd}$Im)Co$^{I}$] ($S$ = 1).

| | | | |
|---|---|---|---|
| Co | 0.01943510093939 | 0.20111443695809 | 0.13156469263406 |
| O | 3.30488090700605 | 0.33292417084783 | 1.11506925108512 |
| H | 2.62260697926238 | 0.36541020529820 | 0.42069147606050 |
| C | 1.25057187288696 | -0.93447197277285 | -0.80797657384072 |
| N | 2.29529218116196 | -1.77076780992380 | -0.54379537548687 |
| C | 2.79356606522212 | -2.05143722926144 | 0.80296703566686 |
| C | 3.83071622283398 | -0.97115019517433 | 1.18260722739675 |
| H | 4.66844731083099 | -1.05971941790563 | 0.47285964801792 |
| C | 1.64912175892458 | -2.04200130525656 | 1.81860596447986 |
| H | 1.12804879919277 | -1.06578757782800 | 1.78578512333346 |
| H | 0.90803515034303 | -2.80805211836767 | 1.53476457407599 |
| C | 3.48940598204216 | -3.41490226100338 | 0.86259079239594 |
| H | 2.77122944599505 | -4.19802914132078 | 0.56333120180505 |
| H | 4.33228701821309 | -3.45199768551401 | 0.15333909511455 |
| C | 4.34901174683091 | -1.22802528808643 | 2.59398503342753 |
| H | 5.07408464090073 | -0.43251175425520 | 2.83553535135734 |
| C | 2.18676166374744 | -2.29514277080823 | 3.22504770379031 |
| H | 1.34110225400348 | -2.27535996628774 | 3.93410014562374 |
| C | 4.02075685246847 | -3.67678903771987 | 2.27042772284622 |
| H | 4.51337046091311 | -4.66407909330470 | 2.28331442162778 |
| C | 5.03387542713698 | -2.59162984431587 | 2.63125743109383 |
| H | 5.88477911877357 | -2.61583375181472 | 1.92704979275640 |
| H | 5.44484652550268 | -2.77472109122561 | 3.63965549042614 |
| C | 3.19124857373511 | -1.20327714729874 | 3.58894262536011 |
| H | 2.70193672089056 | -0.21480599736835 | 3.57984856565501 |
| H | 3.57696988008973 | -1.36661142055884 | 4.61067942340446 |
| C | 2.86828288245167 | -3.66068739031458 | 3.27046815595623 |

**Table A4.11, continued**

| | | | |
|---|---|---|---|
| H | 2.14255763298954 | -4.45646111342485 | 3.02463053653986 |
| H | 3.24524305331539 | -3.86575015231953 | 4.28846017724578 |
| C | 2.92459376534094 | -2.12861620139994 | -1.72299324004723 |
| H | 3.79489016419438 | -2.77630518191389 | -1.76814940463270 |
| C | 2.23080415918192 | -1.52998646676480 | -2.72544129860843 |
| H | 2.41899766423774 | -1.56229976135694 | -3.79470436538719 |
| N | 1.19188476983619 | -0.82767532971247 | -2.16230326807158 |
| C | -1.51025122798390 | -0.29914661462279 | -0.88750419031246 |
| N | -2.80829201697533 | -0.66965783074689 | -0.73789358608896 |
| C | -3.44098067678922 | -0.92464778760456 | 0.55977784377018 |
| C | -2.91699137597502 | 0.06536903009012 | 1.60535509751140 |
| H | -1.81537551883748 | -0.03004589214250 | 1.67716840292331 |
| H | -3.12650925343525 | 1.09639515439825 | 1.27232110859715 |
| C | -4.96335879368329 | -0.76542031830978 | 0.46685208521527 |
| H | -5.20697546234569 | 0.25077793935966 | 0.10985844856077 |
| H | -5.37846484433400 | -1.48047504286372 | -0.26269043389166 |
| C | -3.12454107737817 | -2.35306287981083 | 1.03054794971459 |
| H | -3.49053667145972 | -3.07366325497053 | 0.27778006694184 |
| H | -2.02860967785272 | -2.47433447178973 | 1.09609254719649 |
| C | -3.55519048453258 | -0.20247825983571 | 2.96622444156109 |
| H | -3.15087490431725 | 0.52015097575413 | 3.69613735911873 |
| C | -5.60769977202669 | -1.02559821367923 | 1.82857620341979 |
| H | -6.70017734700750 | -0.90369899135455 | 1.73009958106339 |
| C | -3.77280981946295 | -2.61973999892081 | 2.38855234390683 |
| H | -3.53500788309837 | -3.65021773542757 | 2.70528659662185 |
| C | -3.22776316664847 | -1.62645336203754 | 3.41401413205840 |
| H | -2.13435250344078 | -1.75002437681329 | 3.51970560821821 |

**Table A4.11, continued**

| | | | |
|---|---|---|---|
| H | -3.67242336801888 | -1.82299491207893 | 4.40617997337485 |
| C | -5.06880574981382 | -0.03332913301651 | 2.85566452988284 |
| H | -5.31382418871221 | 1.00025230159481 | 2.55154381540863 |
| H | -5.54636472584284 | -0.20477024109121 | 3.83722376739460 |
| C | -5.28726196468223 | -2.45211722157426 | 2.27396050888859 |
| H | -5.69689283588172 | -3.17748622898169 | 1.54788087581989 |
| H | -5.76690440892036 | -2.66254306463527 | 3.24673031596990 |
| C | -3.38398227439197 | -0.88441746664553 | -1.97915196761653 |
| H | -4.41641406174626 | -1.19012432877642 | -2.11760221587176 |
| C | -2.42198897903827 | -0.62302306621624 | -2.90126401635754 |
| H | -2.47688470579854 | -0.65962346416160 | -3.98607857989300 |
| N | -1.27928443816289 | -0.26512121626682 | -2.22280696565940 |
| C | 0.43598997126386 | 1.77459221456097 | -0.89522423067636 |
| N | 0.89013391116116 | 3.04112067392145 | -0.70555787833138 |
| C | 0.95450651567204 | 3.75318253554897 | 0.57325800679369 |
| C | 0.12088484254560 | 5.04193676564753 | 0.49262596927208 |
| H | 0.49218571904733 | 5.68126011335770 | -0.32663755044238 |
| H | -0.92461646349907 | 4.77863385047286 | 0.25318133419012 |
| C | 0.39392508646383 | 2.89320594067804 | 1.70814781313341 |
| H | -0.65116845269576 | 2.62160253111325 | 1.48370255423981 |
| H | 0.97001720737427 | 1.95239380727112 | 1.78082392072928 |
| C | 2.40896749933103 | 4.11896834011408 | 0.90703767443047 |
| H | 3.00950023649589 | 3.19437509488244 | 0.96587314209293 |
| H | 2.83442673897875 | 4.73678842466368 | 0.09747038113331 |
| C | 0.19072739775147 | 5.80438804292998 | 1.81531325855146 |
| H | -0.40912823789965 | 6.72687935842262 | 1.72801845596460 |
| C | 0.46387290408137 | 3.65132663628549 | 3.03463216858731 |

**Table A4.11, continued**

| | | | |
|---|---|---|---|
| H | 0.05631118407054 | 3.00354193761018 | 3.82992689981686 |
| C | 2.47304056982854 | 4.88198953445984 | 2.22981813498938 |
| H | 3.52538166880362 | 5.13684768424700 | 2.44454287653286 |
| C | 1.64503706884049 | 6.16187331878678 | 2.12115895482904 |
| H | 2.05212967236343 | 6.81158284748686 | 1.32529742821938 |
| H | 1.70401792614862 | 6.73156392223881 | 3.06587781971081 |
| C | -0.36698349333534 | 4.92923139835114 | 2.93540841277474 |
| H | -1.42404537733750 | 4.67977267349639 | 2.73216462264789 |
| H | -0.34062821985260 | 5.47530694248427 | 3.89558262201855 |
| C | 1.91569169522849 | 4.00536927629842 | 3.34972945455115 |
| H | 2.51971507722039 | 3.08527480463760 | 3.44890323565299 |
| H | 1.97463482528398 | 4.53835746940774 | 4.31569180754600 |
| C | 1.29099981815815 | 3.58818576439624 | -1.91066263247981 |
| H | 1.70506970937155 | 4.58896993764207 | -2.00347394784787 |
| C | 1.05373883245279 | 2.64612733850461 | -2.85957203173509 |
| H | 1.25820992595641 | 2.68610900676678 | -3.92574419195438 |
| N | 0.49684010633794 | 1.55300179315433 | -2.23698396567795 |
| B | 0.12262017548815 | 0.13401407330935 | -2.80097933685218 |
| C | 0.00886002807786 | 0.05253226993439 | -4.41582539668717 |
| C | -0.46162179114276 | 1.13413983217661 | -5.17944854426986 |
| H | -0.69035174299174 | 2.08539743331083 | -4.69143604943076 |
| C | -0.68630816199731 | 1.03891815330136 | -6.55234673497790 |
| H | -1.04900251179059 | 1.91201227702754 | -7.10469120919189 |
| C | -0.46170731471530 | -0.16384701922775 | -7.21671512575116 |
| H | -0.63298436205054 | -0.24449480104264 | -8.29488251442779 |
| C | -0.03863920929103 | -1.26893790500439 | -6.48284861095297 |
| H | 0.11454705576036 | -2.23240528852402 | -6.98002427522515 |

**Table A4.11, continued**

| | | | |
|---|---|---|---|
| C | 0.18094525299722 | -1.15677249112943 | -5.11041983258629 |
| H | 0.47075814324335 | -2.05996987931792 | -4.56672966945925 |

**Table A4.12.** Coordinates for the optimized structure of $[PhB(^{Ad}Im)_2(^{\bullet Ad}Im)Co^{III}OH]^+$ ($S$ = ½, **4$^{rad}$**).

| | | | |
|---|---|---|---|
| Co | 0.05557433141473 | 0.06141845698909 | -0.00428871025414 |
| O | 1.01603461969346 | 0.15288283847656 | 1.45990724182166 |
| H | 1.95998535802581 | -0.11320288827907 | 1.50384004497164 |
| C | 1.21433668674237 | -0.94873553439104 | -1.07433584239891 |
| N | 2.24953607995327 | -1.79213058997714 | -0.79631507041712 |
| C | 2.66372730026368 | -2.35981121650206 | 0.50752737243224 |
| C | 3.32231428448749 | -1.33286134505890 | 1.36928218228989 |
| H | 3.94231010827599 | -0.58804579699794 | 0.87408257141878 |
| C | 1.46294296376498 | -3.00719493778031 | 1.21549011569622 |
| H | 0.65736279216341 | -2.26979694492794 | 1.33502801292788 |
| H | 1.07881928634495 | -3.82310079007705 | 0.57958213770192 |
| C | 3.73042940539143 | -3.46968849503282 | 0.31531163370132 |
| H | 3.31857632851942 | -4.27449489900477 | -0.31889112179730 |
| H | 4.62131711161293 | -3.05813772090004 | -0.18555521353163 |
| C | 3.69275934476882 | -1.81649226169924 | 2.72483463326511 |
| H | 4.11981608243956 | -0.99369226078234 | 3.32007678862474 |
| C | 1.88851475136007 | -3.54480963134988 | 2.58019899407708 |
| H | 0.99897247995303 | -3.96280141258028 | 3.08248483456765 |
| C | 4.14667925132093 | -4.03231902845790 | 1.67581944205610 |
| H | 4.90458489056472 | -4.81428806346396 | 1.49876485540370 |
| C | 4.75113075950490 | -2.92370540167513 | 2.53305502810699 |
| H | 5.65241256457998 | -2.50792931132719 | 2.05046189358828 |

**Table A4.12, continued**

| | | | |
|---|---|---|---|
| H | 5.05634462933254 | -3.31904381241274 | 3.51842996650114 |
| C | 2.46933085238699 | -2.41422431358870 | 3.42853114305216 |
| H | 1.70959052232224 | -1.63316710109890 | 3.60024190824168 |
| H | 2.76838539895236 | -2.80182157449108 | 4.41789550138123 |
| C | 2.93797462859478 | -4.63434978187244 | 2.38602885482066 |
| H | 2.52005437618498 | -5.46492452936407 | 1.79024297616728 |
| H | 3.24260544929513 | -5.05286216908247 | 3.36117882809495 |
| C | 2.86711316260432 | -2.12866547369361 | -1.98135387049182 |
| H | 3.73035917241270 | -2.78052414281837 | -2.03630535125017 |
| C | 2.19465905068388 | -1.50746489269261 | -2.98106172642090 |
| H | 2.39025898634758 | -1.50421042449640 | -4.04841116672203 |
| N | 1.16331058982671 | -0.81778550650918 | -2.41142288619811 |
| C | -1.38524938551440 | -0.49378169219113 | -1.08611603763611 |
| N | -2.59302294171523 | -1.03653470150343 | -0.79392974509032 |
| C | -3.13191775132692 | -1.38886406207553 | 0.52922499785291 |
| C | -2.37199321877543 | -0.65796285909512 | 1.63000964403687 |
| H | -1.29892088617486 | -0.92414086411203 | 1.58907230770230 |
| H | -2.46863531321015 | 0.42938779645408 | 1.48368445397913 |
| C | -4.61181612327883 | -0.99371289183304 | 0.62904530877143 |
| H | -4.71115707445960 | 0.09324921040056 | 0.46251867646291 |
| H | -5.20181520576601 | -1.50322827745996 | -0.14992740937932 |
| C | -2.99522721376348 | -2.90328126944483 | 0.74656301439836 |
| H | -3.53957335903110 | -3.44080330171774 | -0.04900528762549 |
| H | -1.93045122918199 | -3.18547997039942 | 0.66616782994630 |
| C | -2.91276653708498 | -1.04646944076283 | 3.00695535063095 |
| H | -2.33213415238017 | -0.50748895092158 | 3.77446811031165 |
| C | -5.16217793348141 | -1.38174282253092 | 2.00244973910524 |

**Table A4.12, continued**

| | | | |
|---|---|---|---|
| H | -6.22663624561209 | -1.09534020223533 | 2.04657725694928 |
| C | -3.55102153856095 | -3.28525311973132 | 2.11778412069973 |
| H | -3.44791742986664 | -4.37562593064561 | 2.25143659737768 |
| C | -2.76756063580793 | -2.55412230197852 | 3.20657456325766 |
| H | -1.70142677952749 | -2.84422615326239 | 3.16954252498802 |
| H | -3.14677995252980 | -2.83934691860017 | 4.20360380903879 |
| C | -4.38505582441016 | -0.65216997276461 | 3.09505784093950 |
| H | -4.49424639833352 | 0.44103414177181 | 2.97876789937351 |
| H | -4.78742780824235 | -0.91513439161728 | 4.08922159942019 |
| C | -5.02560471653319 | -2.89202590296207 | 2.19535644875083 |
| H | -5.60333348174701 | -3.42825080021023 | 1.42111455743212 |
| H | -5.44463650772568 | -3.18668828903640 | 3.17361205228346 |
| C | -3.23231586215913 | -1.36035304536693 | -1.97388189432287 |
| H | -4.21598772909586 | -1.81867253327516 | -2.00147408797344 |
| C | -2.40396621789262 | -1.00208920578300 | -2.98912514292386 |
| H | -2.53301008809094 | -1.08425338427973 | -4.06495823754031 |
| N | -1.28008898619382 | -0.46973913946069 | -2.41961087985856 |
| C | 0.16313765422051 | 1.55353200110083 | -1.11058352846874 |
| N | 0.34605231246706 | 2.86105976869792 | -0.79524201462510 |
| C | 0.18074541373200 | 3.52004418311361 | 0.51922546812990 |
| C | -0.21679674594617 | 4.99051302937992 | 0.32232664681643 |
| H | 0.57984480169048 | 5.53611145594901 | -0.20876469410023 |
| H | -1.13258376194676 | 5.05157952774114 | -0.29120230232583 |
| C | -0.94006291113242 | 2.82968558047527 | 1.29632560161834 |
| H | -1.87266189227352 | 2.86221682354542 | 0.70822353550742 |
| H | -0.67751679948112 | 1.77241934608618 | 1.46102632186946 |
| C | 1.48377831178355 | 3.47496803577611 | 1.32721132100472 |

**Table A4.12, continued**

| | | | |
|---|---|---|---|
| H | 1.79148281839766 | 2.42627316919095 | 1.46537150833110 |
| H | 2.27821700028683 | 3.99012269367541 | 0.75893481955816 |
| C | -0.43161299722317 | 5.66490322499689 | 1.67803545522576 |
| H | -0.71630546312017 | 6.71569727778168 | 1.49953893208581 |
| C | -1.13603754339242 | 3.49523033777134 | 2.65738985929090 |
| H | -1.93353633286096 | 2.95829308362305 | 3.19922379659517 |
| C | 1.27290664577300 | 4.15202206809288 | 2.68366110593391 |
| H | 2.21680655483768 | 4.10152994165690 | 3.25287985845301 |
| C | 0.87022395089759 | 5.61042439325121 | 2.47594993845610 |
| H | 1.66790024732689 | 6.15441294074937 | 1.93891963941296 |
| H | 0.73810117941114 | 6.11094553217451 | 3.45154958151499 |
| C | -1.53986553923248 | 4.95149631591751 | 2.44618212284880 |
| H | -2.48945411593416 | 5.00475259482497 | 1.88432786234412 |
| H | -1.70917121212204 | 5.44575541612656 | 3.41922466530511 |
| C | 0.16824671789263 | 3.42627557191157 | 3.45164327435363 |
| H | 0.45253605965199 | 2.37356495578518 | 3.62559922096376 |
| H | 0.02868107134119 | 3.89280381651549 | 4.44291402469208 |
| C | 0.65737982132019 | 3.54361212297514 | -1.95305265698980 |
| H | 0.86763529115699 | 4.60681667142527 | -1.96954804534010 |
| C | 0.62420144719767 | 2.65069687125705 | -2.97368716643187 |
| H | 0.83233563792094 | 2.79797818423240 | -4.02871861310627 |
| N | 0.27705692171219 | 1.43912423163817 | -2.44073409058265 |
| B | 0.03543988954683 | 0.04009387909176 | -3.07231821348437 |
| C | -0.10242324190682 | -0.03600051610877 | -4.67022556842399 |
| C | -0.65041995326851 | 1.02445848266062 | -5.41091862933040 |
| H | -0.93229042575842 | 1.95533423514404 | -4.91267522119273 |
| C | -0.88850645812775 | 0.92745358927150 | -6.78090334553420 |

**Table A4.12, continued**

| | | | |
|---|---|---|---|
| H | -1.31134204026072 | 1.78180479205330 | -7.31873566167255 |
| C | -0.60040801184367 | -0.25308137056913 | -7.45953696744123 |
| H | -0.78213339194393 | -0.33327292655911 | -8.53575621052576 |
| C | -0.10073973791814 | -1.33851941722017 | -6.74533961210941 |
| H | 0.10285551110765 | -2.28548831687375 | -7.25504741558765 |
| C | 0.13247384317603 | -1.22843480026370 | -5.37573761652400 |
| H | 0.48468040022822 | -2.11913659451501 | -4.84866296930148 |

**Table A4.13.** Coordinates for the optimized transition state between $[PhB(^{Ad}Im)_2(^{\bullet Ad}Im)Co^{III}OH]^+$ (**4**$^{\mathbf{rad}}$) and $[PhB(^{Ad}Im)_2(^{HOAd}Im)Co^{II}]^+$ (**4**$^{\mathbf{reb}}$) ($S$ = 1/2).

| | | | |
|---|---|---|---|
| Co | 0.29931202677007 | -0.03178422971223 | -0.31923947198092 |
| O | 1.48327660233678 | 0.36614333220257 | 0.95392929323769 |
| H | 2.29286293127473 | 0.82108883999150 | 0.70798476482498 |
| C | 1.39320181012115 | -1.06522271851569 | -1.40738365671929 |
| N | 2.45736040807864 | -1.84381080976203 | -1.09591459395317 |
| C | 2.83930023305119 | -2.30887587475406 | 0.25117524024314 |
| C | 3.41907757926945 | -1.21168624317169 | 1.06983044376552 |
| H | 4.00765568035392 | -0.45572689582896 | 0.55896086233167 |
| C | 1.62573352523501 | -2.92678408954917 | 0.96121188788138 |
| H | 0.81486394942637 | -2.18531478964098 | 1.01329615158338 |
| H | 1.25605405032576 | -3.77695805521272 | 0.36363088478113 |
| C | 3.93849596387127 | -3.39693917884316 | 0.17220946670157 |
| H | 3.56952495585560 | -4.25452288591676 | -0.41810525243246 |
| H | 4.83372747569483 | -2.99490048258063 | -0.32928101785870 |
| C | 3.74414435453638 | -1.58042410631424 | 2.46589201806356 |
| H | 4.12321561949409 | -0.70538283821594 | 3.01680405295667 |
| C | 2.00637153265175 | -3.37174100427685 | 2.37015272567720 |

**Table A4.13, continued**

| | | | |
|---|---|---|---|
| H | 1.10881378661439 | -3.78697967729463 | 2.86055426038749 |
| C | 4.31432526370032 | -3.84882024628115 | 1.58447665537737 |
| H | 5.10291228231124 | -4.61551195401158 | 1.49921693364868 |
| C | 4.84543430084260 | -2.66317903664559 | 2.38733839733924 |
| H | 5.75208324942541 | -2.24894306627295 | 1.91356470374007 |
| H | 5.12282878422286 | -2.98099946400346 | 3.40859098446764 |
| C | 2.51791524300393 | -2.17284311208141 | 3.16602999543080 |
| H | 1.73013286058855 | -1.40668562618835 | 3.25801564427455 |
| H | 2.79397767852700 | -2.48707192845101 | 4.18765135229133 |
| C | 3.09287508399774 | -4.43945691528593 | 2.28344196907668 |
| H | 2.72161156353424 | -5.31647123566280 | 1.72457652968472 |
| H | 3.36712072839492 | -4.78895743266683 | 3.29419337879611 |
| C | 3.09254967450553 | -2.20713143875470 | -2.26514548409034 |
| H | 3.98064440343939 | -2.82846888975056 | -2.28894144322373 |
| C | 2.39282082584401 | -1.65319535744437 | -3.28871731193848 |
| H | 2.59076234500643 | -1.68482120550008 | -4.35548169393914 |
| N | 1.33024699688885 | -0.98238809239352 | -2.74348108369935 |
| C | -1.16633146629881 | -0.63270637252987 | -1.32075767373272 |
| N | -2.38346586315837 | -1.10044527596223 | -0.96319152690086 |
| C | -2.88275289334170 | -1.28033420653009 | 0.40267101088959 |
| C | -1.85430655201019 | -0.76098425117761 | 1.40258812308223 |
| H | -0.90614884262994 | -1.31713704950511 | 1.27970404695008 |
| H | -1.66949715611610 | 0.31080446338493 | 1.21632573698424 |
| C | -4.18718484612061 | -0.49569830685649 | 0.60282084534846 |
| H | -4.00241252438647 | 0.57360651108915 | 0.39812338999180 |
| H | -4.95016645944854 | -0.84139322444963 | -0.11474437582285 |
| C | -3.13656543725426 | -2.76840613584222 | 0.68024395562271 |

**Table A4.13, continued**

| | | | |
|---|---|---|---|
| H | -3.87988594120124 | -3.16003142038701 | -0.03490890652363 |
| H | -2.20019797533292 | -3.33252582965525 | 0.52422624691064 |
| C | -2.35294623735265 | -0.94766589281323 | 2.83598757600256 |
| H | -1.58315047414233 | -0.56563189387758 | 3.52732511485121 |
| C | -4.69525870583203 | -0.68717972107967 | 2.03223221846110 |
| H | -5.63588938909399 | -0.12307144957851 | 2.15060341787062 |
| C | -3.64412963821910 | -2.95095668986545 | 2.11030134167893 |
| H | -3.82414558099309 | -4.02483850317241 | 2.28810086538215 |
| C | -2.59740318681106 | -2.43306043427080 | 3.09476237482323 |
| H | -1.65415273484267 | -2.99839415913937 | 2.98306973716202 |
| H | -2.94418426382316 | -2.58235940355877 | 4.13242662883961 |
| C | -3.65264364920574 | -0.16647403262527 | 3.01930059990485 |
| H | -3.47449970287501 | 0.91192854088461 | 2.85587101121843 |
| H | -4.01807936071821 | -0.28145528602207 | 4.05490091695316 |
| C | -4.94723812398843 | -2.17233099037373 | 2.28994304335955 |
| H | -5.71719318171366 | -2.55417155946104 | 1.59571171324452 |
| H | -5.33490138386813 | -2.31708761268794 | 3.31370874999576 |
| C | -3.09887327514535 | -1.41478276391872 | -2.10226306259216 |
| H | -4.10825355601493 | -1.81593333461885 | -2.07047965871143 |
| C | -2.29821285651242 | -1.12547842954028 | -3.16242373079750 |
| H | -2.48218313770602 | -1.22392289823066 | -4.22908119917142 |
| N | -1.11755874157116 | -0.64636004930749 | -2.65843610020593 |
| C | 0.32870522814779 | 1.48169149416711 | -1.44239792260596 |
| N | 0.48504993022875 | 2.81566210972099 | -1.22603888262417 |
| C | 0.29957517256889 | 3.60090096438085 | 0.01923808367775 |
| C | -0.33865132710983 | 4.96027090875186 | -0.31863921456152 |
| H | 0.31240593246586 | 5.54014705087905 | -0.99115077689763 |

**Table A4.13, continued**

| | | | |
|---|---|---|---|
| H | -1.29634630043807 | 4.79658778011418 | -0.84307982171017 |
| C | -0.63933519403985 | 2.87418962421727 | 0.98205139258646 |
| H | -1.60602350836219 | 2.68642397754966 | 0.48367427558641 |
| H | -0.19776814646169 | 1.90579331059948 | 1.25338926819927 |
| C | 1.64596350633691 | 3.85749673327611 | 0.70710915979887 |
| H | 2.12324233667516 | 2.89579499865237 | 0.95469235878274 |
| H | 2.31751324404896 | 4.39274942166474 | 0.01315145118228 |
| C | -0.55177732943366 | 5.78098639659387 | 0.95359458623775 |
| H | -1.00459988393643 | 6.74638020240038 | 0.67005560026262 |
| C | -0.84252970720385 | 3.69244248953773 | 2.25678727290213 |
| H | -1.50777742159472 | 3.12485108714451 | 2.93050364920337 |
| C | 1.43259542663626 | 4.67825232341694 | 1.98048442484478 |
| H | 2.41148658170432 | 4.84326933561171 | 2.46233118793804 |
| C | 0.79910879207697 | 6.02179470931802 | 1.62542227854325 |
| H | 1.46390028300124 | 6.59032146746689 | 0.95053682904025 |
| H | 0.66453722740961 | 6.63044592340702 | 2.53698667885656 |
| C | -1.47738064832679 | 5.03450057808454 | 1.90840200252411 |
| H | -2.46578876914782 | 4.87931390533234 | 1.43993655646439 |
| H | -1.64108735149871 | 5.63021742952433 | 2.82390690876077 |
| C | 0.51013372713657 | 3.91693435297184 | 2.93222285311025 |
| H | 0.96355813101215 | 2.94820631431799 | 3.20832448532411 |
| H | 0.37581715916733 | 4.49005963092755 | 3.86666764814291 |
| C | 0.77752660414704 | 3.42114221106165 | -2.43208744436916 |
| H | 0.97428663792591 | 4.48321727723587 | -2.52565014683466 |
| C | 0.74588527587137 | 2.46029591791570 | -3.38758900453972 |
| H | 0.93309769537351 | 2.53746705977164 | -4.45420176653911 |
| N | 0.42470625631919 | 1.28244337827279 | -2.77064969395612 |

**Table A4.13, continued**

| | | | |
|---|---|---|---|
| B | 0.17212032042960 | -0.14137294466742 | -3.36717577180946 |
| C | -0.02549153042191 | -0.23364612172129 | -4.95833666562549 |
| C | -0.66879862749181 | 0.78725891230549 | -5.67816745443858 |
| H | -0.98515333968615 | 1.70146547199494 | -5.16869922928495 |
| C | -0.95370147619285 | 0.67021332010314 | -7.03742087041420 |
| H | -1.45101169579762 | 1.49343978602639 | -7.55995323763112 |
| C | -0.61648532886126 | -0.49215673867366 | -7.72549324616148 |
| H | -0.83457477575603 | -0.58780633946459 | -8.79369573401225 |
| C | -0.01824634824643 | -1.53963354979538 | -7.03092138058355 |
| H | 0.22801338582687 | -2.47254494869909 | -7.54779288332065 |
| C | 0.26065758190139 | -1.40967150860330 | -5.67137434703713 |
| H | 0.69185164212989 | -2.27255133262362 | -5.15737347480791 |

**Table A4.14.** Coordinates for the optimized structure of [PhB($^{Ad}$Im)$_2$($^{\bullet Ad}$Im)Co$^{II}$OH] ($S$ = 1).

| | | | |
|---|---|---|---|
| Co | 0.06369617392836 | -0.06709999016762 | 0.11882329059910 |
| O | -0.01193895833218 | -0.07010251442704 | 1.98511531993723 |
| H | 0.75312209978117 | -0.53248267674595 | 2.33883738970004 |
| C | 0.63276623494190 | -1.61640053038003 | -0.98069617020520 |
| N | 1.15236199285524 | -2.85682289653550 | -0.85326851124405 |
| C | 1.41207545082308 | -3.48535749410422 | 0.44134988155972 |
| C | 2.14417061597876 | -2.54894427349600 | 1.34022078481487 |
| H | 2.80320127775259 | -1.81042157217616 | 0.89744024900487 |
| C | 0.08682181682054 | -3.90271888683791 | 1.10745071924542 |
| H | -0.55746983298982 | -3.01319462699635 | 1.19876006522299 |
| H | -0.42891725485764 | -4.63012288334589 | 0.45579914547775 |
| C | 2.29043458181157 | -4.74711698259693 | 0.29332060061131 |

**Table A4.14, continued**

| | | | |
|---|---|---|---|
| H | 1.77572314504882 | -5.49765089771827 | -0.33233723365443 |
| H | 3.23797355532089 | -4.48322405414526 | -0.20647049162347 |
| C | 2.39559093877628 | -3.07605619299092 | 2.70649340295501 |
| H | 2.91310361927371 | -2.32210081718093 | 3.32143163060577 |
| C | 0.36127267790586 | -4.51012343025231 | 2.48149175102731 |
| H | -0.60028973133063 | -4.79211272463037 | 2.94444203985608 |
| C | 2.56416419107033 | -5.34388723526440 | 1.67490496966954 |
| H | 3.20224715888081 | -6.23520956618702 | 1.54632185483188 |
| C | 3.28465206366556 | -4.32793221063218 | 2.55865975707711 |
| H | 4.25564452671959 | -4.05102792714104 | 2.11200747124111 |
| H | 3.49190280819252 | -4.76297594857682 | 3.55362649820921 |
| C | 1.07012846087019 | -3.48388596868219 | 3.36336719293613 |
| H | 0.42892345118224 | -2.59697491621258 | 3.50361285059199 |
| H | 1.26517789327070 | -3.91100097957908 | 4.36316026725157 |
| C | 1.24238306368862 | -5.74732438452985 | 2.32583520916893 |
| H | 0.73005733401319 | -6.50477930545747 | 1.70595198117388 |
| H | 1.43129778545547 | -6.20764910167287 | 3.31184632607187 |
| C | 1.33732424934432 | -3.42551944417778 | -2.09730915719389 |
| H | 1.74376995406624 | -4.42064623122485 | -2.24703596433511 |
| C | 0.92943275030816 | -2.50091466015535 | -3.00451166042925 |
| H | 0.92017781131782 | -2.55283262021921 | -4.08923696022957 |
| N | 0.49959804298667 | -1.39475429064693 | -2.30607882540955 |
| C | -1.65212793306787 | 0.21621972320519 | -0.93475427179741 |
| N | -2.93282565852771 | 0.61242546515193 | -0.73322522818976 |
| C | -3.58968925539943 | 0.69296034374202 | 0.58336326670873 |
| C | -2.93082611558908 | 1.78047921916412 | 1.44104161749252 |
| H | -1.85943491707963 | 1.55093772133884 | 1.55551978764667 |

**Table A4.14, continued**

| | | | |
|---|---|---|---|
| H | -3.01456109813806 | 2.75146996596019 | 0.92103860948921 |
| C | -5.07492699501190 | 1.03519165129200 | 0.42631246568517 |
| H | -5.18805246786659 | 2.00918045859912 | -0.08011879922840 |
| H | -5.57338612749665 | 0.27414681659311 | -0.19908723467204 |
| C | -3.47503792898184 | -0.65755927125856 | 1.30216731868925 |
| H | -3.95330827552522 | -1.43637704797158 | 0.68180505392488 |
| H | -2.41016784175399 | -0.92086368700184 | 1.40985179461545 |
| C | -3.60527346633368 | 1.84982704186892 | 2.81198351673006 |
| H | -3.11026327065087 | 2.63285923972726 | 3.41258323843792 |
| C | -5.75083213497799 | 1.10210870993886 | 1.79619968371093 |
| H | -6.81663330576744 | 1.34740755583111 | 1.64755455973535 |
| C | -4.14597278038066 | -0.58342702064054 | 2.67330847464324 |
| H | -4.04124929856073 | -1.56188569484851 | 3.17373216433783 |
| C | -3.47152859801667 | 0.49938955957356 | 3.51578996963012 |
| H | -2.40613347227987 | 0.25414381519079 | 3.66546564955452 |
| H | -3.94058476353828 | 0.54681928436389 | 4.51529347494645 |
| C | -5.08447174371336 | 2.18759640476501 | 2.63966862845461 |
| H | -5.19778254814030 | 3.17206482846033 | 2.15054254717889 |
| H | -5.57764496734110 | 2.25686381056662 | 3.62588155106442 |
| C | -5.62495036832818 | -0.24795413494227 | 2.49836967152047 |
| H | -6.12597592290775 | -1.03325729618939 | 1.90379895641167 |
| H | -6.12895252488656 | -0.21283740189515 | 3.48104158394313 |
| C | -3.52564301971372 | 0.92505782471010 | -1.93959014811546 |
| H | -4.54794921004603 | 1.27372996021134 | -2.03595922216068 |
| C | -2.59324176838737 | 0.69904036242322 | -2.89989422193082 |
| H | -2.66377752123867 | 0.85076256736657 | -3.97267654382361 |
| N | -1.46106451931277 | 0.23360169007828 | -2.27619769587322 |

**Table A4.14, continued**

| | | | |
|---|---|---|---|
| C | 1.06389809860685 | 1.28159407271517 | -1.03078232542794 |
| N | 1.73990268356666 | 2.44811851533469 | -0.89541847836058 |
| C | 2.22261176912422 | 2.99234906287331 | 0.38596761685814 |
| C | 3.05609726783337 | 4.25679275225681 | 0.15586174305004 |
| H | 3.91239847144745 | 4.03161826073866 | -0.50352583145035 |
| H | 2.44374471392829 | 5.02704539803491 | -0.34330016830830 |
| C | 1.03598668500260 | 3.34917383315952 | 1.28985777862550 |
| H | 0.40133316997791 | 4.09281472620917 | 0.77581041139392 |
| H | 0.42841463600851 | 2.44465764992443 | 1.45478791995905 |
| C | 3.09774945105301 | 1.95175207020501 | 1.09573470903700 |
| H | 2.50536963833928 | 1.03597331283408 | 1.25710705536250 |
| H | 3.94879174482974 | 1.68566243359634 | 0.44387592899049 |
| C | 3.56087812543834 | 4.80654404939305 | 1.48988979903567 |
| H | 4.15761474805544 | 5.71336404319881 | 1.29095910594992 |
| C | 1.53788934935576 | 3.90185555204132 | 2.62442396019964 |
| H | 0.66770641618617 | 4.14630482760733 | 3.25820665597338 |
| C | 3.59685684057213 | 2.50343083976326 | 2.43044451351718 |
| H | 4.21719593487649 | 1.73487240745895 | 2.92365240419847 |
| C | 4.42964217227281 | 3.75866999777450 | 2.18171527457591 |
| H | 5.30590338970265 | 3.51650602677942 | 1.55336385883464 |
| H | 4.81622308458426 | 4.15658033460553 | 3.13723382828501 |
| C | 2.36871190287227 | 5.15916073103336 | 2.37734760308078 |
| H | 1.75058813318307 | 5.93485069149856 | 1.89022126650605 |
| H | 2.72041894327457 | 5.57999873697118 | 3.33648846364123 |
| C | 2.40297768973572 | 2.85009819789392 | 3.31983207904684 |
| H | 1.80688737052172 | 1.94405250974623 | 3.52692965629583 |
| H | 2.75730292287363 | 3.23575471395128 | 4.29280882089673 |

**Table A4.14, continued**

| | | | |
|---|---|---|---|
| C | 1.89372985288695 | 3.05078955413819 | -2.12691303669840 |
| H | 2.39825647677833 | 3.99926547221097 | -2.27498828281010 |
| C | 1.31290427588253 | 2.22641498058434 | -3.03599566980725 |
| H | 1.20184009880711 | 2.35977260635241 | -4.10768244935817 |
| N | 0.83722625900091 | 1.13080198922610 | -2.35765875650764 |
| B | -0.04783314843593 | -0.04998257418333 | -2.90062330532018 |
| C | -0.04384809115748 | -0.21663021559315 | -4.51161950956089 |
| C | 1.09913062529908 | 0.05168375929653 | -5.28319393374272 |
| H | 1.99545490109815 | 0.45812286949376 | -4.80686966644022 |
| C | 1.15530585523013 | -0.21281588353634 | -6.65103590508528 |
| H | 2.06670211458692 | 0.01983617997231 | -7.21131791526171 |
| C | 0.06226679929035 | -0.78096843619827 | -7.29954921726155 |
| H | 0.09912854690553 | -0.98809177565803 | -8.37374391793472 |
| C | -1.06961621187552 | -1.10319585267885 | -6.55550869164074 |
| H | -1.92840376925563 | -1.57906650682950 | -7.03994525921394 |
| C | -1.11045774297696 | -0.83163327323561 | -5.18869714564346 |
| H | -2.00214667642536 | -1.13842619740932 | -4.63517817917925 |